Interfacial fractures: thermal effects and material disorder

Tom Vincent-Dospital

UNIVERSITÉ DE STRASBOURG

ÉCOLE DOCTORALE 413

Institut de Physique du Globe de Strasbourg
en cotutelle avec l'Université d'Oslo

THÈSE présentée par :

Tom VINCENT-DOSPITAL

soutenue le : **03 novembre 2020**

pour obtenir le grade de : **Docteur de l'université de Strasbourg**

Discipline/ Spécialité : Géophysique / Physique de la rupture

Fracturation interfaciale : effets thermiques et désordre matériel

THÈSE dirigée par :

M. TOUSSAINT Renaud	DR CNRS, université de Strasbourg
M. MÅLØY Knut Jørgen	Pr, université d'Oslo
M. FLEKKØY Pr. Eirik G.	Pr, université d'Oslo

THÈSE co-encadrée par :

M. Alain Cochard	MCF, université de Strasbourg

RAPPORTEURS :

Mme. AHARONOV Einat	Pr, Hebrew University of Jerusalem
M. WEISS Jérôme	DR CNRS, Université Grenoble Alpes, ISTerre

AUTRES MEMBRES DU JURY :

Mme. TANGUY Anne	Pr, INSA Lyon
M. BONAMY Daniel	Senior Researcher, CEA Saclay
M. SANTUCCI Stéphane	CR CNRS, ENS Lyon

PhD Thesis

Interfacial fractures: thermal effects and material disorder

Field of study:	Geophysics
Speciality:	Rupture dynamics
Author / Candidate:	**Tom Vincent-Dospital**
Research department:	Institut de physique du Globe de Strasbourg (IPGS) - UMR 7516
Cotutelle:	Department of Physics, Université d'Oslo
Location:	IPGS, Université de Strasbourg, Strasbourg
Thesis director:	**Renaud Toussaint** (DR CNRS, Université de Strasbourg)
Co-directors:	**Knut Jørgen Måløy** (Pr, Université d'Oslo) **Eirik G. Flekkøy** (Pr, Université d'Oslo) **Alain Cochard** (MCF, Université de Strasbourg)
Doctoral school:	ED413 – Sciences de la Terre, de l'univers et de l'environnement
Jury:	**Einat Aharonov** (Pr, Hebrew University of Jerusalem) **Jérôme Weiss** (DR CNRS, Université Grenoble Alpes, ISTerre) **Anne Tanguy** (Pr, INSA Lyon) **Daniel Bonamy** (Senior Researcher, CEA Saclay) **Stéphane Santucci** (CR CNRS, ENS Lyon)

Foreword

Dear reader,

The manuscript you are about to read will, among other things, mention spider webs, neural receptors and the surface temperature of stars. Had you expected a thesis that deals on the physics of rupture, fear not. You are indeed reading one. Yet, going off to a messy start seemed to be rather appropriate. After all, what are fractures if not a form of disorder?

In itself, producing a PhD thesis is a process that, as many things in life, holds a fair share of disorder. To learn and, as far I am now allowed to state, to research are activities that are often subject to an intermittent progression. The course of knowledge is bound to get pinned by various obstacles, being either interesting points to elucidate or annoying setbacks to live with or go around. When these obstacles are finally overcome, one's reasoning can then avalanche to some rewarding conclusions. The role of the brain, in this matter, or should I plainly say thinking, is likely to investigate enough possible mental paths, that are hopefully not completely randomly chosen but certainly not entirely pre-lighten, so that difficulties can be vanquished. As a not-so-subtle analogy with the topic of the present thesis, that is, how disorder affects the rupture of matter, the heterogeneous (quenched) barriers in the way of our learning may be, in part, overcome by the (thermal) disorder of our thinking.

While I have here tried to state that the present document is not the output of a long and quiet river, I hope that you will find it to be, itself, ordered enough to be pleasant to go through.
This manuscript is mainly composed of different research articles, some of them being now published when the others are, either currently undergoing the chaotic route of scientific publishing, or are pending for a first submission. In between these articles, one will find some additional elements that were better judged to lie in this thesis report only.
Because the work that I present was made possible by the collaboration between the University of Strasbourg and the University of Oslo (among other actors), you will find all points to be dealt with in English, and some intermediate summaries to also be translated into French. Og for fullstendighet er nettopp denne setningen skrevet på norsk[1].

Before jumping into the summary and the first chapter of the present manuscript, and thus, into some actual fracture dynamics, I would like to thank every person who was involved, directly or indirectly, in this project, and who helped me achieve it. A more formal, nominative, and hopefully nearly exhaustive acknowledgement section will come at the end of the present manuscript.

I wish you, dear reader, a pleasant reading.

[1] *And, for completeness, this very sentence (which is here translated) is written in Norwegian*

Avant-propos (*French / Français*)

Cher lecteur,

Le manuscrit que vous êtes sur le point de lire va, entre autres, parler de toiles d'araignées, de récepteurs neuronaux et de la température de surface des étoiles. Si vous vous attendiez à une thèse traitant de la physique de la rupture, n'ayez crainte. C'est bien ce que vous lisez. Néanmoins, une introduction un peu chaotique semblait à propos. Après tout, que sont les fractures si elles ne sont une forme de désordre ?

En soi, produire une thèse est déjà synonyme, comme beaucoup de choses de la vie, d'une part certaine de désordre. Apprendre et, autant que je puisse à présent le dire, rechercher sont des activités dont la progression est souvent intermittente. Le savoir est de nature à être ralenti par de nombreux obstacles, prenant parfois la forme de points à élucider de premier intérêt, parfois de désillusions que l'on doit accepter. Quand ces obstacles sont enfin franchis, le raisonnement peut enfin accélérer vers des conclusions gratifiantes. Dans ce processus, le rôle du cerveau, ou devrais-je simplement dire de la pensée, est sans doute d'étudier assez de cheminements mentaux potentiels, de préférence pas tout à fait aléatoires mais jamais complètement balisés, afin de vaincre les difficultés rencontrées. L'analogie que nous dessinons ici avec l'objet de la présente thèse, à savoir l'impact du désordre sur la fracturation des matériaux, manque certainement un peu de subtilité. Les barrières hétérogènes (gelées) sur le chemin de la connaissance peuvent, en partie, être franchies par le désordre (thermique) de notre pensée.

Bien que j'aie ici insinué que ce manuscrit n'est pas le résultat d'un travail qui s'apparente à un long fleuve tranquille, j'espère en revanche que vous le trouverez, lui-même, assez ordonné pour que sa lecture soit plaisante.
Cette thèse est surtout composée de différents articles de recherche, certains d'entre eux à present publiés quand d'autres suivent la route chaotique de la publication scientifique, ou bien seront soumis pour la première fois prochainement. Intercalant ces articles, vous trouverez également du contenu additionnel, qu'il fut jugé préférable de réserver à ce manuscrit.
Le travail que je présente étant le fruit d'une collaboration entre l'université de Strasbourg et l'université d'Oslo (entre autres acteurs), il est rédigé principalement en anglais, et certaines parties (dont celle-ci) sont traduites en français. Og for fullstendighet er nettopp denne setningen skrevet på norsk[2].

Avant d'enchainer avec l'abstract et le premier chapitre de ce travail, j'aimerais remercier toute personne qui a participé, de près ou de loin, à la réalisation de ce projet. Bien sûr, une section de remerciement plus formelle, nominative et, je l'espère, quasi-exhaustive viendra à la fin de ce manuscrit.

Je vous souhaite, cher lecteur, une lecture agréable.

[2] *Et, par souci d'exhaustivité, cette phrase-ci (ici traduite) est écrite en norvégien.*

Abstract

What are fractures if not a form of disorder?

During the rupture of a brittle elastic medium, a portion of the external mechanical load, provided to the matrix, is dissipated in a plastic zone at the fracture tip. The entropy rises. This irreversible dissipation, which can be characterized by a macroscopically measurable energy release rate, derives from various physical processes. In particular: the growth of the crack surfaces and the nucleation of new defects in the solid matrix, the emission of mechanical and electromagnetic waves propagating in the medium and dumped in the far field and, finally, a rise in temperature from the intermolecular friction, directly inside the plastic zone.

Such a rise in temperature, that is for instance observable by placing an infrared camera in front of a teared paper sheet, is often regarded as a mere consequence of the rupture. However, more than a marker for the damage, it could, backwardly, have a significant impact on the fracture dynamics. The growth of cracks can, indeed, be described as a thermally activated process, even when the heterogeneities of a material control the shape of crack fronts and the intermittency of their propagation. To understand the kinetics of rupture, it is then paramount to study the temperature field around progressing fractures, and to evaluate an accurate energy budget for this process.

This question is, of course, of importance in material sciences and in everyday engineering, to correctly grasp the toughness of matter and of structures. It is also rather central in geosciences, where the instability of some seismic faults is suspected to derive from the friction induced heat at their moving walls. In particular, the localized melting and deterioration of fault planes and the thermo-pressurization of their in situ fluids may lead to some slip-weakening and, thus, to brutal rock motions in the lithosphere.

The extremely slow growth of subcritical cracks can be accurately described by simple thermodynamics laws, such as an Arrhenius growth law. In this framework, the thermal agitation at the rupture tip allows to overcome the energy barriers that hold matter together. Thus, a rise in temperature at the tip can lead to an increase in the fracture velocity, as understood by statistical physics, and without requiring a phase change of the matrix or an overpressure of its pore fluids. In the present thesis, we study this possibility and propose an activation law in which the fracture induced heat is reintroduced. Such a heat is modeled by a standard Fourier diffusion law, and is proportional to the total energy release rate of the fracture. The hence described dynamics holds a positive feedback: the faster the crack, the hotter it is and the faster it becomes.

We then show that, from a specific mechanical load, which corresponds to a particular crack propagation velocity, this phenomenon can lead to so-called thermal avalanches. The facture shifts from a slow creep regime to a brutal, dynamical, one. Thus, we describe rupture as a first order phase transition, where the order parameter is the propagation velocity and where the external field is the mechanical load. This framework in particular explains the intermittent stick-slip propagation of cracks, which is typically observed in brittle rupture, but also explains the brittle-ductile transition of matter, corresponding to a critical point (second order transition) in our phase transition problem. Indeed, when a material is hot

enough. The thermal avalanches are inhibited as the temperature elevations become negligible compared to the thermal background, and the material is then ductile.

We then compare this model to some data sets from the literature, gathered during the rupture of two widely different polymers: polymethylmethacrylate (PMMA) and a pressure sensible adhesive (PSA), which is typical for the glue used to design standard roller tapes. We show that the dynamics of rupture of these two materials can be quantitatively reproduced by the model over more than six orders of magnitude of propagation velocities, using only physical parameters that are realistic. Thus, a high velocity fracturing can still be considered as subcritical (as understood by an Arrhenius law), but in an intense thermal bath.
We indeed infer from this model comparison to experimental data that, during the rupture of PMMA and PSA, the fracture fronts can reach thousands of degrees, on the length scale of a few atoms and during small time intervals. Although impressive, such high temperatures have long been theorized, and they thus explain the brittleness of matter. We, in particular, discuss how they are compatible with the fractoluminescence phenomenon, that is, the emission of visible light during rupture.

The experimental bench working is limited to a few polymers because only few studies report both the very slow and very fast velocities for given materials, mainly because measuring such a large range in the kinetics is challenging. However, slow creep has been characterized for many materials, from the weakest glasses to the toughest metals. We then compare these slow dynamics to our model features. We show that the intrinsic resistance of all solids is always comparable to a covalence energy, and that the actual macroscopic tenacity of matter derives only from the length scale around the crack tips over which heat is released. The bigger this length, the lesser the tip stress and the stronger the material. We also show that the model allows, when monitoring creep, to approximately predict the critical load at which fractures will evolve to a fast stage. Thermal dissipation is thus both the strength and the weakness of matter.

Of course, a slow enough crack may, in theory, never experience a thermal avalanche. In this case, one can neglect the fracture induced temperature elevations and approximate the tip temperature as constant. The model we present then allowed, in prior works, to successfully account for the mean dynamics of interfacial fronts in PMMA, with various loading conditions.
When the rupture interfaces hold some disorder in their tenacity, the fracture fronts become rugous, and their propagation becomes intermittent. By adding to the model an elastic redistribution of the stress along the fronts, we show that many features of this intermittency can be reproduced. Namely, the local propagation velocity distribution and correlation functions, the growth law and the fracture morphology. These matches confirm that a thermodynamics description of rupture is particularly relevant, even when the cracks are slow enough for any thermal induced effect to be negligible.
Finally, the velocity of a fracture likely derives from the interaction between the quenched disorder of the material where it propagates and the thermal disorder at its tip. The asperities of a solid can in particular help to trigger thermal avalanches.

In Earth sciences, accounting for the disorder along fault surfaces has gathered more and more interest, as it is suspected that this disorder plays an important role in the intermittency of earthquakes. The heterogeneity of friction along fault planes is often considered. However, the anisotropy of this friction, which arises from the anisotropy in the topography of the fault surfaces, is rarely studied. To characterize this frictional anisotropy, we present a novel experimental set-up, based on the 3D printing of actual

faults, whose topography was measured in the field. We show that an earthquake along a direction other than the main tectonic stress direction is possible, notably because of the frictional anisotropy.

Finally, and as an illustration that the main topic of this thesis, heat dissipation in rupture, has not yet revealed all of its secrets, we propose a new theory to explain the perception of mechanical pain by the human body. Indeed, when our biological tissues are damaged, the related elevations in temperatures are likely to be captured by our neural thermo-sensors. Thus, the feeling of mechanical pain could, in part, arise from some thermal measurements.

Abstract (*French / Français*)

Qu'est-ce qu'une fracture sinon du désordre ?

Lors de la rupture d'un milieu élastique fragile, une partie du chargement extérieur fourni à la matrice est dissipée dans une zone plastique en tête de fissure. L'entropie augmente. Cette dissipation irréversible, qui peut-être caractérisée par un taux de libération d'énergie macroscopiquement mesurable, s'appuie sur divers mécanismes physiques. En particulier : l'accroissement de la surface de la fissure ainsi que la nucléation de nouveaux défauts dans la matrice solide, l'émission d'ondes mécaniques et électromagnétiques propagées dans le milieu et amorties au loin et, enfin, l'élévation de la température induite par friction intermoléculaire, directement au sein de la zone plastique.

Cette élévation de température, que l'on peut par exemple observer en plaçant une caméra thermique devant une feuille de papier que l'on déchire, est souvent considérée comme un simple effet secondaire de la fracturation. Néanmoins, plus qu'un marqueur de l'endommagement, elle pourrait, en retour, avoir un impact significatif sur la dynamique de la rupture. La propagation de fractures peut, en effet, être décrite comme thermiquement activée, y compris lorsque les hétérogénéités du matériau dictent la forme d'un front d'endommagement et l'intermittence de son avancée. Pour comprendre la cinétique de rupture, il est donc primordial de s'intéresser au champ de température autour des fissures se propageant, et de réaliser un budget énergétique précis.

Cette question est bien sûr importante en science des matériaux et en ingénierie, pour la compréhension de la résistance des solides et des structures qui nous entourent au quotidien. Elle est aussi centrale en sciences de la Terre, où il est suspecté que l'instabilité de certaines failles est due à la chaleur induite par friction / fracturation. En particulier, la fonte et la dégradation localisée des plans de failles ou la pressurisation thermique de leurs fluides in situ peuvent amener à un adoucissement ('slip-weakening') et donc à des mouvements brusques des roches en présence.

Il est à noter que la propagation de fissures sous critiques, extrêmement lentes, a pu être précisément décrite par des lois simples de thermodynamique de type lois d'Arrhenius. Dans cette description, l'agitation thermique en pointe de rupture permet de vaincre les barrières énergétiques, atomistiques, qui soudent la matière. Ainsi une hausse de température en pointe de fissure peut entrainer une accélération de l'endommagement, au sens de la physique statistique, sans pour autant nécessiter un changement de phase dans la matrice ou une surpression du fluide interstitiel.
Dans cette thèse, nous étudions cette possibilité et proposons une loi d'activation dans laquelle l'élévation thermique en tête de rupture est réintroduite. Cette dernière est modélisée par une loi de diffusion de Fourier et est proportionnelle au taux de libération d'énergie total de la fracture. La dynamique ainsi décrite contient une boucle de rétroaction positive : plus une fracture progresse rapidement, plus sa pointe est chaude, et plus elle accélère.

Nous montrons alors que, à partir d'un chargement mécanique particulier, correspondant à une vitesse de propagation donnée, ce phénomène peut s'emballer et donner naissance à des avalanches, qualifiées plus loin de thermiques. La fracture passe d'un régime de fluage ('creep') très lent à un régime dynamique

brutal. Ainsi, nous décrivons la rupture comme une transition de phase du premier ordre, où le paramètre d'ordre est la vitesse de propagation et où le champ externe est le chargement mécanique. Cette description explique notamment la propagation saccadée ('stick-slip') typiquement observée dans la rupture fragile, mais aussi la transition fragile-ductile de la matière, qui correspond à un point critique (transition de second ordre) dans notre transition de phase. En effet, lorsqu'un matériau est porté à plus haute température ambiante, les effets thermiques induits par la rupture deviennent négligeables, et les avalanches thermiques disparaissent.

Nous comparons ensuite ce modèle avec des données de la littérature pour la rupture de deux polymères très différents : le polyméthacrylate de méthyle (PMMA) et un adhésif sensible à la pression (PSA), typique des colles utilisées dans les rouleaux adhésifs transparents. Nous montrons que les courbes de charges pour la rupture de ces deux matériaux peuvent être reproduites quantitativement par notre modèle sur plus de six ordres de grandeurs en vitesse, en utilisant uniquement des paramètres physiques d'ordres de magnitude réalistes. Ainsi, la rupture à grande vitesse de la matière peut toujours être considérée comme un phénomène sous-critique (décrit par une loi d'Arrhenius), dans un bain thermique intense.
Nous déduisons en effet de cette comparaison avec des données expérimentales que, lors de la rupture rapide de PMMA ou de PSA, les fronts de fissure peuvent atteindre des températures de plusieurs milliers de degrés, à l'échelle de quelques atomes et sur temps courts. Bien qu'impressionnantes, de telles températures ont depuis longtemps été théorisées. Elles permettent donc d'expliquer la rupture brutale de la matière, et nous discutons notamment de leur compatibilité avec le phénomène de fractoluminescence, c'est-à-dire l'émission de lumière dans le visible lors de la rupture.

Si les comparaisons expérimentales susmentionnées se limitent à quelques polymères, c'est que peu d'études rapportent, pour un même solide, à la fois les très basses et les très hautes vitesses de propagation, notamment du fait de la difficulté de les mesurer sur une si large gamme de vitesse. En revanche, la fracture lente de nombreux matériaux, des verres les plus fragiles aux métaux les plus tenaces, a été étudiée par le passé, et nous comparons dans cette thèse ces dynamiques lentes avec notre modèle. Nous montrons ainsi que la résistance intrinsèque de chaque matériau est toujours similaire, proche d'une barrière énergétique de covalence, et que la différence de ténacité entre, par exemple, une roche et un métal ne tient qu'à l'échelle spatiale autour des fronts à laquelle la dissipation thermique a lieu. Plus cette échelle est grande, plus la contrainte en pointe de rupture est limitée, et plus le matériau est résistant mécaniquement. Nous montrons aussi que le modèle permet, connaissant les courbes de chargement à basse vitesse, de prédire le chargement critique de rupture pour la plupart des matériaux. La dissipation thermique est donc à la fois la force et la faiblesse de la matière.

Bien sûr, une fracture, si elle est assez lente, peut ne jamais connaitre d'avalanche thermique. Dans ce cas, il est possible de négliger l'élévation thermique et de considérer que la température en pointe de rupture reste constante. Le modèle que nous présentons a alors permis, dans des travaux plus anciens ne prenant pas en compte la chauffe, de décrire avec succès l'avancée moyenne de fronts de fissure interfaciaux dans le PMMA, sous différents régimes de chargement.
Lorsque les interfaces de rupture présentent un certain désordre dans leur ténacité, les fronts deviennent rugueux et leur propagation intermittente. En ajoutant à notre modèle une redistribution élastique de la contrainte le long des fronts, nous montrons qu'il permet, additionnellement, de reproduire de nombreuses observables de cette intermittence. En particulier : les distributions et corrélations de vitesses locales le

long de la fracture, sa loi de croissance et sa rugosité. Ceci est une nouvelle confirmation qu'une description thermodynamique de la rupture est particulièrement adaptée, même lorsque les fronts sont assez lents pour que des effets thermiques induits soient négligeables.
Finalement, la vitesse d'une fracture résulte certainement, en grande partie, de l'interaction entre le désordre dans le matériau où elle progresse et le désordre thermique à sa pointe, et les aspérités d'un solide peuvent aider au déclenchement d'avalanches thermiques.

En sciences de la Terre, la description du désordre le long des surfaces de failles a attiré de plus en plus d'intérêt, étant suspecté que ce désordre joue un rôle important dans l'intermittence des séismes. L'hétérogénéité de la friction le long des plans de failles est souvent considérée. Pourtant, l'anisotropie de cette friction, découlant de l'anisotropie de la topographie des surfaces en présence, est rarement étudiée. Pour caractériser cette anisotropie, nous présentons un nouveau dispositif expérimental, fondé sur l'impression en 3D de surfaces de failles mesurées sur le terrain. Nous montrons qu'un glissement suivant une direction autre que la direction principale du chargement tectonique est possible, du fait de l'anisotropie de friction.

Finalement, et pour illustrer que l'objet principal de cette thèse, la dissipation thermique dans la rupture, est loin d'avoir divulgué tous ses secrets, nous proposons une nouvelle théorie sur la perception de la douleur mécanique par le corps humain. En effet, lorsque nos tissus biologiques sont endommagés, les élévations de température locale accompagnant probablement les dommages pourraient être détectées par nos capteurs thermiques neuronaux. La sensation de douleur mécanique pourrait donc, en partie, relever de mesures thermiques.

Table of contents

INTRODUCTION

Breaking into things and not breaking things

Most theses about the physics of rupture, which are published today, probably start by quoting the work of Alan A. Griffith and George R. Irwin, and the present document will not be an exception.
The somewhat military background of these works (both men were engineers of the twentieth century, respectively at the British Royal Aircraft Establishment and at the US Naval Research Laboratory) is not particularly surprising. I am a man lucky enough to be born in western Europe in the 1990s, so that war is, fortunately, not something I have much experience of. But war is often said to act as a catalyst for the advance of technical disciplines. More particularly, and by nature, its most martial component involves the propagation / prevention of fractures in fellow human bodies, or in whatever structure they might be defended with, so that it has often be the art of breaking things in the first place.
More positively, the physics of rupture has also been, from its very start, that of building stronger materials and structures: a constructive work rather than a work of destruction. In this context and, I admit, rather cheesily, I can only hope that writing this thesis will be welcomed as an interesting addition to the discipline of rupture physics. In any case, it has been for me a rewarding experience.

In the following introduction, I aim to provide you, dear reader, with a general scientific background for the understanding of this thesis, but also for how this thesis started in the first place.

On the temperature of cracks

The energy dissipation, as heat, which occurs at the tip of a moving crack inside a solid matrix, is a phenomenon well known by the rupture community. It was introduced as early as in the 1950s, to complete the earlier and seminal work by Griffith [1] (1921), on the strength of materials.
Griffith stated the importance of preexisting cracks and defaults on this strength, and experimentally showed that they were to progress if loaded beyond an intrinsic material threshold. Theoretically, this threshold was proposed to derive from the density in surface energy of materials γ, in $\mathrm{J\,m^{-2}}$, the energy needed to create a surface in a solid. As a crack holds two opposing surfaces, Griffith's threshold would then be written in the form:

$$G = 2\gamma, \tag{1}$$

where G is today referred to as the (critical) energy release rate. Here, no energy dissipation is at stake, and G, in this context, can roughly be estimated using the typical energy of molecular bonds U_c keeping matter together and to the typical size d_0 of these bonds:

$$2\gamma \sim \frac{U_c}{d_0^2}. \tag{2}$$

With U_c in the order of a few electronvolts and d_0 in that of a few ångströms (e.g., [2]), one can then predict G in the order of a few joules per square meter, which was in good agreement with Griffith's experiments on the rupture of glass. However, this values was far too low to describe the rupture of many other materials, notably that of the less brittle ones.
Thirty years later, Irwin [3] modified Griffith's criterion of rupture. The excess in energy needed to break through matter, when compared to 2γ, was traced back to the plasticity around moving crack tips, that many rupturing materials display. Such plasticity (i.e., an irreversible – inelastic – dissipation of the matrix potential energy as a fracture progresses) was not encompassed by the work of Griffith, which described the reversible balance between the solid elastic potential energy and the surface energy of its included cracks. The new theoretical framework for the resistance of matter, that is still massively considered today, was then of the form:

$$G = 2\gamma + G_{\mathrm{dissipation}}, \tag{3}$$

where $G_{\mathrm{dissipation}}$ accounts for all mechanical potential energy that is dissipated as a crack advances by a given unit of area.
Various phenomena are responsible for such an energy dissipation. One of them is the nucleation of dislocations and defaults in the plastic zone along the crack path, as it involves the creation of some additional surface energy, not quantifiable by measuring the apparent growth of the fracture. Another one, which has of course been of major

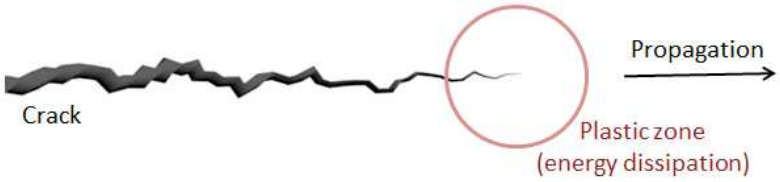

FIG. 1. Schematic of the plastic area at the tip of a moving crack. This zone, which may be complex, holds the energy dissipation $G_{\text{dissipation}}$.

interest to geophysicists in the understanding of earthquakes, is the emission of mechanical waves (e.g., [4]) that will propagate to the far field and progressively be damped by molecular friction. Note that such a friction is already to involve a distributed (and thus negligible) rise in temperature by Joule heating away from the crack. Closer to the tip, the strong matrix plasticity also likely involves the release of some heat, that is, of a disordered molecular motion, which was early identified as a likely significant part of the energy dissipation.
Because such heat release is now concentrated in a small volume around the tip, the subsequent temperature elevation might be important. Soon, very high figures of hundreds or thousands of degrees were either theorised, for instance by Rice and Levy [5] (1969), or measured, notably by Fuller et al. [6] (1975). Measuring the very local temperature of a crack tip is not a trivial thing to do and, in the case of the experiments by Fuller et al. [6] done on glassy polymers, the characterisation of thermoluminescence was used. We have here a fourth, electromagnetic, way for the dissipation of the potential energy of a fracturing matrix, which has been observed in various occasions, for instance in tape peeling [7, 8] and in the rupture of glass [9].

Towards significant thermal effects

Although potentially massive, the rise in temperature at the crack tip is, today, only rarely taken into consideration in describing the dynamics of cracks. Interestingly, however, it was early proposed as a likely cause for the brittleness of matter, by Marshall et al. [10] (1974). Indeed, if hot enough, it might well reduce the material elastic modulus (soften the matter) in the plastic zone, allowing for an easier molecular strain at the crack tip, and hence to a weakened material. The same principle was, more recently, advocated by Carbone and Persson [11] (2005).
Such an importance of thermal effects in rupture has also quickly become a topic in seismology, which explains why the current thesis took place, for the most part, at the 'Institut de Physique du Globe' of Strasbourg. Indeed, eroded fault planes sometimes display partly melted and recrystallised surfaces [12], which, along the thermo-pressurisation of their in situ fluids [13, 14] and the thermal degradation of the walls' minerals [15], could explain the instability of some faults.
A few years ago, as I was still a Master student in geosciences, I had the opportunity to co-author an article by Renaud Toussaint [16], who became the supervisor of the present thesis. By studying the energy budget of cracks progressing in paper sheets, with an infrared camera and numerical simulations of the temperature evolution around the crack fronts, it was concluded that the temperature of fast moving crack tips could reach that of the self-ignition of paper. Thus, fast rupture could be favoured by the thermal dissipation due to some potential microfiber combustion around the fracture fronts.
Here is again the idea that some rupture-induced thermal effects are prone to weaken matter, and this is the lead idea that will be defended in this thesis.

On the kinetics of rupture

One would have here noticed that I have started mentioning the velocity of cracks, and Toussaint et al. [16] (2016), in line with older publications (e.g., [5, 11, 17]), notably showed how the temperature elevation at a crack tip was proportional to the amount of dissipated energy (accounting, in the tearing of paper, to a non negligible 12% of it) but also, in part, to the front velocity. Thus, a minimum growth rate is required for a crack to be considered as hot.
Originally, brittle rupture was described as a rather binary phenomenon. When loaded, a crack could either resist or brutally propagate. In this early description, the actual velocity of the fractures was less important than the load threshold at which they would brutally progress. Yet, it was early acknowledged that this binary description was too limited, because slow cracks (or creeping cracks) could be observed in many materials, at velocities orders of magnitude less than that of a dynamical one. In practice, and in the Griffith's framework briefly introduced above,

it means that a material had to be characterised by a function of the fracture velocity V:

$$\begin{aligned} G &= G(V), \\ G &= 2\gamma + G_{\text{dissipation}}(V), \end{aligned} \tag{4}$$

rather than by a unique number G. The, priorly discussed, binary description of fracture arose from the non-monotonous character of this function, which holds a strong hysteresis (e.g., [10], or see Fig. 2) and two stable propagation phases: a very slow one (almost static for an overlooking observer), and a fast one, with rupture front speed in the order of a mechanical wave velocity [18]. Such a complex behaviour was not, however, completely understood. That is, it lacked a comprehensive reason for the dependence in velocity of $G(V)$. One suggestion by Maugis and Barquins [19] (1978) was to reinterpret the Griffith/Irwin criteria as:

$$G = 2\gamma \left[1 + \phi(T, V)\right], \tag{5}$$

where $\phi(T, V)$ is a function related to viscoelastic losses or internal friction at the crack tip, and T is the temperature. But one still needed to accurately model such a viscous friction.

The kinetics of creep

Other explanations were given to the slowest observed branch of $G(V)$, that is, to creeping cracks. One of them was stress corrosion, that is, the chemical degradation of the matrix in a given corrosive environment helped by a preexisting strain on its atomic structure. Various experimental works have shown that the kinetics of cracks is highly dependent on environmental factors such as temperature [20], the vapour pressure in air (e.g., [21]) or the pH (e.g., [22]). Due to the inherent chemical interactions in this description, thermodynamics naturally rose as a framework to describe the kinetics of cracks. In an Arrhenius-like framework:

$$V_{\text{creep}} = V_0 \exp\left[\frac{-E_{\text{corrosion}}(\sigma)}{k_B T}\right], \tag{6}$$

where V_0 is a nominal velocity, k_B is Boltzmann's constant and $E_{\text{corrosion}}$ is the activation energy for the corrosive reaction at the tip, which depends on the stress σ.
From the seminal work of Brenner [23] (1962), it was however early felt that, although definitely at stake in some instances, stress corrosion was not necessary to obtain slow cracks, as those could be observed in inert environments or in vacuum. It was proposed that, if rupture occurs when the stress acting on an atomic link is high enough to break this link, this process could then be thermally activated because thermal agitation translates into a fluctuation in stress (e.g., [24, 25]). Corrosion is thus not necessary for a crack to creep.

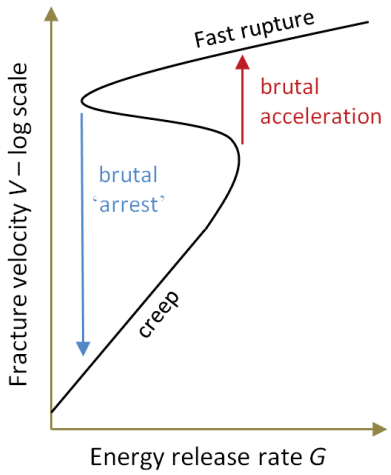

FIG. 2. Schematic of the energy release rate - velocity dependence. Notice the two propagation regimes and the hysteresis in between. The slow branch typically displays exponential trends, which has motivated Eq. (6) or (7).

Over the past decades, the team supervising this PhD, has run extensive experiments of creeping interfacial fractures propagating between sintered polymethylmethacrylate (PMMA) plates, that presented some disorder in fracture energy, introduced pre-sintering by a random sand blasting process. This experimental set-up allows to both monitor the average velocity of the hence rugous crack fronts and the intermittency of their dynamics. It was in particular shown by Lengliné et al. [26] (2011) that, in several loading scenarios, the creep velocity V of the crack was well represented by a, thermally activated, Arrhenius law and a scalar (velocity independent) fracture energy, intrinsic to the material. In addition, by taking into account the redistribution of stress along the rugous fronts, Cochard et al. [27] (2018) could also reproduce, with the same Arrhenius law, the fronts rugosity and the distribution of local propagation velocity. Part of the present thesis will bring further evidences that creep in disordered media can be explained by simple thermal activation.
The slowest rupture regime can thus be well described by stating that materials have a given energy barrier to be broken, denoted G_c, which is similar to the activation energy of a chemical reaction even when no stress corrosion is at stake. Under low mechanical load, this barrier can then be overcome by the molecular kinetics energy of the thermal bath. The higher the energy level at which the crack propagates ($G(V)$), the closer to the barrier G_c it already is, and the faster the propagation. The subsequent law has the form:

$$V_{\text{creep}} = V_0 \exp\left[\frac{-E(G_c, G)}{k_B T}\right], \tag{7}$$

where E is an activation energy depending on the intrinsic barrier G_c and the energy level G at which the crack already propagates.

The proposed reasons for fast rupture and the main topic of this thesis

If creep can thus be accurately modelled with a simple statistical physics law, a question still stands on the transition between the slow, likely thermally activated, crack propagation and the abrupt one.
The various thermal effects, which we have earlier discussed, have been considered as the lead suspects in this transition, being either a change in phase (softening) of the solid matrix [10, 11] or, in some materials, the onset of auto-induced combustion [16] (that is a form of brutal stress corrosion). The transition then occurs when the creep velocity is enough for the tip to be warm enough, so that either of these phenomena becomes significant. We here refer to such phenomena as 'thermal weakening' or 'thermal runaway'.
Another, non thermal, explanation was also proposed by Slepyan [28] (1981). The fast rupture is obtained by the emission of phonons, when the propagation velocity is high enough. In other words, high frequency mechanical waves disturbing the molecular links ahead of the front can be generated as the crack advances, and can maintain the rupture at a velocity in the order of that of the matrix Rayleigh waves.

In this thesis, we propose a novel model (introduced in chapter I) for the propagation of cracks and for thermal weakening, that encompasses both the creep regime and the dynamical rupture. Contrarily to the propositions presented above, we do not consider that a change in phase affects the matrix or that some environmental chemical reactions are necessary to explain either creep or thermal weakening. We rather consider that the velocity of crack is described by Eq. (7), where one needs to take into account the temperature elevation of running cracks to describe their fast velocity.
We show (in chapters II and III) that such a description allows a quantitative reproduction of the rupture at all velocities in many materials, and we additionally discuss its ability to describe creep in disordered interfaces (in chapter IV). Two side works are also included in this thesis: a study of how material disorder affects the frictional characteristic of faults (chapter V), and a discussion on the idea that thermal effects in rupture might be responsible for a sense of mechanical pain in the human body (chapter VI).

---

[1] A. Griffith. The Phenomena of Rupture and Flow in Solids. *Philosophical Transactions of the Royal Society of London A: Mathematical, Physical and Engineering Sciences*, 221(582-593):163–198, January 1921. ISSN 1471-2962. doi: 10.1098/rsta.1921.0006.
[2] G. B. Kaufman. Inorganic chemistry: principles of structure and reactivity, 4th ed. *Journal of Chemical Education*, 70 (10):A279, 1993. doi:10.1021/ed070pA279.1.
[3] G. R. Irwin. Analysis of stresses and strains near the end of a crack traversing a plate. *Journal of Applied Mechanics*, 24: 361–364, 1957.

[4] J. W. Morrissey and J. R. Rice. Crack front waves. *Journal of the Mechanics and Physics of Solids*, 46(3):467 – 487, 1998. ISSN 0022-5096. doi:10.1016/S0022-5096(97)00072-0.
[5] J. R. Rice and N. Levy. Local heating by plastic deformation at a crack tip. *Physics of Strength and Plasticity*, pages 277–293, 1969.
[6] K. N. G. Fuller, P. G. Fox, and J. E. Field. The temperature rise at the tip of fast-moving cracks in glassy polymers. *Proceedings of the Royal Society of London A: Mathematical, Physical and Engineering Sciences*, 341(1627):537–557, 1975. ISSN 0080-4630. doi:10.1098/rspa.1975.0007.
[7] M. Barquins and M. Ciccotti. On the kinetics of peeling of an adhesive tape under a constant imposed load. *International Journal of Adhesion and Adhesives*, 17(1):65 – 68, 1997. ISSN 0143-7496. doi:10.1016/S0143-7496(96)00020-6.
[8] C. Camara, J. Escobar, J. R. Hird, and S. J Putterman. Correlation between nanosecond x-ray flashes and stick–slip friction in peeling tape. *Nature*, 455:1089–92, 11 2008. doi:10.1038/nature07378.
[9] G. Pallares, C. L. Rountree, L. Douillard, F. Charra, and E. Bouchaud. Fractoluminescence characterization of the energy dissipated during fast fracture of glass. *Europhysics Letters*, 99(2):28003, 2012.
[10] G. P. Marshall, L. H. Coutts, and J. G. Williams. Temperature effects in the fracture of PMMA. *Journal of Materials Science*, 9(9):1409–1419, Sep 1974. ISSN 1573-4803. doi:10.1007/BF00552926.
[11] G. Carbone and B. N. J. Persson. Hot cracks in rubber: Origin of the giant toughness of rubberlike materials. *Phys. Rev. Lett.*, 95:114301, Sep 2005. doi:10.1103/PhysRevLett.95.114301.
[12] D. McKenzie and J. N. Brune. Melting on Fault Planes During Large Earthquakes. *Geophysical Journal International*, 29 (1):65–78, 08 1972. ISSN 0956-540X. doi:10.1111/j.1365-246X.1972.tb06152.x.
[13] H. Noda, E. M. Dunham, and J. R. Rice. Earthquake ruptures with thermal weakening and the operation of major faults at low overall stress levels. *Journal of Geophysical Research: Solid Earth*, 114(B7), 2009. doi:10.1029/2008JB006143.
[14] C. Wibberley and T. Shimamoto. Earthquake slip weakening and asperities explained by fluid pressurization. *Nature*, 436: 689–92, 09 2005.
[15] J. Sulem and V. Famin. Thermal decomposition of carbonates in fault zones: Slip-weakening and temperature-limiting effects. *Journal of Geophysical Research: Solid Earth*, 114(B3), 2009. doi:10.1029/2008JB006004.
[16] R. Toussaint, O. Lengliné, S. Santucci, T. Vincent-Dospital, M. Naert-Guillot, and K. J. Måløy. How cracks are hot and cool: a burning issue for paper. *Soft Matter*, 12:5563–5571, 2016. doi:10.1039/C6SM00615A.
[17] R. Weichert and K. Schönert. Heat generation at the tip of a moving crack. *Journal of the Mechanics and Physics of Solids*, 26(3):151 – 161, 1978. ISSN 0022-5096. doi:10.1016/0022-5096(78)90006-6.
[18] L. B. Freund. Crack propagation in an elastic solid subjected to general loading. *Journal of the Mechanics and Physics of Solids*, 20(3):129 – 152, 1972. ISSN 0022-5096. doi:10.1016/0022-5096(72)90006-3.
[19] D. Maugis and M. Barquins. Fracture mechanics and the adherence of viscoelastic bodies. *Journal of Physics D: Applied Physics*, 11(14):1989–2023, oct 1978. doi:10.1088/0022-3727/11/14/011.
[20] A. G. Atkins, C. S. Lee, and R. M. Caddell. Time-temperature dependent fracture toughness of PMMA. *Journal of Materials Science*, 10:1394–1404, 1975. ISSN 1573-4803. doi:10.1007/BF00540830.
[21] S. M. Wiederhorn. Influence of water vapor on crack propagation in soda-lime glass. *Journal of the American Ceramic Society*, 50(8):407–414, 1967. doi:10.1111/j.1151-2916.1967.tb15145.x.
[22] K. Sadananda and P. Shahinian. Effect of environment on crack growth behavior in austenitic stainless steels under creep and fatigue conditions. *Metallurgical Transactions A*, 11:267–276, 1980. doi:10.1007/BF02660631.
[23] S. S. Brenner. Mechanical behavior of sapphire whiskers at elevated temperatures. *Journal of Applied Physics*, 33(1): 33–39, 1962. doi:10.1063/1.1728523.
[24] S. Santucci, L. Vanel, and S. Ciliberto. Subcritical statistics in rupture of fibrous materials: Experiments and model. *Phys. Rev. Lett.*, 93:095505, Aug 2004. doi:10.1103/PhysRevLett.93.095505.
[25] L. Vanel, S. Ciliberto, P.-P. Cortet, and S. Santucci. Time-dependent rupture and slow crack growth: elastic and viscoplastic dynamics. *Journal of Physics D: Applied Physics*, 42(21):214007, oct 2009. doi:10.1088/0022-3727/42/21/214007.
[26] O. Lengliné, R. Toussaint, J. Schmittbuhl, J. E. Elkhoury, J. P. Ampuero, K. T. Tallakstad, S. Santucci, and K. J. Måløy. Average crack-front velocity during subcritical fracture propagation in a heterogeneous medium. *Phys. Rev. E*, 84:036104, Sep 2011. doi:10.1103/PhysRevE.84.036104.
[27] A. Cochard, O. Lengliné, K. J. Måløy, and R. Toussaint. Thermally activated crack fronts propagating in pinning disorder: simultaneous brittle/creep behavior depending on scale. *Philosophical Transactions of the Royal Society A : Mathematical, Physical and Engineering Sciences*, 2018. doi:10.1098/rsta.2017.0399.
[28] L.I. Slepyan. Dynamics of a crack in a lattice. *Soviet Physics, Doklady*, 26:538–540, 1981.

Chapter I

Thermal weakening of cracks and brittle-ductile transition: a phase model

---

Where we introduce our thermal model for the brittleness of matter

---

Published

Vincent-Dospital et al., Physical Review Materials 4, 023604, 2020, doi: PhysRevMaterials.4.023604

Résumé (*French abstract*):

L'adoucissement thermique des fissures et la transition fragile-ductile de la matière : un modèle de phase.

Nous présentons ici un modèle pour la propagation thermiquement activée de fissures dans des matrices élastiques. Cette propagation est supposée être un phénomène sous-critique, dont la cinétique est décrite par une loi d'Arrhenius. Dans cette loi, nous prenons en compte l'évolution thermique de la pointe de rupture, supposant qu'une partie de l'énergie mécanique dissipée au cours de l'endommagement se retrouve sous forme de chaleur dans une 'zone de process' plastique. Nous montrons qu'un tel modèle mène à une propagation de fissures avec deux phases : une première phase lente, dans laquelle l'élévation de température n'a que peu d'effet et où la rupture est surtout gouvernée par le chargement mécanique et la ténacité du matériau, et une seconde phase rapide, dans laquelle un adoucissement thermique cause des vitesses de propagation plus importantes. Une telle dualité dans la physique de la rupture peut expliquer la propagation typiquement saccadée de fissures en cas de rupture fragile, ce que nous illustrons avec des simulations numériques de fissures en mode I se propageant dans des milieux fins et désordonnés. En sus, nous prédisons l'existence d'une température ambiante limite au-dessus de laquelle tout adoucissement thermique est impossible. Nous proposons ce phénomène critique comme une nouvelle explication à la transition fragile-ductile de la matière solide.

Thermal weakening of cracks and brittle-ductile transition of matter: a phase model

Tom Vincent-Dospital,[1, 2, *] Renaud Toussaint,[1, 2, †] Alain Cochard,[1] Knut Jørgen Måløy,[2] and Eirik G. Flekkøy[2]

[1] *Université de Strasbourg, CNRS, IPGS UMR 7516, F-67000 Strasbourg, France*
[2] *SFF Porelab, The Njord Centre, Department of physics, University of Oslo P. O. Box 1048, Blindern, N-0316 Oslo, Norway*

We present a model for the thermally activated propagation of cracks in elastic matrices. The propagation is considered as a subcritical phenomenon, the kinetics of which being described by an Arrhenius law. In this law, we take the thermal evolution of the crack front into account, assuming that a portion of the released mechanical energy is transformed into heat in a zone surrounding the tip. We show that such a model leads to a two-phase crack propagation: a first phase at low velocity in which the temperature elevation is of little effect and the propagation is mainly governed by the mechanical load and by the toughness of the medium, and a second phase in which the crack is thermally weakened and propagates at greater velocity. Such a dual behavior can potentially explain the usual stick-slip in brittle fracturing, and we illustrate how with numerical simulations of mode I cracks propagating in thin disordered media. In addition, we predict the existence of a limiting ambient temperature above which the weakened phase ceases to exist and we propose this critical phenomenon as a novel explanation for the brittle-ductile transition of solids.

I. INTRODUCTION

Of paramount importance in engineering and geophysics, the impact of temperature in fracturing processes have since long been studied. It can simplistically be sorted into two categories: background effects where the temperature is treated as an environmental constant affecting the rates at which the defects of a medium are propagating or healing [1–4] and dynamic effects where the propagation of fractures self-induces a rise in temperature in the vicinity of the crack front [5–9]. In the latter case, the heat elevation can be regarded as more than a secondary effect of the medium's damage: it can be an active process back affecting the crack propagation. This phenomenon will be here referred to as "thermal weakening." Such a weakening has notably been studied in earth science where it is believed to play a role in faults stability and earthquake triggering [10, 11] and it was included in the so-called rate-and-state framework [12] as an explanation for rate weakening faults. Several mechanisms have been proposed to explain thermal weakening, such as the softening [13, 14] or melting of fracture surfaces or the thermo-pressurization of fault fluids [15–17]. We here consider a model which disregards such effects and focuses on the statistical physics consideration of higher reactions rates (i.e., quicker fracture propagation) at higher temperatures, as implied by an Arrhenius law [18]. This model notably showed good agreement with the rupture dynamics, experimentally reported in various polymers [19]. In this work, we further discuss how, in addition, it stands as a physical explanation for the brittle-ductile transition of matter.

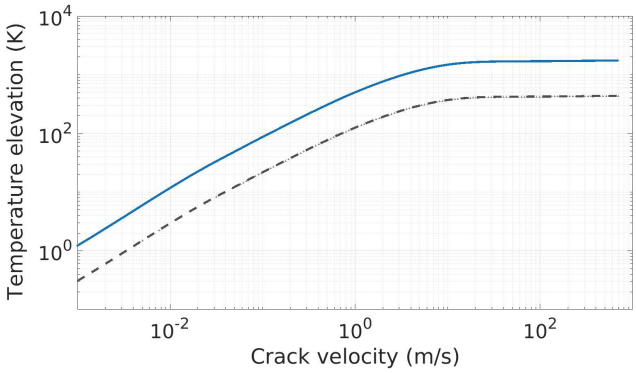

FIG. 1. Steady state values of the temperature elevation. It is obtained by solving Eq. (2) for a crack propagating at constant velocity and for $\phi G = 200\,\mathrm{J\,m^{-2}}$ (plain plot) and $\phi G = 50\,\mathrm{J\,m^{-2}}$ (dotted plot).

II. THE THERMAL WEAKENING MODEL

Arrhenius based models for the velocity of crack fronts have long been considered [1, 2, 4, 20] and have recently been shown to show good agreement with experimental observables of mode I cracks slowly propagating in acrylic glass bodies [21–23]. The rupture is then not considered as a Griffith-like threshold mechanism [24] where the crack only advances for $G > G_c$, where G is the energy release rate of the crack in J m^{-2} (arising from the mechanical load given to the crack front) and G_c the fracture energy of the medium (the energy barrier per surface unit to overcome molecular bonds). It is rather considered as a thermally activated subcritical phenomenon ($G < G_c$) for which the crack velocity is expressed as:

$$V = \alpha\nu\, \mathrm{e}^{\dfrac{\alpha^2(G - G_c)}{k_B T}} \tag{1}$$

* vincentdospitalt@unistra.fr
† renaud.toussaint@unistra.fr

where α is a characteristic size (m) of the fracturing process, that is associated with its energy barrier. $k_B \approx 1.38 \times 10^{-23}\,\mathrm{J\,K^{-1}}$ is the Boltzmann constant, T the absolute temperature at the crack tip and ν the thermal bath collisional frequency. Equation (1), as any Arrhenius law, is a continuous expression of a discrete process arising at the molecular scale. Cochard et al. [23] have recently discussed it at length. The exponential term is the probability (i.e. < 1) for the thermal agitation to exceed the activation energy $-\alpha^2(G-G_c)$ and hence for the crack to advance by a length α. This probability is challenged every $1/\nu$ seconds. In theory ν is also temperature dependent but this is of negligible effect compared to the exponential dependence of the probability term [18] and we hence define $V_0 = \alpha\nu$, the maximum crack velocity obtained when the activation energy is always reached. V_0 shall typically be in the range of the Rayleigh surface wave velocity [25]. Because we consider the thermal evolution around the crack tip we also note $T = T_0 + \Delta T$, where T_0 is the ambient temperature and ΔT any variation away from it at the tip.

Such variations are induced by the dissipation of the mechanical energy given to the elastic matrix in a plastic zone that surrounds the crack tip [26]. There are many processes responsible for such an energy loss, as the creation of new defects surfaces and the emission of mechanical waves, but we here focus on the release of heat. The model we use is based on the work of Toussaint et al. [9]: a portion ϕ of the energy release rate is dissipated on a cylindrical zone of radius l centered around the crack tip. Such a configuration leads to a thermal evolution governed by:

$$\frac{\partial(\Delta T)}{\partial t} = \frac{\lambda}{C}\nabla^2(\Delta T) + \frac{\phi G V}{C\pi l^2} f \tag{2}$$

which is a diffusion equation including a source term. λ is the medium's thermal conductivity in $\mathrm{J\,s^{-1}\,m^{-1}\,K^{-1}}$, C is the volumetric heat capacity in $\mathrm{J\,K^{-1}\,m^{-3}}$, t is the time variable and ∇^2 is the Laplace operator. f is the support function of the heat production zone of surface integral πl^2 (i.e., $f = 1$ in the zone and $f = 0$ otherwise). Solving this equation for a crack propagating at a constant velocity and constant release rate, one can show that the thermal elevation at the tip reaches a steady state after a short transient time. Figure 1 shows the evolution of this steady state as a function of V and for two values of G. See the supplemental material for details on its computation. In our model, we use this relation to describe $\Delta T(V, G)$, thus discarding any transient regime. Equation (1) becomes:

$$V = V_0\, \mathrm{e}^{\dfrac{\alpha^2(G-G_c)}{k_B[T_0 + \Delta T(V,G)]}}. \tag{3}$$

Parameters used for illustration

Note that most of the previously introduced parameters are strongly dependent on the medium in which the crack propagates. The figures we display here use parameters that could be likely for the propagation of interfacial cracks in sintered acrylic glass bodies [21, 22] and are discussed in the supplemental material: $\alpha = 2.5 \times 10^{-11}\,\mathrm{m}$, $G_c = 250\,\mathrm{J\,m^{-2}}$, $T_0 = 293\,\mathrm{K}$, $C = 1.7 \times 10^6\,\mathrm{J\,K^{-1}\,m^{-3}}$, $\lambda = 0.19\,\mathrm{J\,s^{-1}\,m^{-1}\,K^{-1}}$, $V_0 = 1000\,\mathrm{m\,s^{-1}}$, $l = 20\,\mathrm{nm}$ and $\phi = 1$. Note that we use this set of values only to propose some likely orders of magnitude for our parameters, and not to accurately represent the rupture of a specific material, as done in [19].

III. PHASE BEHAVIOR

Equation (3) defines, for a given load G, a function S_G such as: $V = S_G(V)$. To fit the model, the actual velocity at which a crack advances must be a solution of this equation (i.e., be a fixed point for the function S_G) [27]. Figure 2 illustrates that, depending on the value of G, S_G has one to three fixed points: three possible values for the crack velocity. This finite number of solutions arises from the steady-state approximation. If we were to consider the transient regimes, $S_G(V)$ would be, for a front propagating at any velocity V and load G, a target velocity. Any crack not having reached a steady state would thus accelerate or slow down to follow this function. The intermediate fixed point, when it exists, is then unstable (virtually impossible): a crack with a velocity value just above this point ($V < S_G(V)$) is too slow to be steady. The heat generation at the tip is higher than what the diffusion can accommodate, the temperature

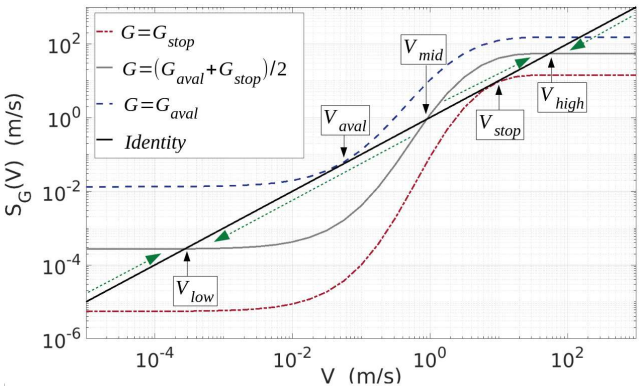

FIG. 2. Representation of $V = S_G(V)$ for three values of G: G_{stop}, G_{aval} ($> G_{\mathrm{stop}}$) and the mid-value between G_{stop} and G_{aval}. The intersections of S_G with the identity plot (straight line) give the possible crack velocities. They are denoted V_{low}, V_{mid} and V_{high} and are emphasized for the intermediate G-plot. V_{aval} and V_{stop} are indicated on the two others plots. The dashed arrows indicate how off-balanced situations evolve to a stable fixed point.

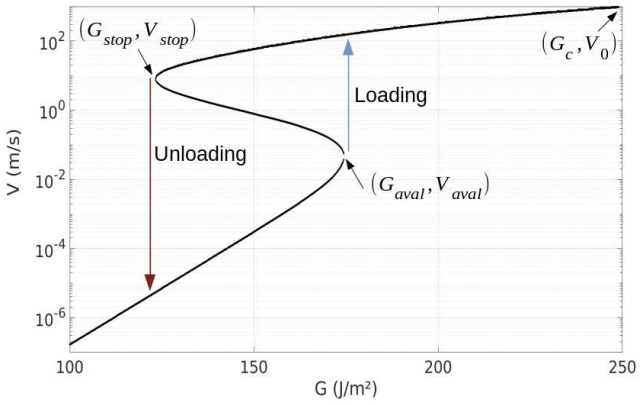

FIG. 3. Solutions for the crack velocity as a function of G for $T_0 = 293\,\mathrm{K}$. All solutions in between V_{stop} and V_{aval} are unstable, any other point is a possible crack velocity. The arrows represent how a crack avalanches of slows down at the phase transition thresholds.

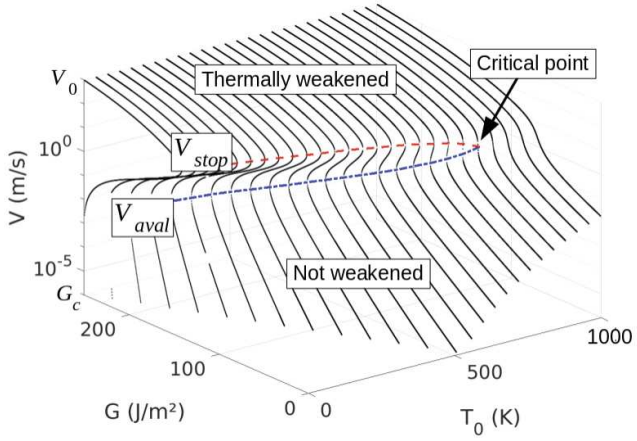

FIG. 4. Solutions for the crack velocity as a function of G and for various T_0. The dashed lines show the $(V_{\mathrm{stop}}, G_{\mathrm{stop}})$ and $(V_{\mathrm{aval}}, G_{\mathrm{aval}})$ couples and converge to the critical point.

rises and the velocity increases to converge to the upper fixed point. On the contrary, if a crack is slightly slower than the intermediate solution ($V > S_G(V)$), the crack cools down to the lower fixed point. We here assume that such transitions happen in a negligible time so the steady velocities are sufficient to describe the main dynamics. The outer solutions of (3) being the only stable ones, the model displays a two-phase behavior. The lower velocity marks a slow phase. The temperature elevation at the crack tip has little effect on the propagation, as $\Delta T(V, G) \ll T_0$. The higher solution corresponds to a thermally weakened phase where $\Delta T(V, G)$ has reached the plateau temperature of Fig. 1. The velocity is there increased as the induced heat is potentially significant compared to the thermal background.

Notice in Fig. 2 that there are two particular values of the load G for which either the lower or the higher phase ceases to exist. We denote them G_{aval} and G_{stop} (with $G_{\mathrm{aval}} > G_{\mathrm{stop}}$) as they correspond to mechanical loads at which a slow crack will have to avalanche to the thermally weakened phase or at which a fast (weakened) crack can only cool down to the slow phase. For G in between these two thresholds, a hysteresis situation holds, there are several solutions for V and the crack might or might not be thermally weakened, depending on the mechanical history. To G_{aval} and G_{stop} correspond some specific velocities $V_{\mathrm{aval}} < V_{\mathrm{stop}}$ in between which a crack cannot propagate, as any solution is there unstable. Figure 3 shows the possible crack velocities for various values of G. One can notice how similar it is to a first order phase transition [28] for the order parameter V associated to avalanches (jumps in V) triggered by variations in the driving field G at temperature T_0. Such a description compares interestingly with various (V, G) branches that are experimentally reported, for instance in the rupture dynamics of pressure adhesives [29, 30], PMMA [21, 31] or elastomers [32] and the model can hence be matched to actual data over decades of velocities [19]. Note that, in the hysteresis domain, we do not discriminate on the relative stability of each phase. One can however argue, by analogy with other phase transition systems [28], that one of the two solutions could only be metastable, that is, in an equilibrium which is less energetically favorable than the one of the alternative phase. In this case, when traveling though an heterogeneous medium where the variations in fracture energy are enough to get shifts from only one state to the other, one of the phase could still be preferential for the crack propagation.

IV. CRITICAL POINT

Besides G, T_0 is the only other parameter of (3) which is not dependent on the medium's properties. Figure 4 thus shows the predicted propagation velocities for various ambient temperatures. Notice the existence of a critical ambient temperature: T_0^*, at which $G_{\mathrm{aval}} = G_{\mathrm{stop}} = G^*$ and $V = V^*$. Beyond T_0^*, the Joule effect cannot overcome the thermal background enough for the crack to be weakened. Increasing the load then only leads to a smooth increase in the velocity. To relate to the theory of critical phenomena in phase transitions [28] we looked for the real numbers β, δ and γ such that:

$$\frac{V - V^*}{V^*} \sim \left(\frac{T_0 - T_0^*}{T_0^*}\right)^{\beta}_{G=G^*} \tag{4}$$

$$\frac{G - G^*}{G^*} \sim \left(\frac{V - V^*}{V^*}\right)^{\delta}_{T_0=T_0^*} \tag{5}$$

$$\frac{G^*}{V^*}\frac{\partial V}{\partial G} \sim \left(\frac{T_0 - T_0^*}{T_0^*}\right)^{-\gamma}_{G=G^*} \tag{6}$$

where $\sim$ stands for a mathematical equivalence in the vicinity of the critical point (any pre-factor is overlooked). These exponents describe how V converges towards V^* beyond the critical point ($T_0 \geq T_0^*$). We also characterized how the hysteresis domain shrinks, looking for β', δ' and γ' such that:

$$\frac{V_{\text{stop}} - V_{\text{aval}}}{V^*} \sim \left(\frac{T_0^* - T_0}{T_0^*}\right)^{\beta'} \tag{7}$$

$$\frac{G_{\text{aval}} - G_{\text{stop}}}{G^*} \sim \left(\frac{V_{\text{stop}} - V_{\text{aval}}}{V^*}\right)^{\delta'} \tag{8}$$

$$\frac{G^*}{V^*}\frac{V_{\text{stop}} - V_{\text{aval}}}{G_{\text{aval}} - G_{\text{stop}}} \sim \left(\frac{T_0^* - T_0}{T_0^*}\right)^{-\gamma'}. \tag{9}$$

With a bisection, we numerically estimated the critical point, checking for the number of solutions of $V = S_G(V)$ (three solutions below T_0^* and one above). Analyzing the shape of the velocity map in the derived vicinity we found: $\beta \approx 1/3$, $\delta \approx 3$, $\gamma \approx 2/3$, and $\beta' \approx 1/2$, $\delta' \approx 3$, $\gamma' \approx 1$ (see the supplemental material). Both sets of exponents respect the scaling relation [28]: $2\beta + \gamma = \beta(\delta + 1)$. We hence derived critical exponents which are, along the phase co-existence domain, the same as the mean field exponents for, say, the liquid-gas transition [28], but different beyond the critical point. The mean field characteristic might arise from the statistical nature of the Arrhenius law only representing an average velocity while consecutive molecular bonds can be overcome at very different speeds. Another interpretation is that it translates the zero-dimensional character of our model. We have indeed disregarded any velocity variations and elastic interactions along the crack front, making the assumption that it is thin or symmetrical enough perpendicularly to the propagation direction.

V. SIMULATIONS OF 0D FRONTS IN DISORDERED MEDIA

Let us finally illustrate the phase transitions with some simulations of such zero-dimensional fronts loaded in mode I. The loading geometry that we consider is shown in Fig. 5. The support body consists in two sintered elastic plates which are progressively separated at the edge. The deflection on the side, $u(t)$ (in m), is increased linearly with time: $u(t) = v_u t$. Using the Euler–Bernoulli beam theory [33], one can compute the energy release rate at the tip of such a system:

$$G(t) = \frac{3Eh^3 {v_u}^2 t^2}{8a(t)^4} \quad \text{if } a \gg h, \tag{10}$$

with E the body Young modulus (in Pa), h half of its thickness and a the crack advancement such as: $V = \partial a/\partial t$. By inserting (10) in (3), we obtain the differential equation in $a(t)$ that governs the crack progression and that we solved with a time step adaptive Runge-Kutta algorithm [34]. We here consider a crack interface with a homogeneous background cohesion $G_c = G_{c_b}$ which is only disturbed by a single tough asperity of length L_a ($G_{c_a} > G_{c_b}$). Figure 5 shows a schematic for this anomaly while Fig. 6 shows, for several values of G_{c_a}, the course of the crack over it and the corresponding evolution of the energy release rate. When the front reaches the asperity, the crack velocity dramatically decreases as it reaches a tougher area. Meanwhile the load G increases because the far field deflection continues to build

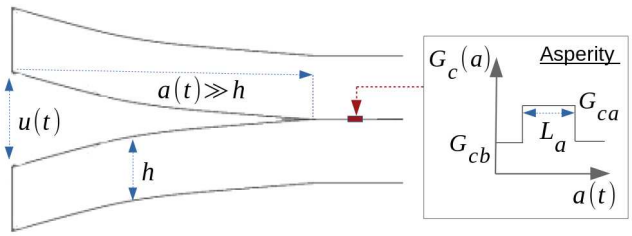

FIG. 5. Geometry for the numerical simulations of zero-dimensional crack fronts overcoming a tough asperity.

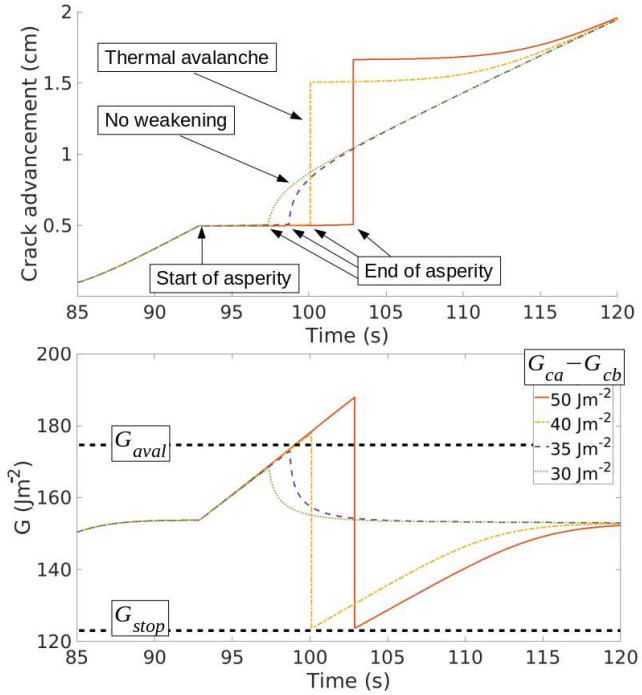

FIG. 6. Numerical simulations for a crack overcoming an asperity as defined by the differential equation from (3) and (10) and for various G_{c_a}. $L_a = 100\,\mu$m, $v_u = 120\,\mu$m s^{-1}, $h = 5$ mm and $E = 3.2$ GPa. The top plot is the crack advancement $a(t)$, the bottom one is the energy release rate $G(t)$. Thermal weakening is or is not triggered depending on the anomaly strength.

up on a now quasi-static crack. Once the anomaly finally gets passed, the simulations show two possible scenarios. If $G_{\text{aval}}(G_{c_b})$ (i.e., the phase shift threshold for the background G_{c_b}) was not reached over the anomaly, then the crack only accelerates back to its pre-asperity state. However, if $G_{\text{aval}}(G_{c_b})$ was overcome, the crack shifts phase and becomes thermally weakened: it avalanches until $G = G_{\text{stop}}$. In Fig. 6, one can read the values of G_{aval} and G_{stop} and remark that they match the theoretical values displayed in Fig. 3. Note that, if the load was to be quickly increased, an avalanche could be triggered without the need for any asperity. We showed, however, how the medium's disorder can lead to some spontaneous thermal weakening of the crack course.

VI. DISCUSSION AND CONCLUSION

By combining an Arrhenius law and the heat equation, we have thus demonstrated the possibility of a thermally activated dynamic phase transition in the propagation of cracks. This phase description may have major implications for the understanding of fracture dynamics. With a rather simple subcritical model, we indeed explain both slow creep regimes and fast ruptures. We do not however strictly disregard over-critical propagations, as $G > G_c$ only implies that the Arrhenius activation energy is null and hence always exceeded. In this case, we predict $V \sim V_0$. Note that at such high velocities, crack fronts tend to complexify [35, 36], and our model might not hold as such, as it only considers single fronts. We derive a tip temperature approaching the 10^4 K range. Although it is high, some experimental characterisations of triboluminescense [7, 8] have shown that fast cracks can reach such a temperature, which only stands on small volumes ($\sim l^2 L$, where L is the length of the front) and short time periods ($\sim l/V$) such that it does not imply a gigantic level of energy nor it necessary leads to local fusion or sublimation of the solid. Note that the temperature merely measures the amplitude of the atoms agitation, and that its statistical definition actually suffers for heat production zones smaller than the molecular scale. While atomic scale simulations [37] would be more appropriate to study the induced heat, such computationally demanding models are often run at given (fixed) temperatures. Yet, some occurrences [38, 39] derive a non negligible induced heat. Besides describing the two phases, we explained the potential shifts from one to the other and point out here how compatible this is with Maugis' reinterpretation [40] of the Griffith criteria [24] and so, with the usual stick-slip in brittle fracturing processes [20, 29], when avalanches get considerably larger than the scales of the in situ quenched disorder. We also showed that above a critical ambient temperature, T_0^*, this phenomenon cannot occur. For materials where T_0^* is lower than the melting point at a given confining pressure, a same solid then displays a different behavior under cool or hot conditions: fragile when cold, but smoother/ductile when warm, as thermal avalanches are inhibited. The model thus could stand as a novel and physical explanation for the fragile-ductile transition of matter. Of course, it might be oversimplifying that to assume that all our parameters stay constant when varying T_0. The general physical principles however remain valid. Previous theories [41–43] actually support the importance of the crack-tip plasticity in the fragile-ductile transition, but rather relate it to the nucleation and mobility of dislocations ahead of the front. Such processes are compatible with induced thermal elevation [38], but are not directly captured by our mesoscopic description of the heat production zone.

Finally, and although we presented a mode I model, we suggest that some analogy is to be made with the frictional effects induced in mode II and mode III fracturing. Notably, as frictional heating is believed to be a cause for the instability of some seismic faults, a potential earthquake triggered when overcoming a strong fault plane asperity might indeed be amplified due to thermal weakening. The existence of the critical point would then explain the disappearance of such amplifications at higher depth (i.e., where rocks are in ductile conditions [44]) as the thermal background is there enough to make the frictional heating negligible and, hence, favors creep over brittle ruptures.

ACKNOWLEDGEMENTS AND CONTRIBUTIONS

T.V.-D. developed and analyzed the model and the simulations, and redacted the first versions of the manuscript. R.T. proposed the physical basis of the model and its mathematical formulation. A.C. set the basis for the numerical implementation of the model and the principles of the resolution algorithm. K.J.M. contributed in the interpretation of the model in fracture mechanics applications. E.G.F. contributed to analyze the model in terms of critical point characteristics. All authors participated to the redaction of the manuscript and agreed with the submitted version. The authors declare no competing financial interests in the publishing of this work and acknowledge the support of the IRP France-Norway D-FFRACT, of the Universities of Strasbourg and Oslo and of the CNRS INSU ALEAS program. Readers are welcome to comment and should address to vincentdospitalt@unistra.fr or renaud.toussaint@unistra.fr. See the Supplemental Material at [URL] for a discussion on the parameters we used, details on how to compute the temperature elevation at the crack tip and decades on which we fitted the critical exponents.

[1] S. S. Brenner. Mechanical behavior of sapphire whiskers at elevated temperatures. *Journal of Applied Physics*, 33 (1):33–39, 1962. doi:10.1063/1.1728523.

[2] S. N. Zhurkov. Kinetic concept of the strength of solids. *International Journal of Fracture*, 26(4):295–307, Dec 1984. ISSN 1573-2673. doi:10.1007/BF00962961.

[3] N. Brantut, M. J. Heap, P. G. Meredith, and P. Baud. Time-dependent cracking and brittle creep in crustal rocks: A review. *Journal of Structural Geology*, 52:17 – 43, 2013. ISSN 0191-8141. doi:10.1016/j.jsg.2013.03.007.

[4] B. Lawn. *Fracture of Brittle Solids*. Cambridge Solid State Science Series. Cambridge University Press, 2 edition, 1993. doi:10.1017/CBO9780511623127.

[5] J. R. Rice and N. Levy. Local heating by plastic deformation at a crack tip. *Physics of Strength and Plasticity*, pages 277–293, 1969.

[6] K. N. G. Fuller, P. G. Fox, and J. E. Field. The temperature rise at the tip of fast-moving cracks in glassy polymers. *Proceedings of the Royal Society of London A: Mathematical, Physical and Engineering Sciences*, 341(1627):537–557, 1975. ISSN 0080-4630. doi:10.1098/rspa.1975.0007.

[7] G. N. Chapman and A. J. Walton. Triboluminescence of glasses and quartz. *Journal of Applied Physics*, 54(10): 5961–5965, 1983. doi:10.1063/1.331773.

[8] G. Pallares, C. L. Rountree, L. Douillard, F. Charra, and E. Bouchaud. Fractoluminescence characterization of the energy dissipated during fast fracture of glass. *Europhysics Letters*, 99(2):28003, 2012.

[9] R. Toussaint, O. Lengliné, S. Santucci, T. Vincent-Dospital, M. Naert-Guillot, and K. J. Måløy. How cracks are hot and cool: a burning issue for paper. *Soft Matter*, 12:5563–5571, 2016. doi:10.1039/C6SM00615A.

[10] S. Braeck and Y. Y. Podladchikov. Spontaneous thermal runaway as an ultimate failure mechanism of materials. *Phys. Rev. Lett.*, 98:095504, Mar 2007. doi: 10.1103/PhysRevLett.98.095504.

[11] J. R. Rice. Heating and weakening of faults during earthquake slip. *Journal of Geophysical Research: Solid Earth*, 111(B5), 2006. doi:10.1029/2005JB004006.

[12] H. Noda, E. M. Dunham, and J. R. Rice. Earthquake ruptures with thermal weakening and the operation of major faults at low overall stress levels. *Journal of Geophysical Research: Solid Earth*, 114(B7), 2009. doi: 10.1029/2008JB006143.

[13] G. P. Marshall, L. H. Coutts, and J. G. Williams. Temperature effects in the fracture of PMMA. *Journal of Materials Science*, 9(9):1409–1419, Sep 1974. ISSN 1573-4803. doi:10.1007/BF00552926.

[14] G. Carbone and B. N. J. Persson. Hot cracks in rubber: Origin of the giant toughness of rubberlike materials. *Phys. Rev. Lett.*, 95:114301, Sep 2005. doi: 10.1103/PhysRevLett.95.114301.

[15] A. W. Rempel and J. R. Rice. Thermal pressurization and onset of melting in fault zones. *Journal of Geophysical Research: Solid Earth*, 111(B9), 2006. doi: 10.1029/2006JB004314.

[16] C. Wibberley and T. Shimamoto. Earthquake slip weakening and asperities explained by fluid pressurization. *Nature*, 436:689–92, 09 2005.

[17] J. Sulem and V. Famin. Thermal decomposition of carbonates in fault zones: Slip-weakening and temperature-limiting effects. *Journal of Geophysical Research: Solid Earth*, 114(B3), 2009. doi:10.1029/2008JB006004.

[18] G. G. Hammes. *Principles of Chemical Kinetics*. Academic Press, 1978.

[19] T. Vincent-Dospital, R. Toussaint, S. Santucci, L. Vanel, D. Bonamy, L. Hattali, A. Cochard, K. J. Måløy, and E. G. Flekkøy. How heat controls fracture. preprint, 2019. URL https://arxiv.org/pdf/1905.07180.pdf.

[20] S. Santucci, L. Vanel, and S. Ciliberto. Subcritical statistics in rupture of fibrous materials: Experiments and model. *Phys. Rev. Lett.*, 93:095505, Aug 2004. doi: 10.1103/PhysRevLett.93.095505.

[21] O. Lengliné, R. Toussaint, J. Schmittbuhl, J. E. Elkhoury, J. P. Ampuero, K. T. Tallakstad, S. Santucci, and K. J. Måløy. Average crack-front velocity during subcritical fracture propagation in a heterogeneous medium. *Phys. Rev. E*, 84:036104, Sep 2011. doi: 10.1103/PhysRevE.84.036104.

[22] K. T. Tallakstad, R. Toussaint, S. Santucci, J. Schmittbuhl, and K. J. Måløy. Local dynamics of a randomly pinned crack front during creep and forced propagation: An experimental study. *Phys. Rev. E*, 83:046108, 04 2011.

[23] A. Cochard, O. Lengliné, K. J. Måløy, and R. Toussaint. Thermally activated crack fronts propagating in pinning disorder: simultaneous brittle/creep behavior depending on scale. *Philosophical Transactions of the Royal Society A : Mathematical, Physical and Engineering Sciences*, 2018. doi:10.1098/rsta.2017.0399.

[24] A. Griffith. The Phenomena of Rupture and Flow in Solids. *Philosophical Transactions of the Royal Society of London A: Mathematical, Physical and Engineering Sciences*, 221(582-593):163–198, January 1921. ISSN 1471-2962. doi:10.1098/rsta.1921.0006.

[25] L. B. Freund. Crack propagation in an elastic solid subjected to general loading. *Journal of the Mechanics and Physics of Solids*, 20(3):129 – 152, 1972. ISSN 0022-5096. doi:10.1016/0022-5096(72)90006-3.

[26] G. R. Irwin. Analysis of stresses and strains near the end of a crack traversing a plate. *Journal of Applied Mechanics*, 24:361–364, 1957.

[27] D. K. Arrowsmith and C. M. Place. *An introduction to dynamical systems*. Cambridge University Press, 1990.

[28] H. B. Callen. *Thermodynamics and an introduction to thermostatistics; 2nd ed.* Wiley, 1985.

[29] M.-J. Dalbe, S. Santucci, P.-P. Cortet, and L. Vanel. Strong dynamical effects during stick-slip adhesive peeling. *Soft Matter*, 10:132–138, 2014. doi: 10.1039/C3SM51918J.

[30] M. Barquins and M. Ciccotti. On the kinetics of peeling of an adhesive tape under a constant imposed load. *International Journal of Adhesion and Adhesives*, 17(1): 65 – 68, 1997. ISSN 0143-7496. doi:10.1016/S0143-7496(96)00020-6.

[31] M.L. Hattali, J. Barés, L. Ponson, and D. Bonamy. Low velocity surface fracture patterns in brittle material: A newly evidenced mechanical instability. In *THERMEC 2011*, volume 706 of *Materials Science Forum*, pages 920–924. Trans Tech Publications Ltd, 1 2012. doi: 10.4028/www.scientific.net/MSF.706-709.920.

[32] Y. Morishita, K. Tsunoda, and K. Urayama. Velocity transition in the crack growth dynamics of filled elastomers: Contributions of nonlinear viscoelasticity. *Phys. Rev. E*, 93:043001, Apr 2016. doi: 10.1103/PhysRevE.93.043001.

[33] T. L. Anderson. *Fracture Mechanics: Fundamentals and Applications*. Taylor and Francis, 2005.

[34] J. R. Dormand and P. J. Prince. A family of embedded Runge-Kutta formulae. *Journal of Computational and Applied Mathematics*, 6(1):19 – 26, 1980. ISSN 0377-0427. doi:10.1016/0771-050X(80)90013-3.

[35] K. Ravi-Chandar and B. Yang. On the role of microcracks in the dynamic fracture of brittle materials. *Journal of the Mechanics and Physics of Solids*, 45(4):535–563, apr 1997. doi:10.1016/s0022-5096(96)00096-8.

[36] J. Fineberg, S. P. Gross, M. Marder, and H. L. Swinney. Instability in dynamic fracture. *Phycal Review Letter*, 67: 457–460, Jul 1991. doi:10.1103/PhysRevLett.67.457.

[37] C. L. Rountree, Rajiv K. K., E. Lidorikis, A. Nakano, L. Van Brutzel, and P. Vashishta. Atomistic aspects of crack propagation in brittle materials: Multimillion atom molecular dynamics simulations. *Annual Review of Materials Research*, 32(1):377–400, 2002. doi: 10.1146/annurev.matsci.32.111201.142017.

[38] T. C. Germann, B. L. Holian, P. S. Lomdahl, D. Tanguy, M. Mareschal, and R. Ravelo. Dislocation structure behind a shock front in fcc perfect crystals: Atomistic simulation results. *Metallurgical and Materials Transactions A*, 35(9):2609–2615, Sep 2004. ISSN 1543-1940. doi:10.1007/s11661-004-0206-5.

[39] P. R. Budarapu, B. Javvaji, V. K. Sutrakar, D. Roy Mahapatra, G. Zi, and T. Rabczuk. Crack propagation in graphene. *Journal of Applied Physics*, 118(6):064307, 2015. doi:10.1063/1.4928316.

[40] D. Maugis. Subcritical crack growth, surface energy, fracture toughness, stick-slip and embrittlement. *Journal of Materials Science*, 20(9):3041–3073, Sep 1985. ISSN 1573-4803.

[41] P. B. Hirsch, S. G. Roberts, and J. Samuels. The brittle-ductile transition in silicon. *Proceedings of the Royal Society of London. A. Mathematical and Physical Sciences*, 421(1860):25–53, 1989. doi:10.1098/rspa.1989.0002.

[42] D. Tanguy. Constrained molecular dynamics for quantifying intrinsic ductility versus brittleness. *Phys. Rev. B*, 76:144115, Oct 2007. doi:10.1103/PhysRevB.76.144115.

[43] A. Hartmaier and P. Gumbsch. Thermal activation of crack-tip plasticity: The brittle or ductile response of a stationary crack loaded to failure. *Phys. Rev. B*, 71: 024108, Jan 2005. doi:10.1103/PhysRevB.71.024108.

[44] C. H. Scholz. The brittle-plastic transition and the depth of seismic faulting. *Geologische Rundschau*, 77(1):319–328, Feb 1988. ISSN 1432-1149. doi: 10.1007/BF01848693.

Thermal weakening of cracks and brittle-ductile transition of matter: a phase model

SUPPLEMENTAL MATERIAL

Tom Vincent-Dospital,[1, 2, *] Renaud Toussaint,[1, 2] Alain Cochard,[1] Knut Jørgen Måløy,[2] and Eirik G. Flekkøy[2]

[1] *Université de Strasbourg, CNRS, IPGS UMR 7516, F-67000 Strasbourg, France*
[2] *SFF Porelab, The Njord Centre, Department of physics, University of Oslo P. O. Box 1048, Blindern, N-0316 Oslo, Norway*

In this supplemental material, we explain the parameters that we used for illustration in the main manuscript. We also provide analytical approximations for the temperature elevation at the crack tip and details how the critical exponents were derived. Although it is not essential to the core comprehension of our letter, we do refer to it. Therefore, for an easier understanding of the present material, we invite the reader to keep an eye onto the main manuscript, which references are marked with a 'M'. For instance: Eq. (M1).

CHOSEN PARAMETERS (FOR ILLUSTRATION)

Most of the parameters that we introduced in our model are strongly dependent on the medium in which the crack propagates. The chosen ones, for the figures of the main manuscript, use values we believe to be likely for the propagation of interfacial cracks in sintered polymethyl methacrylate (PMMA) bodies [1, 2]. Lengliné et al. [1] have derived the main parameters of the Arrhenius law with experiments done at room temperature and for slow crack growth such that it is unlikely that a significant heat was released at the crack tip. In this experiments, V was indeed reported to increase exponentially with G, meaning that $\Delta T(V, G)$ is negligible in Eq. (M3). They found $\alpha \sim 2.5 \times 10^{-11}\,\mathrm{m}$ which is surprisingly less than the typical size of molecular bonds, one Ångström. It was proposed [1], as a possible explanation, that it is a consequences of the off-plane processes in the advance of a crack (a number of off-plane bonds have to be broken for the planar interface to advance by a projected length α). Alternatively, it could be the translation that that only a part of the mechanical energy is consumed in breaking bonds [3]. A nominal velocity $V_0 \times \exp[-\alpha^2 G_c/(k_B T_0)]$ was also measured, although the contributions of V_0 and G_c were not individually resolved. We however used $V_0 = 1000\,\mathrm{m\,s^{-1}}$, of the order of magnitude of the Rayleigh wave velocity [4] ($\approx 1280\,\mathrm{m\,s^{-1}}$ in Plexiglas [5]). This leads to $G_c = 250\,\mathrm{J\,m^{-2}}$. Note that to relate to the probabilistic molecular description of the Arrhenius law, one could also consider V_0 as the average molecular velocity from the kinetics theory [6]. If we approximate it as for unimolecular gas, $V_0 \sim \sqrt{8 k_B T_0/(\pi m)}$ where m is the mass of a molecule), it ranges from 100 to $1000\,\mathrm{m\,s^{-1}}$ for molecular masses from $100\,\mathrm{g\,mol^{-1}}$ (MMA molecule scale) to $10\,\mathrm{g\,mol^{-1}}$ (atomic scale). Typical thermal constants for the Plexiglas were chosen as per the manufacturer specifications [7]: $C = 1.7 \times 10^6\,\mathrm{J\,K^{-1}\,m^{-3}}$ and $\lambda = 0.19\,\mathrm{J\,s^{-1}\,m^{-1}\,K^{-1}}$. Finally, we chose a radius for the heat production zone of $l = 20\,\mathrm{nm}$ corresponding to the scale of a few methyl methacrylate units, and we assume for simplicity that $\phi = 1$: most of the energy contributes to the Joule effect and the other dissipation processes are comparatively negligible.
Note that such parameters are not accurately calibrated to match the actual rupture dynamics in interfacial PMMA. The purpose of this discussion is mainly to highlight the different orders of magnitude at stake in our presented model.

TEMPERATURE ELEVATION AT THE CRACK TIP

As stated in the main manuscript, the temperature evolution at the moving crack tip is dictated by the following equation:

$$\frac{\partial(\Delta T)}{\partial t} = \frac{\lambda}{C}\nabla^2(\Delta T) + \frac{\phi G V}{C\pi l^2} f \tag{1}$$

which is a diffusion equation including a source term. f is the support function of the thermal emission zone of surface integral πl^2 (we used $f = 1$ in the zone and $f = 0$ otherwise). It can notably be solved for the tip temperature using the diffusion Green's function [8]:

$$\Delta T(t) = \int_{-\infty}^{t} \mathrm{d}t' \iiint_{PZ(t')} \mathrm{d}v\, \frac{\phi G V}{C\pi l^2} \frac{\mathrm{e}^{\frac{-Cr^2}{4\lambda(t-t')}}}{[\frac{4\pi\lambda}{C}(t-t')]^{\frac{3}{2}}} \tag{2}$$

$$\text{with } r = r(\mathbf{dr}, t', t) = \| - \int_{t'}^{t} \mathbf{V}\mathrm{d}t'' + \mathbf{dr} \|$$

where $\mathrm{d}v$ is the volume of an elementary heat source of the advancing thermal process zone (PZ). This source is, at time t', located at a distance r from the crack tip at time t. We denote $\mathbf{dr}$ the positioning vector from the PZ center to the elementary source. See Fig. 1 for an illustration of these parameters. The time integration of

(2) adds up the whole history of sources position, while the volumetric integral sums the contribution, for a given time t', of infinitesimal heat sources of the emission zone. The steady state which we used in our model is then the limit of $\Delta T(t)$ for large times ($t \longrightarrow +\infty$), assuming V and G are constant.

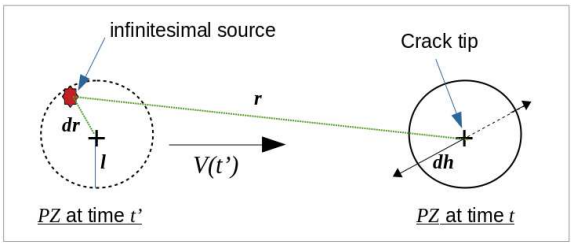

FIG. 1. Illustration of the geometric parameters used in Eq. (2). dh is perpendicular to the figure perspective.

Analytical approximation

For constant crack velocity and energy release rate, the temperature elevation at the steady state can be approximated [9]. When the crack propagates slowly, the temperature at the crack tip is constrained by the diffusion process. The heat production zone dissipates an energy $\phi G V \tau_0 dh$ during the time $\tau_0 = l/V$ that it has spent over the tip location. dh is the length of a crack front element. This energy is diffused over a roughly cylindrical volume with radius equal to the skin depth of diffusion δ over the time τ_0. The section of such a cylinder is given by $\pi\delta^2 \approx \lambda\tau_0/C$, leading to:

$$\Delta T_{\text{slow}} = \frac{(\phi G V \tau_0 dh)}{C(\pi\delta^2 dh)} = \phi G \frac{V}{\lambda}. \tag{3}$$

In this case, because of the small velocity, l is small compared to δ. However, for cracks propagating fast enough $\delta \ll l$. The diffusion is then negligible and all of the energy stays in the emission zone of section πl^2:

$$\Delta T_{\text{fast}} = \frac{(\phi G V \tau_0 dh)}{C(\pi l^2 dh)} = \frac{\phi G}{\pi C l}. \tag{4}$$

Note that ΔT_{fast} is the actual temperature at which the tip evolves in the weakened phase. Finally when $\delta \sim l$, the dissipated energy can only diffuse away from the heat production zone perpendicularly to the crack motion [9] and is spread over an ellipsoidal cross-section $\pi(\delta + l)l \approx 2\pi\delta l$, such as:

$$\Delta T_{\text{mid}} = \frac{(\phi G V \tau_0 dh)}{C(2\pi\delta l dh)} = \phi G \sqrt{\frac{V}{4\pi C \lambda l}}. \tag{5}$$

Fig. 2 illustrate the validity of these three approximations, showing the full solution of the diffusion equation (1) together with asymptotes (3) to (5). We show that, for slow cracks, the temperature increases linearly with the propagation velocity. At higher V, it however reaches a plateau constrained by the size of the heat production zone.

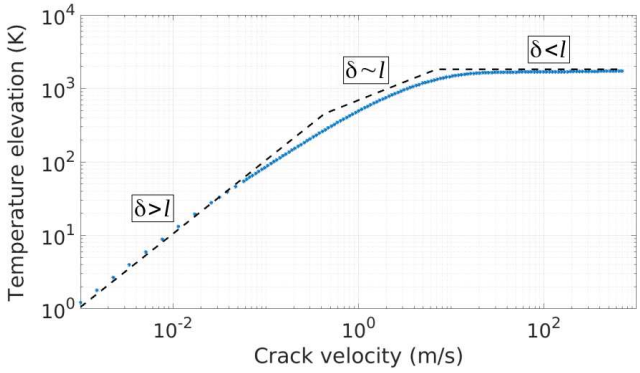

FIG. 2. Steady state values of the temperature elevation (blue dots) obtained by solving the diffusion equation (1) for a crack propagating at constant velocity for $\phi G = 200\,\text{J}\,\text{m}^{-2}$. The plotted asymptotes are the approximations (pre-factors included) from Eq. (3) to Eq. (5).

Transient time

Let us now move away from the thermal steady state hypothesis. We consider a tip which does not move before $t_0 = 0\,\text{s}$ and propagates at velocity V and energy release rate G afterwards. Similarly to the steady state temperature, the transient time for its rise in temperature, τ, is velocity dependent. For a fast propagating crack, the heat is not effectively evacuated away from the emission zone. The transient time then only corresponds to the maximum duration that the tip position stays in this zone:

$$\tau_{\text{fast}}(V) \sim \frac{l}{V}. \tag{6}$$

For a slow crack, however, the characteristic time of the heat diffusion is to be considered. We can derive it by writing in Eq. (2) that $r^2 \sim [V(t-t')]^2 + l^2$ (see Fig. 1). When the first term of this sum dominates, the heat kernel behaves as $\exp[-(t-t')/\tau_{\text{mid}}]$ with:

$$\tau_{\text{mid}}(V) \sim \frac{4\lambda}{CV^2}. \tag{7}$$

Overall, the quicker the crack progression, the shorter the thermal transient time. This is actually of convenience for our steady state approximation. For hot cracks, say propagating at velocities higher than $10\,\text{m}\,\text{s}^{-1}$ (see Fig. 2), we have $\tau_{\text{fast}} < 10^{-9}\,\text{s}$, which can be neglected for standard crack dynamics. Truly though, for

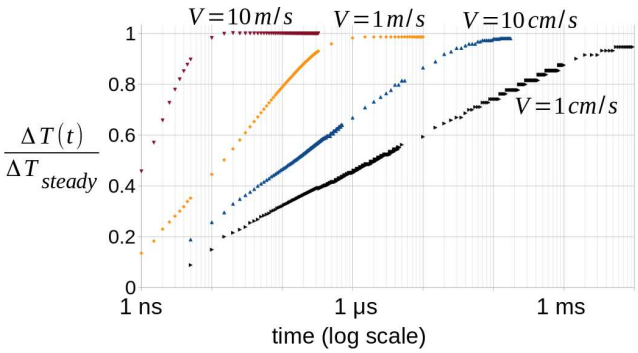

FIG. 3. Transient response for the heating of a crack propagating at constant V and G. The ratio of the tip temperature elevation and its steady state is shown for various velocities. One can read the actual value of ΔT_{steady} in Fig. 2.

slower cracks, say $V = 1\,\text{cm}\,\text{s}^{-1}$, τ_{mid} gets in the millisecond range. In this case, however, we have $\Delta T \ll T_0$ and the Joule heating can anyway be neglected. For completeness, a third transient time also affects the thermal inertia. When the velocity is small enough for $r^2 \sim [V(t-t')]^2 + l^2$ to be dominated by l^2, one can consider:

$$\tau_{\text{slow}} \sim \frac{Cl^2}{4\lambda}, \tag{8}$$

which in our case is a negligible $10^{-9}\,\text{s}$.
The transient regimes for various velocities are displayed in Fig. 3 for illustration. As mentioned, it corresponds to a cold crack that instantaneously accelerates from a full stop to a given constant velocity. It is of course a construction of the mind, as, in practice, our model predicts V to evolve according to its Arrhenius subcritical growth. For instance, we explained in our manuscript how a velocity of $1\,\text{m}\,\text{s}^{-1}$ corresponds to an unstable regime, so that what is shown in Fig. 3 for this velocity won't actually happen. The purpose this figure and of the expressions of τ_{fast}, τ_{mid} and τ_{slow} is to give more insight on how quick the transition to stable regimes would be. The discussion on how negligible are the transient regimes stays of course parameter dependent and one should keep in mind that our steady state model is an approximation that could hold more or less for different parameters values.

MORE ON THE CRITICAL POINT

We ran a bisection to numerically estimate the position of the critical point (CP). This bisection checked, for any temperature T_0, the maximum number of solutions of $V = S_G(V)$ to decide whether $T_0 > T_0^*$ (a unique solution for any G) or $T_0 < T_0^*$ (three solutions in the hysteresis domain). Numerical errors in this decision process imply some inaccuracy on the derived critical point. This, in

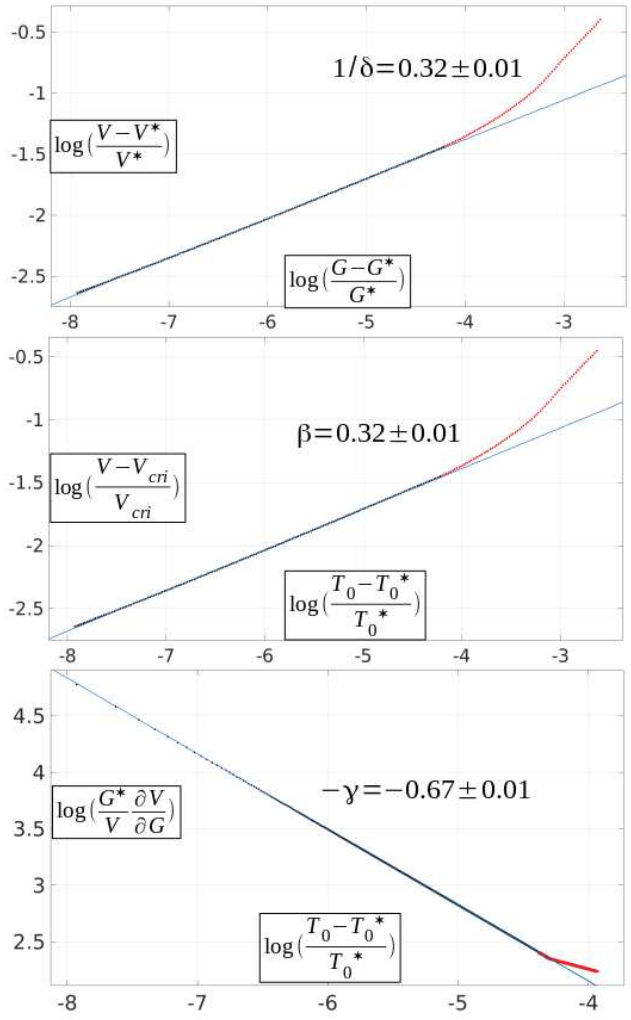

FIG. 4. Representation in the log-log domains (base 10) of the V surface (i.e., Fig. M4) along particular directions in the vicinity of the critical point. Black points were numerically derived from Eq. (M3) and the plain lines are the linear fits from which the red points were discarded. These fits are done beyond the critical point ($T_0 > T_0^*$).

return, leads to poorly determined critical exponents, as they are fitted in the direct neighborhood of the CP. We thus had to refine the position of the critical point with an iterative inversion in the vicinity of the firstly estimated location. The principle was to find T_0^* and G^* in this vicinity such that the velocity range on which to fit the exponents is maximized. The chosen procedure was to: first derive an a priori exponent β_1 in a direct neighborhood of the first CP estimation, then chose a smaller vicinity in which to vary the CP position, compute for each of these positions a more local β_2 value, derive a new CP position by minimizing $|\beta_2 - \beta_1|$, iterate. Choosing smaller and smaller vicinities, this method allowed us to get a more accurate critical point and hence to expand the ranges on which to fit our final exponents. The cor-

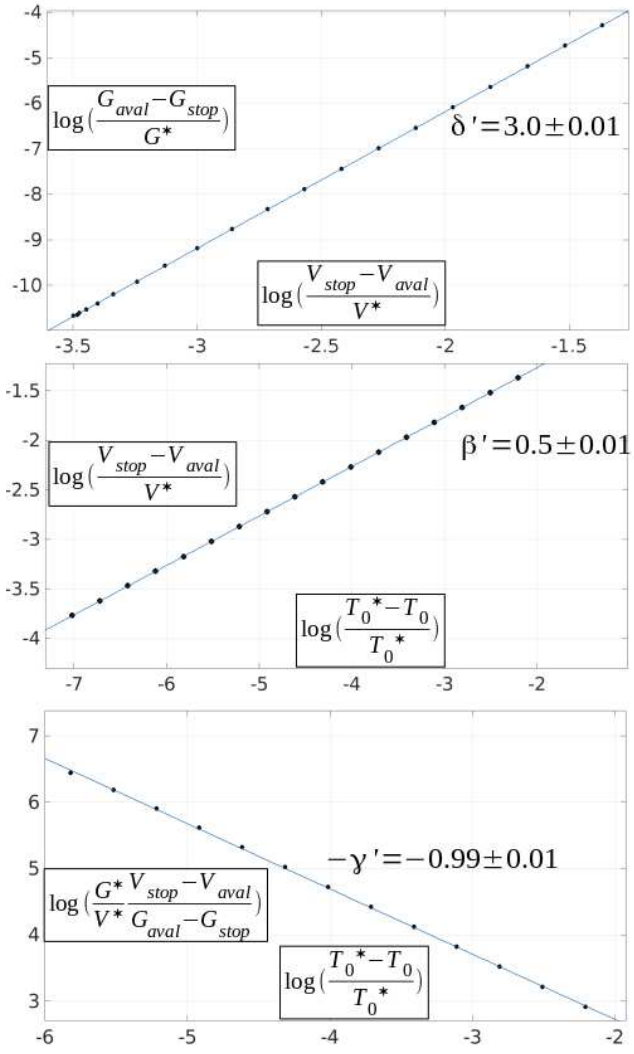

FIG. 5. Representation in the log-log domains (base 10) of the V surface (i.e., Fig. M4) along particular directions in the vicinity of the critical point. Black points were numerically derived from Eq. (M3) and the plain lines are the linear fits. These fits are done on the phase co-existence curve ($T_0 < T_0^*$).

responding decades and the respective exponents fits are shown in Fig. 4 and 5. We consider the reduced parameters $\Delta T_0/T_0^*$ and $\Delta G/G^*$, where $\Delta T_0 = T_0 - T_0^*$ and ΔG stands either for $G - G*$ or $G_{\text{aval}} - G_{\text{stop}}$ depending on the exponents (see Eq. (M4) to (M9)). Varying these parameters, the fits of the crack velocity function extend on at least three and a half decades (for β, δ and γ) and up to five decades (for β' and δ').

* vincentdospitalt@unistra.fr

[1] O. Lengliné, R. Toussaint, J. Schmittbuhl, J. E. Elkhoury, J. P. Ampuero, K. T. Tallakstad, S. Santucci, and K. J. Måløy. Average crack-front velocity during subcritical fracture propagation in a heterogeneous medium. *Phys. Rev. E*, 84:036104, Sep 2011. doi: 10.1103/PhysRevE.84.036104.

[2] K. T. Tallakstad, R. Toussaint, S. Santucci, J. Schmittbuhl, and K. J. Måløy. Local dynamics of a randomly pinned crack front during creep and forced propagation: An experimental study. *Phys. Rev. E*, 83:046108, 04 2011.

[3] L. Vanel, S. Ciliberto, P.-P. Cortet, and S. Santucci. Time-dependent rupture and slow crack growth: elastic and viscoplastic dynamics. *Journal of Physics D: Applied Physics*, 42(21):214007, oct 2009. doi:10.1088/0022-3727/42/21/214007.

[4] L. B. Freund. Crack propagation in an elastic solid subjected to general loading. *Journal of the Mechanics and Physics of Solids*, 20(3):129 – 152, 1972. ISSN 0022-5096. doi:10.1016/0022-5096(72)90006-3.

[5] A. Zerwer, M. A. Polak, and J. C. Santamarina. Wave propagation in thin plexiglas plates: implications for Rayleigh waves. *NDT and E International*, 33(1):33 – 41, 2000. ISSN 0963-8695. doi:10.1016/S0963-8695(99)00010-9.

[6] G. G. Hammes. *Principles of Chemical Kinetics*. Academic Press, 1978. ISBN 978-0-12-321950-3. doi: doi.org/10.1016/B978-0-12-321950-3.50005-0.

[7] Technical information, PLEXIGLAS GS/XT. Technical report, Evonik Industries AG, 2013. URL https://www.plexiglas.de/sites/lists/pm/documentsap/211-1-plexiglas-gs-xt-en.pdf.

[8] H. S. Carslaw and J. C. Jaeger. *Conduction of Heat in Solids*. Oxford: Clarendon Press, 1959.

[9] R. Toussaint, O. Lengliné, S. Santucci, T. Vincent-Dospital, M. Naert-Guillot, and K. J. Måløy. How cracks are hot and cool: a burning issue for paper. *Soft Matter*, 12:5563–5571, 2016. doi:10.1039/C6SM00615A.

TO GO BEYOND (UNPUBLISHED RELATED POINTS)

Abstract

In the next few pages, I continue the discussion on the validity of the steady state model introduced in the preceeding article. I also give a few analytical approximations related to the simulations that were presented there.

A. Steady state versus transient time simulation

In the previous pages, we discuss the various thermal transition times τ, depending on the crack velocity V. As a rough indication, the steady state approximation should hold as long as τ is short enough compared to the time scale of the system's mechanical variations (i.e., the time scales of $\partial V/\partial t$ and $\partial G/\partial t$). Notably, it should hold as long as:

$$V\left|\frac{\partial V}{\partial t}\right|^{-1} \gg \tau(V), \tag{1}$$

and

$$G\left|\frac{\partial G}{\partial t}\right|^{-1} \gg \tau(V). \tag{2}$$

These condition might well be met when the crack stays in a given phase (i.e., either the slow or the weakened state). Our steady state model however predicts some instantaneous velocity variation when a crack transits from one phase to the other, leading to $\partial V/\partial t = \pm\infty$, and to very quick variations in load when a crack avalanches. It implies that at least (1) cannot be verified on the transition thresholds, when $V = V_{\text{aval}}$ or $V = V_{\text{stop}}$, and the phase shifts might hence be poorly described by the steady state approach.
At this point, we should mention that the steady state simulations shown in the previous article, that were performed using a time step adaptive Runge-Kutta algorithm [1], actually failed where the crack acceleration diverges. To stabilise the solver around the phase transitions, so that we could still show you these simulations, we used the

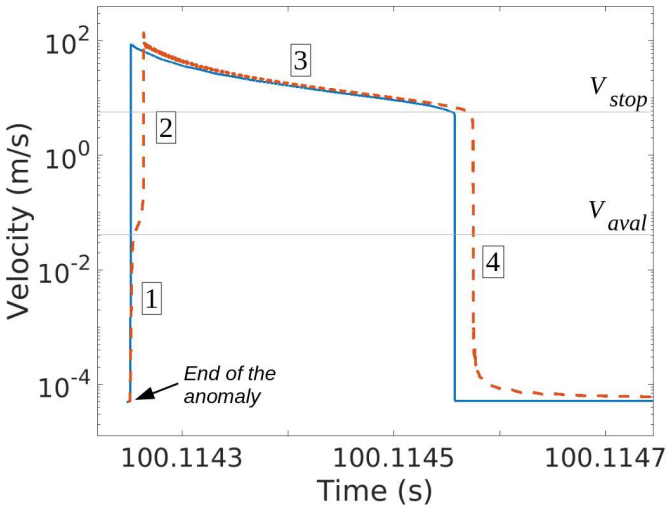

FIG. 1. Velocity of a crack weakened on exiting a stronger toughness anomaly. The plain plot is a steady state only simulation while the dotted plot uses Eq. (3). Labels correspond to: (1) increase of V as G_c drops on the asperity exit, (2) transition to the weakened phase as $V > V_{\text{aval}}$ in which the transient time τ is velocity dependent., (3) avalanche until $V < V_{\text{stop}}$ and (4) transition back to the low velocity phase, which is instantaneous with the steady state model but requires the crack to cool down with the full model.

approximation $\Delta T(t) \sim \Delta T(t - dt)$, where dt is the numerical time step. In other words, we introduced a numerical response time in the solver dynamics, that is nonphysical but negligible as far less than what τ should actually be. To further validate such a steady state computation, we compare it, in Fig. 1, with a simulation in which the governing equation for the temperature elevation, which was (see Fig. 1 of the preceding supplementary information [2])

$$\Delta T(t) = \int_{-\infty}^{t} \mathrm{d}t' \iiint_{PZ(t')} \mathrm{d}v \, \frac{\phi G V}{C\pi l^2} \frac{\exp\left[\dfrac{-Cr^2}{4\lambda(t-t')}\right]}{\left[\dfrac{4\pi\lambda}{C}(t-t')\right]^{\frac{3}{2}}} \tag{3}$$

$$\text{with } r = r(\mathbf{dr}, t', t) = \| - \int_{t'}^{t} \mathbf{V}\mathrm{d}t'' + \mathbf{dr} \|$$

is fully resolved using the total mechanical history of the crack propagation (the history and V and G along the crack position). Thus, this figure compares a steady state simulation (with only a negligible numerical response time, as just discussed) to a fully time dependent computation, where the thermal transient regime is resolved. Similarly to the simulations presented in the main article, we here look at the passage of the crack over a tough, rectangular, anomaly in fracture energy. Figure 1 focuses on the moment when the crack leaves the tough asperity, accelerates to the weakened phase and then, when cool enough, gets back to the slow one. It shows that the phase transitions are, as expected, slightly anticipated when using the steady state model. However the avalanche size is not significantly affected and the overall dynamics shall be well approximated as long as the sum of the transient response times, on acceleration and cooling down, is small compared to the avalanche duration.

B. One asperity simulations: Analytical stick time and avalanche size

In this section, we now come back to the numerical simulations presented in the main manuscript, with a rectangular asperity in the media fracture energy. For convenience, Fig. 2 here reminds of the G outputs for these simulations. Under the chosen loading geometry, we propose an approximate and analytical condition for such anomaly to trigger a thermal avalanche. We also give the pre-avalanche stick time (the time during which the slowed crack loads up on the anomaly) and the avalanche size, should it be triggered.

1. Stick time

Let us first look at the time during which the crack loads up over the G_c anomaly. We assume that this anomaly size is small compared to the priorly developed crack length ($L_a \ll a_0$) and that it is overcome while staying in the low velocity (creep) phase (i.e., $\Delta T \sim 0$ and $G_c = G_{c_a}$) in a negligible time Δt_a compared to the pre-anomaly loading time t_0 ($\Delta t_a \ll t_0$). In this case, the equation describing the energy release rate of the crack in our cantilever loading geometry,

$$G(t, a) = \frac{3Eh^3 {v_u}^2 t^2}{8a^4}, \tag{4}$$

which gives G as a function of time and of the crack advance, can be linearized to derive the evolution of the energy release rate over the asperity:

$$\begin{aligned} G(t_0 + \Delta t, a) &\approx \frac{3Eh^3 {v_u}^2 (t_0^2 + 2t_0\Delta t + \cancel{\Delta t^2})}{8(a_0 + \cancel{\Delta a})^4} \\ &\approx G_0 \left(1 + \frac{2\Delta t}{t_0}\right) \end{aligned} \tag{5}$$

which corresponds to the linear regime observed in Fig. 2, and where G_0 is the energy release rate at the entrance of the anomaly and $\Delta t \leq \Delta t_a$ and $\Delta a \leq L_a \ll a_0$ are the time and the distance already overcome on it.
Let us notice that the size of the anomaly writes as

$$L_a = \int_{t_0}^{t_0 + \Delta t_a} V(t) dt, \tag{6}$$

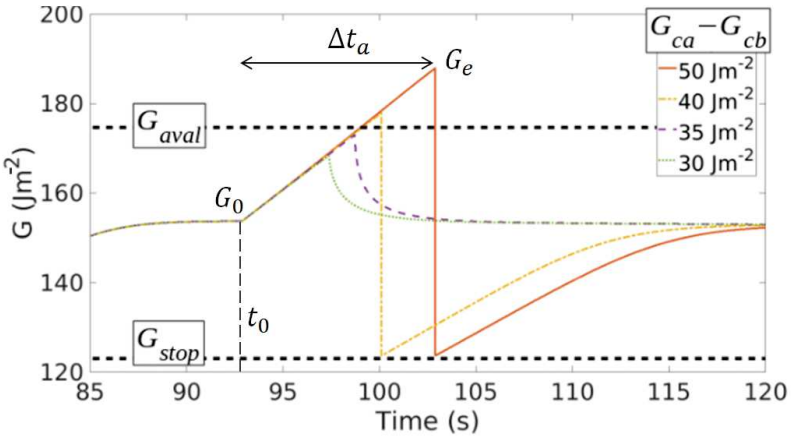

FIG. 2. Numerical simulations for a crack overcoming a rectangular asperity in fracture energy G_c, for various anomaly strengths $G_{ca} - G_{cb}$. The time and load on the entrance of the asperity are t_0 and G_0. The time needed to overcome it is Δt_a and the load on it exit is G_e. These two latter parameters are approximated by Eqs. (8) and (9).

where V is dictated by the governing, cold, Arrhenius law

$$V = V_0 \exp\left[\frac{\alpha^2(G(t) - G_{ca})}{k_B T_0}\right]. \tag{7}$$

in which the evolution of $G(t)$ when passing the anomaly is given by Eq. (5). One can then deduce from Eq. (6) the time Δt_a needed for the crack to vanquish the asperity:

$$\Delta t_a = \frac{t_0}{2}\frac{k_b T_0}{G_0 \alpha^2} \ln\left(1 + \frac{2L_a}{V_0 t_0}\frac{G_0\alpha^2}{k_b T_0} \exp\left[\frac{\alpha^2(G_{c_a} - G_0)}{k_b T_0}\right]\right). \tag{8}$$

Inserting (8) in (5), we deduce the energy release rate upon exiting the asperity: $G_e = G(\Delta t_a)$. To trigger a thermal avalanche, this value must exceed G_{aval} which leads to the following condition:

$$\begin{aligned} &G_e = G_0 + \frac{k_b T_0}{\alpha^2} \ln\left(1 + \frac{2L_a}{V_0 t_0}\frac{G_0\alpha^2}{k_b T_0} \exp\left[\frac{\alpha^2(G_{c_a} - G_0)}{k_b T_0}\right]\right) \\ &G_e > G_{\text{aval}}. \end{aligned} \tag{9}$$

In particular, this condition depends on the pre-asperity load and crack length (from G_0 and t_0) and on the shape of the asperity (from L_a and G_{c_a}).

2. *Avalanche length*

In case $G_e > G_{\text{aval}}$ so that thermal weakening is indeed triggered, one can also derive the length of the avalanche Δa_{aval} by assuming that its duration Δt_{aval} is negligible compared to the total loading time ($\Delta t_{\text{aval}} \ll t_0 + \Delta t_a$) and noticing that the evolution of G (i.e., Eq. (4)) can in this case be approximated as:

$$\begin{aligned} G(t_0 + \Delta t_a + \Delta t', a) &\approx \frac{3Eh^3 {v_u}^2 (t_0 + \Delta t_a + \cancel{\Delta t'})^2}{8(a_0 + \cancel{L_a} + \Delta a')^4}, \\ &\approx G_e \left(\frac{a_0}{a_0 + \Delta a'}\right)^4, \end{aligned} \tag{10}$$

which corresponds to the rapid drop in G in Fig 2 and where $\Delta a' \leq \Delta a_{\text{aval}}$ and $\Delta t' \leq \Delta t_{\text{aval}}$ are the avalanche progression in space and time. Equation (10) is valid until the end of the thermal weakening phase (i.e., until $G = G_{\text{stop}}$) which gives an approximation for Δa_{aval}:

$$\Delta a_{\text{aval}} = a_0 \left[\left(\frac{G_e}{G_{\text{stop}}}\right)^{1/4} - 1\right] \tag{11}$$

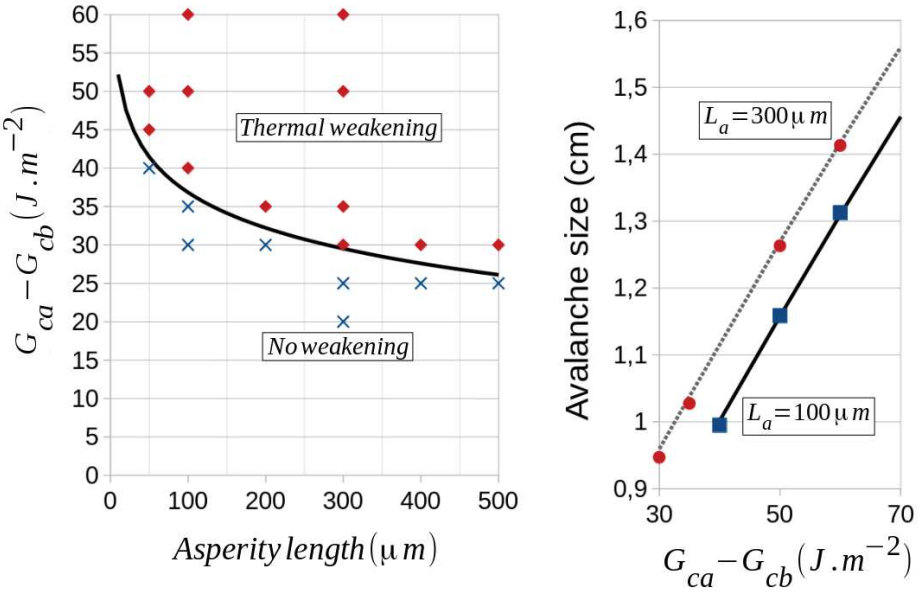

FIG. 3. Thermal avalanches induced by rectangular toughness anomalies. (Left): The crosses correspond to simulations where no thermal weakening has been triggered while the squares are simulations where the crack course is punctually weakened. The plain line is the weakening criteria of Eq. (9). (Right): Size of the avalanches for two widths of asperity and varying asperity toughness as per numerical simulations (symbols) and as per Eq. (11) (lines). $G_0 = 153.7$ J m^{-2} and $t_0 = 92.9$ s as per Fig. 2.

Figure 3 validates the approximations from Eqs. (9) and (11) by comparing them to the results of various numerical simulations.

[1] J. R. Dormand and P. J. Prince. A family of embedded Runge-Kutta formulae. *Journal of Computational and Applied Mathematics*, 6(1):19 – 26, 1980. ISSN 0377-0427. doi:10.1016/0771-050X(80)90013-3.

[2] T. Vincent-Dospital, R. Toussaint, A. Cochard, K. J. Måløy, and E. G. Flekkøy. Thermal weakening of cracks and brittle-ductile transition of matter: A phase model. *Physical Review Materials*, 02 2020. doi:10.1103/PhysRevMaterials.4.023604.

Chapter II

How heat controls fracture: the thermodynamics of creeping and avalanching cracks

Where the model is compared to the fragile rupture of two polymers

Accepted for publication
Vincent-Dospital et al., Soft Matter, 2020, doi: 10.1039/d0sm010
Now released: Soft Matter, 2020,16, 9590-9602

Résumé (*French abstract*):

Comment la chaleur contrôle la rupture :
la thermodynamique du fluage et de la fissuration brutale

Bien que d'importance cruciale en science des matériaux, la dynamique de propagation des fissures manque toujours d'une explication physique exhaustive. En particulier, la transition de leur comportement de fluage lent à un régime dynamique rapide est un point clef, puisqu'elle mène à l'endommagement total d'un matériau si la taille d'une avalanche rapide atteint celle du système. Nous montrons ici qu'une approche thermodynamique simple peut en fait décrire cette complexité dans la rupture, et décrire notamment des courbes de charge force-vitesse non monotones, fréquemment observées dans les tests mécaniques de divers matériaux. Nous considérons une rupture thermiquement activée, couplée avec la production et la diffusion de chaleur en pointe de fissure. Dans ce cadre, l'élévation de température affecte uniquement la vitesse sous-critique de propagation, et non les propriétés mécaniques de la matière. Nous montrons que cette description reproduit quantitativement la rupture de deux polymères différents (l'ouverture en mode I de polymethylmethacrylate (PMMA) et le pelage de rouleaux adhésifs), des régimes de fracturation les plus lents aux fissures les plus rapides, sur sept ou neuf ordres de grandeur de vitesse. En particulier, le régime le plus rapide est obtenu avec une augmentation de la température du front de milliers de kelvins, à l'échelle moléculaire autour de la tête de fissure. Bien que surprenantes, de telles températures extrêmes sont pourtant en phase avec diverses observations expérimentales : la fracto-luminescences (l'émission de lumière visible pendant la rupture) et une morphologie complexe des surfaces de fracture post-mortem, possiblement due à la sublimation de bulles dans la matrice.

How heat controls fracture: the thermodynamics of creeping and avalanching cracks

Tom Vincent-Dospital,[1,2,*] Renaud Toussaint,[1,2,†] Stéphane Santucci,[3,4] Loïc Vanel,[5] Daniel Bonamy,[6] Lamine Hattali,[7] Alain Cochard,[1] Eirik G. Flekkøy,[2] and Knut Jørgen Måløy[2]

[1] *Université de Strasbourg, CNRS, Institut de Physique du Globe de Strasbourg, UMR 7516, F-67000 Strasbourg, France*
[2] *SFF Porelab, The Njord Centre, Department of physics, University of Oslo, N-0316 Oslo, Norway*
[3] *Université de Lyon, ENS de Lyon, Université Claude Bernard, CNRS, Laboratoire de Physique, F-69342 Lyon, France*
[4] *Mechanics of disordered media laboratory, Lavrentyev Institute of Hydrodynamics of the Russian Academy of Science*
[5] *Université de Lyon, Université Claude Bernard, CNRS, Institut Lumière Matière, F-69622 Villeurbanne, France*
[6] *Université Paris-Saclay, CNRS, CEA Saclay, Service de Physique de l'Etat Condensé, F-91191 Gif-sur-Yvette, France*
[7] *Université Paris-Sud, CNRS, Laboratoire FAST, UMR 7608, F-91405 Orsay, France*

While of paramount importance in material science, the dynamics of cracks still lacks a complete physical explanation. The transition from their slow creep behavior to a fast propagation regime is a notable key, as it leads to full material failure if the size of a fast avalanche reaches that of the system. We here show that a simple thermodynamics approach can actually account for such complex crack dynamics, and in particular for the non-monotonic force-velocity curves commonly observed in mechanical tests on various materials. We consider a thermally activated failure process that is coupled with the production and the diffusion of heat at the fracture tip. In this framework, the rise in temperature only affects the sub-critical crack dynamics and not the mechanical properties of the material. We show that this description can quantitatively reproduce the rupture of two different polymeric materials (namely, the mode I opening of polymethylmethacrylate (PMMA) plates, and the peeling of pressure sensitive adhesive (PSA) tapes), from the very slow to the very fast fracturing regimes, over seven to nine decades of crack propagation velocities. In particular, the fastest regime is obtained with an increase of temperature of thousands of kelvins, on the molecular scale around the crack tip. Although surprising, such an extreme temperature is actually consistent with different experimental observations that accompany the fast propagation of cracks, namely, fractoluminescence (i.e., the emission of visible light during rupture) and a complex morphology of post-mortem fracture surfaces, which could be due to the sublimation of bubbles.

I. INTRODUCTION

The rupture of solids is often described by empirical observations rather than by fully understood physical models. One of the earliest formalisms is that by Griffith in 1921 [1]: the propagation of cracks is described as a threshold phenomenon, only obtained when loading their encompassing matrix above a critical fracture energy. To the first order, this view matches the behavior of brittle bodies, which suddenly snap passed a certain elastic deformation. Analytical models of cracks propagating in lattices suggested [2–5] that such an instability arises from the discrete nature of matter at the atomic scale. Indeed, these models revealed a minimum propagation velocity, comparable to that of the mechanical waves in the considered material, above which the advance of a fracture tip through the network of molecular bonds can be self maintained by the emission of high frequency phonons. There, the energy binding two lattice nodes is defined as a covalence-like barrier [6]. While this description [2] does not allow for slow propagation, it is acknowledged that a crack loaded well below the fast rupture threshold is still growing, but at creeping rates that are orders of magnitude below that of a 'dynamic' fracture (e.g., [7, 8]). An approach to explain such a creep in a way that is compatible with Griffith's formalism [1] is to consider that the fracture energy is not an intrinsic material property, but is instead a particular function of the propagation velocity (e.g., [9]). One hence simply obtains a lower crack speed if providing a lesser mechanical load. Alternatively, the creep regime is well modelled [7, 8, 10–16] by thermally activated sub-critical laws such as Arrhenius-like growth rates (e.g., [17]), and thermodynamics has thus emerged as a framework to describe the slow failure. In such descriptions, that are sometimes referred to as 'stress corrosion', a variation of fracture energy with velocity is not particularly called for, as the molecular agitation allows the crack to progress at loads below an intrinsic rupture threshold.

In practice, and depending on the material being broken, both the slow and the fast propagation regimes can be observed for a same range of applied loads [18, 19]. A hysteresis holds and the growth rate of a fracture is then depending on the actual mechanical history, rather than only on the instantaneous mechanical load. Maugis and Barquins [20, 21] early suggested that the description of the slow and the fast regimes, as well as that of the hysteresis, could be qualitatively unified by reinterpreting Griffith's criteria [1], if one could account for the temperature and velocity dependent viscoplasticity that occurs around crack tips [22, 23]. More specifically,

* vincentdospitalt@unistra.fr
† renaud.toussaint@unistra.fr

Marshall et al. [18] and then Carbone and Persson [24, 25] proposed that the induced heat associated to such a plasticity might locally soften the matter around a crack and that some thermal weakening (i.e., the abrupt transition from slow creep to fast failure due to a thermal process) arises from the related reduction of the material elastic moduli.

In this work, we propose a quantitative unifying model of the two propagation regimes that disregards such a softening effect, hence stating that some variations in the material mechanical properties are not necessarily required to obtain a slow-to-fast-crack transition. We focus instead on how the thermal dissipation, and the subsequent rise in tip temperature, affect the front sub-critical growth, as understood by statistical physics and an Arrhenius-like law. In some previous works, we indeed studied how such sub-critical laws, at fixed room temperature, well describe creep; in fibrous and polymeric materials (namely, paper sheets and polymethylmethacrylate, PMMA), they notably account for the mean kinetics of slow rupture fronts under various loading conditions [14, 15, 26]. When, in addition, taking into account these media structure and heterogeneities in fracture energy, such sub-critical laws also reproduce the intermittent dynamics of failure; in particular, the size distribution of crack jumps [13] and the front roughening properties [16]. Here we neglect any spatial variation of the fracture energy, but let the crack tip temperature vary as a function of the front velocity and of the applied mechanical load. Indeed, in a previous experimental and theoretical study of the tearing-induced heating in paper sheets [27], we were able to relate the temperature field around moving cracks to a certain percentage of the mechanical energy which gets converted into heat as the tip advances. More recently, this rise in temperature was fed back into a sub-critical growth law and showed [28] that one can thus obtain a dynamics model holding numerous qualitative similarities with the observed behavior of cracks, namely, two stable phases of propagation and a critical point that is similar to a brittle-ductile transition (e.g., [29]). Here, this model is first reintroduced (section II) and then shown to quantitatively capture the fracturing dynamics of two different polymeric materials, over the full range of velocities (section III), namely, acrylic glass (PMMA) and pressure sensitive adhesives (PSA). In both these media, some extensive experimental work has been carried out by different groups to quantify the two rupture regimes (e.g., see Refs. [9, 30–35] for PMMA and Refs. [19, 36–38] for PSA) and our proposed model accounts for the experimental curves of applied load versus crack velocity, from the slowest (micrometers per second) cracks to the fastest (hundreds of meters per second) ones. Such a match suggests that the growth of cracks could be sub-critical (i.e., as stated by the model) over a far wider velocity range than what is commonly accepted, that is, even at propagation velocities approaching that of mechanical waves. Indeed, we infer that the load threshold at which cracks typically shift to the fast phase is actually smaller than the intrinsic rupture energy, as a result from the boosted thermal activation around the front. In particular, we predict that crack tips can reach thousands of degrees on the molecular scale (i.e., over a few atoms around the front), when they quickly avalanche. Although such high temperatures are today rarely considered, they have long been proposed (e.g., Rice and Levy [39]), and we here discuss (section IV) how they are inline with several observables that sometimes accompany the fast propagation of cracks, namely, the emission of visible light at their tips (i.e., fractoluminescence [40–42]) and the existence of bubbles on their postmortem surfaces, that can nucleate secondary rupture fronts [43, 44].

II. FROM THERMAL CREEPING TO THERMAL WEAKENING

A. The kinetics of sub-critical rupture

We here consider a refinement of the propagation model already introduced by Vincent-Dospital et al. [28], that did not compare it to any actual, experimental, crack propagation. Let us start by restating the various components of this model.

We consider the velocity V of cracks to be ruled by the competition, at their tips, between breaking and healing processes [45] (or see Ref.[46], chpt 5.5.1). As many authors before us (e.g.,[7, 8, 46]), we propose that these processes are, at least in part, sub-critical, and are governed by some Arrhenius-type laws (e.g.,[17], chpt. 1.8.1). The activation energies of these laws are thus exceeded by the thermal bath according to a probabilistic Boltzmann distribution[17]. The rupture activation energy can then be written as $(U_c - U)$: the difference between the mechanical energy U that is stored in the tip bond and a critical rupture energy U_c, at which this bond fails. The latter should typically be comparable to a few electronvolts, which is a standard value for atomic covalence (e.g., see appx. E in Ref.[6]). Of course, depending on the studied material, U_c could also be dominated by the typically weaker binding energies of hydrogen or Van der Waals bonds, and its actual value may thus lie within a few orders of magnitude. In any case, as we are here introducing a mesoscopic law for the rupture dynamics (i.e., an Arrhenius growth), U_c should be understood as a mean material property, representative of the various strengths of the links that break along a crack course. Such a statistical definition will also apply to most of the parameters that we will henceforward consider. Similarly to the rupture barrier, the activation energy to heal the atomic connections can be written as $(U_h + U)$. There, U_h is an intrinsic repulsive energy barrier that two atoms need overcome to bond, in addition to which the thermal bath at the healing link also needs to compensate for the applied stretch U of the tip. With these considerations,

the propagation velocity of a crack is then modelled by

$$V = \nu d_0 \exp\left(-\frac{U_c - U}{k_B T}\right) - \nu d_0 \exp\left(-\frac{U_h + U}{k_B T}\right), \quad (1)$$

where the first term is the forward rupture velocity of the crack and the second one is the backward healing velocity. In this equation, we denote $d_0 \sim 2\,\text{Å}$ the inter-atomic distance, k_B is Boltzmann's constant $\sim 1.38 \times 10^{-23}$ $\text{m}^2\,\text{kg}\,\text{s}^{-2}\,\text{K}^{-1}$, T is the absolute temperature at the crack tip and ν is the collision frequency in the molecular bath (e.g., [17], chpt. 4.1). Each exponential in Eq. (1) is a probability term (i.e., the probability, challenged every $1/\nu$ second, that the thermal bath exceeds one of the activation energies and that the crack hence advances or retreats by a step d_0). As such, these terms cannot be greater than 1 and, while the healing one always meets this condition, $U \geq U_c$ corresponds to an over-critical propagation regime where

$$V = \nu d_0 \left[1 - \exp\left(-\frac{U_h + U}{k_B T}\right)\right]. \quad (2)$$

The product νd_0 is a maximal velocity, that we will further denote V_0, at which a fracture front can advance, when its tip atomic bonds snap each time they are challenged and never heal. In theory [17], the frequency ν is temperature dependent, with $V_0 \sim \sqrt{k_B T/m}$ where m is the mass of an atom or a molecule, but this dependence is small compared to that of the neighbouring exponential terms, so that we here neglect it. In our context of rupture kinetics, and more practically, it was notably proposed [5, 47] that such a nominal velocity V_0 is in the order of that of the medium Rayleigh waves, as quicker fractures then propagate in a specific supersonic regime [48, 49], which is not here considered.

In our description, U is the physical quantity that describes the load of a crack on the microscopic level, and that governs most of its dynamics. However, at the lab scale, U is not a measurable quantity. The energetic level at which a crack progresses is rather characterized by the macroscopic energy release rate G, which is the amount of energy that a fracture dissipates to grow by a given unit of measurable area [1]. This energy dissipation may be of diverse nature, and is to cause a relative reduction in potential energy near the tip. We will denote $N > 1$ the factor for this reduction, so that $U \sim d_0^2 G/N$. More commonly, mechanical shielding is described with the introduction of a plastic process zone of radius ξ around the crack front, where the dissipation occurs. To follow this canonical framework, we define a radius ξ that is relative to the length of an atom link, such that $2\xi/d_0 = N$. The intensity of the mechanical shielding (i.e., the relation between the potential energy U stored in the rupturing bond and the macroscopic energy dissipation G) then writes as

$$U \sim \frac{d_0^3 G}{2\xi}, \quad (3)$$

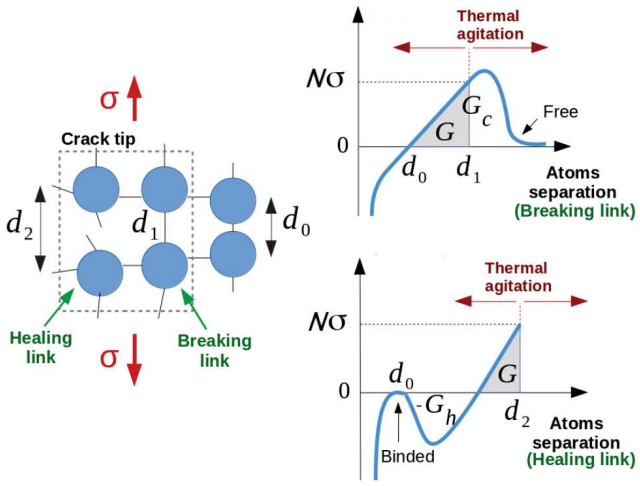

FIG. 1. (Left): simplified atomic view of the breaking/healing site at the crack tip. (Top right): Generic tip stress σ normalised by the stress shielding factor N versus atom separation for the active breaking link. (Bottom right): Generic tip stress normalised by the stress shielding factor versus atom separation for the active healing link. The grey areas are the energy release rate G. At this load, d_1 and d_2 are the mean extensions of, respectively, the breaking and the healing link, while d_0 is the unstressed atom separation. On the breaking link graph: the area below the curve for $d > d_0$ is the intrinsic surface fracture energy G_c. The thermal agitation may overcome the remaining $G_c - G$ barrier. Although the healing link is initially broken, an energy input is required to move the two particles closer to each other, due to the neighbouring unbroken links stretched at a load G. In addition, when the atoms separation gets smaller, the thermal agitation also needs to overcome a repulsive energy barrier G_h (the area below the atoms separation axis in this figure) before reforming the bond.

By additionally introducing $G_c = 2\xi U_c/d_0^3$ and $G_h = 2\xi U_h/d_0^3$, the respective equivalents in the energy release rate framework of U_c and U_h, one can re-write Eqs. (1) and (2) as functions of G:

$$V = V_0\left[\exp\left(-\frac{d_0^3(G_c - G)}{2\xi k_B(T_0 + \Delta T)}\right) - \exp\left(-\frac{d_0^3(G_h + G)}{2\xi k_B(T_0 + \Delta T)}\right)\right] \quad \text{when } G < G_c$$

$$V = V_0\left[1 - \exp\left(-\frac{d_0^3(G_h + G)}{2\xi k_B(T_0 + \Delta T)}\right)\right] \quad \text{when } G \geq G_c. \quad (4)$$

We have here also written T as $T_0 + \Delta T$, where T_0 is the absolute room temperature ($\sim 296\,\text{K}$) and ΔT is any deviation from this background value, as we will proceed to propose that the tip temperature can vary.

Note finally that one could also write this relation as a function of the mechanical stress σ that is applied at the crack tip, using $G(d) = \int_{d_0}^{d} N\sigma(d')\mathrm{d}d'$, where d_0 is the nominal separation of atoms in an unloaded matrix (i.e., at $G = 0$) and d is the actual atom separation at the crack tip. Figure 1 illustrates such a link between G and

σ and summarizes, in a simplified atomistic view, how the thermal bath allows to overcome the surface energy barriers for breaking and healing atomic bonds, $G_c - G$ and $G_h + G$, as per Eq. (4).

B. Heat dissipation and tip temperature rise

In the model we have introduced, one needs to further account for the energy which is dissipated around the running tip (G), as, even if it is mechanically lost, we will here show that it can maintain a strong effect on the crack dynamics. While the energy dissipation can be of several forms, ranging from the emission of mechanical waves [50] damped in the far field, to the nucleation of defaults in the matrix [51] (i.e., crazing [9, 52]), we here focus on the release of heat around the fracture tip [27, 40]. We thus call ϕ the percentage of G that is converted into some local rise in internal energy, and hence in temperature, and denote l the typical size over which this process occurs. As the heat, released on a production zone of area πl^2 close to the tip, is to diffuse in the whole bulk, the resulting temperature elevation ΔT can be modelled (e.g., [27]) by the standard diffusion equation:

$$\frac{\partial(\Delta T)}{\partial t} = \frac{\lambda}{C}\nabla^2(\Delta T) + \frac{\phi G V}{C\pi l^2} f, \tag{5}$$

where λ is the medium's thermal conductivity, and C is the volumetric heat capacity. The last term of this equation is a source term only valid in the heat production zone. The support function f of this zone is 1 inside of it and 0 otherwise, and the thermal source term is proportional to $\phi G V$, that is the dissipated power per unit of crack length deposited in the advancing zone. Although governed by Eq. (5), ΔT at the rupture front can approximate to far simpler expressions. It was indeed shown [27] that, at low propagation velocities, the temperature elevation at the centre of the heat production zone (i.e., the crack tip) is only governed by the diffusion skin depth $\delta = \sqrt{\lambda\tau/(\pi C)}$ upon the passage of the production zone of extension l within the time $\tau = l/V$. For fast cracks however, when δ becomes smaller than l, the generated heat can barely diffuse out of its source zone and ΔT is then constrained by l. We thus have

$$\Delta T_{\text{slow}} \sim \frac{\phi G V \tau}{C(\pi\delta^2)} = \frac{\phi G V}{\lambda}, \tag{6}$$

$$\Delta T_{\text{fast}} \sim \frac{\phi G V \tau}{C(\pi l^2)} = \frac{\phi G}{\pi C l}. \tag{7}$$

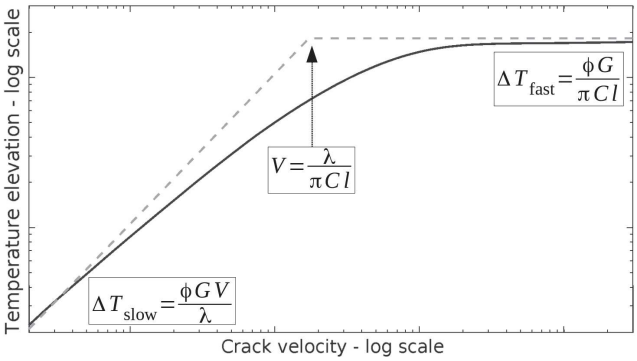

FIG. 2. Steady thermal elevation at a crack tip for various propagation velocities, due to the diffusion equation (5) (plain plot). The approximations ΔT_{fast} and ΔT_{slow}, from Eqs. (6) and (7), are shown for comparison (dotted plots). The axes are not annotated for the sake of generality.

Figure 2 shows the general evolution of ΔT at the tip with V, according to Eq. (5) solved by numerically integrating the heat diffusion kernel [53]. Note that ΔT in Eq. (5) is a temperature field as shown for instance in the inset of Fig. 3, but we are here mainly interested in its value at the centre of the heat production zone (i.e., where the rupture process occurs). Figure 2 also shows how the two expressions of Eqs. (6) and (7) approximate for the tip temperature.

C. Model phase behavior

We have now derived the two constitutive equations of our fracture dynamics model: Eq. (4), that gives the velocity of a crack as a function of its tip temperature, and Eq. (5), that governs the thermal state around a progressing front. In a previous work [28], we have simultaneously solved these two equations and, focusing on their steady state, showed that they predict two stable phases for the propagation of cracks. These two behaviors are shown by the plain curve in Fig. 3, and are there labelled 'Slow stable phase' and 'Fast stable phase'. The first one, as its name suggests, is a slow one, where ΔT stays small compared to T_0, such that the growth rate is mainly governed by the medium fracture energy G_c (i.e., as indicated by Eq. (4)). This slow branch ceases to exist beyond a particular load $G = G_a$. The second phase is reached when the generated heat (and hence ΔT) significantly overcomes the background temperature. From the Arrhenius law (4), the growth rate then significantly increases, so that the crack is said to be thermally weakened. Note, in Fig. 3, how both phases coexist for a certain range of energy release rates: a hysteresis situation holds (e.g., between $G = 300\,\text{J m}^{-2}$ and $G = G_a$ in Fig. 3). When this is the case, the model also predicts [28] a third phase, that is, by contrast, unstable and hence shall be difficult to be recorded experimentally.

III. COMPARISON TO EXPERIMENTAL RESULTS

Interestingly, this phase description in our model matches key observations of fracturing experiments. The

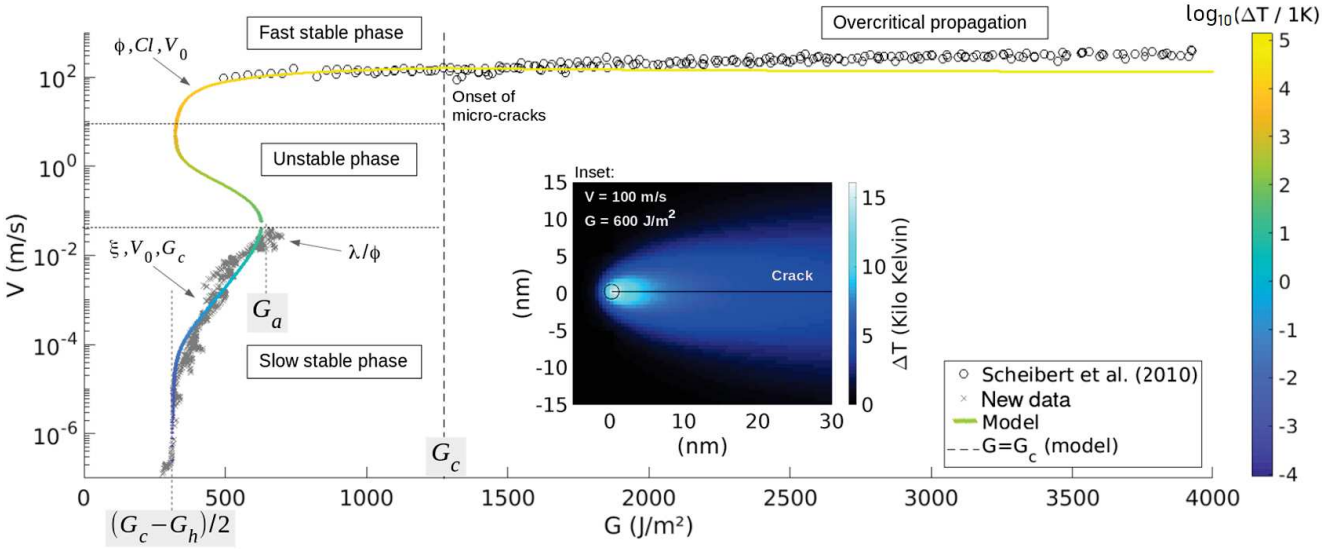

FIG. 3. Crack velocity V as a function of the energy release rate G as predicted by Eqs. (4) and (5) (plain curve) and fitted to the PMMA experimental data [32]. The arrows indicate to which model parameters each part of the curve is mainly sensitive, and the main color scale specifies at which temperature the crack tip is modelled to be. The load G_a is an avalanche threshold beyond which a front can only propagate quickly and G_c is the modelled microscopic energy barrier for rupture. Below the asymptote at $(G_c - G_h)/2$, fronts cannot propagate forward due to some dominating healing processes. The inset shows, for a given point of the curve: $V \sim 100\,\mathrm{m\,s^{-1}}$ and $G \sim 600\,\mathrm{J\,m^{-2}}$, the associated modelled temperature field around the front. For readability, the color map is there different from the main one, and the circle corresponds to the tip of radius l, where the extra heat is emitted. ΔT of the main model curve is the value at the centre of the circle. At loads beyond $G = G_c$, micro-cracks begin to nucleate [32], as shown further in Fig 4, which shows a zoom of the fast branch.

abrupt transition, passed a load threshold, from slow cracks to fast cracks, can indeed be interpreted as a phase transition [28], and the usual stick-slip of fronts is a good indicator that some hysteresis holds in the physical laws that rule the rupture dynamics [21, 28]. We then proceed to test our model against two sets of experimental data, where both the energy release rate G and the velocity V of the slow creep and the fast propagation stages were well quantified, as we detail in the next sections.

A. The rupture of PMMA

First, we look into a data set acquired when breaking polymethylmethacrylate plates (PMMA) at room temperature ($T_0 = 296\,\mathrm{K}$). A wedge is driven into Perspex® bodies, resulting in cracks for which two stable (G, V) branches are indeed recorded [32]. These results are shown in Fig. 3. There, the fast branch, with propagation velocities above $100\,\mathrm{m\,s^{-1}}$, was reported by Scheibert et al. [32], and the slow creeping branch is here published for the first time for this given PMMA (see appendix A for details on how it is obtained). When forcing the rupture velocity between these two regimes (i.e., above a specific creep velocity of $4\,\mathrm{cm\,s^{-1}}$ and below $\sim 100\,\mathrm{m\,s^{-1}}$), some stick-slip is observed in the dynamics of the fronts, as reported by Hattali et al. [54].
Figure 3 then compares both experimental branches with our proposed model. We thus pursue by detailing how each parameter was fitted (i.e., how the model was calibrated to the data), based on asymptotic read-offs. We classically start by wondering how well the slow propagation phase is represented by an Arrhenius law of constant temperature. In the model, this corresponds to a linear $\ln(V)$ to G relationship that holds at low velocity, where ln is the natural logarithm. There, ΔT is negligible compared to the background T_0 and G is high enough for the healing terms of Eq. (4) to be secondary (i.e., the terms involving G_h in this equation), leading to

$$\ln(V) = G\left[\frac{d_0^3}{2\xi k_B T_0}\right] + \left[\ln(V_0) - \frac{d_0^3 G_c}{2\xi k_B T_0}\right]. \quad (8)$$

In the data, this equation shall describe the portion of the plot lying between 10^{-4} and 10^{-2} $\mathrm{m\,s^{-1}}$, and the slope there, approximately $0.02\,\mathrm{m^2\,J^{-1}}$, hence constrains $d_0^3/(2\xi k_B T_0)$ and so the equivalent length for the crack mechanical shielding ξ to be in the order of 50 nm. Additionally, the intercept of Eq. (8) with the V axis (i.e., the second term in brackets) links V_0 and G_c. We earlier stated the former to be comparable to the medium Rayleigh velocity [32], $880\,\mathrm{m\,s^{-1}}$ in this particular polymer, so that we can deduce the rupture threshold G_c to be about $1300\,\mathrm{J\,m^{-2}}$. This value, together with that of ξ, gives a fracture energy $U_c = G_c d_0^3/(2\xi)$ comparable to 1 eV, which is satisfyingly consistent with a covalence-like barrier. Next, the healing threshold G_h can be inferred

from the vertical asymptote at $G = 300\,\mathrm{J\,m^{-2}}$, below which healing seems to prevail as cracks do not propagate forward [45]. Equation (4) predicts this asymptote for $G = (G_c - G_h)/2$, when the healing term equals the breaking one, such that $G_h \sim 650\,\mathrm{J\,m^{-2}}$. Let us now focus on the maximum G in the slow stable phase, denoted G_a (for 'avalanche') in Fig. 3, around $V = 4\,\mathrm{cm\,s^{-1}}$. It is modelled by Eq. (4) once ΔT is high enough compared to T_0 to trigger a phase transition, which, as per Eq. (6), mainly depends on the λ/ϕ ratio. By tuning this ratio, and appreciating the fit (see appendix B), we have deduced it to be around $0.9\,\mathrm{J\,s^{-1}\,m^{-1}\,K^{-1}}$. As the PMMA conductivity, $\lambda = 0.18\,\mathrm{J\,s^{-1}\,m^{-1}\,K^{-1}}$, is known [55], we can approximate $\phi \sim 20\%$. Note that at this particular point (at $G = G_a$), the polymer suddenly breaks (e.g., [20, 56]), as $\partial V/\partial G \to +\infty$ and the velocity has to jump to the fast regime. Consequently, G_a is often seen as a macroscopic critical energy release rate, which in our description is less than the intrinsic microscopic energy barrier (i.e., $G_a < G_c$). This difference is here directly related to the thermal conductivity λ of the medium, and the avalanche to a fast rupture arises when the diffusion can no longer cope with the crack velocity, so that heat is no longer efficiently diffused away from the tip. The characteristic size l on which this heat is generated is the only parameter that remains to be determined. As, according to the model, the crack needs to be hot enough to explain some fast fronts at low mechanical load (i.e., the slower part of the fast branch in Fig. 3, around $100\,\mathrm{m\,s^{-1}}$), we can estimate the limiting factor of ΔT_{fast}, Cl (see Eq. (7)). Matching the data set in this area (see appendix B), and using [55] $C \sim 1.5 \times 10^6\,\mathrm{J\,K^{-1}m^{-3}}$, we have deduced l to be in the nanometer range. This magnitude happens to be in the same order as the earlier derived ξ. We thus predict that most of the induced molecular agitation is introduced on the closest atoms around the crack tip, which coincides with the length scale for the energetic shielding of the tip. Noteworthily, such a nanometer scale appears to be close to the typical entanglement scale of polymers [57] (i.e., the density of polymeric chains crossing points in the matrix).

To quantify how well the model accounts for the experimental data, we computed, for each data point, the relative orthogonal distance ε_d to the model, that is

$$\varepsilon_d(G_d, V_d) = \min_m \sqrt{\left[1 - \frac{G_m}{G_d}\right]^2 + \left[1 - \frac{\log_{10}(V_m)}{\log_{10}(V_d)}\right]^2}, \tag{9}$$

where the subscript d stands for 'data' and m for 'model'. We are thus looking at a relative fit mismatch along the G axis and a relative fit mismatch, in order of magnitude, along the V axis. For any particular measurement point below $G = G_c$, ε_d is at most 16%. An average error for the whole fit, $\bar{\varepsilon} = \mathrm{mean}_d(\varepsilon_d)$, can also be inferred. To do so, we first have regularly under-sampled the experimental data onto $40\,\mathrm{J\,m^{-2}}$ wide bins, keeping there only the mean G_d and the mean $\log_{10}(V_d)$. This way, and doing so separately for the two propagation branches (see appendix C, Fig. 15), no bias is introduced on $\bar{\varepsilon}$ by the strong difference in measure density along the experimental (V_d, G_d) curve (i.e., see Fig. 3). The thus derived overall fit error computes to $\bar{\varepsilon} = 4\%$, below $G = G_c$. We discuss, in the next section, the fit beyond G_c and further discuss the accuracy of the inverted parameters in appendix B.

B. On the fast crack velocity in PMMA

Our simple sub-critical model hence matches most of the rupture dynamics of PMMA, from slow to fast velocities. In Fig. 3 however, an increase in velocity holds in the experimental data beyond $G = G_c$, and is not properly accounted for. To highlight this mismatch, we display in Fig. 4 the fast branch with an optimised display scale. It has been shown [33] that, beyond a particular load, the global front velocity is impacted by the fracture instabilities that occur at high speed. Indeed, passed this threshold, fronts get more complex as micro-cracking occurs [32, 43, 44], that is, as micro-cracks form and propagate in the fracture plane ahead of the main front. Such micro-cracks are shown in Fig. 4. And, at an even higher

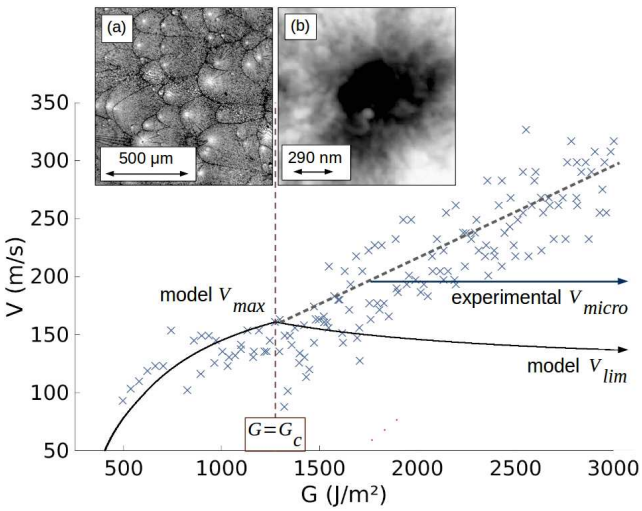

FIG. 4. Zoom on the PMMA fast propagation branch presented in Fig. 3, and as per Eqs. (4) and (5). Beyond a load comparable to the modelled G_c threshold, some micro-cracks start to nucleate, impacting the overall propagation velocity as explained by Guerra et al. [33]. The individual velocity of each micro-crack stays however constant at $V = V_{\mathrm{micro}}$. The validity of our single front model is limited passed this point, although it does predict a velocity plateau V_{lim}, as per Eq. (10), and a velocity maximum V_{max}, which are comparable to V_{micro}. Inset (a): Fractography of the secondary micro-cracks on a postmortem fracture surface. White areas mark their nucleation centres. Inset (b): Atomic Force Microscopy of a nucleating cavity at the centre of a micro-crack. As proposed in section IV D, it could derive from the sublimation of localised bubbles around the main front, due to some intense thermal effects.

load, micro-branching also comes into play, and aborted out-of-plane secondary cracks are observed [31, 58–60]. For the PMMA that is here studied, the micro-cracks were observed [32] at velocities above $165\,\mathrm{m\,s^{-1}}$, which approximately corresponds in the model to $G > G_c$. Beyond this threshold, the apparent macroscopic speed of the front, V, increases with the micro-cracks growing density, while the individual velocity of each micro-front, however, was inferred to stay constant [33], around $V_{\mathrm{micro}} \sim 200\,\mathrm{m\,s^{-1}}$, as illustrated in Fig. 4.
Such a plateau in the propagation speed is somewhat consistent with our description (see Fig. 4). But this being said, it is clear that our unique front model shows limitations as soon as fronts complexify. We can still push this discussion on the fast regime a bit further. A question of interest about the rupture of PMMA has been why the maximal observed crack velocity was significantly lower than the theoretical Rayleigh speed [32] (i.e., about $200\,\mathrm{m\,s^{-1}}$ rather than $880\ \mathrm{m\,s^{-1}}$). Equation (4) gives here some insight, as it does predict a plateau velocity V_{lim} as the applied G gets very large. Indeed, besides preventing the crack advance at very low loads, the sub-critical healing processes significantly limit the fast growth rate, as the tip temperature is modelled to be high. More specifically, by inserting ΔT_{fast} (7) in Eq. (4), and by looking at the high loads asymptotic regime of the healing term, we predict V to be limited by $c_0 = d_0^3 C$, the individual heat capacity of atom bounds:

$$V_{\mathrm{lim}} \sim V_0 \left[1 - \exp\left(-\frac{d_0^3(1+\cancel{G_h/G})}{2\xi k_B(\cancel{T_0/G} + \phi/[\pi C l])}\right)\right] \sim V_0 \left[1 - \exp\left(-\frac{\pi c_0}{2k_B}\ \frac{l}{\xi\phi}\right)\right]. \tag{10}$$

In this expression, the crossed out terms are neglected in regard to the neighbouring ones. Note however that Eq. (10) is mainly illustrative, as the plateau it describes occurs in a domain where our single front model does not strictly apply. Note also that the value $V_{\mathrm{lim}} \sim 100\,\mathrm{m\,s^{-1}}$ is smaller than the modelled maximum individual propagation velocity $V_{\mathrm{max}} \sim 160\,\mathrm{m\,s^{-1}}$, which is obtained for $G = G_c$ rather than for $G \to +\infty$ (see Fig. 4).

C. The detachment of Pressure Sensitive Adhesives

We now pursue the comparison with the reported rupture of another material, acrylic based pressure sensitive adhesives (PSA), that typically happens when unrolling some office tape. In particular, the peeling dynamics of Scotch® 3M 600 rolls (composed of a polyolefin rigid backing coated with a layer of synthetic acrylic adhesive) has been thoroughly studied in the last decades (e.g., [19, 37, 61]); we here fit our model to two compatible (G, V) data sets that were published by Dalbe et al. [37] and by Barquins and Ciccotti [19]. These data sets are shown in Fig. 5. Two stable modes of front detachment (i.e., a fast one and a slow one) are reported [19], similarly to those governing the rupture in PMMA. Additionally, some (unstable) stick-slip in the rupture dynamics is also observed [37] when peeling with an average velocity between $V \sim 15\,\mathrm{cm\,s^{-1}}$ and $V \sim 20\,\mathrm{m\,s^{-1}}$.
Overlaying this experimental data, Fig. 5 also displays a calibrated version of our model. The model parameters were inverted as follows, with a similar asymptotic analysis as what was done for PMMA. As no significant healing threshold displays at low velocity, we have only assumed that G_h is high enough to completely neglect the healing processes (i.e., the healing term in Eq. (4) is small if G_h is high). Of course, this absence of threshold, below which no forward propagation of the crack is observed, could also only indicate that $(G_c - G_h)/2 < 0$ or that this value (i.e., illustrated on the PMMA data in Fig. 3) is less than the minimum energy release rate that was investigated in the tape experiments. We discuss this particular point further in appendix D. We now invert the length ξ, which is, again, given by the slope of the slow phase and is here about 10 nm. As no healing is now supposed to be at play, the nominal velocity V_0 is given by the highest velocity records: $V_0 \sim 30\,\mathrm{m\,s^{-1}}$ as V_0 is the maximum value then predicted by Eq. (4). Satisfyingly, this value compares well with the magnitude of a mechanical wave velocity in PSA, that is, $\sqrt{\mu/\rho}$, where μ is, for instance, the shear modulus of the adhesive [62], 0.1 to 1 MPa, and ρ is its volumetric mass [63], about $10^3\,\mathrm{kg\,m^{-3}}$. Next, from Eq. (8), the intercept of the slow branch with the ordinate (zero G) axis indicates $G_c \sim 150\,\mathrm{J\,m^{-2}}$. Rather logically, and with the inverted value of ξ, this again corresponds to a value of fracture energy $U_c \sim 1\,\mathrm{eV}$. Note also that G_c is again higher than the transition load G_a at which a creeping front jumps to a fast regime. From this transition load, arising in the model from the temperature rise at low velocity (6), we also infer λ/ϕ to be in the order of $0.1\,\mathrm{J\,s^{-1}\,m^{-1}\,K^{-1}}$. As the adhesive's conductivity λ lies in the same range [64], a consequent portion of G should be released into heat: $\phi \sim 1$. Of course, ϕ cannot be exactly one, as other dissipating processes than heat diffusion are likely to dissipate a part of G (see the discussion in section IV). According to our inversion however, this part ought to be small. Finally, by varying l and by matching the coolest points of the fast phase, we estimate this parameter, which limits the highest tip temperature (i.e., Eq. (7)), to be in the nanometer range. This value, for the length scale of the heat production zone, is again rather consistent with the inverted magnitude of ξ, that is, the equivalent length scale for the mechanical shielding of the tip. Note also that both ξ and l are interestingly comparable to what was obtained for PMMA, and in the order of a polymeric entanglement density [57].
As shown in Fig. 5 and with this set of parameters, the model accounts for most of the tape peeling dynamics. More quantitatively, for all the particular data points of the two stable phases, the fit error ε_d (as defined by

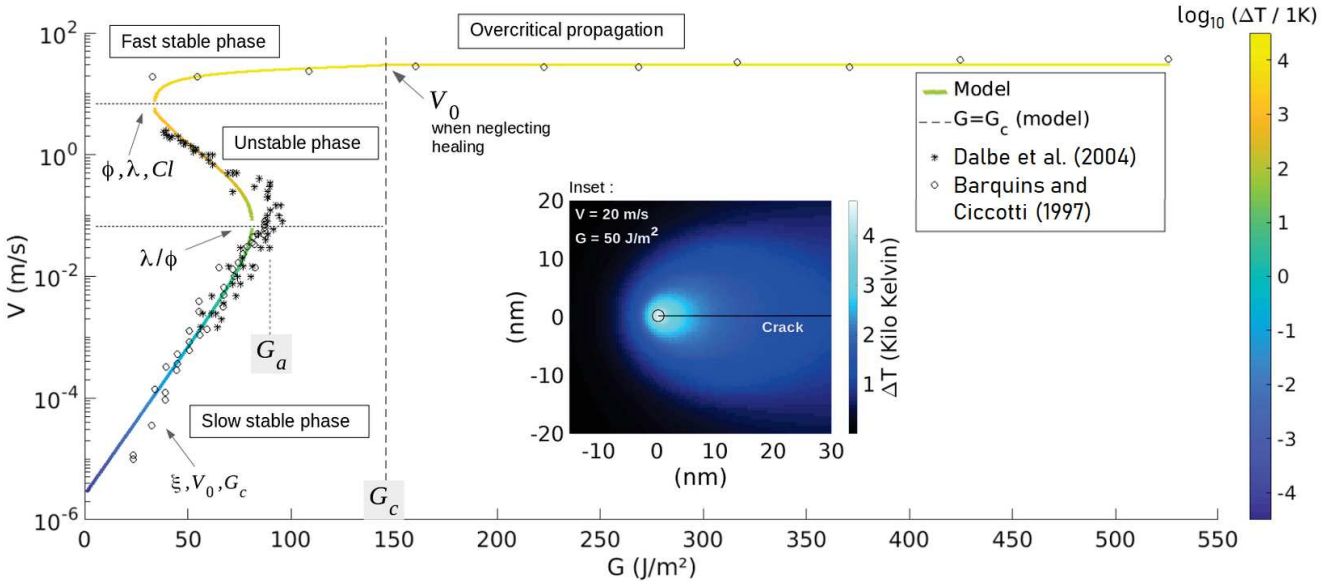

FIG. 5. Crack velocity V as a function of the energy release rate G as predicted by Eq. (4) and (5) (plain curve) and fitted to the tape experimental data [19, 37]. The unstable branch was not actually measured and the data points there are only averaged V versus G for a crack that undergoes stick-slip, in the given set-up, between the slow and the fast phase. The arrows indicate to which model parameters each part of the curve is mainly sensitive, and the main color scale specifies at which temperature the crack tip is modelled to be. The load G_a is an avalanche threshold beyond which peeling fronts can only propagate quickly and G_c is the modelled microscopic energy barrier for rupture. The inset shows the associated modelled temperature field around the front, at the onset of the fast to slow phase shift ($G = 50\,\mathrm{J\,m^{-2}}$, $V = 20\,\mathrm{m\,s^{-1}}$). For readability, the color map is there different from the main one, and the circle corresponds to the tip of radius l, where the extra heat is emitted. ΔT of the main model curve is the value at the centre of the circle.

Eq. (9)) is less than 20%. We also computed a mean fit error $\bar{\varepsilon} = \mathrm{mean}_d(\varepsilon_d)$ for the stable phases. To do so, and as done for PMMA, we first averaged the data points onto $10\,\mathrm{J\,m^{-2}}$ wide bins, so that no densely populated part of the measured curve dominate the value of $\bar{\varepsilon}$ (see appendix C, Fig. 16). We thus computed $\bar{\varepsilon} = 5\%$.

Note that, in comparison to the fast branch for the failure of PMMA (i.e., as discussed in section III B), it would be of interest to know if the critical load $G = G_c$ also approximately corresponds to the apparition of some new rupture modes. Yet, the high velocity branch of the tape data is bound to relatively large uncertainties (the loading system of Barquins and Ciccotti [19] involved dropping weights from an elevated balcony, illustrating the challenges in fast peeling measurements), so that it does not allow a more thorough analysis.

D. Parameter summary

In Tab. I, we summarises all the parameters's values, that we have inverted or supposed for the rupture of PMMA and PSA. The accuracy of these values is further discussed in appendix B.

Parameter	PMMA	PSA	Unit
V_0	880	30	$\mathrm{m\ s^{-1}}$
G_c	1300	150	$\mathrm{J\ m^{-2}}$
G_h	650	-	$\mathrm{J\ m^{-2}}$
ξ	50	10	nm
l	1	1	nm
ϕ	0.2	~ 1	[-]
λ	0.1	0.18	$\mathrm{J\ s^{-1}\ m^{-1}\ K^{-1}}$
C	1.5	1	$\mathrm{MJ\ m^{-3}\ K^{-1}}$
G_c/G_a	1.8	1.6	[-]
U_c	1	1	eV
N	500	100	[-]

TABLE I. Summary of all model parameters considered for the rupture of PMMA and PSA, as discussed in section III. A value $d_0 \sim 2\,\text{Å}$ has been assumed in the derivation of these parameters. For completeness, the related quantities $G_c/G_a = U_c/U_a$, $U_c = G_c d_0^3/(2\xi)$ and the shielding factor $N = 2\xi/d_0$ are also specified.

IV. DISCUSSIONS

For two different polymeric materials, we thus have shown how a thermally activated fracture process, coupled with the dissipation and diffusion of heat, can simply explain many features of the dynamics of both creeping and fast cracks, and the shifts from one state to the other. Such novel match, over seven to nine decades of propagation velocities and with only very simple physics considerations, could shade some new light on fracture mechanics, as thermal effects are often discarded.

A. How hot is too hot for a crack tip? Some light from fractoluminescence

To explain the fast propagation branch, we have notably predicted the front temperature to reach several thousands of degrees. Such high values are difficult to confirm experimentally, especially as they are to stand only on a few nanometers during short avalanches. There exist however, indirect hints toward the existence of an important temperature elevation in a variety of brittle materials fracturing at high speed.

For instance, the analysis of some fracture roughness in cleaved quasi-crystals has revealed a damage zone of size anomalously large for this class of materials, and this was stated to result from a local temperature elevation of about 500 K at the moving crack tip [65].

Several experimental works in glass and quartz [40–42] also managed to indirectly measure ΔT to indeed reach thousands of degrees, by characterising the photons emission from the tips of some moving cracks and by comparing it to the blackbody radiation theory [66]. In the case of tape, when peeling fast enough to be in the stick-slip regime, a blue tribo-radiation can similarly be observed [19, 67], and it was established that this radiation only occurs during the fast propagation phases of the cycle [19]. A direct example of such an emission is shown in Fig. 6, and its color could well correspond to the central wavelength λ_{peak} associated, via Wien's law [66], with a blackbody temperature compatible with our model:

$$\lambda_{\text{peak}} = \frac{b}{T_0 + \Delta T} \sim 400\,\text{nm}, \tag{11}$$

where b is Wien's displacement constant $\sim 0.0029\,\text{m K}$ and ΔT is about 7000 K at a load just passed the stick-slip threshold $G = 90\,\text{J m}^{-2}$ (see Fig. 5). The intensity of the observed light, which is visible in the dark but not under normal lightening, seems to also be consistent with the model. According to the Stefan–Boltzmann law [66], we indeed expect a radiated power in the order of

$$P = s(T_0 + \Delta T)^4 hl \sim 1\,\text{mW}, \tag{12}$$

where $s \sim 5.67\times10^{-8}\,\text{W m}^{-2}\,\text{K}^{-4}$ is the Stefan–Boltzmann constant, and h the tape width (2 cm) so that hl is the total area that significantly emits light. Note that such a power only accounts for a negligible part of the energy that is dissipated as the front advances, as $P/(GVh) \sim 10^{-4}$. For a human eye at a distance $D \sim 10\,\text{cm}$, it corresponds to a light luminance of about $eP/(4\pi D^2) \sim 1\,\text{cd m}^{-2}$, using a blackbody luminous efficacy [68] e of 100 lumens per watt. With a pupil opening of about $10\,\text{mm}^2$, such a luminance is in the order of 10 trolands (Td) [69], which does fit that of a flickering (i.e., the front has a stick-slip motion) radiation that is only visible in the dark, as those approximately range between 0.01 and 100 Td [69]. While the eye is persistent, a camera sensor of size $S \sim 10\,\text{mm}^2$, placed at the same distance, would capture an averaged power $\gamma PS/(4\pi D^2) \sim 100\,\text{nW}$, where $\gamma \sim 0.1$ is a typical ratio of time during which the front is in the fast phase compared to the total recording time, when peeling at a slow average velocity (i.e., $\sim 15\,\text{cm s}^{-1}$) [37]. The magnitude of this power is interestingly close to the 10 nW that were successfully measured by Camara et al. [67] for the luminescence of another adhesive roll.

For a given PMMA, Fuller et al. [70] also tried to quantify the temperature elevation around a quick fracture, both with the thermoluminescence technique and by using a liquid crystal coating on the matrix, whose color was thermosensitive [71]. For cracks propagating at $400\,\text{m s}^{-1}$ and faster, they measured heat efficiencies of about $2000\,\text{J m}^{-2}$, which is fairly compatible with the value we have derived for ϕG (a $400\,\text{m s}^{-1}$ speed is obtained for $G > 4000\,\text{J m}^{-2}$ in Fig. 3 and ϕ was inferred to be about 0.2). This experimental work [70] also estimated the instantaneous temperature elevation of the fractures to be about 500 K over a 0.5-µm-thick area around the front. Such a thickness for the heat source was however acknowledged to be rather uncertain, as the measure sensibility for this parameter was limited. We remark that the same energy spread on the $l \sim 10\,\text{nm}$ thickness which we have here inferred would give a temperature rise of 10^4 K and more, as predicted by our model (see Fig. 3).

Truly, fractoluminescence could emanate from other mechanisms than some hot matter radiation. It was for

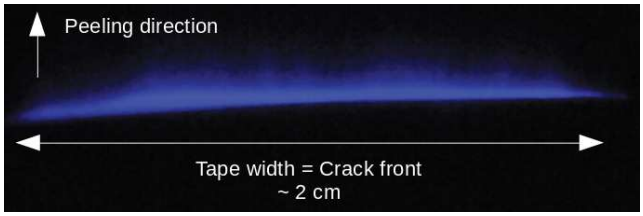

FIG. 6. Blue radiation emitted when quickly peeling tape beyond the stick-slip threshold (i.e., at an average velocity greater than 15 cm s^{-1}, see Fig. 5). This picture was captured in the dark by a standard reflex camera (ISO: 25600, shutter speed: 1/2 s, focal length: 60 mm, aperture: f/4). The low shutter speed ensures that enough light enters the camera, but then covers many stick-slip cycles of the peeling dynamics [37]. Such fractoluminescence could be the mark of a very hot crack front [40–42] when unrolling tape.

instance proposed [67, 72] that it partly arises from the molecules excitation of the fracture in situ air, by some electrical discharges between the two crack planes. Both these phenomena could surely coincide and, in any case, the light emission is an indication that some extreme and localised phenomena are at stake during fast failure. In that way, the thermodynamics model we propose holds some compatibility with that of Slepyan [2], where the abrupt advance of cracks derives from the emission of high frequency phonons, that excite atom bonds ahead of the tip, but that do not necessary thermalize.
Some relatively recent atomistic simulations [73] seem nonetheless to confirm that the atoms at a moving front can undergo a significant heat. In a modelled graphene, Budarapu et al. [73] thus inferred a 200 K temperature rise, over a $43\,\mathrm{nm} \times 43\,\mathrm{nm}$ area surrounding a running tip. This estimation is interestingly compatible with the thermal maps presented in Figs 3 and 5, for which the mean temperature is respectively 950 K and 350 K, when recomputed on a similar $1800\,\mathrm{nm}^2$ surface upon the front. Note that atomistic simulations might naturally be more proper than our mesoscopic description, in particular because the small scales (l) and high excitation frequencies (V/l) at play could call for more complicated models [74, 75] than plain Fourier diffusion, Arrhenius growth or blackbody radiation. Yet, atomistic simulations are by nature far heavier to run, requiring an accurate description of the atomic interactions onto femtosecond time steps.

B. Is a simple model too simple?

It is actually surprising that the proposed simple mesoscopic model can describe the propagation of cracks, when such a propagation, in reality, displays many complex phenomena. For instance, we have completely neglected the impact of crazing on the crack dynamics [36, 52], that is, the formation of defaults and fibrils at relatively large scales around the fracture front (i.e., a hundred of micrometers in PMMA and up to millimeters in PSA), while such large scale plasticity is often considered to have a strong effect on the growth of cracks (e.g., [36, 52]). Yet, crazing is not incompatible with our thermal weakening model, which only states that a significant part of the mechanical energy should be dissipated far closer to the crack front (i.e., over a few nanometers), and that this very local dissipation should be that of a first effect on the crack dynamics. In this description, crazing is then a consequence of the front progression rather than its main cause. In a similar way, many other known failure phenomena, such as the emission of mechanical waves during rupture [50], complicated creep laws from the corrosive interactions between the fracture fluid and the fracture tip (e.g., [46], chpt. 5.4), or the complexification of fronts at high propagation velocities [44], are not directly encompassed by Eqs. (4) and (5), but are not in conflict with the model either.

The simplicity of the model can actually be considered as one of its strength, as the physics that it describes could apply to many different materials and not only to polymers. Accurately testing this idea would however require the full (G, V) curves of more materials, and those are often not trivial to obtain experimentally at all velocities. Such experimental work could yet be rewarding, as we have here shown that matching the model to some (G, V) curves can give some valuable insights on the rupture of matter. Our quantification for each model parameter stays however rather approximate, and we have mainly derived their orders of magnitude. We have, in particular, assumed that they were all constant for a given material, while most could be velocity or temperature dependent [18, 24, 76]. For instance, the fact that PSA exhibits a larger scale viscous behavior (i.e., including fibrillation and heating over millimeters around the tip) at lower velocity [36] could indicate that the heat production size l decreases with the crack speed in this medium. It is especially known that the elastic moduli in PSA are strongly temperature dependent [62], and this was actually proposed by Maugis [21] and Carbone and Persson [24] as the driving cause for failure instability in rubber-like materials. We have, besides, considered both PMMA and PSA as homogeneously tough while G_c is bound to present some quenched disorder. While such heterogeneities should not affect the stable propagation branches, as long as G and V are then understood quantities which are averaged over a few G_c correlation lengths, it could be of importance for the accuracy of the loads at which the phase transitions occur [28], as slow cracks shall preferentially avalanche on weaker zones and fast cracks stop on stronger locations. In the case of PSA, we have furthermore considered that peeling was a cohesive process (i.e., that it occurs inside the adhesive), while a bi-materials interfacial model would be more appropriate, as the crack essentially propagates at the interface between the substrate and the glue [77].
These numerous limitations being stated, the parameters we have inverted are nonetheless in rather satisfying orders of magnitude, confirming the physical relevance of the model. Indeed, the intrinsic fracture energy in both materials $U_c = d_0^3 G_c/(2\xi)$ is comparable to one electron-volt, which is typical for an energy that bonds atoms (e.g., see appx. E in Ref. [6]). Because our proposed description is statistical, one should remember that U_c is a mean material feature, for a rupture process that is made of several types of bond breaking. As a rough example, $U_c \sim 1\,\mathrm{eV}$ may indicate that the crack consummates in average three weak links (such as hydrogen or Van des Waals bonds of respective energies [6] ~ 0.1 and $\sim 0.01\,\mathrm{eV}$) for every stronger connection that snaps (say, one C–C link of an acrylic chain, of covalence energy [6] $\sim 4\,\mathrm{eV}$). The nanometric scale l for the heat generation may well correspond to the typical entanglement density in polymers [57] (the density of polymeric chains crossing points in the matrix), below which atoms have more freedom to vibrate, and which is known to affect some

rupture properties (e.g., [52, 57]). It is also coherent that the generation of heat was inferred to occur over a length scale comparable to ξ, the equivalent radius describing the energy shielding of the tip. We have indeed derived that the former is a strong cause for the latter, as the heat efficiency ϕ was inverted to be non negligible (i.e., $\phi \sim 0.2 - 1$).

C. Tip stress and front shielding

A nanometric scale (i.e., comparable to ξ or l) has been noteworthily observed in the rupture of other materials. One example is the length scale of a light radiating (and hence likely thermal) zone around running fracture tips in glass [42]. In carbonate rocks, it is also the typical size of some observed nanograins that form along sliding seismic fault planes [78]. Such a nano-damage explains the glossy and reflective aspect displayed by some faults (often referred to as fault mirrors), as their typical surface roughness is then comparable to the wavelengths of visible light. The origin of this damage, however, is debated as, below 1 µm, plasticity is expected to dominate over brittleness in this material and asperities should hence deform rather than break. Noteworthily, some intense thermal effects, arising from the frictional heat, such as some fast melting and cooling or the thermal decomposition of carbonates, were proposed to solve this apparent paradox [79].

Similarly, for the materials that we have here studied, the usual predictions for the size of the shielding process zones are far larger than ξ. In PMMA, for instance, it is in the order of $\xi_{\text{macro}} \sim GE/\sigma_y^2 \sim 200\,\mu\text{m}$, where $\sigma_y \sim 100\,\text{MPa}$ is the tensile yield stress of the bulk polymer and $E \sim 3\,\text{GPa}$ its Young modulus [55]. However, in that description, σ_y is a stress that is averaged over a macroscopic sample, and is likely not representative of the actual energy density around the defaults of this sample. It was notably reported that a Dugdale [80] like cohesion model (i.e., σ is homogeneously equal to σ_y in a process zone of radius ξ_{macro}), poorly accounts for fast rupture in PMMA [81]. Naturally, ξ_{macro} is still to bear some significance, in particular as a characteristic length scale for crazing in acrylic glass [52], where a portion within $(1 - \phi)$ of the release rate G is to be dissipated, either by the creation of dislocations [51], the emission of waves [42, 50] or residual thermal effects. But ξ was inverted as an equivalent size, only defined by $2\xi/d_0 = N$ with N the damping of the tip potential energy U due to the energy dissipation. We solely inverted N to be around 100 and 500 for respectively PSA and PMMA, and many links might well snap and heal far away from the tip, allowing for crazing.

Still, most of the rupture is likely to occur very close to the front where the stress is to be the highest. We can estimate such a stress at the tip by considering a simplified expression for the elastic energy stored in rupturing bonds:

$$U \sim d_0^3 \frac{\sigma^2}{2E}, \tag{13}$$

which, with Eq. (3), is equivalent to the well known form for the limitation of an otherwise divergent stress at the tip of cracks, predicted by the general elasticity theory (e.g., [46]):

$$\sigma \sim \sqrt{\frac{GE}{\xi}}. \tag{14}$$

In the case of PMMA, such a computed stress is as high as 7 GPa, and we thus predict a high atomic strain σ/E of about 200% at the onset to fast rupture (i.e., for U equal to $U_c/1.8$ as per Tab. I). Such a strain shall be likely at a fracture tip for the strong intermolecular deformation immediately before failure. Of course, the simply linear elastic Eq. (13) is unlikely to be valid at 200% strain, and we also considered describing U with a Morse potential [82], that is

$$\frac{U}{U_c} \sim \left(1 - \exp\left[-\sqrt{\frac{Ed_0}{2U_c}}(d - d_0)\right]\right)^2, \tag{15}$$

which, at the onset of fast rupture, predicts a strain $(d - d_0)/d_0 \sim 400\%$. While this dual-particles potential stays, by nature, a strong approximation in the complex rupture of a polymer, it is worth reminding that the model which we have introduced does not rely on a particular shape of the inter-atomic potentials (i.e., neither on Eq. (13) or on Eq. (15)), but only on their average dissociation energy U_c.

D. Front complexification

Overall, our derivation of $\xi \ll \xi_{\text{macro}}$ only suggests that process zones are heterogeneous objects, dissipating a higher density of energy in their centre than at their periphery. In particular, it was shown that a few tens of micrometers (i.e., a portion of ξ_{macro}) is a typical distance at which the secondary micro-cracks nucleate from the main front in PMMA [33] and, as shown in Fig. 4, the imaging of some postmortem rupture surfaces reveals that these micro-cracks initially grow from isolated spherical cavities at their centre, of radius about 300 nm. We here propose that such cavities could correspond to bubbles, forming by sublimation [83] on weak locations of the process zone, and leading to some micro-fractures once having grown to a critical size. While remaining to be confirmed, such a sublimation process would definitely require some local but very high temperatures in the crazing area. Indeed, to nucleate ahead of the main front, the observed cavities have to form during less than $\xi_{\text{macro}}/V \sim 1\,\mu\text{s}$, and the pyrolysis of PMMA to methyl methacrylate (MMA) only reaches such a reaction

rate at temperatures T_b that are beyond 1000 kelvins [83]. In return, and assuming that the ideal gas law approximately applies (e.g., [17], chpt. 4), some bubbles forming at this temperature would hold an internal pressure $\rho R T_b/M$, where $M = 0.1\,\mathrm{kg\,mol^{-1}}$ is the MMA molecular mass [84], $\rho = 1200\,\mathrm{kg\,m^{-3}}$ is the volumetric mass of the solid PMMA [55] and R is the ideal gas constant. This value computes to at least 100 MPa, which is comparable to the surrounding bulk compressive strength [55]. The evolution from pressurised pores to propagating micro-cracks would then be coherent.

Thus, in addition to explaining, as shown in this work, the first order dynamics of singular fronts, concentrated thermal processes could also be responsible for their complexification at high propagation velocities. In the case of acrylic glass, we have notably inferred (see section III B) that the appearance of the secondary fronts approximately coincides with energy release rates that are close to the (modelled) intrinsic barrier G_c. This concomitance could be explained by the need for new dissipation processes, when cracks propagate over-critically ($G > G_c$) so that some extra energy is brought to the rupture system. Such an idea is notably re-enforced by the fact that the density of nucleated micro-cracks was inferred to be proportional to a value comparable to $G - G_c$, as shown by Guerra et al. [33].

V. CONCLUSION AND PERSPECTIVES

We presented a new and general model for the kinetics of cracks. The main physical elements that were introduced in this model are, only, a sub-critical (Arrhenius-like) growth rate and the dissipation and diffusion of heat around fracture tips (where the applied mechanical stress is concentrated), an immediate consequence of the latter being the possibility for crack fronts to reach thousands of degrees temperatures. Interestingly, these different elements have, separately, long been considered or observed in the physics of rupture (e.g., [7, 18, 39, 85]), but had not previously been combined for comparison with some experimental data. In doing so, we here showed that the rupture of two materials (namely, PMMA and PSA) can be quantitatively reproduced over many decades of propagation velocities, from slow creep regime to fast propagation.

Thus, we inferred that the propagation of a crack can be sub-critical, even at velocities approaching that of the mechanical waves in the surrounding matrix, due to its potentially very high tip temperature. We also suggested that the microscopic healing process around a fracture front can significantly constrain the fast velocity regime, from the strong thermal activation at such temperatures, while it is often considered that healing is only relevant for very slow cracks. The existence of thousands of degree temperatures is actually supported by many experimental works that study the visible fractoluminescence of fast fronts [40–42, 70]. In some instance [73], it has also been modelled by some atomistic simulations, and we additionally showed, in the present work, the existence of bubble forming in the process zones of cracks in PMMA. We proposed that these bubbles could well originate from some local sublimation of the polymer near crack tips. As they are located at the nucleation centres of secondary fracture fronts, we also suggested that the complexification of cracks at high velocities could derive, as the rest of the propagation dynamics, from some thermally activated processes. Finally, for the two materials that we have studied, we have inferred that the mechanical stress around cracks remains an increasing quantity inside the process zones up to a few nanometers from the tip. Such a nanometric scale matches the typical size over which the heat was inferred to be generated, making thermal dissipation the likely main process that shields rupture fronts from mechanical failure.

In theory, the model could be reversed, and the fast propagation of cracks under a minimum load could be triggered by a very local heating of their fronts. Related experiments could for instance be performed with localized light pulses on material that are thin or transparent enough, for the heat elevation to be controlled. Certainly, elevated ambient temperatures are known to have a strong impact on the kinetics of fractures, both in the lab (e.g., [30, 86]) and in nature [87].

Noteworthily, the proposed model, and its ability to explain some actual crack dynamics, stresses the importance of the heat conductivity of materials on their macroscopic strength. A high conductivity indeed allows to evacuate the extra internal energy away from the fronts, thus delaying any thermal weakening. As a general statement, many strong materials happen to be good conductors, such as metals, graphene [88] or spider silk [89]. For the latter, it was in particular shown that, contrarily to most materials, its conductivity actually increases with deformation [89], which could well be a natural defence mechanism for the stability of arachnid webs. Designing human-made solid matrices that can replicate such a behavior on the molecular scale could then become a new important target of material sciences.

Finally, we suggest that most of the physics that we have introduced to study mode I fractures shall also be valid for mixed-mode fracturing as well as for solid friction. The latter is actually suspected to hold some non negligible, thermal related, weakening mechanisms (e.g., [90]), which could notably be a key in geophysics in understanding the stability of seismic faults. Such mechanisms might be diverse, and may include the thermal pressurisation of fault fluids [91, 92] or some changes in the fault planes minerals phase (i.e., such as melting or thermal decomposition) [93]. We propose that they could also be related to a thermally boosted sub-critical slip, in the sense of statistical physics and similarly to the model we have here developed.

ACKNOWLEDGEMENTS AND CONTRIBUTIONS

T.VD. developed and analysed the model and redacted the manuscript. R.T. proposed the physical basis of the model and its mathematical formulation. A.C. worked on its numerical implementations. D.B. and L.H. provided the PMMA data and images. S.S. and L.V. gave direct insights on the tape experiments. K.J.M. and E.G.F. contributed in the interpretation of the model in fracture mechanics applications. All authors participated to the redaction of the manuscript and agreed with the submitted version. The authors declare no competing interests in the publishing of this work. We acknowledge and are grateful for the support of the IRP France-Norway D-FFRACT, of the Universities of Strasbourg and Oslo and of the CNRS INSU ALEAS program. We thank the Research Council of Norway through its Centres of Excellence funding scheme, project number 262644. We are also thankful for the support of the Russian Government, through its grant number 14.W03.31.0002. Readers are most welcome to contact the authors for discussion.

Appendix A: Method for the measure of crack velocity versus energy release rate in PMMA

As part of the PMMA data was not published before (i.e., the slow propagation branch), we describe, in this section, the method that was used to acquire it.
Wedge splitting fracture tests are used to measure both the slow and fast $V(G)$ branches in PMMA [32, 54], whose geometry is shown in Fig. 7. Rectangular plates of size 140 mm × 125 mm × 15 mm are first machined from a plate of moulded PMMA (Perspex®). A 25 mm × 25 mm notch is subsequently cut out on one of the two lateral edges and a 8-mm-long 800-µm-thick groove is finally introduced in the middle of the notch with a diamond saw. To grow slow cracks, an additional seed crack ($\sim$ 2 mm-long) is added at the end of the groove via a razor blade. This crack is loaded in tension by pushing a steel wedge (semi-angle of 15°) in the notch. Two steel blocks equipped with rollers are placed in between the wedge and the specimen notch to limit the parasitic mechanical dissipation through plastic deformations or friction at loading contacts. As a result, the vicinity of the crack tip can be assumed to be the sole dissipation source for mechanical energy in the system. The wedge speed is first set to 1.6 µm s^{-1}. The force F, applied by the wedge to the specimen, increases linearly with time up to a point F_c above which the seed crack starts to propagate. Above this point, F decreases with time. We let the crack propagate over a distance of about 10 mm. This ensures reproducible initial conditions with a long-enough well-defined sharp seed crack. The specimen is then unloaded (unloading wedge speed: 16 µm s^{-1}). The specimen is then loaded again at a constant prescribed wedge speed V_{wedge}, which has been varied from 1.6 µm s^{-1} to 1.2 mm s^{-1}.

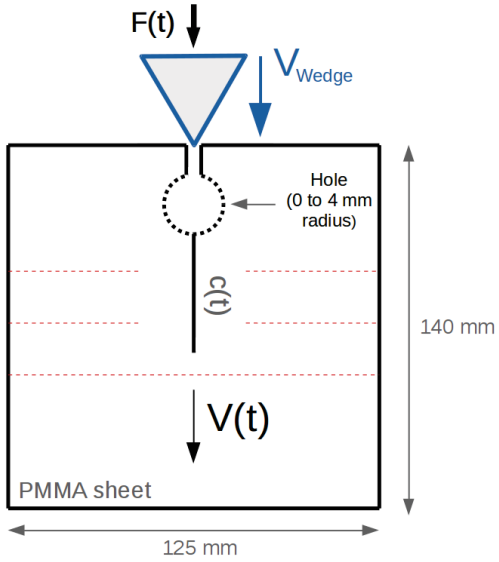

FIG. 7. Schematic of the experimental set-up used to measure the crack energy release rate G and its corresponding propagation velocity $V(t)$ in PMMA. See Refs. [32, 54] for details. The hole is used to store some potential energy in the PMMA sheet for fast propagation experiments and is replaced by only a seed crack for slow ones. The dashed horizontal lines represent conductive metallic lines deposited onto the sample to measure the fast crack velocity with an oscilloscope.

During each fracture test, the force $F(t)$ is monitored in real-time via a cell force mounted on the system (S-type Vishay load cell). A camera (USB2 uEye from IDS) is also used to image crack propagation at the specimen surface (space and time accuracy of 125 µm and 0.1 s). A coarse approximation of the crack speed can be obtained by differentiating the position of the crack tip observed on the successive images. However, a more accurate signal $V(t)$ is obtained from the force signal (see Ref. [94] for details on the method). Indeed, in a linear elastic isotropic material like PMMA, the specimen stiffness $k(t) = F(t)/(V_{\text{wedge}}t)$ is a continuous decreasing function of the crack length, $c(t)$, that is set by the specimen geometry only. This function has been obtained using finite element calculations on the exact experimental geometry (Cast3M software, 2D simulation assuming plane stress conditions); it was checked that the obtained k versus c curve coincides with the experimental curves obtained by plotting $k(t)$ as a function of the crack length measured by the camera. The idea is then to use this curve $k(c)$, and the corresponding inverse function k^{-1}, to infer the time evolution of crack length $c(t)$ from the signal $F(t)$: $c(t) = k^{-1}[F(t)/(V_{\text{wedge}}t)]$. Time derivation of the so-obtained $c(t)$ provides a signal $V(t)$ about 50 times less noisy than that directly obtained from the camera images. The knowledge of $c(t)$ and $F(t)$ also allows determining the time evolution of the energy release rate, $G(t)$. Indeed, the total amount of mechanical energy provided to the specimen is $F^2(t)/[2k(c(t))]$. Dif-

ferentiating this stored energy with respect to c directly provides $G(t)$. The slow branch of Fig. 3 then provides the observed $V(t)$ as a function of $G(t)$. The results from twelve fracture experiments are gathered in this branch and differ by their V_{wedge} value.
To grow fast cracks and measure $V(G)$ in the fast stable phase, the seed crack has been replaced by a hole of tunable radius (1 to 4 mm) drilled at the end of the groove [32]. This delays fracture and increases the potential energy stored in the specimen at the initiation of crack growth. The time evolution of $V(t)$ is measured by monitoring, via an oscilloscope, the successive rupture of parallel 500-µm-large metallic lines (chromium/gold) deposited on the surface. That of the stress intensity factor K is obtained via finite element analysis (see Ref. [32] for details). The time evolution of the mechanical energy release rate is then deduced: $G = K^2/E$ where the Young modulus E in the studied PMMA have been measured to be $E = 2.8\,\text{GPa}$. The fast branch of Fig. 3 then provides the observed $V(t)$ as a function of $G(t)$. The results from five fracture experiments are gathered in this branch; they differ by the amount of stored elastic energy at crack growth initiation.

Appendix B: Parameters sensitivity

We here show, on the PMMA data, how varying the model parameters around their inferred values impacts the model fit, thus giving the reader a better feeling for their individual effect and sensitivity. In each of the figures 8 to 14, a unique parameter of the model varies while the others are kept to the exact values used for the fit presented in Fig. 3: $\xi = 56\,\text{nm}$, $V_0 = 880\,\text{m s}^{-1}$, $G_c = 1275\,\text{J m}^{-2}$, $G_h = 650\,\text{J m}^{-2}$, $\phi = 20\%$, $\lambda = 0.18\,\text{J s}^{-1}\,\text{m}^{-1}\,\text{K}^{-1}$, $C = 1.5 \times 10^6\,\text{J m}^{-3}\,\text{K}^{-1}$, $l = 1\,\text{nm}$ and $T_0 = 296\,\text{K}$. These seven plots show the fits up to the apparition of the secondary micro-cracks (see section III B and Fig. 4), after which the model does not apply as such. Naturally, some care should be taken when interpreting the inverted parameters (i.e., ξ, G_c, G_h, ϕ and l) beyond their actual orders of magnitude. For instance, ξ and G_c were fitted by a linear regression (i.e., Eq. (8)) on the data which lies between $G = 350$ and $G = 700\,\text{J m}^{-2}$ in Fig. 3, and the above values ($\xi = 56\,\text{nm}$ and $G_c = 1275\,\text{J m}^{-2}$) were obtained with a coefficient of determination R^2 equal to 0.85. Allowing R^2 to drop down to 0.75 during this fit gives ξ in a 30 to 80 nm range and G_c between 950 and $1500\,\text{J m}^{-2}$. G_h being directly deduced from G_c (and from the vertical asymptote at low velocity in Fig. 3), the uncertainty on its value is comparable to that of G_c, that is, a few hundreds of joules per square meter. Let us

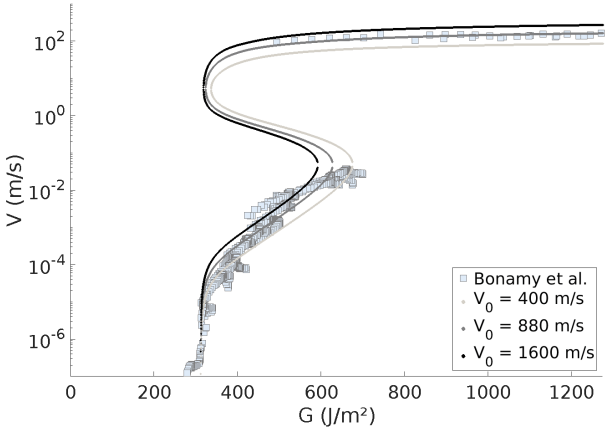

FIG. 8. Effect of varying the nominal velocity, V_0, on the fit to the PMMA data. The propagation velocity is roughly proportional to V_0, but also modifies the positions of the phase transitions.

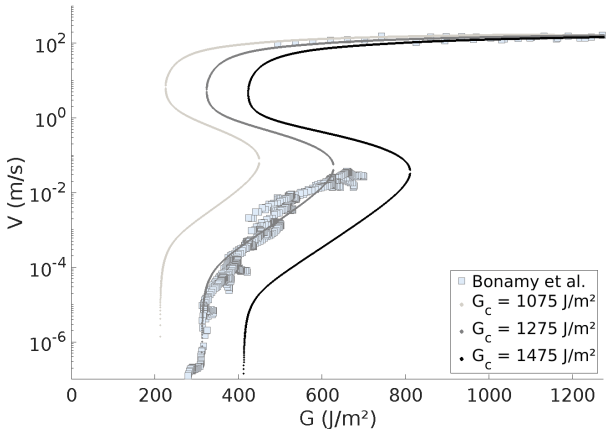

FIG. 9. Effect of varying the breaking energy barrier, G_c, on the fit to the PMMA data. At a given load G, the higher G_c, the slower the crack. The transitions between the three propagation modes (fast, slow, and dominated by healing) are also affected: a medium with a stronger barrier needs a heavier load to transit to a weaker state.

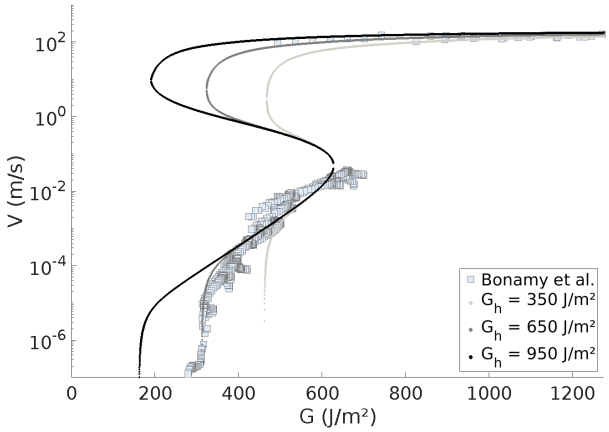

FIG. 10. Effect of varying the healing energy barrier, G_h, on the fit to the PMMA data. A crack that heals more easily needs a higher load to actually propagate forward or to stay in the high velocity regime.

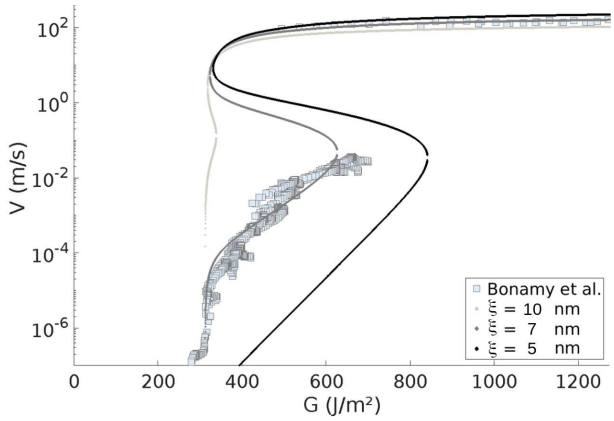

FIG. 11. Effect of varying the stress cut-off scale ξ, on the fit to the PMMA data. ξ mainly controls the slope and the intercept of the low velocity branch. A small change in ξ significantly modifies this branch as well as the threshold to the fast regime.

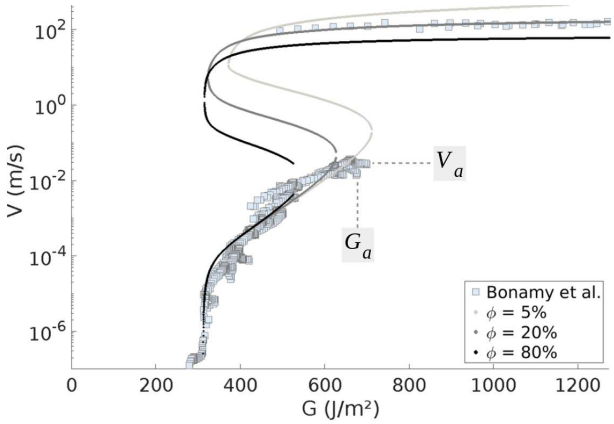

FIG. 12. Effect of varying the ratio of energy converted to heat, ϕ, on the fit to the PMMA data. The maximum velocity increases with ϕ as the tip temperature is higher. The threshold from the slow to the fast branch (i.e., the (G_a, V_a) point) shifts towards a lower G as a lighter load is required for the temperature to significantly deviate from T_0.

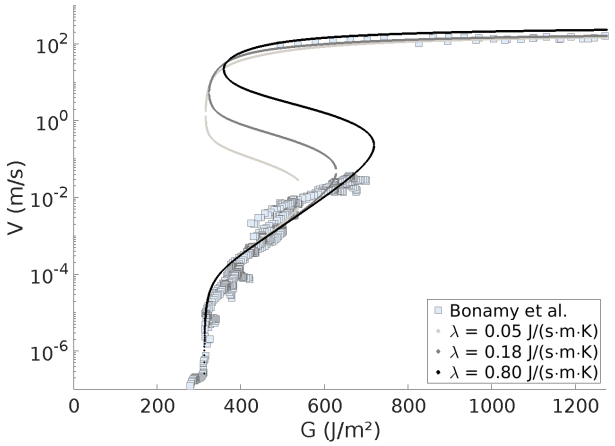

FIG. 13. Effect of varying the thermal conductivity, λ, on the fit to the PMMA data. With a higher λ, the heat is better evacuated: the slow to fast branch threshold shifts towards higher G and V. The fast regime is not very sensitive to λ, as ΔT is there constrained by l.

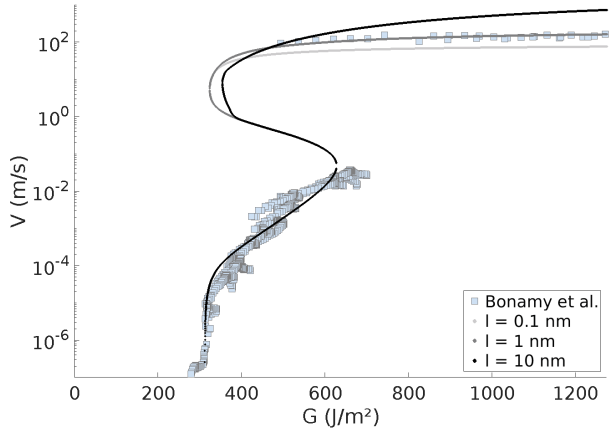

FIG. 14. Effect of varying the heat production zone radius, l, on the fit to the PMMA data. l mainly impacts the plot curvature on the high velocity branch. No effect is observed on the slow branch, as the thermal elevation there is constrained by the diffusion skin depth rather than by l (see Eq. (6)).

now assess the accuracy of ϕ. In the model, this parameters mainly controls which is the fastest point of the slow velocity branch (e.g., as shown in Fig. 12), after which cracks have to avalanche [28]. We then compare the experimental value for this particular point (obtained at $G = G_a$ and $V = V_a$, see Fig 12) to the model prediction of the same point. We quantify the error there as the euclidean distance between these points, in the sense of Eq. (9). Such a relative, unitless, error minimizes to 10% for $\phi = 0.25$ and, should we allow it to rise up to 30%, we obtain ϕ to be between 0.15 and 0.30. Finally, let us assess the accuracy of the inversion for the length scale of the heat production zone l. We vary l and compute the same relative euclidean error in average over the fast velocity branch (i.e., the location where the model is mostly sensitive to l, see Fig. 14). This error now minimizes to 5% for $l = 1\,\text{nm}$ and, letting it reach 30%, we infer l to lie in a 0.1 nm to 2 nm range.

These uncertainties in the parameter inversion are somewhat high, but we here quantify an atomic scale process based on macroscopic measurements, so that this is not particularly surprising. One also needs to add up the experimental inaccuracy for V and G (see the data spread in Fig. 3), as well as the limitations of our very first order physical model, as discussed in section IV B. Still, overall, the data is well explained over eight decades of velocities and with parameters that are in physically reasonable orders of magnitude.

Appendix C: Data binning to compute a mean fit error

To compute a mean fit error $\bar{\varepsilon} = \text{mean}_d(\varepsilon_d)$, where ε_d is defined by Eq. (9), we first binned the PMMA and PSA data points onto coarse bins using a running average on both stable branches, as explained in the core text (see section III). This was done to avoid the densely populated parts of the data sets to dominate on the value of the inferred $\bar{\varepsilon}$. Figures 15 and 16 show the result of this data decimation.

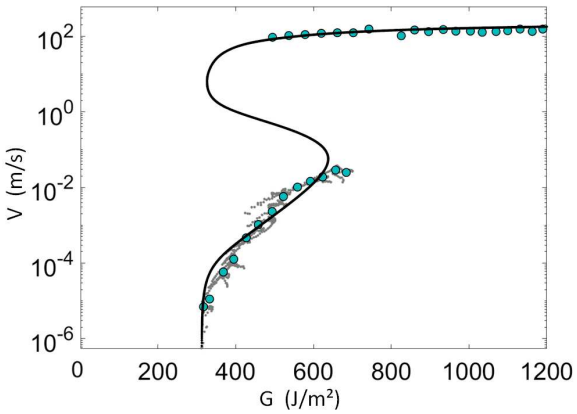

FIG. 15. Under sampled PMMA data (blue circles), using a running average on 40 J m^{-2} bins. The dots are the original data points and the black line the fitted model. With this decimated data set, the mean fitting error is $\bar{\varepsilon} = 4\%$. The data is only shown to the onset of micro-cracking (i.e., see section III B), beyond which the model does not apply as such.

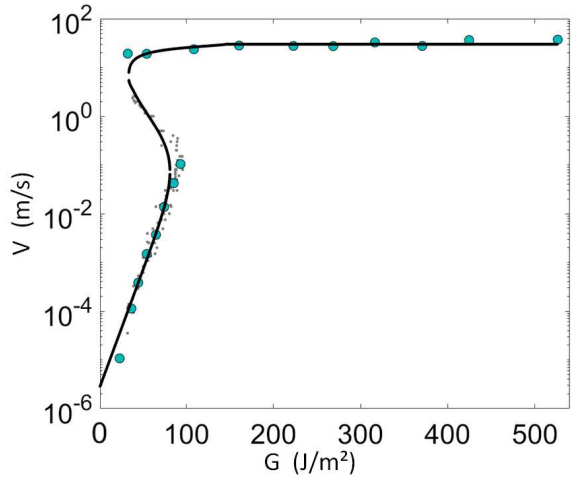

FIG. 16. Under sampled PSA data (blue circles), using a running average on 10 J m^{-2} bins. The dots are the original data points and the black line the fitted model. With this decimated data set, the mean fitting error is $\bar{\varepsilon} = 5\%$.

Appendix D: Healing processes in tape

We considered the healing processes to be negligible in order to describe the dynamics of unrolling tape, as no low velocity constant G asymptote arising from crack healing displays in the (G, V) data (i.e., in Fig. 5). Such an absence would, however, also happen if G_c was to be smaller than G_h, as the asymptote is obtained for $(G_c - C_h)/2$. Thus, the healing energy barrier could still be comparable to the breaking one, and so still significantly impact the high velocity propagation branch, when the crack tip is hot enough for healing to be non negligible (as predicted by Eq. (4)). Of course, an accurate quantification of this effect suffers from the absence of the asymptote as it is the only good constraint for G_h. Figure 17 shows for instance a model

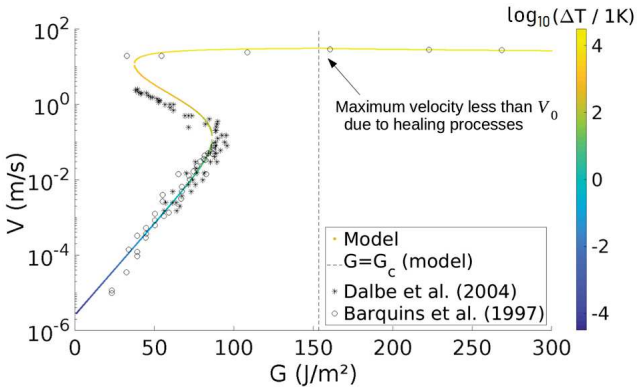

FIG. 17. Fit of the Scotch® 3M 600 data [19, 37] with a model including healing processes. The unstable (middle) branch of the model should not necessarily match the data point which are averaged G and V values for a front that stick-slips.

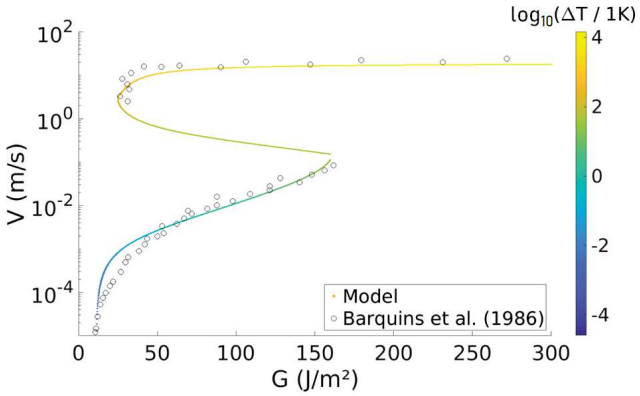

FIG. 18. Fit of the peeling data for another roller tape: Scotch® 3M 602 data [95]. The lack of linearity at low velocity calls for healing processes in our model. Note also the curvature on the lower end of the high velocity branch, not present in the other data sets that we show but rather compatible with our proposed model.

not disregarding healing, and compares it with the tape

data. The match is there improved compared to the fit presented in Fig. 5 as we have now an additional degree of freedom. The fit parameters in this figure are as follow: $\xi = 9\,\mathrm{nm}$, $V_0 = 70\,\mathrm{m\,s^{-1}}$, $G_c = 154\,\mathrm{J\,m^{-2}}$, $G_h = 200\,\mathrm{J\,m^{-2}}$, $\phi \sim 1$, $\lambda = 0.2\,\mathrm{J\,s^{-1}\,m^{-1}\,K^{-1}}$, $C = 10^6\,\mathrm{J\,m^{-2}\,K^{-1}}$, $l = 1\,\mathrm{nm}$ and $T_0 = 296\,\mathrm{K}$.
Note that Barquins et al. [95], who released part of the data presented in Fig. 17, also provided similar measurements for another type of roller tape, Scotch® 3M 602 (see Ref. [95], in French). For this new medium, an asymptote does seem to display at low velocity on the $(G,\ V)$ plot, calling for healing processes in our description, as shown in Fig. 18. We there propose a fit with the following parameters: $\xi = 40\,\mathrm{nm}$, $V_0 = 200\,\mathrm{m\,s^{-1}}$, $G_c = 500\,\mathrm{J\,m^{-2}}$, $G_h = 480\,\mathrm{J\,m^{-2}}$, $\phi = 60\%$, $\lambda = 0.3\,\mathrm{J\,s^{-1}\,m^{-1}\,K^{-1}}$, $C = 10^6\,\mathrm{J\,m^{-3}\,K^{-1}}$, $l = 1\,\mathrm{nm}$ and $T_0 = 296\,\mathrm{K}$.

[1] A. Griffith. The Phenomena of Rupture and Flow in Solids. *Philosophical Transactions of the Royal Society of London A: Mathematical, Physical and Engineering Sciences*, 221(582-593):163–198, January 1921. ISSN 1471-2962. doi:10.1098/rsta.1921.0006.

[2] L.I. Slepyan. Dynamics of a crack in a lattice. *Soviet Physics, Doklady*, 26:538–540, 1981.

[3] Sh. A. Kulakhmetova, V. A. Saraikin, and L. I. Slepyan. Plane problem of a crack in a lattice. *Mechanics of Solids*, 19:102–108, 1984.

[4] M. Marder. Slepyan's dynamic contribution to studies of fracture. *Philosophical Transactions of the Royal Society A: Mathematical, Physical and Engineering Sciences*, 2019.

[5] M. Marder and S. Gross. Origin of crack tip instabilities. *Journal of the Mechanics and Physics of Solids*, 43(1):1 – 48, 1995. ISSN 0022-5096. doi:10.1016/0022-5096(94)00060-I.

[6] G. B. Kaufman. Inorganic chemistry: principles of structure and reactivity, 4th ed. *Journal of Chemical Education*, 70(10):A279, 1993. doi:10.1021/ed070pA279.1.

[7] S. S. Brenner. Mechanical behavior of sapphire whiskers at elevated temperatures. *Journal of Applied Physics*, 33 (1):33–39, 1962. doi:10.1063/1.1728523.

[8] S. N. Zhurkov. Kinetic concept of the strength of solids. *International Journal of Fracture*, 26(4):295–307, Dec 1984. ISSN 1573-2673. doi:10.1007/BF00962961.

[9] W. Döll and L. Könczöl. Micromechanics of fracture under static and fatigue loading: Optical interferometry of crack tip craze zones. In *Crazing in Polymers Vol. 2*, pages 137–214. Springer Berlin Heidelberg, 1990. ISBN 978-3-540-46192-0.

[10] L. Golubović and S. Feng. Rate of microcrack nucleation. *Phys. Rev. A*, 43:5223–5227, May 1991. doi: 10.1103/PhysRevA.43.5223.

[11] Y. Pomeau. Brisure spontanée de cristaux bidimensionnels courbés. *Compte Rendu de l'Académie des Sciences Paris*, 314 II:553–556, 1992.

[12] S. Roux. Thermally activated breakdown in the fiber-bundle model. *Phys. Rev. E*, 62:6164–6169, Nov 2000. doi:10.1103/PhysRevE.62.6164.

[13] S. Santucci, L. Vanel, and S. Ciliberto. Subcritical statistics in rupture of fibrous materials: Experiments and model. *Phys. Rev. Lett.*, 93:095505, Aug 2004. doi: 10.1103/PhysRevLett.93.095505.

[14] L. Vanel, S. Ciliberto, P.-P. Cortet, and S. Santucci. Time-dependent rupture and slow crack growth: elastic and viscoplastic dynamics. *Journal of Physics D: Applied Physics*, 42(21):214007, oct 2009. doi:10.1088/0022-3727/42/21/214007.

[15] O. Lengliné, R. Toussaint, J. Schmittbuhl, J. E. Elkhoury, J. P. Ampuero, K. T. Tallakstad, S. Santucci, and K. J. Måløy. Average crack-front velocity during subcritical fracture propagation in a heterogeneous medium. *Phys. Rev. E*, 84:036104, Sep 2011. doi: 10.1103/PhysRevE.84.036104.

[16] A. Cochard, O. Lengliné, K. J. Måløy, and R. Toussaint. Thermally activated crack fronts propagating in pinning disorder: simultaneous brittle/creep behaviour depending on scale. *Philosophical Transactions of the Royal Society A: Mathematical, Physical and Engineering Sciences*, 377(2136):20170399, 2019. doi: 10.1098/rsta.2017.0399.

[17] G. G. Hammes. *Principles of Chemical Kinetics*. Academic Press, 1978. ISBN 978-0-12-321950-3. doi: 10.1016/B978-0-12-321950-3.50005-0.

[18] G. P. Marshall, L. H. Coutts, and J. G. Williams. Temperature effects in the fracture of PMMA. *Journal of Materials Science*, 9(9):1409–1419, Sep 1974. ISSN 1573-4803. doi:10.1007/BF00552926.

[19] M. Barquins and M. Ciccotti. On the kinetics of peeling of an adhesive tape under a constant imposed load. *International Journal of Adhesion and Adhesives*, 17(1): 65 – 68, 1997. ISSN 0143-7496. doi:10.1016/S0143-7496(96)00020-6.

[20] D. Maugis and M. Barquins. Fracture mechanics and the adherence of viscoelastic bodies. *Journal of Physics D: Applied Physics*, 11(14):1989–2023, oct 1978. doi: 10.1088/0022-3727/11/14/011.

[21] D. Maugis. Subcritical crack growth, surface energy, fracture toughness, stick-slip and embrittlement. *Journal of Materials Science*, 20(9):3041–3073, Sep 1985. ISSN 1573-4803.

[22] E. Orowan. Energy criteria of fracture. Technical report, Massachusetts Institute of Technology, Cambridge Departement of Mechanical Engineering, 1954.

[23] G. R. Irwin. Analysis of stresses and strains near the end of a crack traversing a plate. *Journal of Applied Mechanics*, 24:361–364, 1957.

[24] G. Carbone and B. N. J. Persson. Hot cracks in rubber: Origin of the giant toughness of rubberlike materials. *Phys. Rev. Lett.*, 95:114301, Sep 2005. doi: 10.1103/PhysRevLett.95.114301.

[25] G. Carbone and B. N. J. Persson. Crack motion in viscoelastic solids: The role of the flash temperature. *The European Physical Journal E*, 17:261 – 281, 2005. doi: 10.1140/epje/i2005-10013-y.

[26] S. Santucci, P.-P. Cortet, S. Deschanel, L. Vanel, and S. Ciliberto. Subcritical crack growth in fibrous materials. *Europhysics Letters (EPL)*, 74(4):595–601, may 2006. doi:10.1209/epl/i2005-10575-2.

[27] R. Toussaint, O. Lengliné, S. Santucci, T. Vincent-Dospital, M. Naert-Guillot, and K. J. Måløy. How cracks are hot and cool: a burning issue for paper. *Soft Matter*, 12:5563–5571, 2016. doi:10.1039/C6SM00615A.

[28] T. Vincent-Dospital, R. Toussaint, A. Cochard, K. J. Måløy, and E. G. Flekkøy. Thermal weakening of cracks and brittle-ductile transition of matter: A phase model. *Physical Review Materials*, 02 2020. doi:10.1103/PhysRevMaterials.4.023604.

[29] C. H. Scholz. The brittle-plastic transition and the depth of seismic faulting. *Geologische Rundschau*, 77(1):319–328, Feb 1988. ISSN 1432-1149. doi:10.1007/BF01848693.

[30] A. G. Atkins, C. S. Lee, and R. M. Caddell. Time-temperature dependent fracture toughness of PMMA. *Journal of Materials Science*, 10:1394–1404, 1975. ISSN 1573-4803. doi:10.1007/BF00540830.

[31] J. Fineberg, S. P. Gross, M. Marder, and H. L. Swinney. Instability in dynamic fracture. *Physical Review Letters*, 67(4):457–460, jul 1991. doi:10.1103/physrevlett.67.457.

[32] J. Scheibert, C. Guerra, F. Célarié, D. Dalmas, and D. Bonamy. Brittle-quasibrittle transition in dynamic fracture: An energetic signature. *Phys. Rev. Lett.*, 104: 045501, Jan 2010. doi:10.1103/PhysRevLett.104.045501.

[33] C. Guerra, J. Scheibert, D. Bonamy, and D. Dalmas. Understanding fast macroscale fracture from microcrack post mortem patterns. *Proceedings of the National Academy of Sciences*, 109(2):390–394, 2012. ISSN 0027-8424. doi:10.1073/pnas.1113205109.

[34] K. J. Måløy, S. Santucci, J. Schmittbuhl, and R. Toussaint. Local waiting time fluctuations along a randomly pinned crack front. *Phys. Rev. Lett.*, 96:045501, Jan 2006. doi:10.1103/PhysRevLett.96.045501.

[35] K. T. Tallakstad, R. Toussaint, S. Santucci, J. Schmittbuhl, and K. J. Måløy. Local dynamics of a randomly pinned crack front during creep and forced propagation: An experimental study. *Phys. Rev. E*, 83:046108, 04 2011.

[36] C. Creton and C. Ciccotti. Fracture and adhesion of soft materials: a review. *Reports on Progress in Physics*, 79(4):046601, mar 2016. doi:10.1088/0034-4885/79/4/046601.

[37] M.-J. Dalbe, S. Santucci, P.-P. Cortet, and L. Vanel. Strong dynamical effects during stick-slip adhesive peeling. *Soft Matter*, 10:132–138, 2014. doi:10.1039/C3SM51918J.

[38] V. De Zotti, K. Rapina, P.-P. Cortet, L. Vanel, and S. Santucci. Bending to kinetic energy transfer in adhesive peel front microinstability. *Phys. Rev. Lett.*, 122: 068005, Feb 2019. doi:10.1103/PhysRevLett.122.068005.

[39] J. R. Rice and N. Levy. Local heating by plastic deformation at a crack tip. In *Physics of Strength and Plasticity*, pages 277–293. M.I.T. Press, Cambridge, Mass., 1969.

[40] R. Weichert and K. Schönert. Heat generation at the tip of a moving crack. *Journal of the Mechanics and Physics of Solids*, 26(3):151 – 161, 1978. ISSN 0022-5096. doi:10.1016/0022-5096(78)90006-6.

[41] G. N. Chapman and A. J. Walton. Triboluminescence of glasses and quartz. *Journal of Applied Physics*, 54(10): 5961–5965, 1983. doi:10.1063/1.331773.

[42] G. Pallares, C. L. Rountree, L. Douillard, F. Charra, and E. Bouchaud. Fractoluminescence characterization of the energy dissipated during fast fracture of glass. *Europhysics Letters*, 99(2):28003, 2012.

[43] A. Smekal. On the fracturing processes underlying the brittle behavior of materials under uniaxial and multiaxial loading (translated from german). *Oesterreichisches Ingenieur-Archiv*, 7:49–70, 1953.

[44] K. Ravi-Chandar and B. Yang. On the role of microcracks in the dynamic fracture of brittle materials. *Journal of the Mechanics and Physics of Solids*, 45(4):535–563, apr 1997. doi:10.1016/s0022-5096(96)00096-8.

[45] J.R. Rice. Thermodynamics of the quasi-static growth of Griffith cracks. *Journal of the Mechanics and Physics of Solids*, 26(2):61 – 78, 1978. doi:10.1016/0022-5096(78)90014-5.

[46] B. Lawn. *Fracture of Brittle Solids*. Cambridge Solid State Science Series. Cambridge University Press, 2 edition, 1993. doi:10.1017/CBO9780511623127.

[47] L. B. Freund. Crack propagation in an elastic solid subjected to general loading. *Journal of the Mechanics and Physics of Solids*, 20(3):129 – 152, 1972. ISSN 0022-5096. doi:10.1016/0022-5096(72)90006-3.

[48] J. L. Huang and A. V. Virkar. High speed fracture in brittle materials: Supersonic crack propagation. *Engineering Fracture Mechanics*, 21(1):103 – 113, 1985. ISSN 0013-7944. doi:10.1016/0013-7944(85)90057-8.

[49] M. J. Buehler, F. F. Abraham, and H. Gao. Hyperelasticity governs dynamic fracture at a critical length scale. *Nature*, 426:141 – 146, 2003. doi:10.1016/0013-7944(85)90057-8.

[50] J. W. Morrissey and J. R. Rice. Crack front waves. *Journal of the Mechanics and Physics of Solids*, 46(3): 467 – 487, 1998. ISSN 0022-5096. doi:10.1016/S0022-5096(97)00072-0.

[51] J. R. Rice and D. C. Drucker. Energy changes in stressed bodies due to void and crack growth. *International Journal of Fracture Mechanics*, 3:19–27, 1967. ISSN 1573-2673. doi:10.1007/BF00188642.

[52] E. J. Kramer. Microscopic and molecular fundamentals of crazing. In H. H. Kausch, editor, *Crazing in Polymers*, pages 1–56, Berlin, Heidelberg, 1983. Springer Berlin Heidelberg. ISBN 978-3-540-38652-0.

[53] H. S. Carslaw and J. C. Jaeger. *Conduction of Heat in Solids*. Oxford: Clarendon Press, 1959.

[54] M.L. Hattali, J. Barés, L. Ponson, and D. Bonamy. Low velocity surface fracture patterns in brittle material: A newly evidenced mechanical instability. In *THERMEC 2011*, volume 706 of *Materials Science Forum*, pages 920–924. Trans Tech Publications Ltd, 1 2012. doi:10.4028/www.scientific.net/MSF.706-709.920.

[55] Technical information, Altuglas sheets. Technical report, Arkema, 2017. URL https://www.altuglas.com/export/sites/altuglas/.content/medias/downloads/literature/UK-brochure-technique-BD.pdf.

[56] M. Parvin. Theoretical prediction of temperature rise at the tip of a running crack. *International Journal of Fracture*, 15(5):397–404, Oct 1979. ISSN 1573-2673. doi:10.1007/BF00023327.

[57] C. S. Henkee and E. J. Kramer. Crazing and shear deformation in crosslinked polystyrene. *Journal of Polymer Science: Polymer Physics Edition*, 22(4):721–737, 1984. doi:10.1002/pol.1984.180220414.

[58] K. Ravi-Chandar and W. G. Knauss. An experimental investigation into dynamic fracture: II. Microstructural aspects. *International Journal of Fracture*, 26(1):65–80, Sep 1984. ISSN 1573-2673. doi:10.1007/BF01152313.

[59] E. Sharon, S. P. Gross, and J. Fineberg. Local crack branching as a mechanism for instability in dynamic fracture. *Physical Review Letters*, 74(25):5096–5099, jun 1995. doi:10.1103/physrevlett.74.5096.

[60] T. Goldman Boué, G. Cohen, and J. Fineberg. Origin of the microbranching instability in rapid cracks. *Physical Review Letters*, 114(5), feb 2015. doi: 10.1103/physrevlett.114.054301.

[61] V. De Zotti, K. Rapina, P.-P. Cortet, L. Vanel, and S. Santucci. Bending to kinetic energy transfer in adhesive peel front microinstability. *Phys. Rev. Lett.*, 122: 068005, Feb 2019. doi:10.1103/PhysRevLett.122.068005.

[62] C. Creton. Pressure-sensitive adhesives: An introductory course. *MRS Bulletin*, 28(6):434–439, 2003. doi: 10.1557/mrs2003.124.

[63] S. G. Robert, A. Morse, E. Siband, D. Dupin, S. P. Armes, and J. L. Keddie. Mechanical properties of a waterborne pressure-sensitive adhesive with a percolating poly(acrylic acid)-based diblock copolymer network: Effect of ph. *Journal of Colloid and Interface Science*, 448:8 – 16, 2015. doi:10.1016/j.jcis.2015.01.074.

[64] J. K. Kim, J. W. Kim, M. I. Kim, and M. S. Song. Thermal conductivity and adhesion properties of thermally conductive pressure-sensitive adhesives. *Macromolecular Research*, 14(5):517–523, Oct 2006. ISSN 2092-7673. doi: 10.1007/BF03218718.

[65] L. Ponson, D. Bonamy, and L. Barbier. Cleaved surface of $i-$AlPdMn quasicrystals: Influence of the local temperature elevation at the crack tip on the fracture surface roughness. *Phys. Rev. B*, 74:184205, Nov 2006. doi:10.1103/PhysRevB.74.184205.

[66] P Jain and L. Sharma. The physics of blackbody radiation: A review. *Journal of Applied Science in Southern Africa*, 4:80–101, 02 1998. doi:10.4314/jassa.v4i2.16899.

[67] C. Camara, J. Escobar, J. R. Hird, and S. J Putterman. Correlation between nanosecond x-ray flashes and stick–slip friction in peeling tape. *Nature*, 455:1089–92, 11 2008. doi:10.1038/nature07378.

[68] V. Lampret, J. Peternelj, and A. Krainer. Luminous flux and luminous efficacy of black-body radiation: an analytical approximation. *Solar Energy*, 73(5):319 – 326, 2002. ISSN 0038-092X. doi:10.1016/S0038-092X(02)00119-6.

[69] A. Stockman and L. T. Sharpe. Into the twilight zone: the complexities of mesopic vision and luminous efficiency. *Ophthalmic and Physiological Optics*, 26(3):225–239, 2006. doi:10.1111/j.1475-1313.2006.00325.x.

[70] K. N. G. Fuller, P. G. Fox, and J. E. Field. The temperature rise at the tip of fast-moving cracks in glassy polymers. *Proceedings of the Royal Society of London A: Mathematical, Physical and Engineering Sciences*, 341(1627):537–557, 1975. ISSN 0080-4630. doi: 10.1098/rspa.1975.0007.

[71] James L. Fergason. Liquid crystals in nondestructive testing. *Applied Optics*, 7(9):1729–1737, Sep 1968. doi: 10.1364/AO.7.001729.

[72] H. E. Newton. The luminescence of adhesive tape. *Science*, 89(2316):460 – 461, 1939.

[73] P. R. Budarapu, B. Javvaji, V. K. Sutrakar, D. Roy Mahapatra, G. Zi, and T. Rabczuk. Crack propagation in graphene. *Journal of Applied Physics*, 118(6):064307, 2015. doi:10.1063/1.4928316.

[74] D. W. Tang and N. Araki. On non-fourier temperature wave and thermal relaxation time. *International Journal of Thermophysics*, 18(2):493, Mar 1997. ISSN 1572-9567. doi:10.1007/BF02575178.

[75] S. W. S. McKeever. *Thermoluminescence of Solids*. Cambridge Solid State Science Series. Cambridge University Press, 1985. doi:10.1017/CBO9780511564994.

[76] K. Kitamura. Crack surface energy: Temperature and force dependence. *Materials Transactions*, 49(3):643–649, 2008. doi:10.2320/matertrans.MER2007238.

[77] K. W. Allen. Fundamentals of adhesion and interfaces. *Polymer International*, 41(2):209–210, 1996. doi: 10.1002/pi.1996.210410212.

[78] S. Siman-Tov, E. Aharonov, A. Sagy, and S. Emmanuel. Nanograins form carbonate fault mirrors. *Geology*, 41(6):703–706, 06 2013. ISSN 0091-7613. doi: 10.1130/G34087.1.

[79] R. Han, T. Hirose, and T. Shimamoto. Strong velocity weakening and powder lubrication of simulated carbonate faults at seismic slip rates. *Journal of Geophysical Research: Solid Earth*, 115(B3), 2010. doi: 10.1029/2008JB006136.

[80] D.S. Dugdale. Yielding of steel sheets containing slits. *Journal of the Mechanics and Physics of Solids*, 8(2): 100 – 104, 1960. ISSN 0022-5096. doi:10.1016/0022-5096(60)90013-2.

[81] N. Murphy and A. A. Ivankovic. The prediction of dynamic fracture evolution in PMMA using a cohesive zone model. *Engineering Fracture Mechanics*, 72(6):861 – 875, 2005. ISSN 0013-7944. doi: 10.1016/j.engfracmech.2004.08.001.

[82] P. M. Morse. Diatomic molecules according to the wave mechanics. ii. vibrational levels. *Phys. Rev.*, 34:57–64, Jul 1929. doi:10.1103/PhysRev.34.57.

[83] H. Arisawa and T.B. Brill. Kinetics and mechanisms of flash pyrolysis of poly(methyl methacrylate) (PMMA). *Combustion and Flame*, 109(3):415 – 426, 1997. ISSN 0010-2180. doi:10.1016/S0010-2180(96)00190-3.

[84] S. Shaik, E. Cremades, and S. Alvarez. The periodic table, a universal icon: Its birth 150 years ago, and its popularization through literature art and music. *Angewandte Chemie International Edition*, 58(38):13194–13206, 2019. doi:10.1002/anie.201904584.

[85] G.I. Barenblatt. The mathematical theory of equilibrium cracks in brittle fracture. In *Advances in Applied Mechanics*, volume 7, pages 55 – 129. Elsevier, 1962. doi: 10.1016/S0065-2156(08)70121-2.

[86] N. Brantut, M. J. Heap, P. G. Meredith, and P. Baud. Time-dependent cracking and brittle creep in crustal rocks: A review. *Journal of Structural Geology*, 52:17 – 43, 2013. ISSN 0191-8141. doi:10.1016/j.jsg.2013.03.007.

[87] B. D. Collins and G. M. Stock. Rockfall triggering by cyclic thermal stressing of exfoliation fractures. *Nature Geoscience*, 9:395–400, 2016. ISSN 1752-0908. doi: 10.1038/ngeo2686.

[88] A. Balandin, S. Ghosh, W. Bao, I. Calizo, D. Teweldebrhan, F. Miao, and J. Lau. Superior thermal conductivity of single-layer graphene. *Nano letters*, 8:902–7, 04 2008. doi:10.1021/nl0731872.

[89] X. Huang, G. Liu, and X. Wang. New secrets of spider silk: Exceptionally high thermal conductivity and its ab-

normal change under stretching. *Advanced Materials*, 24 (11):1482–1486, 2012. doi:10.1002/adma.201104668.

[90] J. R. Rice. Heating and weakening of faults during earthquake slip. *Journal of Geophysical Research: Solid Earth*, 111(B5), 2006. doi:10.1029/2005JB004006.

[91] H. Noda, E. M. Dunham, and J. R. Rice. Earthquake ruptures with thermal weakening and the operation of major faults at low overall stress levels. *Journal of Geophysical Research: Solid Earth*, 114(B7), 2009. doi: 10.1029/2008JB006143.

[92] C. Wibberley and T. Shimamoto. Earthquake slip weakening and asperities explained by fluid pressurization. *Nature*, 436:689–92, 09 2005.

[93] J. Sulem and V. Famin. Thermal decomposition of carbonates in fault zones: Slip-weakening and temperature-limiting effects. *Journal of Geophysical Research: Solid Earth*, 114(B3), 2009. doi:10.1029/2008JB006004.

[94] J. Barés, M. L. Hattali, D. Dalmas, and D. Bonamy. Fluctuations of global energy release and crackling in nominally brittle heterogeneous fracture. *Physical Review Letters*, 113(26), dec 2014. doi: 10.1103/physrevlett.113.264301.

[95] M. Barquins, B. Khandani, and D. Maugis. Propagation saccadée de fissure dans le pelage d'un solide viscoélastique. *Compte Rendu de l'Académie des Sciences Paris*, 303:1575–1519, 1 1986.

TO GO BEYOND (UNPUBLISHED RELATED POINTS)

Abstract

We here discuss a few extra points related to the preceding article but that were not included, for space reasons, in the accepted-for-publication version.

A. Model compatibility with irreversible thermodynamics

It should be emphasised that, although the full model we have considered allows for some microscopic crack healing (with the addition of a healing term, described by an Arrhenius rate, in the fronts dynamics in the preceding article), the propagation of cracks is not considered as a reversible phenomenon. Rupture is a dissipative process. One does not recover a fully cured PMMA or PSA body by only waiting during a finite amount of time after having caused an initial damage. In the creep regime, where no significant temperature rise occurs, the proposed model is actually inline with Rice's theorem [1] (or see Ref. [2], chpt. 5.2), which is the condition deriving from the first and second laws of (irreversible) thermodynamics applied to the propagation of quasi-static cracks. It states that the entropy production rate per unit of crack length Λ_{slow} (that is necessarily positive) is of the form

$$\Lambda_{\text{slow}} = \frac{(G-\Gamma)V}{T_0} \geq 0. \tag{1}$$

In this equation, Γ is "the work per unit of area of reversible separation of the surfaces to be fractured" [1], that is $\Gamma = (G_c - G_h)/2$ as per our parameters' definitions. The warmer the crack the more reversible its propagation is. Our model respects the condition of Eq. (1) (as it predicts $V < 0$ if $G < \Gamma$ and $V > 0$ if $G > \Gamma$), and hence respects the ruling laws of irreversible thermodynamics.
When it comes to the fast propagation branch, however, a quasi-static propagation regime, which is a hypothesis lying being Eq. (1), is harder to assume [1], in particular because of the evolving temperature field around the front and because non-negligible inertia effects could be at stake (the rupture velocity approaching that of the mechanical waves). There, irreversible thermodynamics might be oversimplified by Eq. (1). Healing is still modelled to play an important role in this regime (we notably inferred that it limits the maximal crack velocity), so that the question of reversibility is also relevant. Our model was derived neglecting any inertial effect on the load G that is transmitted to the crack tip and, furthermore, we only used the steady state of the equation that governs the front temperature. At high velocity the thermal transient time is indeed small in regards to the experimental conditions for the data sets we have fitted, about $l/V \sim 0.1\,\text{ns}$ (see Ref. [3] for more discussion on this transient time). Thus, our framework is actually a quasi-static one. The local entropy production rate Λ_{fast} at the front may then well be comparable to

$$\Lambda_{\text{fast}} = \frac{(G-\Gamma)V}{T_0 + \Delta T} \geq 0, \tag{2}$$

which is a criterion that is respected by our model, so that irreversible thermodynamics should also be respected by our framework at high propagation velocity.

B. Alternative (more accurate?) sub-critical law

We have, in this thesis, considered some simple forms for the rupture and healing activation energies, that are directly linear with the energy release rate G. Note however that other forms for these activation energies could be considered. For instance, by considering that atoms bonds break at a given stress threshold σ_c (rather than at an energy threshold U_c) and hold a gaussian statistical stress fluctuation, it was proposed [4, 5] that the activation energy should relate to $(\sigma_c - \sigma)^2$ rather than to $\sigma_c^2 - \sigma^2$. The final form for the rupture kinetics retained by Vanel et al. [5] was

$$V = V_1 \sqrt{\frac{T}{T_0}} \left(\frac{\sigma_c}{\sigma_c - \sigma}\right) \exp\left(-\frac{d_0^3(\sigma_c - \sigma)^2}{2Ek_BT}\right), \tag{3}$$

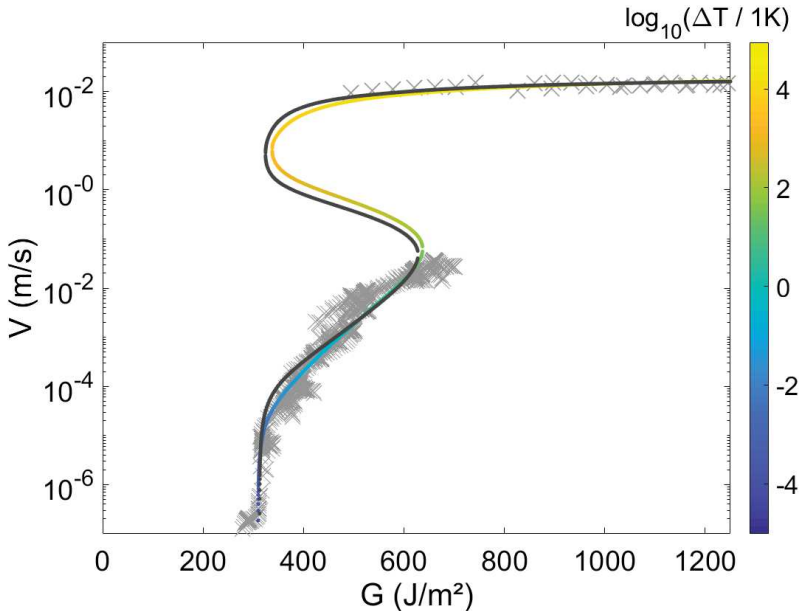

FIG. 1. Model fit to the PMMA data (squares), when considering the sub-critical growth law of Eq. (6) (colored curve, where the colormap describe the tip temperature elevation) or considering the simpler Arrhenius formalism instead (black curve, as considered in the core article). The fit quality in both cases is similar.

where a healing term can be added for completeness, similarly to the one we introduced in ref. [6]:

$$\begin{aligned} V = &V_1\sqrt{\frac{T}{T_0}}\left(\frac{\sigma_c}{\sigma_c-\sigma}\right)\exp\left(-\frac{d_0^3(\sigma_c-\sigma)^2}{2Ek_BT}\right)\\ &+V_1\sqrt{\frac{T}{T_0}}\left(\frac{\sigma_h}{\sigma_h-\sigma}\right)\exp\left(-\frac{d_0^3(\sigma_h-\sigma)^2}{2Ek_BT}\right). \end{aligned} \tag{4}$$

In this expression, the nominal velocities in front of the exponential terms depend both on the tip temperature and on the applied stress, rather than being a constant V_0. Their particular value when $T = T_0$ and $\sigma = 0$ is denoted V_1. Should one want to write this equation as a function of G (for instance to compare this model to experiments were G is measured but σ is vastly unknown), one could use a linear elasticity approximation that was already discussed in the preceding article:

$$\sigma \sim \pm\sqrt{\frac{GE}{\xi}}, \qquad \sigma_c \sim +\sqrt{\frac{G_cE}{\xi}}, \qquad \sigma_h \sim -\sqrt{\frac{G_hE}{\xi}}. \tag{5}$$

Here, I have used the $\pm$ notation in the first equation and opposite signs in the two others as the square root is a positive value while σ is a signed quantity. For instance, let us use the convention $\sigma > 0$ when extending atom links and $\sigma < 0$ when compressing them. The barrier σ_c is then likely to be a positive quantity (one needs to force two atoms to a high distance to separate them) and σ_h a negative quantity (one needs to force two atoms to a short distance to link them together).
Equation (4) is only an approximation for large values of $(\sigma_c - \sigma)$ and $(\sigma_h - \sigma)$ of a more general expression [5] that we can now write as a function of G and for $\sigma > 0$:

$$\begin{aligned} V = &\frac{V_0}{2}\ \mathrm{erfc}\left((\sqrt{G_c}-\sqrt{G})\sqrt{\frac{d_0^3}{2\xi k_B(T_0+\Delta T)}}\right)\\ &-\frac{V_0}{2}\ \mathrm{erfc}\left((\sqrt{G_h}+\sqrt{G})\sqrt{\frac{d_0^3}{2\xi k_B(T_0+\Delta T)}}\right), \end{aligned} \tag{6}$$

where $V_0 = V_1\sqrt{4\pi U_c/(k_BT_0)}$ and erfc is the complementary error function. Interestingly, deriving this equation from the stress σ rather than from the elastic energy U allowed us to properly explain the difference in sign in front of the term in G, and this was not done in the article which precedes the current sections.

With Eq. (6), we can still apply a thermal weakening view (i.e., a potentially hot temperature elevation ΔT, from a thermal dissipation of G, that helps exceed the energy barriers). Such an application to the rupture of PMMA is presented in Fig. 1, where the new fit parameters are: $\xi = 50\,\mathrm{nm}$, $V_0 = 880\,\mathrm{m\,s^{-1}}$, $G_c = 2250\,\mathrm{J\,m^{-2}}$, $G_h = 150\,\mathrm{J\,m^{-2}}$, $\phi = 20\%$, $\lambda = 0.18\,\mathrm{J\,s^{-1}\,m^{-1}\,K^{-1}}$, $C = 1.5 \times 10^6\,\mathrm{J\,m^{-3}\,K^{-1}}$, $l = 1\,\mathrm{nm}$ and $T_0 = 296\,\mathrm{K}$. These parameters are in the same order of magnitude as those inverted with the model we chose in the article, such that none of the two options (anyway very close) is particularly better. The straightforward Arrhenius formalism has no doubt the advantage of being the simplest and most canonical one, while the other one (Eq. (6) here introduced) is probably more suitable when the stress σ approaches the intrinsic critical barrier σ_c, and does not neglect the dependence in temperature and stress of the molecular velocity V_0.

---

[1] J.R. Rice. Thermodynamics of the quasi-static growth of Griffith cracks. *Journal of the Mechanics and Physics of Solids*, 26(2):61 – 78, 1978. doi:10.1016/0022-5096(78)90014-5.

[2] B. Lawn. *Fracture of Brittle Solids*. Cambridge Solid State Science Series. Cambridge University Press, 2 edition, 1993. doi:10.1017/CBO9780511623127.

[3] T. Vincent-Dospital, R. Toussaint, A. Cochard, K. J. Måløy, and E. G. Flekkøy. Thermal weakening of cracks and brittle-ductile transition of matter: A phase model. *Physical Review Materials*, 02 2020. doi:10.1103/PhysRevMaterials.4.023604.

[4] S. S. Brenner. Mechanical behavior of sapphire whiskers at elevated temperatures. *Journal of Applied Physics*, 33(1):33–39, 1962. doi:10.1063/1.1728523.

[5] L. Vanel, S. Ciliberto, P.-P. Cortet, and S. Santucci. Time-dependent rupture and slow crack growth: elastic and viscoplastic dynamics. *Journal of Physics D: Applied Physics*, 42(21):214007, oct 2009. doi:10.1088/0022-3727/42/21/214007.

[6] T. Vincent-Dospital, R. Toussaint, S. Santucci, L. Vanel, D. Bonamy, L. Hattali, A. Cochard, K. J. Måløy, and E. G. Flekkøy. How heat controls fracture: the thermodynamics of creeping and avalanching cracks. *Soft Matter*, 2020. doi: 10.1039/d0sm010. accepted.

Chapter III

Is breaking through matter a hot matter?
A material failure prediction by monitoring creep

Where the load threshold for brittleness, as predicted by the model, is compared to that of numerous materials.

Next submission to Nature Communications

arXiv: 2007.04866

Résumé (*French abstract*):

Rompre la matière est-elle une affaire brulante ?
Une prédiction de la rupture grâce au suivi du fluage

Dans tout domaine où des solides sous contraintes sont en jeu, autrement dit, de la sismologie à l'ingénierie classique, comprendre la résistance de la matière est une question cruciale. Nous discutons ici de la possibilité pour un simple modèle thermiquement activé, qui comprend l'évolution auto-générée de la température en tête de fissure, de prédire la rupture catastrophique d'un vaste variété de matériaux. Il est en particulier montré que la barrière énergétique surfacique intrinsèque, pour rompre les liens moléculaires de nombreux solides, peut facilement être déduite de la dynamique lente du fluage d'une fissure. Cette barrière est, cela-dit, plus haute que le niveau d'énergie auquel la matière fragile casse effectivement, possiblement du fait de l'activation thermique et d'un mécanisme d'adoucissement thermique. Nous proposons une nouvelle méthode pour calculer le taux de libération d'énergie de rupture brutale, s'appuyant seulement sur le suivi du fluage lent, et nous montrons que cette méthode permet de prédire, avec une précision de l'ordre de 50 %, la rupture de plus de vingt matériaux différents, dont les énergies de fracture couvrent plus de quatre ordres de grandeur.

Is breaking through matter a hot matter? A material failure prediction by monitoring creep

Tom Vincent-Dospital,[1,2,*] Renaud Toussaint,[1,2,†] Alain Cochard,[1] Eirik G. Flekkøy,[2] and Knut Jørgen Måløy[2]

[1] *Université de Strasbourg, CNRS, IPGS UMR 7516, F-67000 Strasbourg, France*
[2] *SFF Porelab, The Njord Centre, Department of physics, University of Oslo, Norway*

In any domain involving some stressed solids, that is, from seismology to general engineering, the strength of matter is a paramount feature to understand. We here discuss the ability of a simple thermally activated sub-critical model, that includes the auto-induced thermal evolution of cracks tips, to predict the catastrophic failure of a vast range of materials. It is in particular shown that the intrinsic surface energy barrier, for breaking the atomic bonds of many solids, can be easily deduced from the slow creeping dynamics of a crack. This intrinsic barrier is however higher than the macroscopic load threshold at which brittle matter brutally fails, possibly as a result of thermal activation and of a thermal weakening mechanism. We propose a novel method to compute the macroscopic critical energy release rate of rupture, G_a, solely from monitoring slow creep, and show that this reproduces the experimental values within 50% accuracy over twenty different materials, and over more than four decades of fracture energy.

I. INTRODUCTION: FROM SLOW CREEP TO ABRUPT RUPTURE

Although seminal, the early theoretical descriptions of crack dynamics, such as Griffith's [1] or Slepyan's [2, 3] one, was somewhat binary: beyond a critical mechanical load, matter suddenly breaks. It is however acknowledged that, at load levels below the critical one, a far slower crack propagation already occurs, that will here be referred to as 'creep'. This phenomenon was successfully modelled with Arrhenius-like sub-critical growth laws [4, 5], and is hence sometimes called 'stress corrosion'. With the increasing number of experimental work, the description of such a slow dynamics was quickly refined, and five propagation stages were notably distinguished [5]. Let us start this manuscript by summarising them. Figure 1 illustrates these stages in a V-G plot, where V is the crack velocity for a given load G, which is the 'energy release rate', that is the energy that the fracture consummates to advance by unit surface [1]. At stage 0, while under only a mild mechanical input, cracks do not actually propagate forward. This was notably explained by the existence of some healing processes, that there efficiently compete with the failure ones [4]. From this state, when the load is increased above a given threshold, some slow fracture growth starts to be observed (stage I). The propagation velocity V increases exponentially with the crack's energy release rate G. In a sub-critical (i.e., Arrhenius-like) description, it implies that V is to first order explained by an activation mechanism dependent on G, in a chemical-like rupture reaction [6]. Logically, this regime was observed to also depend on the surrounding temperature and on the fluid that is present in the fracture [7], which affects the chemical reaction involved in molecular bond breaking. When reaching a faster propagation, some velocity plateau might then hold (stage II), possibly as the transport of fluid corrosive elements toward the tip can not efficiently cope with the crack advance. Such plateau is, in this case, only a transition to a sub-critical growth 'in-vacuum-condition', where the dynamics becomes notably insensitive to the fracture fluid (stage III). Finally, when a particular threshold is reached for the energy release rate, the velocity jumps to a far quicker regime: the material fails (stage IV). We will denote[1] this threshold G_a in $\mathrm{J\,m^{-2}}$, with 'a' standing for 'avalanche'.

In this work, we will show how studying the slow creep regime allows to predict this particular failure load. This can lead to methods to characterise natural or lowly controlled materials, where the critical energy release rate G_a is not well known a priori, but where the monitoring of creep allows to infer it. In a previous study [8], we indeed proposed a unifying model of the slow creep and the fast regime, holding a precise quantification of the energy budget and the heating of the crack tip, that is coupled with an Arrhenius-type activation law. We have shown how it accounts, in some polymers [9], for seven decades of propagation velocities and for the transition, at the avalanche load, from creep to sudden failure. Here, we present how well this thermodynamics based model can predict the threshold G_a for a broad range of materials, by comparing its forecasts to actual experimental failure thresholds from twenty data sets from the literature. By doing so, one can actually identify the microscopic rupture energy of the breaking bonds, G_c, and show how this quantity is related to, yet different from, the macro-

* vincentdospitalt@unistra.fr
† renaud.toussaint@unistra.fr

[1] This is usually referred to as G_c in experiments, since it corresponds to the value of the macroscopic energy release rate at which the velocity of fracture propagation jumps to much higher values. By contrast, in this article, we made the choice to design as G_c a microscopic property, and consequently use this different notation G_a for the the macroscopic (observable) critical energy release rate.

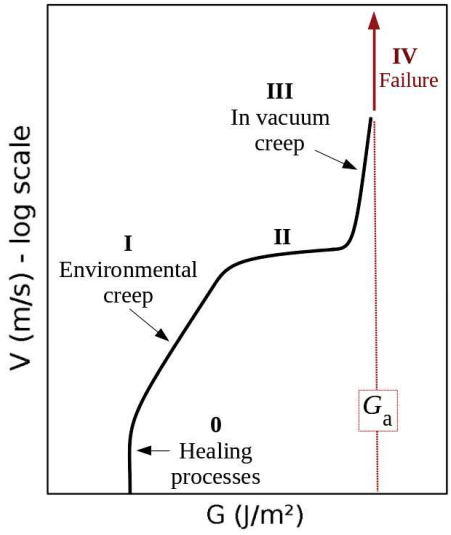

FIG. 1. Summary of the different forward crack velocity regions observed in experimental velocity curves. After *Fracture of Brittle Solids*, Lawn [5]

.

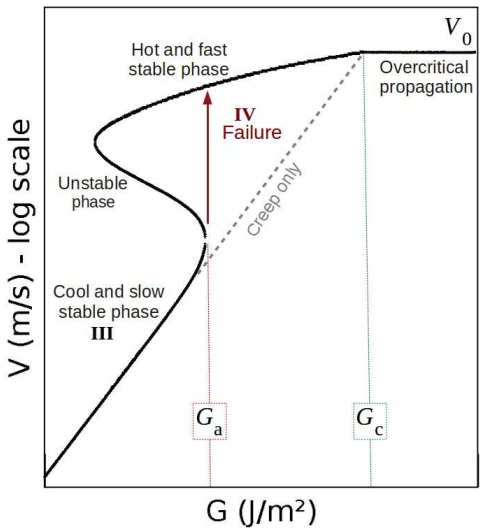

FIG. 2. Modelled crack velocity as a function of energy release rate, as per Eqs. (1) and (2). Stages I, III and IV correspond to the one labelled in Fig. 1. As explained in the text, stages 0 and II are here not covered. In our model, the failure occurs when the cracks becomes hot enough, that is, when $\Delta T \sim T_0$ The dashed line corresponds to a cold case $\Delta T \ll T_0$ in Eq. (1).

scopic G_a. The agreement between the predictions and the realisation is obtained for materials spanning more than 4 orders of magnitude in energy release rate, indicating the robustness of this description among different types of materials and the versatility of the theoretical framework.

II. THE THERMAL WEAKENING MODEL

We consider that the propagation of a crack follows an Arrhenius sub-critical growth law, in which the temperature term accounts for the induced heat generated at the plastic crack tip [10, 11]. Such a model, introduced in Refs.[8] and [9], writes as

$$V = V_0 \min\left[\exp\left(-\frac{d_0^3(G_c - G)}{2lk_B(T_0 + \Delta T)}\right), 1\right] \tag{1}$$

$$\frac{\partial(\Delta T)}{\partial t} = \frac{\lambda}{C}\nabla^2(\Delta T) + \frac{\phi GV}{C\pi l^2}f, \tag{2}$$

where the first equation describes the Arrhenius growth (i.e., the term in brackets is a probability for the thermal bath to overcome an energy barrier), and the second one in the diffusion equation governing the thermal evolution around the crack front. Here, V_0 is a nominal atomic speed related to the collision frequency in the thermal bath, and should typically be comparable to the mechanical wave velocity of the studied media [2, 12]. The activation energy is modelled proportional to $(G_c - G)$, where G_c is the surface energy barrier to overcome in order to break atomic bonds. d_0^3 is the characteristic volume for the bonds ($d_0 \sim 1\,\text{Å}$), k_B is the Boltzmann constant, T_0 the ambient temperature and ΔT any variation away from it at the crack tip. A percentage ϕ of the power consummated per unit of crack length GV is uniformly dissipated as heat over a zone of support function f and of radius l. This heating zone is a subset of the process zone (that is the full extent of plasticity around the tip), and we assume that it also constrains the stress level σ at the tip, as verified in Vincent-Dospital et al. [9]: $\sigma \sim \sqrt{GE/l}$ [5], where E is the materials Young's modulus. This assumption is the reason why l also intervenes in Eq. (1). In Eq. (2), T is the temperature field, its value at the crack tip being $T_0 + \Delta T$ in Eq. (1). Finally, the heat conductivity and volumetric heat capacity of the solid matrix are respectively denoted λ and C.
Note that it was shown [9, 13] that at low velocities (i.e., the creep velocities we are interested in), ΔT computed from Eq. (2) can, more simply, be approximated to

$$\Delta T \sim \frac{\phi GV}{\lambda}, \tag{3}$$

which does not depend on C or l, notably because if the crack advances slowly enough, the temperature elevation is constrained by the heat diffusion skin depth $\sqrt{\lambda l/(\pi CV)}$ rather than the size of the heat production zone, as the former is, in this case, big compared to the latter.
Approximating Eqs. (1) and (2) by their steady state solutions, two stable propagation branches are derived from this model [8], as shown in Fig. 2: a fast phase, which is obtained for a hot crack tip and corresponds to the catastrophic failure of matter, and a slow one corresponding

to the creep regime, when $\Delta T \ll T_0$. In between these two branches, a hysteresis situation holds with a third unstable phase. In this study, we are here mainly interested in the slow to fast regime transition (i.e., that leads to quick material failure).
When approaching this transition, the velocity deviates from its negligible heating asymptotic expression, which is a simple exponential increase with the load G:

$$\ln\left(\frac{V}{V_0}\right) \sim (G - G_c)\left[\frac{d_0^3}{2lk_BT_0}\right], \tag{4}$$

as the rise in temperature ΔT in Eq. (1) becomes comparable to the room temperature T_0. The particular energy release rate G_a is then reached, at which $\partial V/\partial G \to +\infty$, and beyond which the crack can only avalanche to a velocity that is orders of magnitude higher (see Fig. 2). The matter suddenly snaps. As a result of thermal activation, G_a is actually less than the actual surface energy barrier for breaking bonds G_c.
Although rarely regarded today, such an importance of the auto-induced heat to explain brittleness was early developed [14–16]. These studies reckon that the dissipated energy favours failure by locally softening the material at the tip. Our model neglects such a softening effect and instead considers that the reaction rate for rupture is increased from the elevated temperature, only as understood by statistical physics. Of course, both views are not mutually exclusive. In both cases, the G value of interest (i.e., G_a) remains similar: the threshold for which ΔT significantly overcomes the thermal background, so that a quick avalanche can be generated.

III. MODEL PREDICTIONS VERSUS REPORTED FAILURES

Extensive fracturing experiments on numerous materials can be found in the literature. Hence, we can compare the model predictions of G_a to some experimentally reported avalanche thresholds, that are often referred to as 'critical energy release rate' or 'material toughness', although it does not correspond to what is here denoted G_c, that is an intrinsic (microscopic) medium property not directly measurable at lab scale.
Note that Eq. (1) does not account for all of the creep regimes summarized in Fig. 1, that one can meet with an experimental test, but displays a unique low velocity slope (i.e., from Eq. (4)). We have indeed discarded any healing processes, needed to explain stage 0, as they are beyond the topic of the current study. Such processes can however be included in the model [9]. We have also assumed no rate-limiting environmental factor, that is, no significant chemical interaction of the matrix with the fracture fluid (i.e., no stage I or II). We have hence restricted our comparison to experimental data to such a case, although distinguishing it with certitude is not always straightforward. When available, we have notably used data sets of dry experiments or with lowly corrosive fracture fluids. Note however that, when some fluid-matrix interaction does take place, the model can still be somewhat applied, if failure is preceded by a unique slope (i.e., if it occurs before the slope break between stages I and II), or after it, once clearly having entered in regime III. In this case, the definition of the surface energy barrier G_c may slightly change: from an intrinsic strength of the solid to an equivalent strength under a given chemical environment.
To predict G_a, it is of course needed to know, for each material, the values of the model constitutive parameters. Although they are not many, most of these parameters are not usually considered, and are hence unknown. It is however possible to estimate their order of magnitude from known material properties, or to assess them from the slow (creep) part of the loading curve. We have first considered that V_0 is of the order the mechanical wave velocity. It could ideally be that of the Rayleigh waves [12], but it is often simpler to rather estimate the shear wave velocity of solids, $V_S \sim \sqrt{\mu/\rho}$, as the shear modulus μ and the density ρ of most materials are easily available. The heat conductivity λ is also known in most cases, and T_0 is nothing but the room temperature at which a given reported experiment took place. We assume the interatomic space d_0 to be 1 Å. While it could be two or three times bigger depending on the materials, which would have an order of magnitude effect on the term d_0^3, this uncertainty would only impact the estimation of l, as the ratio d_0^3/l is here of importance. We indeed have to deduce l and G_c from the slope and intercept of the slow sub-critical growth, that is, from the two terms of Eq. (4) fitted to the experimental curves with the fit parameters a and b: $\ln(V) = a + bG$. This gives

$$l = \frac{d_0^3}{2bk_BT_0} \tag{5}$$

$$G_c = \frac{2k_BT_0}{d_0^3}\big[ln(V_0) - a\big]. \tag{6}$$

This implies that we can predict G_a if relying on some creep observations, that can yet be at loads far below the failure threshold. The only remaining model parameter, the percentage ϕ of energy converted into heat is mostly unknown. While qualitative statements, such as larger ϕ in metals rather than, say, polymers, are tempting, we have here arbitrarily fixed this percentage to 50 % in all materials, except for a couple of instances where we could estimate it [9, 13].
Note that, while the velocity is often reported in relation to the stress intensity factor K rather than the energy release rate G, we have here converted from one to the other with the following relation: $G \sim K^2/E$ [5] to derive a and b, and then l and G_c. Backwardly, with the here proposed method, we will thus predict the tough-

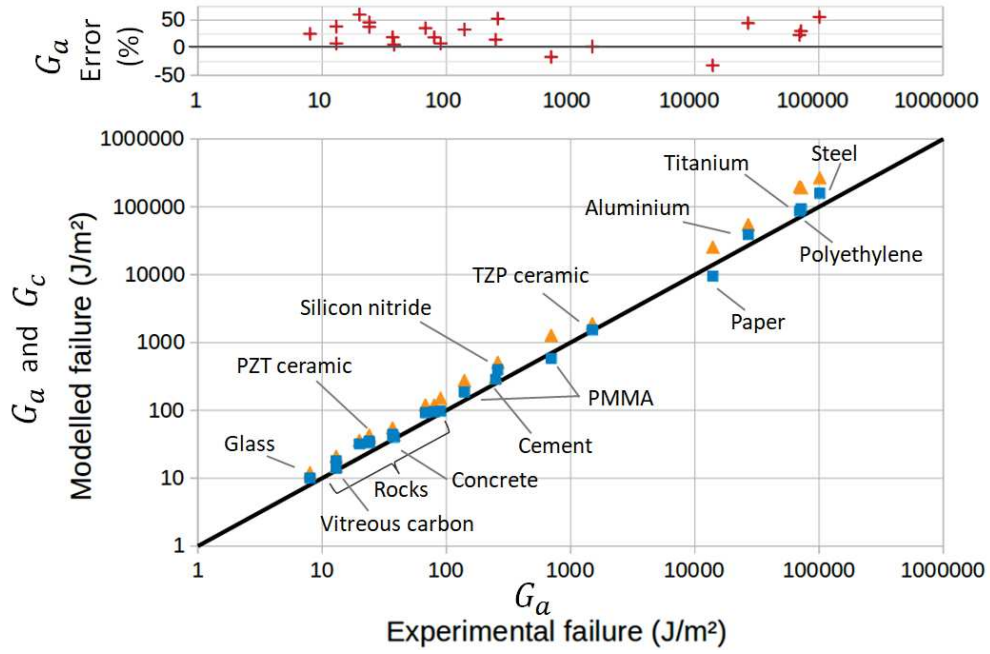

FIG. 3. (Bottom): Modelled G_a thresholds (squares) and modelled surface energy barrier G_c (triangles) compared to the experimental thresholds from the literature. The black line is the identity. The labels locate different materials. The unlabelled rock materials are quartz, sapphire, granite and andesite. See the supplementary material for an exhaustive list. (Top): Relative error on the avalanche threshold.

ness, $K_c \sim \sqrt{EG_a}$, based on the creep measurement. Indeed, all the introduced parameters can now be estimated, and we did so for twenty materials for which the creeping behaviour was studied in the literature [9, 17–34]. The corresponding G to V curves and the inferred parameters values are shown in the supplementary material. We can then solve the full two non linear equations (1) and (2), now taking into account the temperature rise ΔT. The inflection of this model, if it exists, where $\partial V/\partial G \to +\infty$ (see Fig. 2), can be identified as G_a and compared to the reported experimental thresholds. This comparison is summarised for all the media in Fig. 3, and our model displays there a good general description of catastrophic failure. In the same figure, the surface energy barrier G_c is also displayed for comparison, as well as the relative error made in the estimation of G_a.

IV. ANALYTICAL APPROXIMATION

While, to derive the modelled G_a, one should compute the full crack dynamics (i.e., as displayed in Fig. 2), and search for the points where $\partial G/\partial V = 0$, we explain in the supplementary material how Eqs. (1) and (2) also approximately lead to:

$$G_a \sim \frac{\lambda T_0}{\phi V_0} \frac{\exp(R_a)}{R_a}. \tag{7}$$

where R_a is the activation energy at the avalanche threshold counted in thermal energy units: $R_a = d_0^3(G_c - G_a)/(2lk_BT_0)$. As this ratio notably depends on G_a, Eq. (7) only implicitly defines the threshold. It however gives further insight on the influence of each parameter and, although a numerical solver is still required, it is simpler and far quicker than finding the accurate solution, and potentially easy to use in engineering applications. We show, in the supplementary material, how this approximation is a slight overestimation of the real solution, by about 0 to 10%.

V. MICROSCOPIC VS MACROSCOPIC FRACTURE ENERGY

In Fig. 3, one can notice that the surface energy barrier G_c is always similar in order of magnitude to the rupture threshold G_a. Yet, the rupture always occurs at a load less than G_c, with G_a being about twice lower in average for all the displayed solids. We have here explained how a weakening mechanism, as the thermal view that we have here developed, allows to account for this discrepancy. Having gathered various exponential creep data, and derived l and G_c from their slope and intercept in their $\ln V$ - G representations, we can notably infer the intrinsic crack energy barrier in each material: $U_c = d_0^3 G_c/(2l)$. As shown in Fig. 4, this quantity is always in the or-

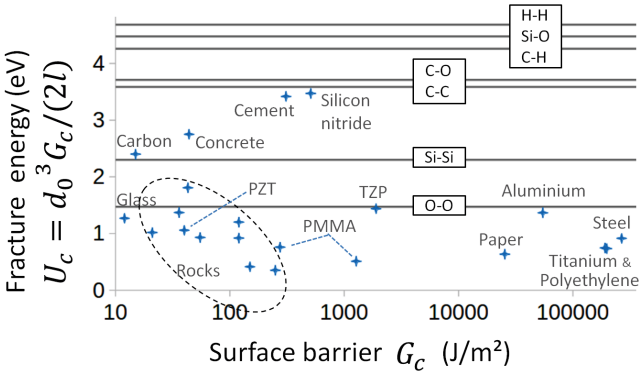

FIG. 4. Microscopic fracture energy $U_c = d_0^3 G_c/(2l)$ as a function of the macroscopic energy barrier G_c, for the same materials as Fig. 3. See the supplementary material for the exhaustive list. Note that the accuracy of U_c is not better than an order of magnitude. The horizontal lines show some typical covalent cohesion energies for comparison [35].

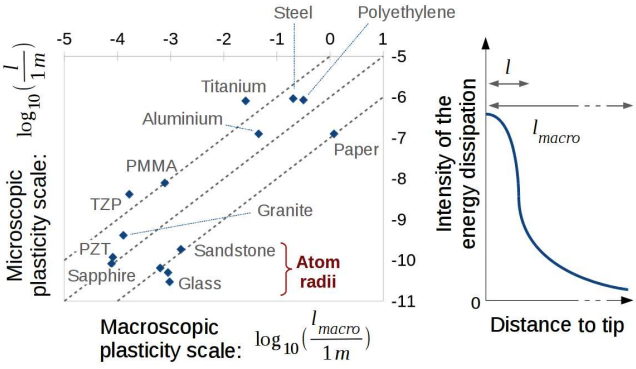

FIG. 5. (Left): Core size of the process zone l, as understood by our model, versus macroscopic plasticity scale l_{macro}, as derived from reported tensile yield stresses. The straight lines mark a factor 10^5, 10^6 and 10^7 between both views. (Right): Simplified spacial distribution of the intensity (arbitrary unit) at which energy is dissipated (i.e., plasticity) around the crack tip, as a possible explanation for the difference in scale. The graph is not to scale as $l_{\text{macro}} \gg l$. The two unlabelled points in the vicinity of Glass represent Quartz and Concrete.

der of 10^{-19} J $\sim$ 1 eV, logically comparable to the energy level that is necessary to unbind single atomic covalent bounds [35]. The actual values of U_c are yet often slightly inferior to the typical covalent strength. This could derive from an averaging effect, with cracks that are prone to follow the weakest paths, that possibly includes inter-molecular bonds (such as Van der Waals and hydrogen links) and dislocations or atomic voids (i.e., when the distance between two consecutive breaking bonds is more than a few ångströms). For instance, in polymers, part of the rupture shall be inter-molecular, and, in rock-type materials, the crack dynamics might benefit from the intrinsic porosity. However, due to the simplicity of the model, care should be taken when interpreting U_c beyond its order of magnitude.

It is clear however that the value of G_c varies by a factor 10^4 for different materials, while its counterpart U_c does not. As most materials have the same U_c and d_0, in order of magnitude, the large variability in G_c (and hence in G_a) that is observed is, in this description, attributable entirely to the variability in the scale for the release of heat. We indeed infer that l varies from the radius of a single atom, for the weakest materials, up to 1 µm, for the ones with the highest G_c (see Fig. 5). The wider the plastic area that shields crack tips, the stronger is matter. But backwardly, we have discussed how the heat dissipation might be the root cause for dramatic ruptures in brittle solids, if the heat is not efficiently evacuated away from the rupture front.

We can compare the values of l with the more typical plastic radius predicted by a Dugdale view [36] of the process zone, $l_{\text{macro}} \sim G_c E/{\sigma_y}^2$, where σ_y is the tensile yield stress, beyond which macroscopic samples lose their elasticity. As shown in Fig. 5, the latter is consistently five to seven orders of magnitude higher than what we predict for l. This likely translates to the fact that plasticity (here understood as the dissipation of mechanical energy in any form) ought to be a rather heterogeneous phenomenon, with a greater density of energy dissipation close to the front than away from it. Thus, the scale of a process zone can be characterised either by its core radius l, where most of the heating due to the dissipation takes place, or by its full extent l_{macro}, where the rheology becomes non elastic. While the former is to include significant thermal losses, the latter can encompass various mechanisms, namely, the nucleation of dislocations, the release of residual heat over a greater volume, the emission of phonons and photons, or even some material change in phase.

Overall, Eq. (1) should be understood as:

$$V = V_0 \exp\left(-\frac{U_c - U(G^{[+]},\, \text{plasticity}^{[-]})}{k_B T\big(\text{plasticity}^{[+]},\, \text{diffusion}^{[-]}\big)}\right), \quad (8)$$

where U is the mechanical energy corresponding to the stress actually transmitted to the crack tip covalent bond of average strength U_c, and where [+] and [–] indicate if the T and U functions are increasing or decreasing with the specified parameters.

VI. DISCUSSION AND CONCLUSION

We have thus presented a model that gives reasonable predictions of the rupture load, over a broad range of materials. We did this with a full expression (Eqs. (1) and (2)), or in simplified forms (Eqs. (1) and (3) or Eq. (7)). This predicted load is still, however, overestimated by about 25% (in average for all media, see the errors in Fig. 3). This could derive from numerous causes. First, most of our parameters were only broadly

estimated, when not arbitrarily fixed. We have in particular assumed that G_c is a homogeneously distributed constant, although it is likely to hold some level of quenched disorder [37, 38]. In this case, the overall creep dynamics (i.e. the slow branch of Fig. 2, described by Eq. (4)) would not be strongly affected, as it shall mainly depend on an average value of G_c. The failure, however, would be prone to occur on weaker locations [8], that are controlled by a lower G_c, which would explain our overestimation on G_a. It corresponds to the common idea that the overall strength of a material is highly dependent on its heterogeneities. Furthermore, the experimental error on the measurement of G_a could also be important, as the avalanches occur in a regime where the crack velocity diverges with G, just before test samples snap at a velocity comparable to that of the mechanical waves. Hence, the last mechanical load accurately measured before rupture is, by essence, to be slightly below the actual physical threshold. Note also that, sometimes, the actual creep stage (i.e., 0 to III in Fig. 1) that we fit to derive our parameters is not unambiguously identifiable on the experimental curves. Besides these considerations, the model is extremely simple, applying mesoscopic laws (i.e., Fourier conductivity and Arrhenius growth) at atomic scales. For instance, a propagative description [39] of the heat transport could be needed, due to the small time and space scales that are here considered. Overall, a transposition of the model into a, more complicated, atomistic solver [40] would be beneficial.

Still, the model we propose gave, in some instances [9], a comprehensive explanation of the full dynamics of failure. Additionally, we have here showed how G_c, the intrinsic surface energy barrier of materials, shall only depend on a heat dissipation scale around the crack tip, and that the accumulation of this induced heat is effectively reducing the mechanical resistance of matter ($G_a < G_c$).

Countering this latter effect could be a key to design advanced strong materials, in particular as some intriguingly tough solids such as graphene [41, 42] or arachnid silks [43], are indeed very conductive. Interestingly, the conductivity of spider threads even increases with deformation [43], which could be a nature made adaptive defence mechanism for the stability of nets, whenever they are pressurized. Replicating such a behaviour with a man-made material would then be an important achievement that could lead to high performance cables or bulk materials. For instance, a first step could be the engineering of highly conductive atomic networks, integrated into strong solid matrices, thus limiting any local rise in temperature that could weaken the matter.

A more down-to-earth application of the model could be the monitoring of structures and infrastructures, as we have shown how their creep rate can be used to predict their failure. This would be of particular interest for bodies that have aged in uncontrolled conditions, in which the change in mechanical properties becomes uncertain with time, but could be inverted from their creep.

Finally, and although we have only treated about fracture in mode I, we suggest that most of the effects that we have discussed shall be valid for mixed-mode fracturing and solid friction. The latter is also suspected to hold some non negligible, thermal related, weakening mechanisms [44, 45], which could notably be a key in geophysics and in understanding the stability of seismic faults. In particular, when increasing the background temperature T_0, it was shown that the model holds a critical point, beyond which not enough heat can be generated to trigger instabilities in the dynamics of cracks [8], which may physically explain the brittle-ductile transition in the Earth's crust [46, 47], below which rocks tend to flow rather than break.

ACKNOWLEDGEMENTS

The authors declare no competing financial interests in the publishing of this work and acknowledge the support of the IRP France-Norway D-FFRACT, of the Universities of Strasbourg and Oslo and of the CNRS INSU ALEAS program. We thank the Research Council of Norway through its Centres of Excellence funding scheme, project number 262644.

[1] A. Griffith. The Phenomena of Rupture and Flow in Solids. *Philosophical Transactions of the Royal Society of London A: Mathematical, Physical and Engineering Sciences*, 221(582-593):163–198, January 1921. ISSN 1471-2962. doi:10.1098/rsta.1921.0006.

[2] L.I. Slepyan. Dynamics of a crack in a lattice. *Soviet Physics, Doklady*, 26:538–540, 1981.

[3] M. Marder. Slepyan's dynamic contribution to studies of fracture. *Philosophical Transactions of the Royal Society A: Mathematical, Physical and Engineering Sciences*, 2019.

[4] J.R. Rice. Thermodynamics of the quasi-static growth of Griffith cracks. *Journal of the Mechanics and Physics of Solids*, 26(2):61 – 78, 1978. doi:10.1016/0022-5096(78)90014-5.

[5] B. Lawn. *Fracture of Brittle Solids*. Cambridge Solid State Science Series. Cambridge University Press, 2 edition, 1993. doi:10.1017/CBO9780511623127.

[6] G. G. Hammes. *Principles of Chemical Kinetics*. Academic Press, 1978. ISBN 978-0-12-321950-3. doi: doi.org/10.1016/B978-0-12-321950-3.50005-0.

[7] N. Brantut, M. J. Heap, P. G. Meredith, and P. Baud. Time-dependent cracking and brittle creep in crustal rocks: A review. *Journal of Structural Geology*, 52:17 – 43, 2013. ISSN 0191-8141. doi:10.1016/j.jsg.2013.03.007.

[8] T. Vincent-Dospital, R. Toussaint, A. Cochard, K. J. Måløy, and E. G. Flekkøy. Thermal weakening of cracks and brittle-ductile transition of matter: A phase model. *Physical Review Materials*, 02 2020. doi: 10.1103/PhysRevMaterials.4.023604.

[9] T. Vincent-Dospital, R. Toussaint, S. Santucci, L. Vanel, D. Bonamy, L. Hattali, A. Cochard, K. J. Måløy, and E. G. Flekkøy. How heat controls fracture: the thermodynamics of creeping and avalanching cracks. *Soft Matter*, 2020. doi:10.1039/d0sm010. accepted.

[10] E. Orowan. Energy criteria of fracture. Technical report, Massachusetts Institute of Technology, Cambridge Departement of Mechanical Engineering, 1954.

[11] G. R. Irwin. Analysis of stresses and strains near the end of a crack traversing a plate. *Journal of Applied Mechanics*, 24:361–364, 1957.

[12] L. B. Freund. Crack propagation in an elastic solid subjected to general loading. *Journal of the Mechanics and Physics of Solids*, 20(3):129 – 152, 1972. ISSN 0022-5096. doi:10.1016/0022-5096(72)90006-3.

[13] R. Toussaint, O. Lengliné, S. Santucci, T. Vincent-Dospital, M. Naert-Guillot, and K. J. Måløy. How cracks are hot and cool: a burning issue for paper. *Soft Matter*, 12:5563–5571, 2016. doi:10.1039/C6SM00615A.

[14] G. P. Marshall, L. H. Coutts, and J. G. Williams. Temperature effects in the fracture of PMMA. *Journal of Materials Science*, 9(9):1409–1419, Sep 1974. ISSN 1573-4803. doi:10.1007/BF00552926.

[15] D. Maugis. Subcritical crack growth, surface energy, fracture toughness, stick-slip and embrittlement. *Journal of Materials Science*, 20(9):3041–3073, Sep 1985. ISSN 1573-4803.

[16] G. Carbone and B. N. J. Persson. Hot cracks in rubber: Origin of the giant toughness of rubberlike materials. *Phys. Rev. Lett.*, 95:114301, Sep 2005. doi: 10.1103/PhysRevLett.95.114301.

[17] O. Lengliné, R. Toussaint, J. Schmittbuhl, J. E. Elkhoury, J. P. Ampuero, K. T. Tallakstad, S. Santucci, and K. J. Måløy. Average crack-front velocity during subcritical fracture propagation in a heterogeneous medium. *Phys. Rev. E*, 84:036104, Sep 2011. doi: 10.1103/PhysRevE.84.036104.

[18] S. Santucci. *Croissance lente thermiquement activée et piégeage d'une fissure dans les matériaux structurés à une échelle mésoscopique : expériences et modèles*. PhD thesis, Ecole normale supérieure de Lyon, www.theses.fr/2004ENSL0288, 2004.

[19] M. Yoda, M. Nabetani, and W. Shim. Creep crack growth in polyethylene under combined mode I and mode II loading. *International Journal of Fracture*, 112(3):21–26, Dec 2001. ISSN 1573-2673. doi:10.1023/A:1022681718523.

[20] S. M. Wiederhorn. Influence of water vapor on crack propagation in soda-lime glass. *Journal of the American Ceramic Society*, 50(8):407–414, 1967. doi: 10.1111/j.1151-2916.1967.tb15145.x.

[21] S.M. Wiederhorn and R.F. Jr. Krause. Crack growth in sapphire. In *Ceramic Engineering and Science Proceedings*, volume 23, pages 71–82. Wiley, 2002.

[22] P. M. Dove. Geochemical controls on the kinetics of quartz fracture at subcritical tensile stresses. *Journal of Geophysical Research: Solid Earth*, 100(B11):22349–22359, 1995. doi:10.1029/95JB02155.

[23] P.G. Meredith and B.K. Atkinson. Fracture toughness and subcritical crack growth during high-temperature tensile deformation of westerly granite and black gabbro. *Physics of the Earth and Planetary Interiors*, 39 (1):33 – 51, 1985. ISSN 0031-9201. doi:10.1016/0031-9201(85)90113-X.

[24] Y. Nara and K. Kaneko. Study of subcritical crack growth in andesite using the double torsion test. *International Journal of Rock Mechanics and Mining Sciences*, 42(4):521 – 530, 2005. ISSN 1365-1609. doi: 10.1016/j.ijrmms.2005.02.001.

[25] J. Holder, J. E. Olson, and Z. Philip. Experimental determination of subcritical crack growth parameters in sedimentary rock. *Geophysical Research Letters*, 28(4):599–602, 2001. doi:10.1029/2000GL011918.

[26] W. Wang, T. Tong, and Q. Yu. Subcritical crack growth induced by stress corrosion in hardened cement paste. In *9th International Conference on Fracture Mechanics of Concrete and Concrete Structures*. FraMCos, 2016. doi: 10.21012/FC9.177.

[27] Y. Nara, M. Takada, D. Mori, H. Owada, T. Yoneda, and K. Kaneko. Subcritical crack growth and long-term strength in rock and cementitious material. *International Journal of Fracture*, 164(1):57–71, Jul 2010. ISSN 1573-2673. doi:10.1007/s10704-010-9455-z.

[28] W. S. Oates, C. S. Lynch, D. C. Lupascu, A. B. K. Njiwa, E. Aulbach, and J. Rödel. Subcritical crack growth in lead zirconate titanate. *Journal of the American Ceramic Society*, 87(7):1362–1364, 2004. doi: 10.1111/j.1151-2916.2004.tb07736.x.

[29] J. Chevalier, C. Olagnon, and G. Fantozzi. Subcritical crack propagation in 3Y-TZP ceramics: Static and cyclic fatigue. *Journal of the American Ceramic Society*, 82(11):3129–3138, 1999. doi:10.1111/j.1151-2916.1999.tb02213.x.

[30] A. G. Evans and S. M. Wiederhorn. Crack propagation and failure prediction in silicon nitride at elevated temperatures. *Journal of Materials Science*, 9(2):270–278, Feb 1974. ISSN 1573-4803. doi:10.1007/BF00550951.

[31] G. Hénaff, G. Odemer, and B. Journet. Creep and creep-fatigue crack growth in aluminium alloys. In *Aluminium Alloys, Theory and Applications*, pages 259–282. IntechOpen, 2011. doi:10.5772/15153.

[32] J. H. Huang and C. J. Altstetter. Internal hydrogen-induced subcritical crack growth in austenitic stainless steels. *Metallurgical Transactions A*, 22(11):2605–2618, Nov 1991. ISSN 1543-1940. doi:10.1007/BF02851354.

[33] S. M. L. Sastry, R. J. Lederich, and B. B. Rath. Subcritical crack-growth under sustained load in Ti-6AI-6V-2Sn. *Metallurgical Transactions A*, 12(1):83–94, Jan 1981. ISSN 1543-1940. doi:10.1007/BF02648512.

[34] J. S. Nadeau. Subcritical crack growth in vitreous carbon at room temperature. *Journal of the American Ceramic Society*, 57(7):303–306, 1974. doi:10.1111/j.1151-2916.1974.tb10906.x.

[35] George B. Kaufman. Inorganic chemistry: principles of structure and reactivity, 4th ed. *Journal of Chemical Education*, 70(10):A279, 1993. doi:10.1021/ed070pA279.1.

[36] D.S. Dugdale. Yielding of steel sheets containing slits. *Journal of the Mechanics and Physics of Solids*, 8(2): 100 – 104, 1960. ISSN 0022-5096. doi:10.1016/0022-5096(60)90013-2.

[37] K. T. Tallakstad, R. Toussaint, S. Santucci, J. Schmittbuhl, and K. J. Måløy. Local dynamics of a randomly pinned crack front during creep and forced propagation: An experimental study. *Phys. Rev. E*, 83:046108, 04 2011.

[38] A. Cochard, O. Lengliné, K. J. Måløy, and R. Toussaint. Thermally activated crack fronts propagating in pinning disorder: simultaneous brittle/creep behavior depending on scale. *Philosophical Transactions of the Royal Society A : Mathematical, Physical and Engineering Sciences*, 2018. doi:10.1098/rsta.2017.0399.

[39] D. W. Tang and N. Araki. On non-fourier temperature wave and thermal relaxation time. *International Journal of Thermophysics*, 18(2):493, Mar 1997. ISSN 1572-9567. doi:10.1007/BF02575178.

[40] C. L. Rountree, Rajiv K. K., E. Lidorikis, A. Nakano, L. Van Brutzel, and P. Vashishta. Atomistic aspects of crack propagation in brittle materials: Multimillion atom molecular dynamics simulations. *Annual Review of Materials Research*, 32(1):377–400, 2002. doi: 10.1146/annurev.matsci.32.111201.142017.

[41] Y. Hwangbo, C-K. Lee, S-M. Kim, J-H. Kim, K-S. Kim, B. Jang, H-J. Lee, S-K. Lee, S.S. Kim, J-H. Ahn, and S-M. Lee. Fracture characteristics of monolayer cvd-graphene. *Scientific Reports*, 4:4439, 03 2014. doi: 10.1038/srep04439.

[42] A. Balandin, S. Ghosh, W. Bao, I. Calizo, D. Teweldebrhan, F. Miao, and J. Lau. Superior thermal conductivity of single-layer graphene. *Nano letters*, 8:902–7, 04 2008. doi:10.1021/nl0731872.

[43] X. Huang, G. Liu, and X. Wang. New secrets of spider silk: Exceptionally high thermal conductivity and its abnormal change under stretching. *Advanced Materials*, 24 (11):1482–1486, 2012. doi:10.1002/adma.201104668.

[44] J. R. Rice. Heating and weakening of faults during earthquake slip. *Journal of Geophysical Research: Solid Earth*, 111(B5), 2006. doi:10.1029/2005JB004006.

[45] GermÃ¡n A. Prieto, Manuel Florez, Sarah A. Barrett, Gregory C. Beroza, Patricia Pedraza, Jose Faustino Blanco, and Esteban Poveda. Seismic evidence for thermal runaway during intermediate-depth earthquake rupture. *Geophysical Research Letters*, 40(23):6064–6068, 2013. doi:10.1002/2013GL058109.

[46] C. H. Scholz. The brittle-plastic transition and the depth of seismic faulting. *Geologische Rundschau*, 77(1):319–328, Feb 1988. ISSN 1432-1149. doi: 10.1007/BF01848693.

[47] E. Aharonov and C. H. Scholz. The brittle-ductile transition predicted by a physics-based friction law. *Journal of Geophysical Research: Solid Earth*, 124(3):2721–2737, 2019. doi:10.1029/2018JB016878.

Is breaking through matter a hot matter? A material failure prediction by monitoring creep

SUPPLEMENTARY MATERIALS

Tom Vincent-Dospital,[1,2,*] Renaud Toussaint,[1,2,†] Alain Cochard,[1] Eirik G. Flekkøy,[2] and Knut Jørgen Måløy[2]

[1] *Université de Strasbourg, CNRS, IPGS UMR 7516, F-67000 Strasbourg, France*
[2] *SFF Porelab, The Njord Centre, Department of physics, University of Oslo, Norway*

CONTENTS

I. ANALYTICAL APPROXIMATION OF THE AVALANCHE THRESHOLD

Let us start this additional material with the analytical approximations of the temperature at a running crack tip. Assuming a quasi-constant velocity and energy release rate, some simplified expressions can indeed be derived (1) for ΔT. At low velocity, the typical diffusion skin depth is large compared to the radius of the heat production zone ($\sqrt{\lambda l/(V\pi C)}/l \gg 1$) and the heat diffusion is hence the ruling process:

$$\Delta T_{\text{slow}} \sim \phi G \frac{V}{\lambda}. \tag{1}$$

At high velocity, however, the rise in temperature is limited by the scale over which heat is produced and:

$$\Delta T_{\text{fast}} \sim \frac{\phi G}{\pi C l}. \tag{2}$$

Between these two cases, and typically for $V \sim \lambda/(\pi C l)$, an intermediate regime holds:

$$\Delta T_{\text{mid}} \sim \phi G \sqrt{\frac{V}{4\pi C \lambda l}}. \tag{3}$$

We invite the reader to a more in-depth derivation of these equations in Toussaint et al. (1) or Vincent-Dospital et al. (2).

* vincentdospitalt@unistra.fr
† renaud.toussaint@unistra.fr

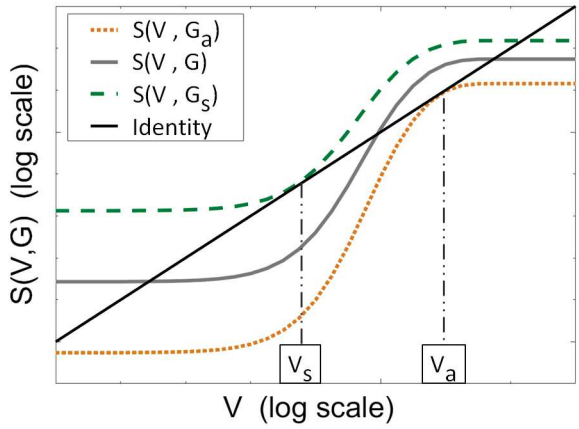

FIG. 1. Representation of $V = S(V, G)$ for three values of G: G_s, G_a and a mid-value between G_s and G_a (plain plot). The intersections of S_G with the identity plot (straight line) give the possible crack velocities for a given energy release rate, as per Eq. (4). The axes are not annotated for the sake of generality. See Ref. (2) for further information.

Now that some straightforward expressions for ΔT are known, we can move on to infer G_a. Our model, the Arrhenius law as considered in the main manuscript, defines a function $S(V, G)$ such that $S(V, G) = V$:

$$S(V,G) = V_0 \min\left[\exp\left(-\frac{\alpha^2[G_c - G]}{k_B[T_0 + \Delta T(V,G)]}\right), 1\right]. \tag{4}$$

To lighten the equations that will follow, we have here denoted α^2 the ratio $d_0^3/(2l)$. We have discussed, in the main manuscript, how this relation might have one to three solutions depending on G (see Fig. 1). Two particular energy release rates mark the passages from a singular to multiple solutions: the avalanche threshold G_a, of interest in this study, and another threshold, G_s, which is the load at which an avalanche has to stop.
All functions being continuously smooth, the switch from one solution to three solutions implies that $S(V, G)$ is tangent to the identity function for these two particular G, as illustrated in Fig 1. G_a and the corresponding velocity V_a must therefore verify the following system of equations:

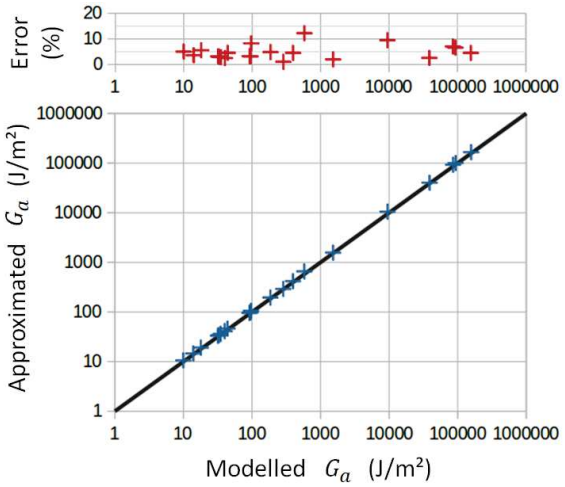

FIG. 2. (Bottom): G_a threshold, as approximated by Eq. (11) versus the accurate numerical solution of the model. The black line is the identity. (Top): Relative error from the approximation

$$S(V,G) = V \tag{5}$$

$$\frac{\partial S}{\partial V}(V,G) = 1. \tag{6}$$

To solve this system, we assume that the transition towards the fast phase happens in a regime where the temperature elevation still increases linearly with the crack velocity (i.e., $\Delta T = \Delta T_{\text{slow}}(V,G)$ (1)). Equation (6) then becomes:

$$\frac{\phi G \lambda \alpha^2 (G_c - G)}{k_b(\lambda T_0 + \phi G V)^2} S(V,G) = 1. \tag{7}$$

Inserting Eq. (5) back into (7) leads to the following quadratic equation in V:

$$\left(\frac{\phi G V}{\lambda T_0}\right)^2 + \left[2 + \frac{\alpha^2(G - G_c)}{k_b T_0}\right] \frac{\phi G V}{\lambda T_0} + 1 = 0. \tag{8}$$

While it might of course hold two solutions, only the lower one is of interest to derive the avalanche threshold G_a. The upper solution would indeed correspond to the 'arrest' of the crack avalanche, but the initial hypothesis of $\Delta T = \Delta T_{\text{slow}}$ would there anyway be wrong, as this 'arrest' occurs while on the quick (hot) propagation branch. Focusing therefore on the lower solution of (8), we have:

$$V_a = \frac{T_0 \lambda}{2\phi G_a}(R_a - 2 - R_a\sqrt{1 - 4/R_a}), \tag{9}$$

with $R_a = \alpha^2(G_c - G_a)/(k_B T_0)$. This equation indicates at which slow velocity a crack avalanches, given the corresponding G_a threshold. Substituting (9) in (5), one finally derives the equality that defines the avalanche threshold:

$$G_a \sim \frac{\lambda T_0}{2\phi V_0} \frac{R_a - 2 - R_a\sqrt{1 - 4/R_a}}{\exp\left(-2/\left[1 - \sqrt{1 - 4/R_a}\right]\right)}. \tag{10}$$

Such an expression gives a fairly good approximation of G_a as predicted by the model. The only hypothesis was indeed the validity of Eq. (1), that is $\sqrt{\lambda l/(V_a \pi C)}/l \gg 1$ and, for the materials that we have studied in our manuscript, this ratio ranges from 300 to 1500. While Eq. (10) is easy to solve for G_a with any numerical method, it can however be further simplified by grossly assuming that $R_a \gg 4$ and by developing the term $\sqrt{1 - 4/R_a}$. We thus obtain the equation presented in the manuscript:

$$G_a \sim \frac{\lambda T_0}{\phi V_0} \frac{\exp(R_a)}{R_a}. \tag{11}$$

Figure 2 shows the quality of the approximation for G_a, off by a few percents as, as shown in Tab. I, the $R_a \gg 4$ hypothesis is not strictly valid.

II. THE ARREST THRESHOLD (FOR COMPLETENESS)

Similarly, one can solve (5) and (6) at the 'arrest' point: the transition from a quick regime back to the low velocity phase, occurring at the particular load G_s. While G_a is vastly reported for a lot of materials, making it the topic of this manuscript, G_s is more rarely reported, so that the following computation is given for completeness. We here assume that the transition arises when the crack cools down from the plateau temperature $\Delta T = \Delta T_{\text{fast}}(G)$ (2), along the intermediate slope defined by $\partial \Delta T/\partial V = \partial \Delta T_{\text{mid}}(V,G))/\partial V$ (3). We thus turn the system into a quadratic equation of $\sqrt{V}$:

$$\left(\frac{\phi G\sqrt{V}}{4\pi\lambda C l T_0}\right)^2 + \left(2 + \frac{\alpha^2(G - G_c)}{2k_b T_0}\right)\left(\frac{\phi G\sqrt{V}}{4\pi\lambda C l T_0}\right) + 1 = 0, \tag{12}$$

the upper solution of which, together with Eq. (5), leads to:

$$V_s = \frac{\pi\lambda C l {T_0}^2}{4(\phi G_s)^2}\left[R_s - 4 + R_s\sqrt{1 - 8/R_s}\right]^2, \tag{13}$$

where $R_s = \alpha^2(G_c - G_s)/(k_B T_0)$. When inserting (13) back into (5), one gets:

$$\frac{4(\phi G_s)^2 V_0}{\pi\lambda C l {T_0}^2} = \frac{\left[R_s - 4 + R_s\sqrt{1-8/R_s}\right]^2}{\exp\left(\dfrac{\alpha^2(G_s - G_c)}{k_b[T_0 + \phi G_s/(\pi C l)]}\right)}. \tag{14}$$

Assuming that $R_s \gg 8$ and $\Delta T_{\text{fast}} \gg T_0$, Eq. (14) further simplifies to:

$$G_s \sim \frac{T_0}{\phi}\sqrt{\frac{\pi C l}{V_0}}\exp\left(\frac{\pi C l T_0}{2\phi G_s}\right) R_s, \tag{15}$$

which gives a relatively simple expression to invert for G_s.

III. MATERIALS CREEP CROSSPLOTS AND PARAMETERS TABLE

A summary of the model parameters considered for each media is also provided in Tab. I. These parameters are deduced, as explained in the main manuscript, from the V to G creep data of these materials, shown in Fig 3 to Fig 20. One can notably notice the variability in fit quality for these datasets, that of course impacts our inversion work, but also how it is not always straight forward to know to which subcritical phase the data correspond (i.e., phase I to III, from environmental induced corrosion to void-like conditions).

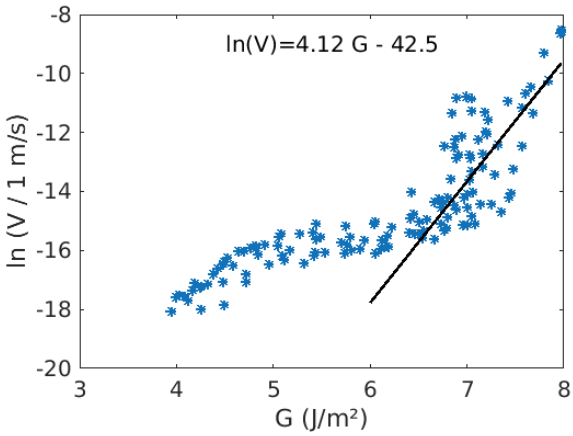

FIG. 3. Creep data of dry soda-lime glass, from Wiederhorn (3), figure 3. A rather complex creep law holds there so that we only roughly fitted the last part.

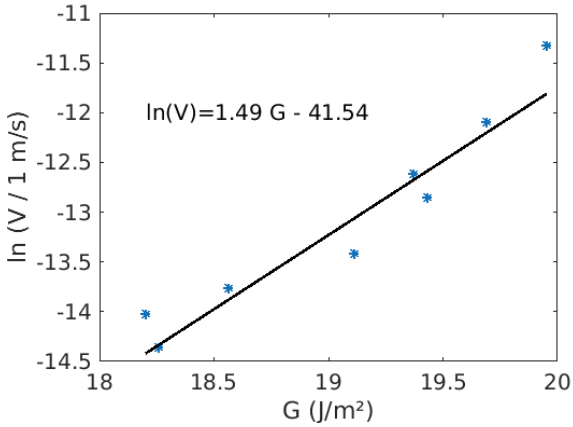

FIG. 4. Creep data of dry sapphire (r-plane), from Wiederhorn and Krause (4).

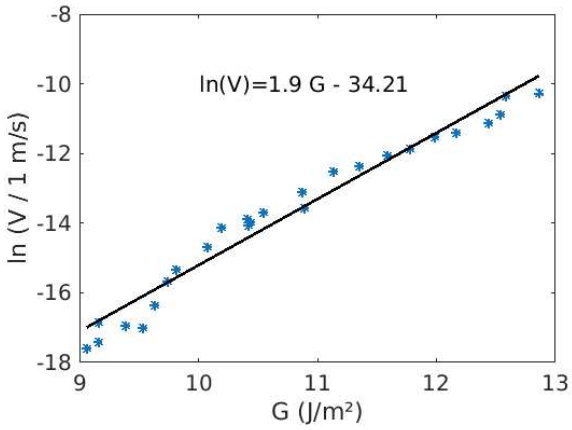

FIG. 5. Creep data of quartz in vacuum, from Dove (5), figure 4.

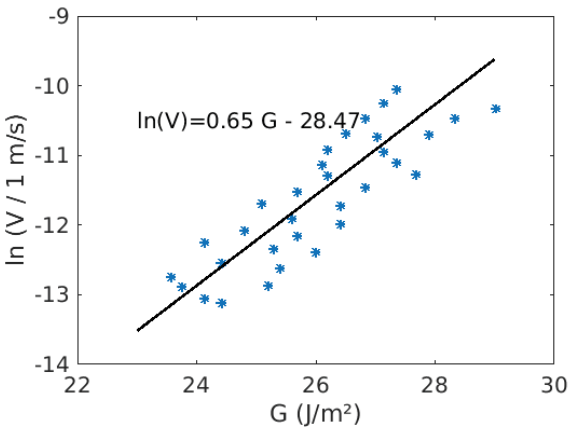

FIG. 6. Creep data of Scioto sandstone, from Holder et al. (6), figure 3.

	λ (SI)	ϕ (-)	V_0 (m/s)	l (Å)	T_0 (K)	G_c (J/m^2)	G_a real (J/m^2)	G_a model (J/m^2)	Ra (-)
Acrylic adhesive	0.4	1	30	10	296	**150**	**90**	**97**	5.7
Paper	0.035	0.12	1300	1000	296	**25000**	**14000**	**9500**	15.6
Bulk PMMA	0.18	0.2	880	80	296	**1300**	**700**	**580**	10.9
Interfacial PMMA	0.18	0.2	880	8	298	**275**	**140**	**190**	13.5
HD Polyethylene	0.4	0.5	900	8500	293	**200000**	**70000**	**87000**	16.6
Soda lime glass	1	0.5	3400	0.3	296	**12**	**8**	**10**	8.3
Sapphire	24	0.5	6000	0.8	296	**36**	**20**	**32**	6
Quartz	8	0.5	3400	0.6	293	**21**	**13**	**18**	5.7
Westerly Granite (ambient)	2	0.5	3000	4	293	**120**	**68**	**92**	8.5
Westerly Granite (hot)	2	0.5	3000	0.7	573	**43**	**24**	**35**	6.8
Kumamoto Andesite	1	0.5	2200	3	330	**120**	**80**	**97**	8.8
Scioto Sandstone	2	0.5	2000	2	296	**55**	**37**	**44**	7.3
Cement paste	1	0.5	2200	3	298	**310**	**250**	**280**	10.7
HSULP Concrete	0.8	0.5	3000	1	293	**44**	**38**	**40**	9.9
Vitreous carbon	5	0.5	2600	0.2	296	**15**	**13**	**14**	7.2
Lead Zirconate Titanate (PZT)	1	0.5	2000	1	296	**40**	**24**	**33**	11.3
Tetragonal zirconia (TZP)	2	0.5	1600	40	298	**1900**	**1500**	**1530**	10.9
Silicon nitride	30	0.5	5500	45	1573	**510**	**260**	**400**	8.9
2650 T6 Aluminium alloy	150	0.5	3100	1000	448	**54500**	**27000**	**39000**	10.1
AISI 310S Stainless Steel alloy	14	0.5	3000	9000	298	**265000**	**102000**	**158000**	13.4
Ti-6A1-6V-2Sn Titanium	7	0.5	3100	8000	298	**190000**	**72000**	**93000**	14.9

TABLE I. Model parameters for various materials of the literature. The real and modelled G_a thresholds are compared in the two former last columns. The cells colour help to highlight standing out values for λ and T_0.

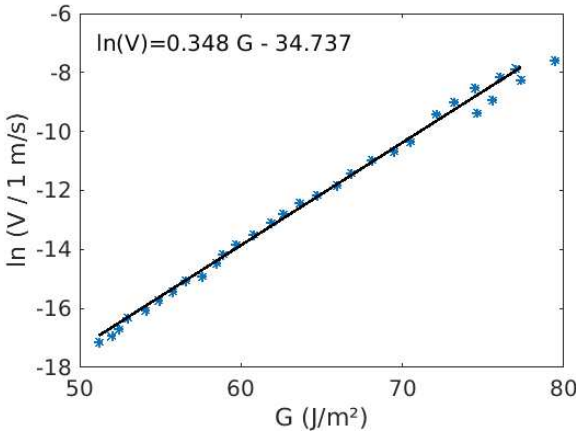

FIG. 7. Creep data of Kumamoto andesite in moist air at 67 °C, from Nara and Kaneko (7), figure 9.

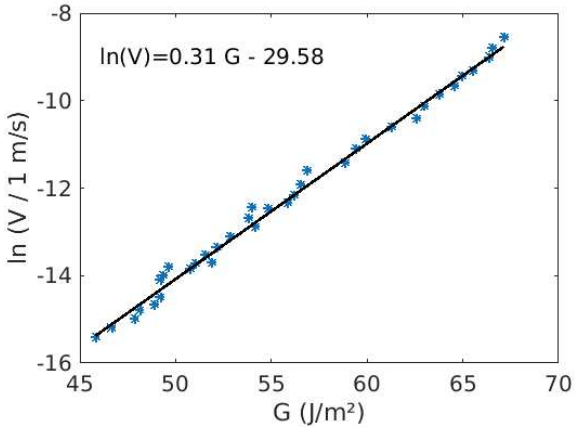

FIG. 8. Creep data of Westerly granite in moist air at 20 °C, from Meredith and Atkinson (8), figure 7.

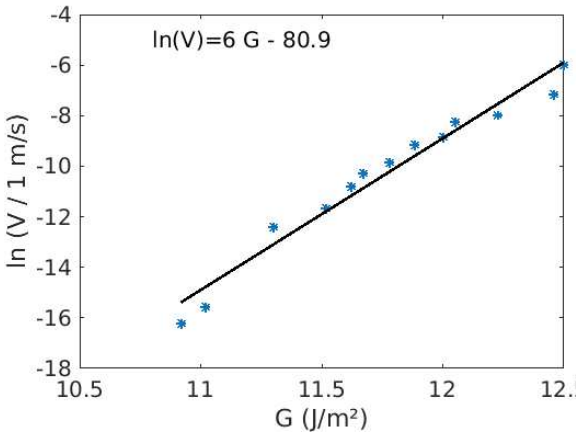

FIG. 9. Creep data of vitreous carbon, from Nadeau (9), figure 4.

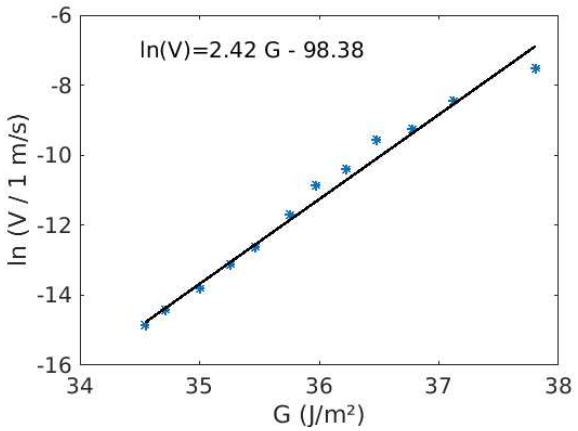

FIG. 10. Creep data of high strength ultra low porosity concrete in moist air, from Nara et al. (10), figure 9.

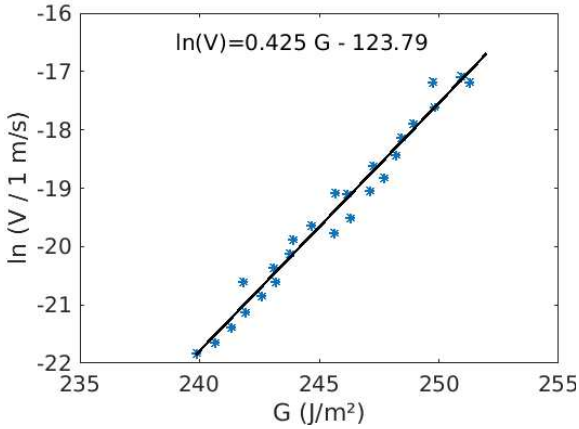

FIG. 11. Creep data cement in water, from Wang et al. (11), figure 4a.

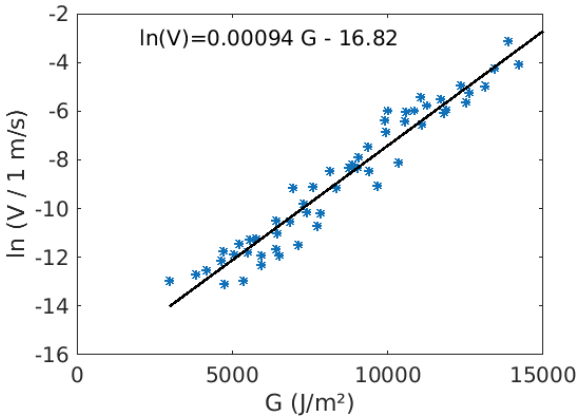

FIG. 12. Creep data of paper in air, from Santucci (12), figure 3.32.

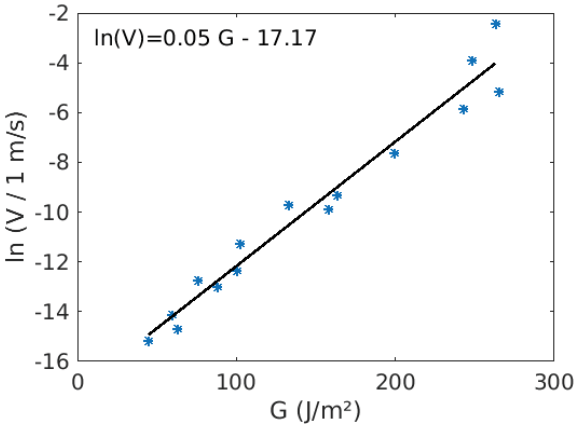

FIG. 13. Creep data of hot silicon nitride at 1200 °C, from Evans and Wiederhorn (13), figure 5.

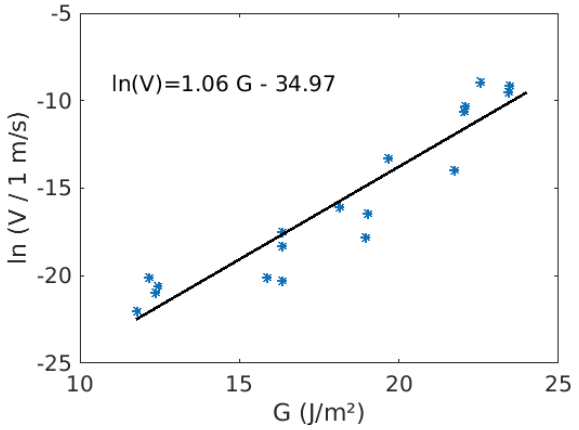

FIG. 14. Creep data of Lead Zirconate Titanate at ambient conditions, from Oates et al. (14), figure 2 (open circuit).

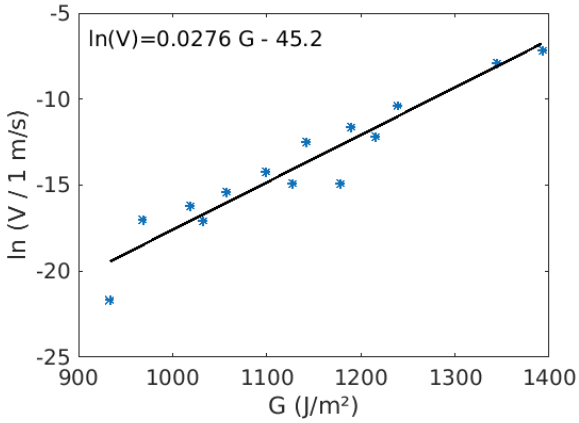

FIG. 15. Creep data tetragonal zirconia (TZP) in vacuum, from Chevalier et al. (15), figure 5.

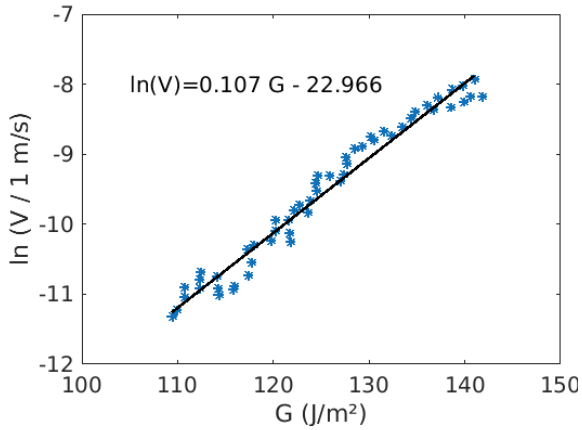

FIG. 16. Interfacial creep data in sintered PMMA plates in air, from Lengliné et al. (16), figure 5.

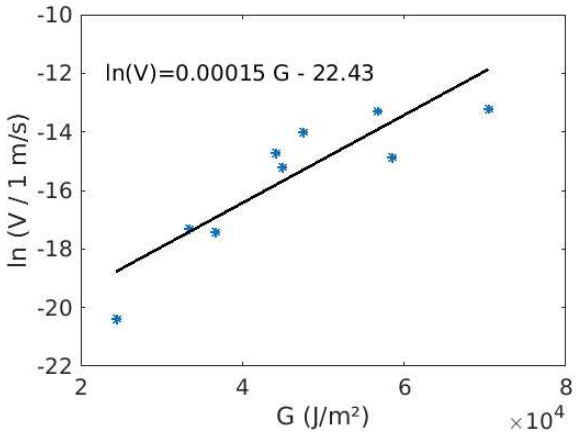

FIG. 17. Creep data of high density polyethylene, from Yoda et al. (17), figure 4.

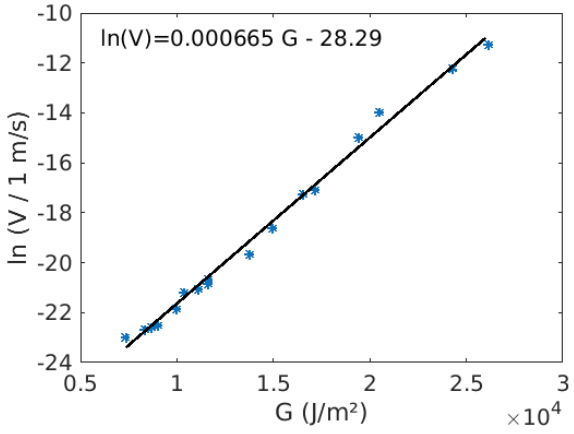

FIG. 18. Creep data of aluminium 2650 T6 alloy in vacuum at 175 °C, from Hénaff et al. (18), figure 6.

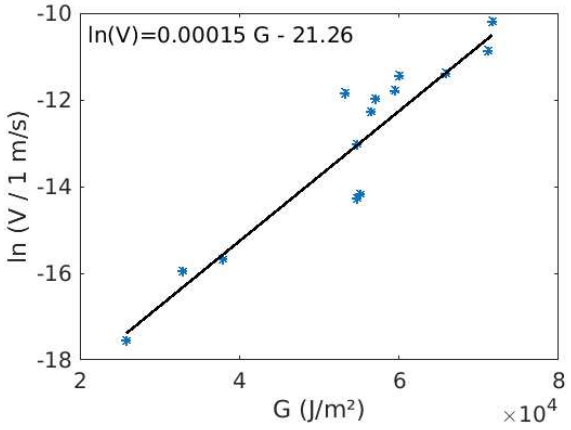

FIG. 19. Creep data in Ti-6A1-6V-2Sn titanium alloy in moist air, from Sastry et al. (19), figure 6a (beta annealed).

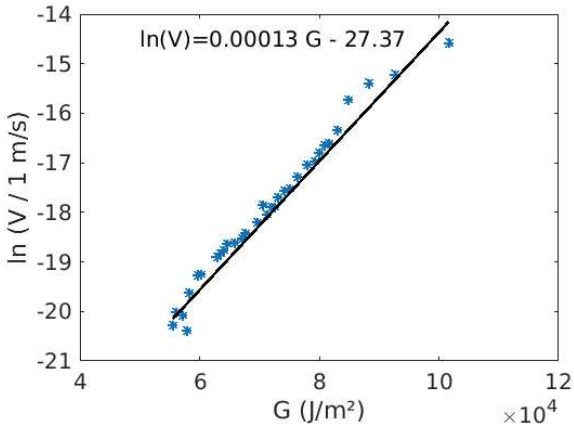

FIG. 20. Creep data of AISI 310S austenitic stainless steel in air, from Huang and Altstetter (20), figure 1 (uncharged plot).

[1] R. Toussaint, O. Lengliné, S. Santucci, T. Vincent-Dospital, M. Naert-Guillot, and K. J. Måløy. How cracks are hot and cool: a burning issue for paper. *Soft Matter*, 12:5563–5571, 2016. doi:10.1039/C6SM00615A.

[2] T. Vincent-Dospital, R. Toussaint, A. Cochard, K. J. Måløy, and E. G. Flekkøy. Thermal weakening of cracks and brittle-ductile transition of matter: A phase model. *Physical Review Materials*, 02 2020. doi: 10.1103/PhysRevMaterials.4.023604.

[3] S. M. Wiederhorn. Influence of water vapor on crack propagation in soda-lime glass. *Journal of the American Ceramic Society*, 50(8):407–414, 1967. doi: 10.1111/j.1151-2916.1967.tb15145.x.

[4] S.M. Wiederhorn and R.F. Jr. Krause. Crack growth in sapphire. In *Ceramic Engineering and Science Proceedings*, volume 23, pages 71–82. Wiley, 2002.

[5] P. M. Dove. Geochemical controls on the kinetics of quartz fracture at subcritical tensile stresses. *Journal of Geophysical Research: Solid Earth*, 100(B11):22349–22359, 1995. doi:10.1029/95JB02155.

[6] J. Holder, J. E. Olson, and Z. Philip. Experimental determination of subcritical crack growth parameters in sedimentary rock. *Geophysical Research Letters*, 28(4):599–602, 2001. doi:10.1029/2000GL011918.

[7] Y. Nara and K. Kaneko. Study of subcritical crack growth in andesite using the double torsion test. *International Journal of Rock Mechanics and Mining Sciences*, 42(4):521 – 530, 2005. ISSN 1365-1609. doi: 10.1016/j.ijrmms.2005.02.001.

[8] P.G. Meredith and B.K. Atkinson. Fracture toughness and subcritical crack growth during high-temperature tensile deformation of westerly granite and black gabbro. *Physics of the Earth and Planetary Interiors*, 39 (1):33 – 51, 1985. ISSN 0031-9201. doi:10.1016/0031-9201(85)90113-X.

[9] J. S. Nadeau. Subcritical crack growth in vitreous carbon at room temperature. *Journal of the American Ceramic Society*, 57(7):303–306, 1974. doi:10.1111/j.1151-2916.1974.tb10906.x.

[10] Y. Nara, M. Takada, D. Mori, H. Owada, T. Yoneda, and K. Kaneko. Subcritical crack growth and long-term strength in rock and cementitious material. *International Journal of Fracture*, 164(1):57–71, Jul 2010. ISSN 1573-2673. doi:10.1007/s10704-010-9455-z.

[11] W. Wang, T. Tong, and Q. Yu. Subcritical crack growth induced by stress corrosion in hardened cement paste. In *9th International Conference on Fracture Mechanics of Concrete and Concrete Structures*. FraMCos, 2016. doi: 10.21012/FC9.177.

[12] S. Santucci. *Croissance lente thermiquement activée et piégeage d'une fissure dans les matériaux structurés à une échelle mésoscopique : expériences et modèles*. PhD thesis, Ecole normale supérieure de Lyon, www.theses.fr/2004ENSL0288, 2004.

[13] A. G. Evans and S. M. Wiederhorn. Crack propagation and failure prediction in silicon nitride at elevated temperatures. *Journal of Materials Science*, 9(2):270–278, Feb 1974. ISSN 1573-4803. doi:10.1007/BF00550951.

[14] W. S. Oates, C. S. Lynch, D. C. Lupascu, A. B. K. Njiwa, E. Aulbach, and J. Rödel. Subcritical crack growth in lead zirconate titanate. *Journal of the American Ceramic Society*, 87(7):1362–1364, 2004. doi: 10.1111/j.1151-2916.2004.tb07736.x.

[15] J. Chevalier, C. Olagnon, and G. Fantozzi. Subcritical crack propagation in 3Y-TZP ceramics: Static and cyclic fatigue. *Journal of the American Ceramic Society*, 82(11):3129–3138, 1999. doi:10.1111/j.1151-2916.1999.tb02213.x.

[16] O. Lengliné, R. Toussaint, J. Schmittbuhl, J. E. Elkhoury, J. P. Ampuero, K. T. Tallakstad, S. Santucci, and K. J. Måløy. Average crack-front velocity during subcritical fracture propagation in a heterogeneous medium. *Phys. Rev. E*, 84:036104, Sep 2011. doi: 10.1103/PhysRevE.84.036104.

[17] M. Yoda, M. Nabetani, and W. Shim. Creep crack growth in polyethylene under combined mode I and mode II loading. *International Journal of Fracture*, 112(3):21–26, Dec 2001. ISSN 1573-2673. doi:10.1023/A:1022681718523.

[18] G. Hénaff, G. Odemer, and B. Journet. Creep and creep-fatigue crack growth in aluminium alloys. In *Aluminium Alloys, Theory and Applications*, pages 259–282. IntechOpen, 2011. doi:10.5772/15153.

[19] S. M. L. Sastry, R. J. Lederich, and B. B. Rath. Subcritical crack-growth under sustained load in Ti-6AI-6V-2Sn. *Metallurgical Transactions A*, 12(1):83–94, Jan 1981. ISSN 1543-1940. doi:10.1007/BF02648512.

[20] J. H. Huang and C. J. Altstetter. Internal hydrogen-induced subcritical crack growth in austenitic stainless steels. *Metallurgical Transactions A*, 22(11):2605–2618, Nov 1991. ISSN 1543-1940. doi:10.1007/BF02851354.

A FEW MORE ANALYTICAL FEATURES OF THE CRITICAL POINT

ABSTRACT

In the preceding article supplementary material, we provided some analytical approximations of the avalanche and arrest thresholds in energy release rate according to our crack propagation model. Here, I am pushing this analytical work slightly further and study the implications of these approximations for the model critical point. To generate the following couple of figures, I have used the same parameters as those proposed in the first chapter of this thesis [1], for the rupture of interfacial PMMA. As a reminder, these parameters were: $V_0 = 1000\,\mathrm{m\,s^{-1}}$, $G_c = 250\,\mathrm{J\,m^{-2}}$, $\alpha^2/(k_B T_0) = 0.15$, $T_0 = 293\,\mathrm{K}$, $l = 20\,\mathrm{nm}$, $\phi = 1$, $\lambda = 0.18\,\mathrm{J/(m\,s\,K)}$, $C = 1.5\,\mathrm{MJ\,m^{-3}}$.

I. WHERE IS THE CRITICAL POINT?

In the previous pages, we derived two systems of equations to approximate G_a, V_a, G_s and V_s, the energy release rates and propagation velocities at the onset and end of avalanches. These systems were:

$$V_a = \frac{T_0 \lambda}{2\phi G_a}(R_a - 2 - R_a\sqrt{1 - 4/R_a}), \tag{1}$$

$$G_a \sim \frac{\lambda T_0}{2\phi V_0}\frac{R_a - 2 - R_a\sqrt{1-4/R_a}}{\exp\left(-2/\left[1-\sqrt{1-4/R_a}\right]\right)}, \tag{2}$$

and

$$V_s = \frac{\pi\lambda C l {T_0}^2}{4(\phi G_s)^2}\left[R_s - 4 + R_s\sqrt{1-8/R_s}\right]^2, \tag{3}$$

$$\frac{4(\phi G_s)^2 V_0}{\pi\lambda C l {T_0}^2} = \frac{\left[R_s - 4 + R_s\sqrt{1-8/R_s}\right]^2}{\exp\left(\dfrac{\alpha^2(G_s - G_c)}{k_b[T_0 + \phi G_s/(\pi C l)]}\right)}. \tag{4}$$

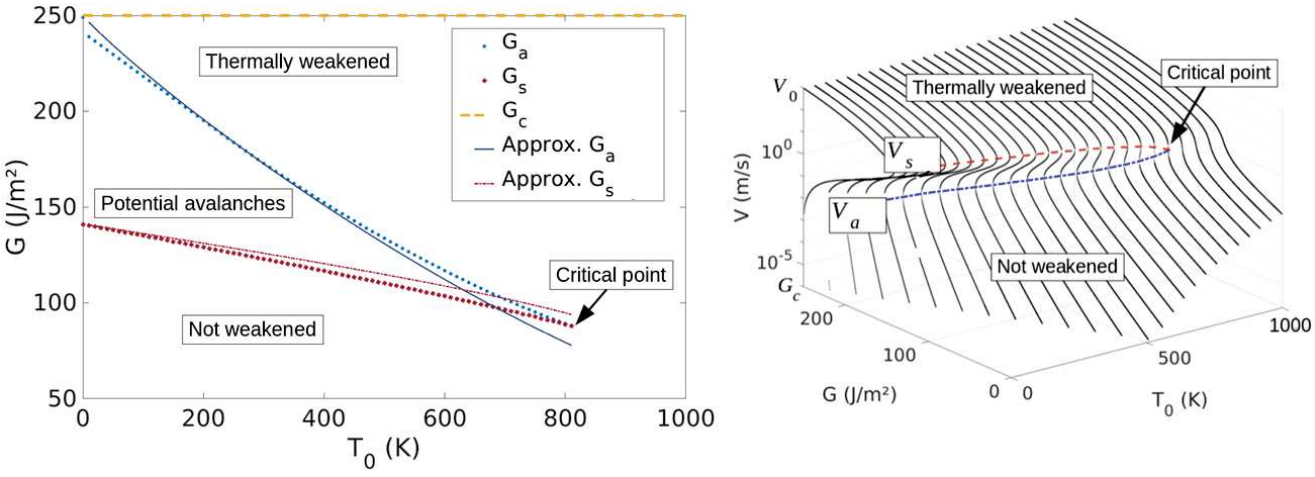

FIG. 1. (left): G_a and G_s as functions of the ambient temperature T_0, both solved numerically as well as using the approximate equations (2) and (4). One can notice the critical point which the approximations are failing to recover quantitatively. The horizontal dashed line at the top is for $G = G_c$ domain. Note: this plot is a top view of the phase diagram of Vincent-Dospital et al. [1], which I have reinserted here (plot on the right).

where all parameters keep the same definition as previously introduced. For various values of the ambient temperature T_0, Fig. 1 graphically compares the G thresholds out of these solutions to the more accurately, numerically, computed ones, derived in Ref. [1] based on the model constitutive Arrhenius law and heat equation. While the match is overall good, one can notice that the critical point is not recovered quantitatively by the analytical approximations from (2) and (4).

Remember however that approximations (2) and (4) each were derived from one of the roots of two second order polynomials. One of this polynomial, in V, was based on the low velocity (cool) approximation for the temperature elevation at the crack front ΔT and allowed to derive the expression for G_a. The other one, in $\sqrt{V}$, was based on the high velocity (hot) approximations for ΔT, and led to the expression for G_s.

At the critical point, such description is not to be valid, as the maximum temperature elevation at the tip is there just enough to trigger a phase shift. Thus, G_a is rather involving a temperature elevation which follows the hot regime rather than the cool one. In other words, in the critical vicinity, both G_a and G_s likely approximate to the two solutions of the, latter, polynomial (that based on the hot front approximations) that I here write again as a reminder:

$$\left(\frac{\phi G\sqrt{V}}{4\pi\lambda C l T_0}\right)^2 + \left(2+\frac{\alpha^2(G-G_c)}{2k_bT_0}\right)\left(\frac{\phi G\sqrt{V}}{4\pi\lambda C l T_0}\right) + 1 = 0, \tag{5}$$

As the discriminant of this polynomial tends to zero, both solutions merge together, leading to $G_a = G_s$, that is, to the critical point. By noting $R = \alpha^2(G_c - G)/k_bT_0$, this discriminant (denoted Δ) is

$$\Delta = \left(\frac{\phi G}{4\pi\lambda C l T_0}\right)^2 \left(\frac{R}{8}-1\right) 2R, \tag{6}$$

and tends to 0 for $R = 8$, for $G = 0$, or for $G = G_c$ (that is $R = 0$). The two latter cases correspond to the particular situations of, relatively, an unloaded crack and an overcritical crack. More generally, at the critical point, one should then get

$$\alpha^2(G_c - G^*) = 8k_bT_0^*, \tag{7}$$

where T_0^* is the critical temperature and G^* the critical energy release rate defining the critical point. The linear domain defined by Eq (7) is then shown in Fig. 2, which also shows the position of the critical point for several sets of parameters, that were numerically computed without approximations. A good match is shown.

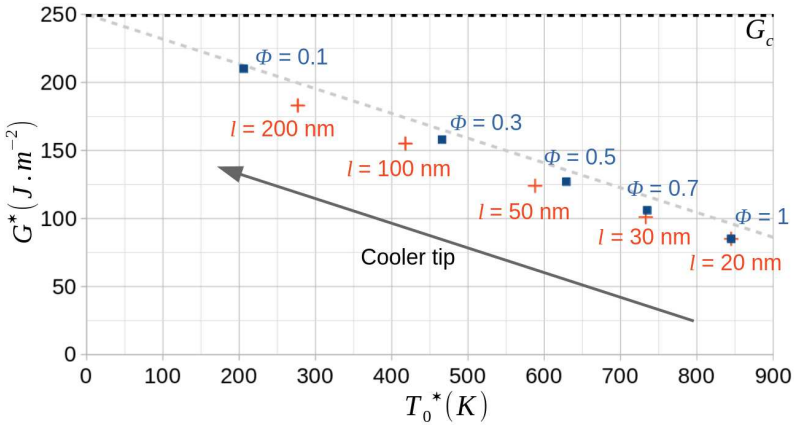

FIG. 2. Critical point location with varying ϕ and l. Points are for $l = 20\,\text{nm}$ and varying ϕ. Crosses are for $\phi = 1$ and varying l. The dotted line is the domain defined by Eq. (7): $\alpha^2(G_c - G^*) = 8k_bT_0^*$. Of course, the warmer a crack front (for higher ϕ and smaller l), the higher is the critical temperature. The horizontal dashed line at the top is for $G = G_c$ domain.

II. DERIVING THE CRITICAL EXPONENT β'

The description of $\sqrt{V_\mathrm{a}}$ and $\sqrt{V_\mathrm{s}}$ around the critical point as approximately the two solutions of a same second order polynomial (i.e., Eq. (5)) also allows to analytically derive the critical exponent $\beta' = 1/2$, inverted in Ref. [1], and which was defined in the critical vicinity by the equivalence:

$$\frac{V_\mathrm{s} - V_\mathrm{a}}{V^*} \sim \left(\frac{T_0^* - T_0}{T_0^*}\right)^{\beta'}. \tag{8}$$

Indeed, the expression for V_a analogous to Eq. (3) is (by only changing the sign in front of the square root of the discriminant):

$$V_\mathrm{a} = \frac{\pi\lambda C l {T_0}^2}{4(\phi G_\mathrm{a})^2}\left[R_a - 4 - R_a\sqrt{1 - 8/R_a}\right]^2. \tag{9}$$

Subtracting (9) to (3) in the critical vicinity ($R_\mathrm{a} \sim R_\mathrm{s} \sim R$), and dropping their prefactor, leads to

$$(V_\mathrm{s} - V_\mathrm{a}) \sim 4\,(R-4)\left(R^2 - 8R\right)^{1/2}. \tag{10}$$

Thus, by dividing the left term of this equivalence by V^* to look at an homogeneous equation, and because R tends to 8 at the critical point, the velocity convergence mainly behaves as

$$\frac{V_\mathrm{s} - V_\mathrm{a}}{V^*} \sim \left(\frac{\alpha^2(Gc - G)}{k_B T_0} - 8\right)^{1/2}. \tag{11}$$

If one only looks at the influence of the ambient temperature in this convergence (which is the spirit of Eq. (8)), we can approximate $G = G^*$, so that

$$\frac{V_\mathrm{s} - V_\mathrm{a}}{V^*} \sim \left(\frac{\alpha^2(Gc - G^*)}{k_B T_0} - 8\right)^{1/2}. \tag{12}$$

By additionally using Eq. (7), we get:

$$\frac{V_\mathrm{s} - V_\mathrm{a}}{V^*} \sim \sqrt{8}\left(\frac{T_0^*}{T_0} - 1\right)^{1/2}, \tag{13}$$

and finally

$$\frac{V_\mathrm{s} - V_\mathrm{a}}{V^*} \sim \left(\frac{T_0^* - T_0}{T_0^*}\right)^{1/2}, \tag{14}$$

which is the expected result.

---

[1] T. Vincent-Dospital, R. Toussaint, A. Cochard, K. J. Måløy, and E. G. Flekkøy. Thermal weakening of cracks and brittle-ductile transition of matter: A phase model. *Physical Review Materials*, 02 2020. doi:10.1103/PhysRevMaterials.4.023604.

Chapter IV
Fracture creep in disordered interfaces: Arrhenius based simulations and comparison of the spatial and temporal intermittency to experimental data

---

Where the model, without thermal weakening but with the redistribution of stress, allows simulating interfacial crack fronts in disordered materials

---

Pending submission, maybe to PRMaterials
see lastly updated version, arXiv: 2010.06865

Résumé (*French abstract*):

Fluage de fissures dans des interfaces désordonnées: simulations basées sur une loi d'Arrhenius et comparaison avec l'intermittence spatiale et temporelle de données expérimentales.

Nous montrons qu'un modèle de fracture sous-critique, couplé avec une redistribution élastique de la contrainte mécanique le long des fronts de rupture rugueux, permet de simuler la dynamique intermittente de fissures expérimentales se propageant dans des interfaces désordonnées. Pour ce, nous supposons que l'énergie de fracture de cette interface (au sens d'un taux de libération d'énergie critique) suit une distribution normale spatialement corrélée, et étudions ensuite des simulations numériques de rupture dans ce milieu. Nous comparons alors divers observables statistiques des résultats ainsi obtenus avec ceux acquis grâce à des expériences de fissuration dans des interfaces rugueuses de polymethylmethacrylate (PMMA), ainsi que reportés dans un manuscrit précédent. Ces observables comptent notamment la distribution des vitesses locales de propagation le long de la fracture, l'exposant de croissance du front, les corrélations spatiales et temporelles du champ de vitesse, la distribution de taille des avalanches de la dynamique intermittente et les coefficients de Hurst du front. La plupart des statistiques simulées montrent un bon accord avec les statistiques expérimentales, et nous proposons ainsi une nouvelle indication que des lois d'activations sous-critiques de type Arrhenius sont adaptées à la description du fluage de fissures.

Fracture creep in disordered interfaces: Arrhenius based simulations and comparison of the spatial and temporal intermittency with that of experimental fronts

Tom Vincent-Dospital,[1,2,*] Alain Cochard,[1] Stéphane Santucci,[3] Knut Jørgen Måløy,[2] and Renaud Toussaint[1,2,†]

[1] *Université de Strasbourg, CNRS, IPGS UMR 7516, France*
[2] *SFF Porelab, The Njord Centre, Department of physics, University of Oslo, Norway*
[3] *Université de Lyon, ENS de Lyon, Université Claude Bernard, CNRS, Laboratoire de Physique, France.*

We present a subcritical fracture growth model, coupled with the elastic redistribution of the acting mechanical stress along rugous rupture fronts. We show the ability of this model to simulate the intermittent dynamics of experimental cracks propagating in disordered interfaces. To this end, we assume that the fracture energy (in the sense of a critical energy release rate) of such interfaces follows a spatially correlated normal distribution, and then run numerical rupture simulations in this material. We compare various statistical features from the hence obtained fracture dynamics to that from experimental cracks propagating in sintered polymethylmethacrylate (PMMA) interfaces, as reported in an earlier manuscript. These features include the distribution of the local growth velocity along the rupture fronts, the growth exponent of these fronts, the spatial and temporal correlations of the velocity fields, the avalanches size distribution of the intermittent dynamics and the fronts Hurst exponents. Most modelled statistics show a good agreement with the experimental ones, and we thus provide new evidence that Arrhenius-like subcritical growth laws are suitable for the description of creeping cracks.

I. INTRODUCTION

In the physics of rupture, understanding the effects that material disorder has on the propagation of cracks is of prime interest. For instance, the overall strength of large solids is believed to be ruled by the weakest locations in their structures, and notably by the voids in their bulk samples [1, 2]. There, cracks tend to initiate as the mechanical stress is concentrated. A growing focus has been brought on models in which the description of the breaking matrix remains continuous (i.e., without pores). There, the material disorder resides in the heterogeneities of the matrix [3–8]. The propagation of a cracks is partly governed by its spatial distribution in surface fracture energy, that is, the heterogeneity of the energy needed to generate two opposing free unit surfaces in the continuous matrix [9], including the dissipation processes at the tip [10]. From this disorder, one can model a rupture dynamics which holds a strongly intermittent behaviour, with extremely slow (i.e., pinned) and fast (i.e., avalanching) propagation phases. In many physical processes, including but not limited to the physics of fracture [11–14], such intermittency is referred to as crackling noise [15, 16].

Over the last decades, numerous experiments have been run on the interfacial rupture of oven-sintered acrylic glass bodies (PMMA) [17–19], in which random heterogeneities in the fracture energy were introduced in a controlled way by sand blasting the interface prior to the sintering process. This method has allowed to study the dynamics of rugous fronts, in particular because the transparent PMMA interface becomes more opaque when broken. Indeed, the generated rough air-PMMA interfaces reflects more light, and the growth of fronts can thus be monitored. Different models [4–6, 8, 20, 21] have successfully described part of the statistical features of the recorded crack dynamics. A recent one (Cochard et al. [8]) is a thermally activated model, based on an Arrhenius law, by contrast to others that are threshold based (the crack only advances when the stress reaches a local threshold). A notable advantage of this subcritical framework is that its underlying processes are, physically, well understood, and Arrhenius-like laws have long been used [22–25] to describe the slow creep of fractures. This subcritical model has proven to describe both the mean behaviour of experimental fronts [26] (i.e., the average front velocity under a given load) and the actual distributions of propagation velocities along these fronts [8]. It has recently been proposed [27, 28] that it might also explain the faster failure of brittle matter, that is, the dramatic propagation of cracks at velocities close to that of mechanical waves, when taking into account the energy dissipated as heat around a progressing crack tip. Indeed, if fronts creep fast enough, their local rise in temperature becomes significant compared to the background one, so that they can avalanche to a very fast phase, in a positive feedback loop [27, 28].

Here, we only consider slow fronts (i.e., fronts that creep slowly enough so that their temperature elevation is supposed to remain negligible). Building on the work of Cochard et al. [8], we study various statistical features that can be generated with this Arrhenius-based model (re-introduced in section II), when simulating the rupture of a disordered interface. By comparing these features to those reported for the PMMA experiment by Tallakstad et al. [19], Santucci et al. [18] and Måløy et al. [17], we show a strong match to the experimental data for many of the scaling laws describing the fracture intermittent dynamics, including the growth of the fracture width

* vincentdospitalt@unistra.fr
† renaud.toussaint@unistra.fr

(section III A), its distribution in local propagation velocity (section III B), the correlation of this velocity in space and time (section IV A), the size of the propagation avalanches (section IV B) and the front Hurst exponents (section IV C). We hence re-enforce the relevance of simple thermodynamics coupled with elasticity in the understanding of rupture mechanics.

II. PROPAGATION MODEL

A. Constitutive equations

We consider rugous crack fronts that are characterised by a varying and heterogeneous advancement $a(x,t)$ along their front, x being the coordinate perpendicular to the average crack propagation direction, a the coordinate along it, and t being the time variable. An example for such a crack front is shown in Fig. 1. At a given time, the velocity profile along the rugous front is modelled to be dictated by an Arrhenius-like growth, as proposed by Cochard et al. [8]:

$$V(x,t) = V_0 \min\left[\exp\left(-\frac{\alpha^2[G_c(x,a) - G(x,t)]}{k_B T_0}\right), 1\right], \tag{1}$$

where $V(x,t) = \partial a(x,t)/\partial t$ is the local propagation velocity of the front at a given time and V_0 is a nominal velocity, related to the atomic collision frequency [30], which is typically similar to the Rayleigh wave velocity of the medium in which the crack propagates [31]. The exponential term is a subcritical rupture probability (i.e., that is between 0 and 1). It is the probability for the rupture activation energy (i.e., the numerator term in the exponential) to be exceeded by the thermal bath energy $k_B T_0$, that is following a Boltzmann distribution [30]. The Boltzmann constant is denoted k_B and the crack temperature is denoted T_0 and is modelled to be equal to a constant room temperature (typically, $T_0 = 298\,\mathrm{K}$).
It corresponds to the hypothesis that the crack is propagating slowly enough so that no significant thermal elevation occurs by Joule heating at its tip (i.e., as inferred by Ref. [27, 28]). Such propagation without significant heating is notably believed to take place in the experiments by Tallakstad et al. [19] that we here try to numerically reproduce, and whose geometry is shown in Fig. 2. Indeed, their reported local propagation velocities V did not exceed a few millimetres per second, whereas a significant heating in acrylic glass is only believed to arise for fractures faster than a few centimetres per second [28, 32].
In Eq. (1), the rupture activation energy is proportional to the difference between an intrinsic material surface fracture Energy G_c (in $\mathrm{J\,m^{-2}}$) and the energy release rate G at which the crack is mechanically loaded, which corresponds to the amount of energy that the crack dissipates to progress by a given fracture area. The front growth being considered subcritical, we have $G < G_c$. We here model the fracture energy G_c to hold some quenched disorder that is the root cause for any propagating crack front to be rugous. This disorder is hence dependent on two position variables along the rupture interface. For instance, at a given front advancement $a(x,t)$, one gets $G_c = G_c(x,a)$. The coefficient α^2 is an area which relate the macroscopic G and G_c values to, respectively, the microscopic elastic energy $U = \alpha^2 G$ stored in the molecular bonds about to break, and to the critical energy $U_c = \alpha^2 G_c$ above which they actually break (see Vanel et al. [25] or Vincent-Dospital et al. [28] for more insight on the α parameter).
Finally, the average mechanical load that is applied on the crack at a given time is redistributed along the evolving rugous front, so that $G = G(x,t)$. To model such a redistribution, we here use the Gao and Rice [3] formalism, which integrates the elastostatic kernel along the front:

$$G(x,t) = \overline{G}(t)\left[1 - \frac{1}{\pi}\mathrm{PV}\int_{x'=-\infty}^{+\infty} \frac{\partial a(x',t)/\partial x'}{x - x'}\mathrm{d}x'\right]. \tag{2}$$

In this equation, $\overline{G}$ is the mean energy release rate and PV stands for the integral principal value. We, in addition, considered the crack front as spatially periodic,

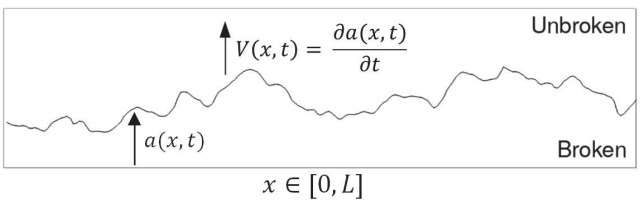

FIG. 1. Crack front a and crack velocity profile V, as defined in this manuscript. The front is supposed to have periodic boundary conditions along x, the coordinate perpendicular to the direction of propagation. The time variable is denoted t. This figure is a top view of Fig. 2.

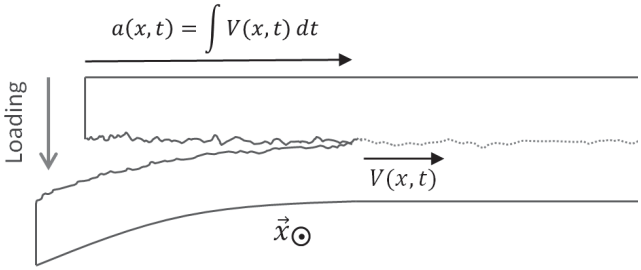

FIG. 2. Separation of two rugous and sintered PMMA plates, as reported by Tallakstad et al. [19]. The rugosity of the (quasi-plane) interface is here massively exaggerated (the plates are centimetres thick while the standard deviation in the interface topography is less than a micrometer [29]). A local position of the front has an advancement $a(x,t)$ and a velocity $V(x,t)$. The out of plane coordinate is x and t is the time variable. This figure is a side view of Fig. 1.

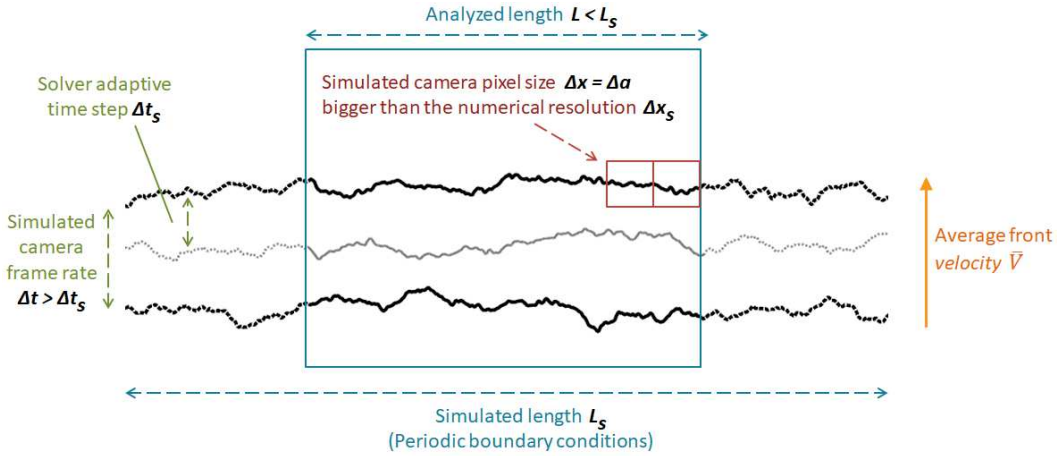

FIG. 3. Illustration of the discretization principles and of the solver and observation grids. Three crack fronts at three successive dates are shown, over which the parameters discussed in section II B are defined.

which allowed us to numerically implement a spectral version of Eq. (2) [33] as explained by Cochard et al. [8]. Equations (1) and (2) thus define a system of differential equations for the crack advancement a, which we have then solved with a time step adaptive Runge-Kutta algorithm [34], as implemented by Hairer et al. [35].

B. Discretization

In this section, we discuss the main principles we have used in choosing the numerical accuracy of our solver. The related parameters are illustrated in Fig. 3.
To possibly reproduce correctly the results of Tallakstad et al. [19], this solver needs to output space and time steps, here denoted Δx_s and Δt_s, at least smaller than those on which the experimental fronts were observed and analysed. Thus, Δx_s needs to be smaller than the experimental resolutions in space (the camera pixel size) $\Delta x = \Delta a$ of about 2 to 5 µm and $1/\Delta t_s$ needs to be higher than the experimental camera frame rate $1/\Delta t$. This frame rate was set by Tallakstad et al. [19] to about $(100\overline{V})/\Delta x$, where $\overline{V}$ is the average front velocity of a given fracture realisation. The propagation statistics of our simulated fronts, henceforward shown in this manuscript, have, for consistency, always been computed on scales comparable to the experimental Δx, Δa, Δt steps. Thus, as $\Delta x_s < \Delta x$ as $\Delta t_s < \Delta t$, we have first decimated the dense numerical outputs on the experimental observation grid, by discarding smaller time scales and by averaging smaller space scales to simulate the camera frame rate and pixel size.
As the experimental camera resolution was 1024 pixels, the lengths L of the crack segments that Tallakstad et al. [19] analysed were $1024\Delta_x = 3$ to 7 mm long, and we have then analyse our numerical simulations on similar front widths. Yet, these simulations were priorly run on longer front segments, $L_s > L$, in order to avoid any possible edge effects in the simulated crack dynamics (for instance in the case where L would not be much bigger than the typical size of the G_c quenched disorder).
Overall, we have checked that the numerical results presented henceforward were obtained using a high enough time and space accuracy for them to be independent of the discretization (see appendix A).

C. Physical parameters values

For the model dynamics to be compared to the experiments [19], one must also ensure that the V_0, α, T_0, G and G_c parameters are in likely orders of magnitude.
As V_0 is to be comparable to the Rayleigh velocity of acrylic glass, we have here used $1\,\mathrm{km\,s^{-1}}$ [36]. Lengliné et al. [26] furthermore estimated the ratio $\alpha^2/(k_B T_0)$ to be about $0.15\,\mathrm{m^2\,J^{-1}}$ and they could approximate the quantity $V_0 \exp(-\alpha^2 \overline{G_c}/[k_B T_0])$ to about $5 \times 10^{-14}\,\mathrm{m\,s^{-1}}$, where $\overline{G_c}$ is the average value of G_c. With our choice on the value of V_0, we then deduce $\overline{G_c} \sim 250\,\mathrm{J\,m^{-2}}$. Note that such a value for the fracture energy, that is to represent the sintered PMMA interfaces, is logically smaller but comparable to that inferred by Vincent-Dospital et al. [28] for the rupture of bulk PMMA (about $1300\,\mathrm{J\,m^{-2}}$). Qualitatively, the longer the sintering time, the closer one should get from such a bulk toughness, but the less likely an interfacial rupture will occur.
We will also consider, in Eq. (2), that the crack is, in average along the front, always loaded with the same intensity (i.e., $\overline{G}(t) = \overline{G}$. Indeed, the experiments [19] were done in regimes where the average load $\overline{G}$ was computed to be almost constant over time, in regard to the typical avalanches duration and to the total analysed experimental time. The actual value of $\overline{G}$, together with the average surface fracture energy of the medium $\overline{G_c}$, then mainly controls the average crack velocity $\overline{V}$. This average velocity was investigated over three orders of magnitudes

in Ref. [19], from 0.03 to 140 µm s^{-1}, which, in our formalism, shall correspond to values of $(\overline{G_c} - \overline{G})$ between 145 and 85 J m^{-2}, which is consistent with the values of $\overline{G}$ measured by Lengliné et al. [26] for cracks propagating at similar speeds. In this manuscript, we will use $\overline{G} = 120\,\mathrm{J\,m^{-2}}$, which corresponds to a propagation velocity of about 1 µm s^{-1}. The statistical description of the crack motion (i.e., that we are here interested in) was experimentally inferred to be independent on $\overline{V}$ and, as per Eqs. (1) and (2), where $\overline{G}$ is only a prefactor, the velocity distribution along the front shall only arise from the disorder in G_c and from the related variations of G due to the non-straight character of the crack front.

III. HETEROGENEOUS FRACTURE ENERGY

Of course, the actual surface fracture energy field in which the rupture takes place will significantly impact the avalanches dynamics and the crack morphology. Such a field is yet a notable unknown in the experimental set-up of Tallakstad et al. [19], as their interface final strength derived from complex sand blasting and sintering processes. Although these processes were well controlled, so that the rough rupture experiments were repeatable, and although the surfaces prior to sintering could be imaged [29], the actual resulting distribution in the interface cohesion was not directly measurable. While this is, to some extent, a flaw in assessing the validity of the model we present, we will here show that a simple statistical definition of G_c is enough to simulate most of the avalanches statistics.

We will indeed consider a normally distributed G_c field around the mean value $\overline{G_c}$ with a standard deviation δG_c and a correlation length l_c. Such a landscape in G_c is shown in Fig. 4, and we proceed to discuss the chosen values of δG_c and l_c in sections III A and III B.

A. Growth exponent and fracture energy correlation length

Among the various statistical features studied by Tallakstad et al. [19], they notably studied the growth exponent β_G of their propagating interfacial fronts. We will here show how it allows to deduce a typical correlation length for the interface disorder.

It was, more specifically, inferred that the standard deviation of the width evolution of a crack front h scales with the crack mean advancement:

$$\mathrm{rms}\big(h(t)\big) = \sqrt{<h(t)^2>_{x,t_0}} \propto \big(\overline{V}t\big)^{\beta_G}. \qquad (3)$$

In this equation, x is a given position along the front, t is a time delay from a given reference date t_0, and h writes as

$$h_{x,t_0}(t) = \big[a(x,t+t_0) - \overline{a}(t+t_0)\big] - \big[a(x,t_0) - \overline{a}(t_0)\big], \quad (4)$$

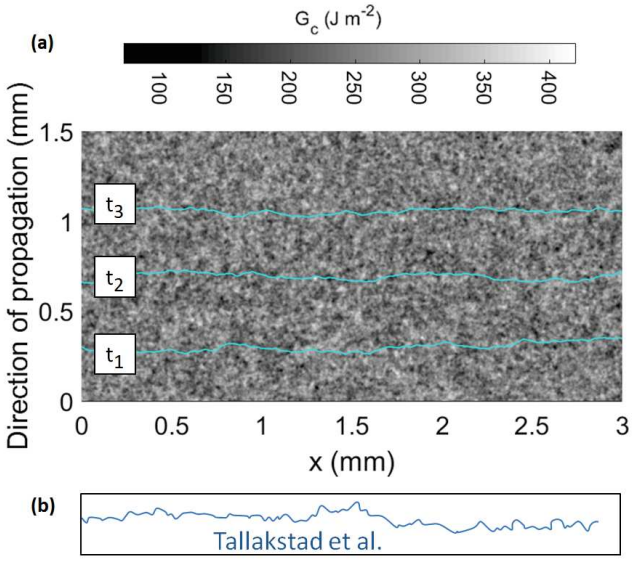

FIG. 4. (a): Normal distribution of the fracture energy G_c considered for the simulations. The average value is $\overline{G_c} = 250\,\mathrm{J\,m^{-2}}$, with a standard deviation $\delta G_c = 35\,\mathrm{J\,m^{-2}}$ and a correlation length $l_c = 50$ µm. The three lines are the modelled propagating front at three different times $t_1 < t_2 < t_3$, using Eqs. (1) and (2). (b): A crack front reported by Tallakstad et al. [19] (Fig. 3 of the experimental paper), plotted on the same spatial scales. One can notice the slight difference in rugosity, likely indicating the limitations of the proposed normal G_c distribution.

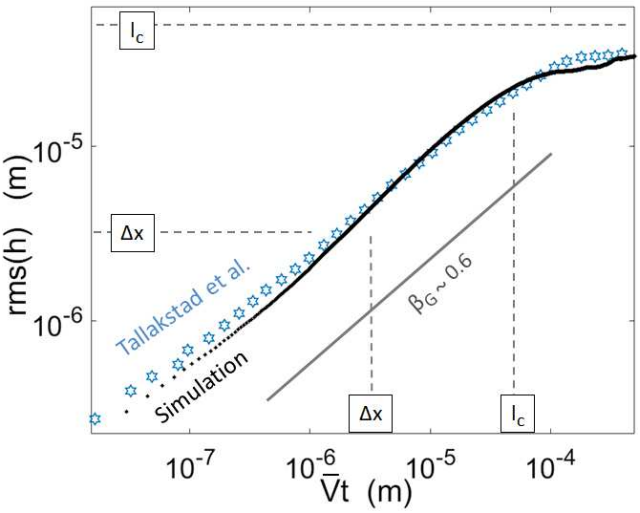

FIG. 5. Standard deviation of the width evolution of the crack front as a function of the mean crack advancement, as defined by Eqs. (3) and (4) for the chosen simulation (plain points) and for the experiments [19] (hollow stars) (out of Fig. 8, Expt. 5 of the experimental paper). The continuous line has a slope $\beta_G = 0.6$ close to that of the experimental points $\beta_G = 0.55$. The dashed lines mark the observation scale Δx, corresponding to the experimental camera pixel size, and the chosen correlation length for the simulation $l_c = 50$ µm.

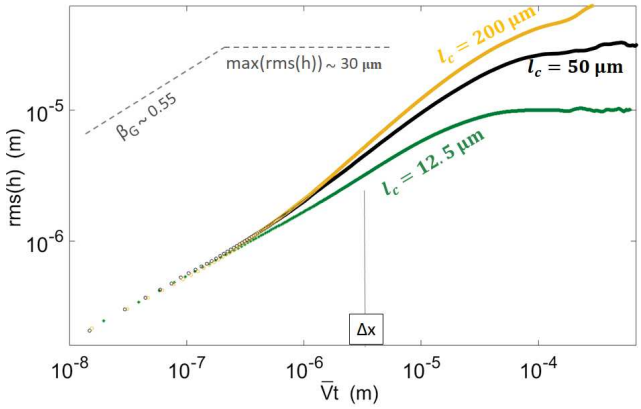

FIG. 6. Standard deviation of the width evolution of the crack front as a function of the mean crack advancement, as defined by Eqs. (3) and (4) for simulations with different correlation lengths l_c. The rest of the parameters are as defined in table I. The slope and plateau of the experimental data (shown in Fig. 5) is marked by the dashed line for comparison.

$\overline{a}$ being the average crack advancement at a given time. The hence defined growth exponent β_G was measured to be about 0.55 by Tallakstad et al. [19]. This value is close to $1/2$, that is, consistent with an uncorrelated growth process (e.g., [37]), such as simple diffusion or Brownian motion. We thus get a first indication on the disorder correlation length scale l_c. Indeed, to display an uncorrelated growth when observed with the experimental resolution ($\Delta x \sim 3\,\mu$m), the fronts likely encountered asperities which size was somewhat comparable to this resolution. By contrast, if these asperities in G_c were much bigger, the growth would be perceived as correlated. Oppositely, if they were much smaller (orders of magnitude smaller), the rugosity of the front would not be measurable, as only the average $\overline{G_c}$ over an observation pixel would then be felt. Furthermore, and as shown in Fig. 5, the exponent β_G was observed on scales $(\overline{V}t)$ up to 100 µm, above which rms(h) stabilised to a plateau value of about 30 µm. A common picture is here drawn as both this plateau value and the typical crack propagation distance at which it is reached are likely to be correlated with l_c, as the front is to get pinned on the strongest asperities at this scale. Note however that care may be needed when interpreting the plateau of rms(h) as it was also proposed that the large scale crossover is only an effect of a limited system size [19].

From all these clues, we have considered, in our simulations, the correlation length of the disorder to be about $l_c = 50\,\mu$m, and we show in Fig. 5 that it allows an approximate reproduction of the front growth exponent and of the plateau at high $(\overline{V})t$. In Fig. 6, we also show how varying l_c impacts rms(h), and, in practice, we have chosen l_c by tuning it and compare these curves to the experimental ones. Noteworthily, the thus chosen l_c is smaller yet comparable to the size of the blasting sand grains ($100 - 300\,\mu$m) that were used [19] to generate the interface disorder. It is also comparable to the correlation length of the blasting induced topographic anomalies $\sim 18\,\mu$m on the post-blasting/pre-sintering PMMA surfaces, as measured by Santucci et al. [29] by white light interferometry.

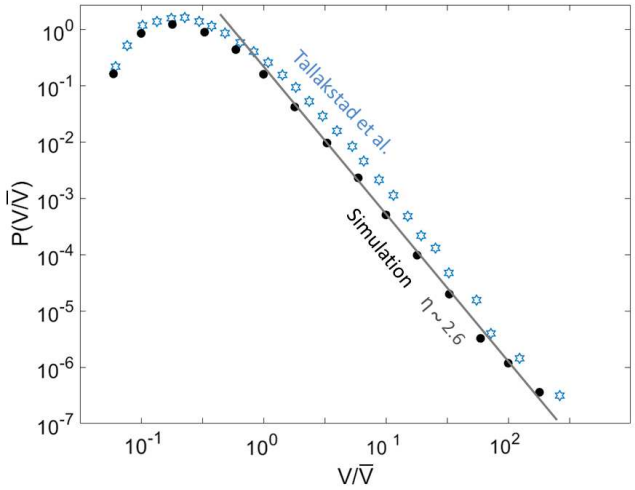

FIG. 7. Probability density function of the local propagation velocity along a simulated front (plain points), computed from the space-time map of Fig. 9. The experimental probability [19] (out of Fig. 5, Expt. 5 of the experimental paper) is shown for comparison (hollow stars). The continuous line has a slope $-\eta = -2.6$ close to that of the experimental points $\eta = 2.55$. This was achieved by setting the standard deviation for the disorder in fracture energy to $35\,\mathrm{J\,m^{-2}}$.

B. Local velocity distribution and fracture energy standard deviation

While the crack advances at an average velocity $\overline{V}$, the local velocities along the front, described by Eq. (1), are, naturally, highly dependent on the material disorder: the more diverse the met values of G_c the more distributed shall these velocities be.

Måløy et al. [17] and Tallakstad et al. [19] inferred the local velocities of their cracks with the use of a so-called waiting time matrix. That is, they counted the number of discrete time steps a crack would stay on a given camera pixel before advancing to the next one. They then deduced an average velocity for this pixel by inverting this number and multiplying it by the ratio between the pixel size and the time between two pictures: $\Delta a/\Delta t$. Such a method, that provides a spatial map $V(x, a)$, was applied to our simulated fronts, and we show a related $V(x, a)$ map in Fig. 9 a. As to any time t corresponds a front advancement $a(x, t)$ (recorded with a resolution Δa), an equivalent space-time map $V(x, t)$ can also be computed, and it is shown in Fig. 9 b. The experimental report [19] presented the probability density function of this latter (space-time) map $P(V/\overline{V})$, and it was inferred

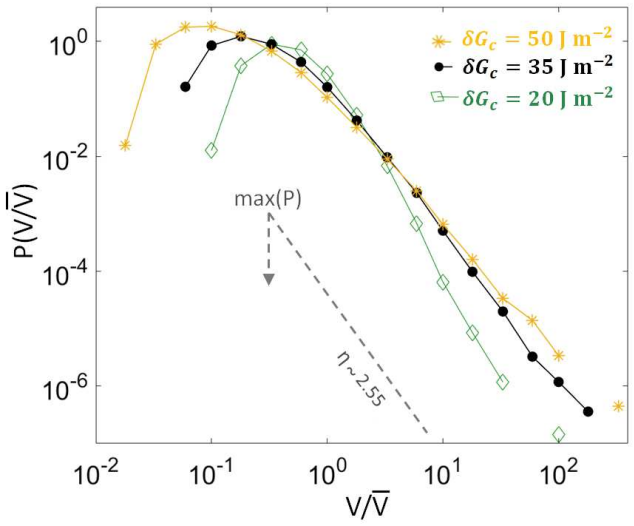

FIG. 8. Probability density function of the local propagation velocity along simulated fronts with three different values of $\delta G_c = 20\,\mathrm{J\,m^{-2}}$. We chose the value of δG_c by tuning it and fitting the slope and maximum of the experimental data, which are illustrated by the dashed line and arrow. The rest of the parameters used in these simulations are as defined in table I.

that, for high values of V, the velocity distribution scaled with a particular exponent $\eta = 2.55$ (see Fig. 7). That is, it was observed that

$$P\left(V/\overline{V}\right) \propto \left(V/\overline{V}\right)^{-\eta}. \tag{5}$$

Cochard et al. [8], who introduced the model that we here discuss, inferred that the η exponent was mainly depending on $\alpha^2(\delta G_c)^2/[k_B T_0(\overline{G_c})^2]$. As all other parameters have been estimated, we can deduce δG_c by varying it to obtain $\eta \sim 2.55$. We show how varying δG_c impacts $P(V/\overline{V})$ and η in Fig. 8. We found $\delta G_c \sim 35\,\mathrm{J\,m^{-2}}$. In Fig. 7, we show the corresponding velocity distribution for a simulation run with this parameter, together with that from Tallakstad et al. [19], showing a good match. Satisfyingly, this value of δG_c is not too far from that found by Lengliné et al. [26] for their fluctuation in the mean fracture energy $\overline{G_c}$, when studying the mean front advancement (i.e., neglecting the disorder) in similar PMMA interfaces, which was about $25\,\mathrm{J\,m^{-2}}$.

IV. FURTHER STATISTICS

We have now inverted the orders of magnitude of all parameters in Eqs. (1) and (2), including a likely distribution for an interface fracture energy representative of the experiments [19] we aim to simulate (i.e., $\overline{G_c}$, δG_c and l_c). For convenience, this information is summarised in table I.

We will now pursue by computing additional statistics of the crack dynamics to compare them to those reported by Tallakstad et al. [19].

	Parameter	Value	Unit
(a)	V_0	1000	m s^{-1}
	$\alpha^2/(k_B T_0)$	0.15	m^2 J^{-1}
	$\overline{G_c}$	250	J m^{-2}
	$\overline{G}$	120	J m^{-2}
	δG_c	35	J m^{-2}
	l_c	50	µm
(b)	$\Delta a = \Delta x$	3	µm
	Δt	10	ms
	L	3000	µm
(c)	Δx_s	1	µm
	Δt_s	~ 5	ms
	L_s	6000	µm

TABLE I. Summary of all parameters that are considered in this manuscript. (a): physical parameters in Eqs. (1) and (2) believed to be representative of the studied creep experiments. (b): observation scale of the modelled fronts, similar to the experimental ones of Tallakstad et al. [19]. (c): the solver grid, finer than the observation scale for numerical accuracy.

A. Local velocities correlations

In particular, we here compute the space and time correlations of the velocities along the front. That is, four correlation functions that are calculated from the $V(x,t)$ and $V(x,a)$ matrices (shown in Fig. 9) and defined as:

$$C_t(\delta t) = \left\langle \frac{\left[V(x,t_0+\delta t) - \overline{V_x}\right]\left[V(x,t_0) - \overline{V_x}\right]}{(\delta V_x)^2} \right\rangle_{t_0}, \tag{6}$$

$$C_{xt}(\delta x) = \left\langle \frac{\left[V(x_0+\delta x,t) - \overline{V_t}\right]\left[V(x_0,t) - \overline{V_t}\right]}{(\delta V_t)^2} \right\rangle_{x_0}, \tag{7}$$

$$C_a(\delta a) = \left\langle \frac{\left[V(x,a_0+\delta a) - \overline{V_x}\right]\left[V(x,a_0) - \overline{V_x}\right]}{(\delta V_x)^2} \right\rangle_{a_0}, \tag{8}$$

$$C_{xa}(\delta x) = \left\langle \frac{\left[V(x_0+\delta x,a) - \overline{V_a}\right]\left[V(x_0,a) - \overline{V_a}\right]}{(\delta V_a)^2} \right\rangle_{x_0}. \tag{9}$$

Here, $\overline{V_x}$ is the mean propagation velocity along x at a given time t_0 in Eq. (6) or at a given position a_0 in Eq. (8). The corresponding δV_x are the velocity standard deviations in the same directions. Similar definitions apply to $\overline{V_t}$, $\overline{V_a}$, δV_t and δV_a in Eqs. (7) and (9). The correlations functions hence defined are the same as those used by Tallakstad et al. [19] on their own data, allowing to display a direct comparison of them in Fig. 10. A good general match is obtained.

One can notice the comparable cut-offs along the x axis (Fig. 10 a and c), indicating that our chosen corre-

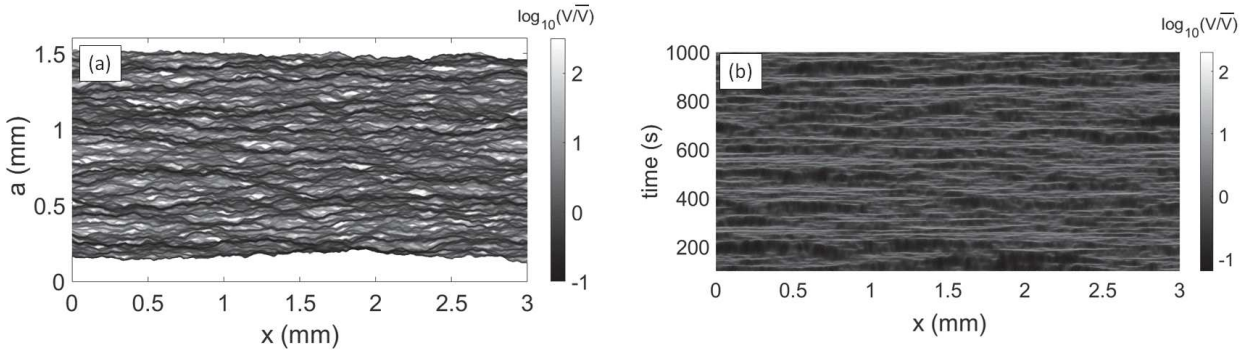

FIG. 9. Local velocity maps $V(x, a)$ in the space-space domain (left) and $V(x, t)$ in the space-time domain (right). Both maps are computed on a resolution similar to that of the experiments by Tallakstad et al. [19], using the waiting time matrix. The velocity are plotted related to the average crack velocity $\overline{V} = 1.5\,\mu\mathrm{m\,s^{-1}}$. Both maps are shown with the same color scale. All parameters used to run the corresponding simulation are summarised in table I.

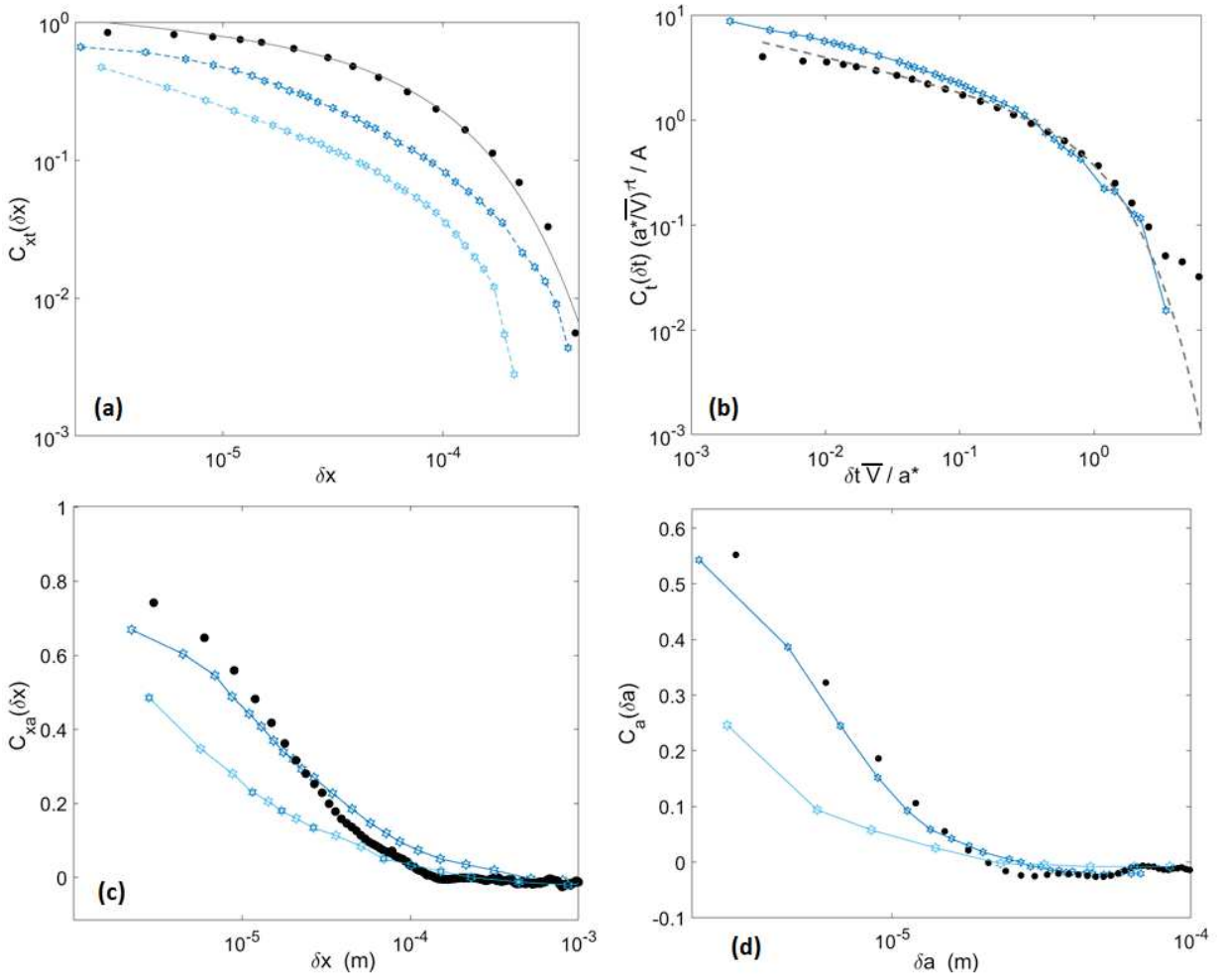

FIG. 10. Local velocity correlation functions in space and time as defined by Eqs. (6) to (9). The plain points were computed from the simulation which parameters are presented in table I and the hollow stars are some of the experimental data points extracted from Tallakstad et al. [19] (Figs. 6 and 7 of the experimental report). In inset (a), the line overlying the numerical data set corresponds to a fit using Eq. (10). Inset (b) is plotted in a domain that allowed a good collapse of the experimental data for many experiments [19]. The parameters A, a^* and τ_t were inverted from Eq. (11), and the related fit is shown by the dashed line overlying the numerical data set. Insets (a), (c) and (d) hold two curves for the experiments, corresponding to two distinct sets of experiments done on two different sintered PMMA bodies.

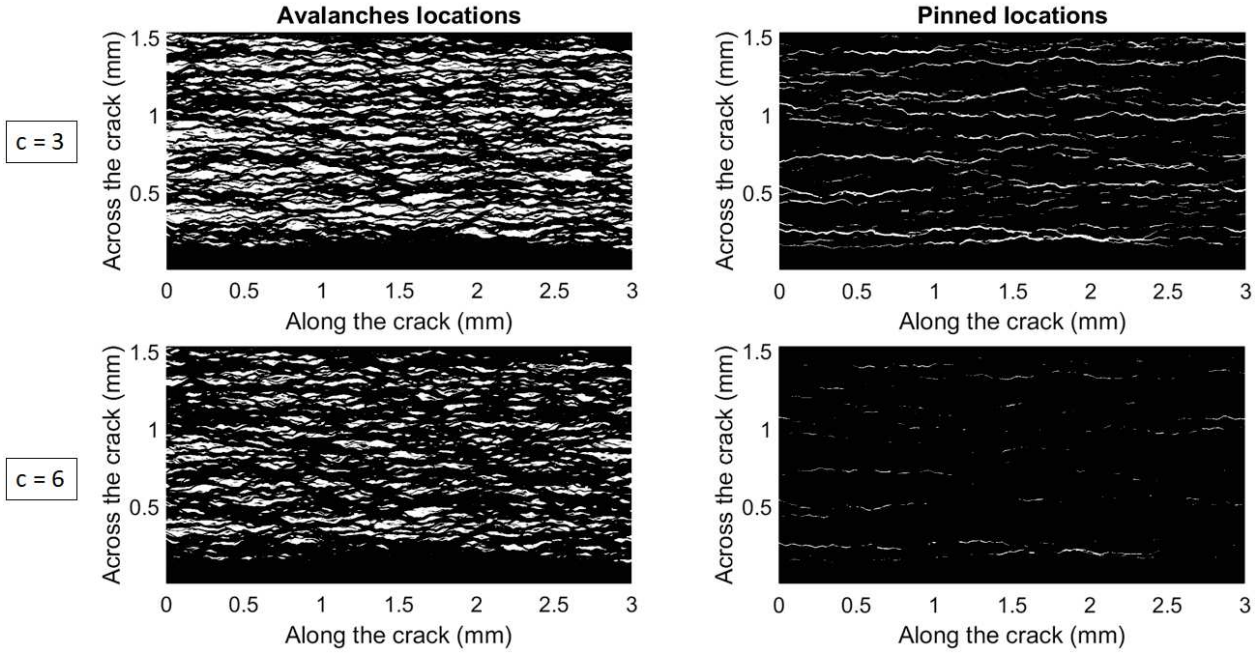

FIG. 11. Positions of the avalanches (left) and pinning locations (right) in the front local velocity map $V(x, a)$ shown in Fig. 9 a, as per Eqs. (12) and (13). Two thresholds are here used to define these maps relatively to the mean velocity: $c = 3$ (top) and $c = 6$ (bottom). The white areas are the locations of interests, of surfaces S, crossline extents l_x and inline extents l_a.

lation length for the interface disorder (l_c inferred in section III A) is a good account of the experiment. Yet, one can notice that C_{xt} (the velocity correlation along the crack front shown in Fig. 10 a) is higher in the numerical case than in the experimental one. It could translates the fact that the experimental disorder holds wavelengths that are smaller than the observation scale Δx, and that our modelled G_c distribution, where $l_c > \Delta x$ is rather simplified.

Tallakstad et al. [19] modelled C_{xt} as

$$C_{xt}(\delta x) \propto \delta x^{-\tau_x} \exp\left(-\frac{\delta x}{x^*}\right), \tag{10}$$

and inverted the values of τ_x and x^* to respectively 0.53 and about 100 µm. Doing a similar fit on the simulated data, we found $\tau_x \sim 0.13$ and $x^* \sim 94\,\mu$m. Our small $\tau_x \sim 0.13$ may derive, as discussed, from the better correlation our simulation displays at small δx (τ_x may in reality tend to zero for smaller scales that those we observe), while the matching x^* probably relates to a satisfying choice we made for l_c.

On the time correlation C_t (Fig. 10 b), one can similarly define the parameters A, τ_t and a^* to fit Eq. (6) with a function

$$C_t(\delta t) \approx A\delta t^{-\tau_t} \exp\left(-\frac{\overline{V}\delta t}{a^*}\right) \tag{11}$$

where A is a constant of proportionality. Fitting this function to Eq. (6) with a least-squares method, we found $\tau_t \sim 0.3$ and $a^* \sim 4.3\,\mu$m. Tallakstad et al. [19] reported $\tau_t \sim 0.43$ and $a^* \sim 7\,\mu$m. Figure 10 b shows the experimental and simulated correlation functions in the $\overline{V}\delta t/a^*$ – $C_t(a^*/\overline{V})^{\tau_t}/A$ domain, as this domain allowed a good collapse of the data from numerous experiments [19]. We show that it also allows an approximate collapse of our modelled correlation on a same trend. Finally, the derived value of a^* consistently matches the apparent cut-off length in the C_a correlation function in Fig. 10 d. This length being of a similar magnitude than that of the observation scale Δa, the crack local velocities appear uncorrelated along the direction of propagation, which is consistent with the $\beta_G \sim 1/2$ growth exponent.

B. Avalanches size and shape

We pursue by characterising the stick-slip motion of our crack fronts and, more specifically, the avalanche (or depinning) and pinning clusters shown by the local front velocity $V(x, a)$. We define an avalanche when the front velocity locally exceed the mean velocity $\overline{V}$ by an arbitrary threshold that we denote c, that is, when

$$V(x, a) > c\overline{V}. \tag{12}$$

Similarly, we state that a front is pinned when

$$V(x, a) < \frac{\overline{V}}{c}. \tag{13}$$

We then map, in Fig. 11 the thus defined avalanching and pinned location of the crack. Following the analysis of Tallakstad et al. [19], we compute for each of these

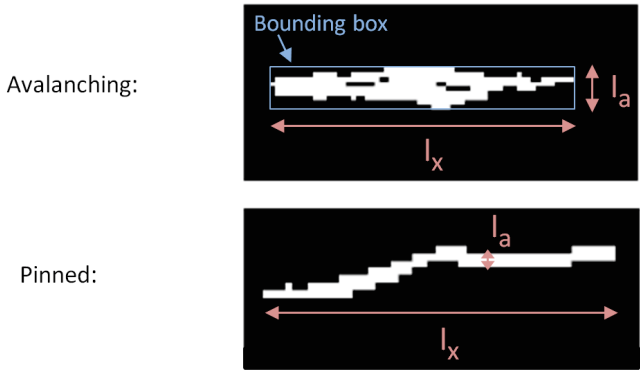

FIG. 12. Difference in definition of l_a for the avalanche (or depinning) and pinning clusters shown in Fig. 11. For the former, l_a is the maximum extent along the a direction. For the latter it is the average width in the same direction. In both cases, l_x is the maximum extent along the x direction and S the full surface (in white) of the cluster. The square pattern marks the pixel size ($\Delta x = \Delta a = 3\,\mu$m).

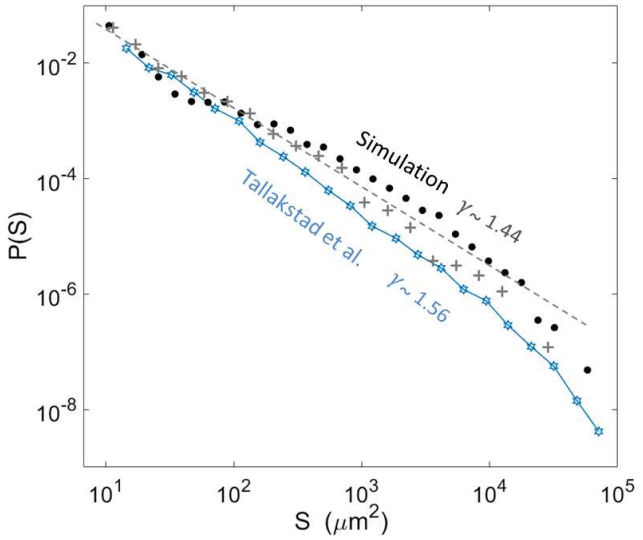

FIG. 13. Probability density function of the surface of the modelled avalanche clusters (plain points) and of the modelled pinning clusters (crosses), for a threshold $c = 3$. The straight dashed line has a slope $\gamma \sim 1.44$, as per Eq. (14). For comparison, the hollow stars shows the experimental probability density function obtained by Tallakstad et al. [19] for the avalanche and pinning clusters (Both are overlapping, see Fig. 10 of their manuscript).

clusters the surface S, the crossline extent l_x (that is, the maximum of the clusters width in the x direction) and the inline extent l_a. The definition chosen for l_a varies for the avalanche clusters, where the maximal extent along the a direction is regarded, or the pinned one, where the mean extent along the a direction is rather used. This choice was made [19] because the pinning clusters tend to be more tortuous so that their maximum span along the

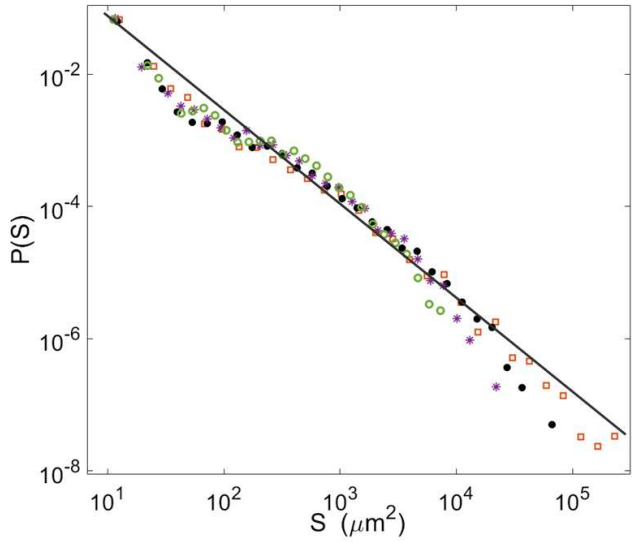

FIG. 14. Probability density function of the surface of the modelled avalanche clusters for various c values: $c = 1.5$ (squares), $c = 3$ (plain points), $c = 6$ (stars), $c = 12$ (circles). The straight line has a slope $\gamma \sim 1.4$, as per Eq. (14).

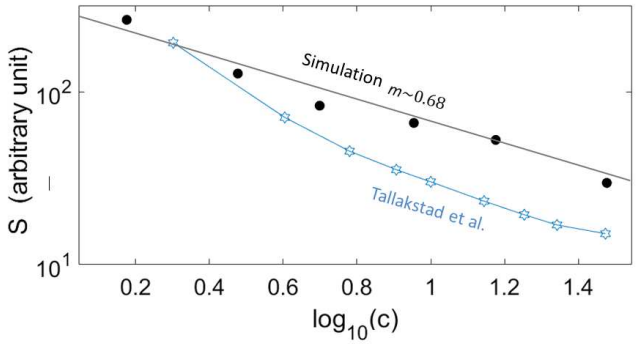

FIG. 15. Variation of the mean avalanche size $\overline{S}$ as a function of the threshold c for the simulation (plain points) and the experiments (hollow stars). The modelled $\overline{S}$ is expressed in pixels (one pixel is 9 μm^2) and the experimental $\overline{S}$ reported by Tallakstad et al. [19] (on their Fig. 13) is in a arbitrary unit, so that the magnitude of both should not here be compared. The straight line has a slope 0.68.

crack direction of propagation is not really representative of their actual extent (see Fig. 12).

In Fig. 13, we show the probability density function of the cluster surface $P(S)$ and compare it to the experimental one. One can notice that it behaves as

$$P(S) \propto S^{-\gamma}, \tag{14}$$

with $\gamma \sim 1.4$. This value is comparable to the exponent inverted experimentally [19], that is, $\gamma \sim 1.56$.

Of course, the size of the avalanche (depinning) clusters highly depends on the chosen threshold c, but we verified, as experimentally reported, that the value of γ inverted from the simulated data is not dependent on c, as shown

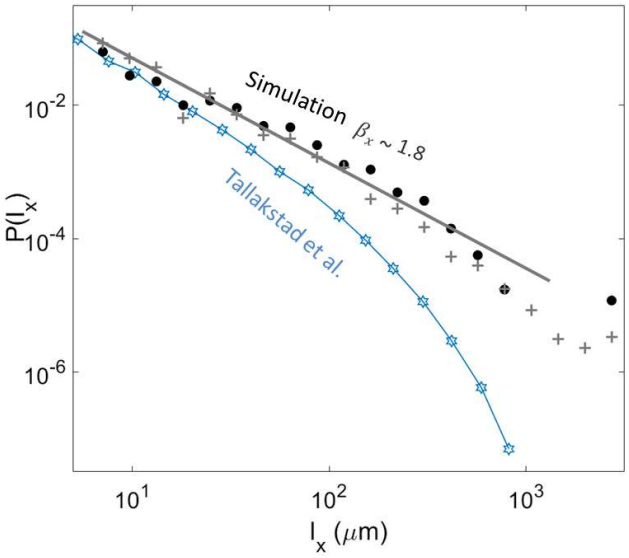

FIG. 16. Probability density function of the crossline extent l_x of the modelled avalanche clusters (plain points) and of the modelled pinning clusters (crosses), for a threshold $c = 3$. The straight line has a slope $\beta_x \sim 1.8$, as per Eq. (15). The hollow stars shows the experimental probability density function obtained by Tallakstad et al. [19] for the pinning clusters (from their Fig. 16a, inset, c=3).

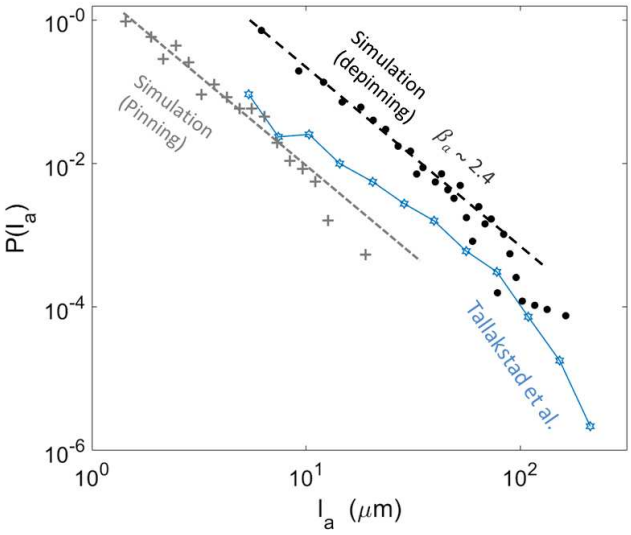

FIG. 17. Probability density function of the inline extent l_a of the modelled avalanche clusters (plain points) and of the modelled pinning clusters (crosses), for a threshold $c = 3$. The two straight dashed lines have a slope $\beta_x \sim 2.4$, inline with that of the experimental data Tallakstad et al. [19] for the pinning clusters (hollow stars, from their Fig. 16b, inset, c=3).

in Fig. 14. We show, in Fig 15, that the mean cluster size $\overline{S}$ varies with c approximately as $\overline{S} \propto c^{-m}$, which $m \sim 0.68$. This value is comparable with the experimental scaling law [19] measured to be $\overline{S} \propto c^{-0.75}$.
We also computed the probability density function of l_x and l_a, that are respectively compared to their experimental equivalent in Figs. 16 and 17. These functions can be fitted with

$$P(l_x) \propto {l_x}^{-\beta_x}, \tag{15}$$

$$P(l_a) \propto {l_a}^{-\beta_a}, \tag{16}$$

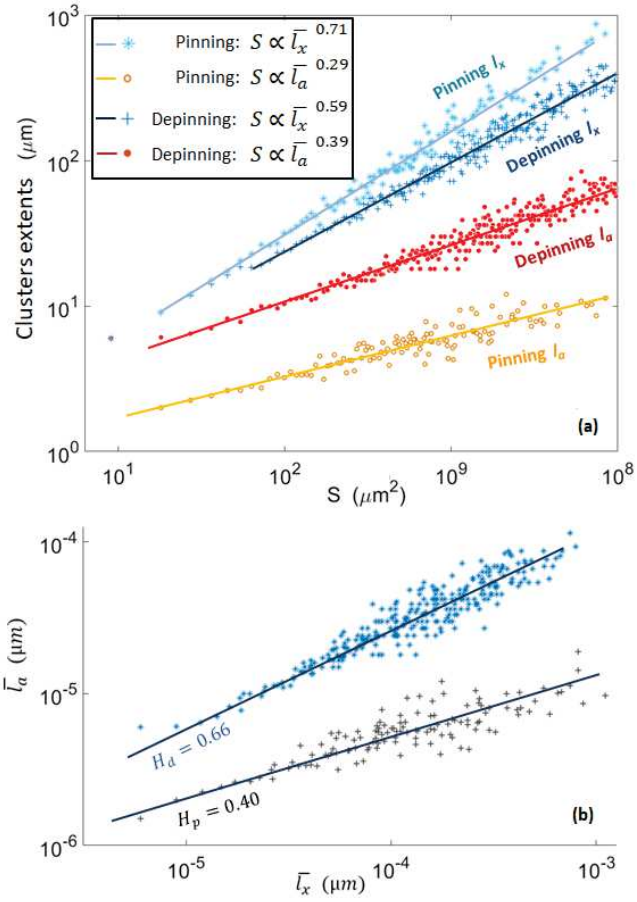

FIG. 18. (Top): Mean linear extents of the simulated pinning and depinning clusters as a function of cluster size. The four data sets are, from top to bottom, $\overline{l_x}$ for the pinning clusters (hollow stars), $\overline{l_x}$ for the avalanche clusters (crosses), $\overline{l_a}$ for the avalanche clusters (plain points), $\overline{l_a}$ for the pinning clusters (hollow points). The straight lines corresponds to the fits described in the inset. See text for the equivalent experimental exponents. (Bottom): Mean inline extent $\overline{l_a}$ as a function of the mean crossline extent $\overline{l_x}$ for the pinning and depinning clusters. The straight lines have a slope of respectively $H_p = 0.40$ and $H_d = 0.66$.

and we found $\beta_x \sim 1.8$, close to the reported experimental value [19] $\beta_x \sim 1.93$. The value we found for $\beta_a \sim 2.4$ is also inline with that of Tallakstad et al. [19], who reported $\beta_a \sim 2.36$.
Finally, we show, in Fig. 18 a, the relations between the clusters surface S and their linear extent $\overline{l_x}$ and $\overline{l_a}$. Here, $\overline{l_x}$ and $\overline{l_a}$ are the mean extents for all the observed clusters sharing a same surface. We could fit these relations with $S \propto \overline{l_x}^{0.71}$ and $S \propto \overline{l_a}^{0.29}$ for the pinning clusters, and with $S \propto \overline{l_x}^{0.59}$ and $S \propto \overline{l_x}^{0.39}$ for the avalanches clusters. It can be compared with the laws observed by Tallakstad et al. [19]: $S \propto \overline{l_x}^{0.63}$ and $S \propto \overline{l_a}^{0.34}$ for the pinning clusters, and $S \propto \overline{l_x}^{0.61}$ and $S \propto \overline{l_x}^{0.41}$ for the avalanches clusters. Note that, from all these exponents, one can easily define H such that $l_a \propto {l_x}^H$, and we thus have $H_d \sim 0.40$ and $H_p \sim 0.66$ for respectively the depinning and pinning clusters (see Fig. 18 b). Thus, the shape of our simulated avalanches and pinned locations is similar to the observed experimental ones.

C. Front morphology

It was suggested [5] that H is a good indicator of the front morphology, as the front shape is to be highly dependent on the aspect ratio of its avalanches. To verify this hypothesis, we computed the advancement fluctuation along the front σ, that is

$$\sigma(\delta x) = \sqrt{< \left(a(x_0 + \delta x, t) - a(x_0, t)\right)^2 >_{x_0,t}}. \qquad (17)$$

While this quantity was not presented by Tallakstad et al. [19], it was provided by other experimental works done on the same set-up [17, 18], and Fig. 19 show σ as reported by these authors, together with that computed in the output of our simulation. One can notice that the numerical fronts are less rugous than the experimental ones, contrarily to what is displayed in Fig. 5. Such a mismatch is here due to the fact that the experiment from Santucci et al., shown in Fig. 19, had more rugous crack fronts than the ones from Tallakstad et al., to which the simulation is calibrated. In both cases, the data sets seem to present two self-affine behaviours (e.g., [37]) with a Hurst exponent ζ that differs at low and high length scales. Noting δx^* the cut-off between these length scales we indeed have:

$$\sigma \propto {\delta_x}^{\zeta^-} \text{ for } \delta x < \delta x^*, \qquad (18)$$

$$\sigma \propto {\delta_x}^{\zeta^+} \text{ for } \delta x > \delta x^*. \qquad (19)$$

We derived $\zeta^- \sim 0.68$ and $\zeta^+ \sim 0.3$ for the simulation, which compare reasonably well to the exponents that were measured experimentally $\zeta^- \sim 0.63$ and $\zeta^+ \sim 0.37$ and which is also relatively close to the values we found for H_d and H_p. The cut-off scale is also similar in both

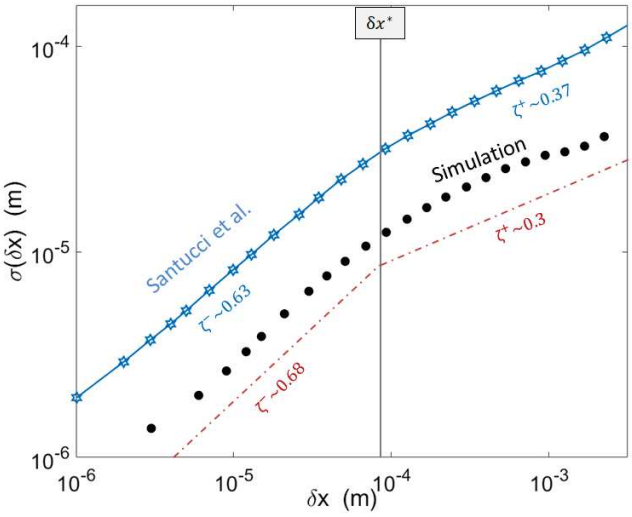

FIG. 19. Advancement fluctuation σ along the crack fronts, as per Eq. (17), for the simulation (plain points) and an experimental data set from Santucci et al. [18] (see their Fig. 2). Different self-affine behaviours are observed above and below the δx^* cut-off, with comparable Hurst exponents ζ. The dashed lines mark the slopes fitted on the simulation data for the two regimes. The experimental points are from a different experiment than those of Tallakstad et al. [19] to which the model was calibrated, explaining the apparent difference in prefactor.

the experimental and numerical cases: $\delta x^* \sim 80\,\mu$m, comparable to the length scale x^* below which the local propagation velocities are correlated.
Note that Cochard et al. [8], analytically analysing the same model as we here study, showed that, at very large scales, it holds a Hurst coefficient $\zeta^+ \sim 0$, and a coefficient $\zeta^+ \sim 0.5$ at very small scales. While these values differs from our estimations, our inverted slopes (and those of the experimental data) might only be two different fits of a smooth transition regime between these two asymptotic behaviours, as already mentioned in Refs. [18] and [8].

V. DISCUSSION AND CONCLUSION

We studied an interfacial fracture propagation model, based only on statistical - subcritical - physics in the sense of an Arrhenius law (Eq. (1)) and on the elastic redistribution of stress along crack fronts (Eq. (2)). Following the work of Cochard et al. [8], we here showed that it allows a good representation of the intermittent dynamics of fracture in disordered media, as it approximately mimics the scaling laws dictating the propagation of experimental fronts, such as their growth exponent, their local velocity distribution and space and time correlations, the size of their avalanches and their self-affine characteristics.

To run our simulations, we had to assume a given distribution for the toughness of the rupturing interface, as this quantity is not directly measurable in the lab. We proposed G_c to be normally distributed with a unique correlation length and, of course, this can only be a rough approximation of the actual fracture energy obtained by Tallakstad et al. [19] by sand blasting and sintering. From this approximation, could arise discrepancies between our simulations and Tallakstad's experiments. We have indeed shown how some of the observed exponents were strongly dependent on the definition of the material disorder. We also have assumed a perfectly elastic crack front, when the local dynamics of creeping PMMA could be visco-elastic in part, particularly below the typical length scale $r \sim GE/\sigma_y^2 \sim 30\,\mu\text{m}$ for plasticity around crack tips (e.g. [1]) in this material, where $\sigma_y \sim 100\,\text{MPa}$ is the tensile yield stress of the polymer and $E \sim 3\,\text{GPa}$ its Young modulus [38].

These points being written, the vast majority of the statistical quantities that we have here studied show a good match to those from the experimental observation, so that both the considered physical model and the interface definition are likely relevant.

It should be noted that, as stated in our introduction, other models have been considered to numerically reproduce the interfacial PMMA experiment, notably, a threshold based fluctuating line model by Tanguy et al. [20], Bonamy et al. [4] or Laurson et al. [5] and a fiber bundle approach by Schmittbuhl et al. [6], Gjerden et al. [21] or Stormo et al. [39]. The former [4, 5, 20] considers a similar redistribution of energy release rate G as proposed in Eq. (2), but with a dynamics that is thresholded rather than following a subcritical growth law. The fronts move forward by one pixel if $G > G_c$, and is completely pinned otherwise. The latter [6, 21, 39], the fiber bundle model, is not a line model. The interface is sampled with parallel elastic fibers breaking at a given force threshold. This threshold is less in the vicinity of the crack than away from it (it is modelled with a linear gradient), explaining why the rupture is concentrated around a defined front, and it holds a random component in order to model the quenched disorder of the interface. An advantage of the fiber bundle model is to be able to describe a coalescence of damage in front of the crack [40] rather than solely describing a unique front. This could likely also be achieved in a subcritical framework, but would require a full 3D modelling rather than only a 2D front. A clear advantage of the Arrhenius based model, however, when compared to the other ones, is to hold a subcritical description that is physically well understood and that is a good descriptor of creep in many materials [1, 25].

For the record, we show in table II a comparison between the different exponents predicted by the three models, that all successfully reproduce some experimental observables.

Despite such a variety in models reproducing the rough dynamics of creep, the present work provides additional indications that a thermodynamics framework in the sense of a thermally activated subcritical crack growth is well suited for the description of creeping cracks. Such a framework has long been considered (e.g., [22–25, 41, 42]), and, additionally to the scaling laws that we have here presented, the proposed model was proven to fit many other observable features of the physics of rupture [8, 26–28]. It accurately recreates the mean advancement of cracks under various loading conditions [8, 26], and, when coupled with heat dissipation at the fracture tip, it also accounts for the brittleness of matter [28] and for its brittle-ductile transition [27].

Indeed, for zero dimensional (scalar) crack fronts, it was shown [28] that the thermal fluctuation at the crack tip, expressed as a deviation of the temperature from T_0 in Eq. (1) can explain the transition between creep and abrupt rupture, that is the transition to a propagation velocity close to a mechanical wave speed V_0, five orders of magnitude higher than the maximal creep velocity V that was here modelled. It was also shown, similarly to many phase transition problems, that such a thermal transition could be favoured by material disorder [27]. Thus, a direct continuation of the present work could be to introduce such a heat dissipation for interfacial cracks in order to study how brittle avalanches nucleate at given positions (typically positions with weaker G_c) to then expand laterally to become bulk threatening events.

Parameter	**Expt.**	**Models**		
		ABM	*FBM*	*TBFLM*
β_G	0.55	0.6	0.52	
η	2.55	2.6	2.56	
τ_x	0.53	0.13	0.4	
x^*	$\sim 100\,\mu\text{m}$	$94\,\mu\text{m}$	-	
β_x	1.94	1.8		
β_a	2.34	2.4		
γ	1.56	1.4	-	1.65
m	0.75	0.68		
ζ^-	0.63	0.68 ($\to 0.5$)	0.67	0.48
ζ^+	0.37	0.3 ($\to 0$)	0.39	0.37
H_d	0.66	0.66	0.6	0.65
H_p	0.55	0.40	0.4	

TABLE II. Comparison of various exponents and cut-off scales derived experimentally [18, 19] (Expt.) and numerically with the present, Arrhenius based, model (ABM), the fiber bundle model [21] (FBM) and the threshold based fluctuating line model [4, 5] (TBFLM).

ACKNOWLEDGEMENT

The authors declare no competing interests in the publishing of this work. They acknowledge the support of the Universities of Strasbourg and Oslo, of the CNRS INSU ALEAS program and of the IRP France-Norway D-FFRACT. We thank the Research Council of Norway through its Centres of Excellence funding scheme, project number 262644.

Appendix A: Solver convergence

We verified that our simulations were accurate enough so that the derived statistical features were not dependent on the steps of the numerical computation grids. In table III, we show the accuracy parameters of two different simulations and show, in Fig. 20, how the modelled crack dynamics is unchanged with both parameter sets.

Parameter	Higher accuracy	Lower accuracy	Unit
Δx_s	0.5	1	µm
Δt_s	~ 1	~ 5	ms
L_s	12000	6000	µm

TABLE III. Two different sets of numerical accuracy parameters corresponding to the results shown in Fig. 20.

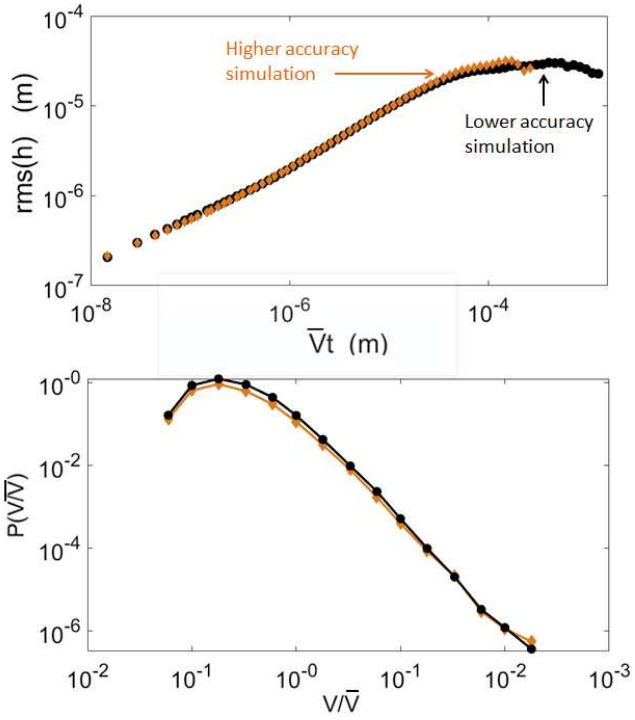

FIG. 20. Crack growth (top) and velocity distribution (bottom) for two simulations with the same physical parameters but different numerical accuracy, as per table III. The points are data from the simulation analysed in this manuscript and the squares were computed on coarser numerical grids. The computed exponents are not significantly affected.

[1] B. Lawn. *Fracture of Brittle Solids*. Cambridge Solid State Science Series. Cambridge University Press, 2 edition, 1993. doi:10.1017/CBO9780511623127.

[2] D.A. Gerard and D.A. Koss. Porosity and crack initiation during low cycle fatigue. *Materials Science and Engineering: A*, 129(1):77 – 85, 1990. ISSN 0921-5093. doi:10.1016/0921-5093(90)90346-5.

[3] H. Gao and J. R. Rice. A First-Order Perturbation Analysis of Crack Trapping by Arrays of Obstacles. *Journal of Applied Mechanics*, 56(4):828–836, 12 1989. ISSN 0021-8936. doi:10.1115/1.3176178.

[4] D. Bonamy, S. Santucci, and L. Ponson. Crackling dynamics in material failure as the signature of a self-organized dynamic phase transition. *Phys. Rev. Lett.*, 101:045501, Jul 2008. doi:10.1103/PhysRevLett.101.045501.

[5] L. Laurson, S. Santucci, and S. Zapperi. Avalanches and clusters in planar crack front propagation. *Phys. Rev. E*, 81:046116, Apr 2010. doi:10.1103/PhysRevE.81.046116.

[6] J. Schmittbuhl, A. Hansen, and G. G. Batrouni. Roughness of interfacial crack fronts: Stress-weighted percolation in the damage zone. *Phys. Rev. Lett.*, 90:045505, Jan 2003. doi:10.1103/PhysRevLett.90.045505.

[7] Z. Danku, F. Kun, and H. J. Herrmann. Fractal frontiers of bursts and cracks in a fiber bundle model of creep rupture. *Phys. Rev. E*, 92:062402, Dec 2015. doi:10.1103/PhysRevE.92.062402.

[8] A. Cochard, O. Lengliné, K. J. Måløy, and R. Toussaint. Thermally activated crack fronts propagating in pinning disorder: simultaneous brittle/creep behavior depending on scale. *Philosophical Transactions of the Royal Society A : Mathematical, Physical and Engineering Sciences*, 2018. doi:10.1098/rsta.2017.0399.

[9] A. Griffith. The Phenomena of Rupture and Flow in Solids. *Philosophical Transactions of the Royal Society of London A: Mathematical, Physical and Engineering Sciences*, 221(582-593):163–198, January 1921. ISSN 1471-2962. doi:10.1098/rsta.1921.0006.

[10] G. R. Irwin. Analysis of stresses and strains near the end of a crack traversing a plate. *Journal of Applied Mechanics*, 24:361–364, 1957.

[11] S. Santucci, R. Planet, K. J. Måløy, and J. Ortín. Avalanches of imbibition fronts: Towards critical pinning. *EPL (Europhysics Letters)*, 94(4):46005, may 2011. doi:10.1209/0295-5075/94/46005.

[12] E. Vives, J. Ortín, L. Mañosa, I. Ràfols, R. Pérez-Magrané, and A. Planes. Distributions of avalanches in martensitic transformations. *Phys. Rev. Lett.*, 72:1694–1697, Mar 1994. doi:10.1103/PhysRevLett.72.1694.

[13] D. M. Dimiduk, C. Woodward, R. LeSar, and M. D. Uchic. Scale-free intermittent flow in crystal plasticity. *Science*, 312(5777):1188–1190, 2006. ISSN 0036-8075. doi:10.1126/science.1123889.

[14] G. Durin and S. Zapperi. Scaling exponents for Barkhausen avalanches in polycrystalline and amorphous ferromagnets. *Phys. Rev. Lett.*, 84:4705–4708, May 2000. doi:10.1103/PhysRevLett.84.4705.

[15] J. P. Sethna, K. A. Dahmen, and C. R. Myers. Crackling noise. *Nature*, 2001. ISSN 1476-4687. doi:10.1038/35065675.

[16] L. Laurson, X. Illa, S. Santucci, K. Tore Tallakstad, K. J. Måløy, and M. J. Alava. Evolution of the average avalanche shape with the universality class. *Nature Communications*, pages 242–250, 2013. ISSN 2041-1723. doi:10.1038/ncomms3927.

[17] K. J. Måløy, S. Santucci, J. Schmittbuhl, and R. Toussaint. Local waiting time fluctuations along a randomly pinned crack front. *Phys. Rev. Lett.*, 96:045501, Jan 2006. doi:10.1103/PhysRevLett.96.045501.

[18] S. Santucci, M. Grob, R. Toussaint, J. Schmittbuhl, A. Hansen, and K.-J. Maløy. Fracture roughness scaling: A case study on planar cracks. *EPL (Europhysics Letters)*, 92(4):44001, nov 2010. doi:10.1209/0295-5075/92/44001.

[19] K. T. Tallakstad, R. Toussaint, S. Santucci, J. Schmittbuhl, and K. J. Måløy. Local dynamics of a randomly pinned crack front during creep and forced propagation: An experimental study. *Phys. Rev. E*, 83:046108, 04 2011. doi:10.1103/PhysRevE.83.046108.

[20] A. Tanguy, M. Gounelle, and S. Roux. From individual to collective pinning: Effect of long-range elastic interactions. *Phys. Rev. E*, 58:1577–1590, Aug 1998. doi:10.1103/PhysRevE.58.1577.

[21] K. S. Gjerden, A. Stormo, and A. Hansen. Local dynamics of a randomly pinned crack front: a numerical study. *Frontiers in Physics*, 2:66, 2014. ISSN 2296-424X. doi:10.3389/fphy.2014.00066.

[22] S. S. Brenner. Mechanical behavior of sapphire whiskers at elevated temperatures. *Journal of Applied Physics*, 33 (1):33–39, 1962. doi:10.1063/1.1728523.

[23] S. N. Zhurkov. Kinetic concept of the strength of solids. *International Journal of Fracture*, 26(4):295–307, Dec 1984. ISSN 1573-2673. doi:10.1007/BF00962961.

[24] S. Santucci, L. Vanel, and S. Ciliberto. Subcritical statistics in rupture of fibrous materials: Experiments and model. *Phys. Rev. Lett.*, 93:095505, Aug 2004. doi:10.1103/PhysRevLett.93.095505.

[25] L. Vanel, S. Ciliberto, P.-P. Cortet, and S. Santucci. Time-dependent rupture and slow crack growth: elastic and viscoplastic dynamics. *Journal of Physics D: Applied Physics*, 42(21):214007, oct 2009. doi:10.1088/0022-3727/42/21/214007.

[26] O. Lengliné, R. Toussaint, J. Schmittbuhl, J. E. Elkhoury, J. P. Ampuero, K. T. Tallakstad, S. Santucci, and K. J. Måløy. Average crack-front velocity during subcritical fracture propagation in a heterogeneous medium. *Phys. Rev. E*, 84:036104, Sep 2011. doi:10.1103/PhysRevE.84.036104.

[27] T. Vincent-Dospital, R. Toussaint, A. Cochard, K. J. Måløy, and E. G. Flekkøy. Thermal weakening of cracks and brittle-ductile transition of matter: A phase model. *Physical Review Materials*, 02 2020. doi:10.1103/PhysRevMaterials.4.023604.

[28] T. Vincent-Dospital, R. Toussaint, S. Santucci, L. Vanel, D. Bonamy, L. Hattali, A. Cochard, K. J. Måløy, and E. G. Flekkøy. How heat controls fracture: the thermodynamics of creeping and avalanching cracks. *Soft Matter*, 2020. doi:10.1039/d0sm010. accepted.

[29] S. Santucci, K. J. Måløy, R. Toussaint, and J. Schmittbuhl. Self-affine scaling during interfacial crack front propagation. In *Dynamics of Complex Interconnected Systems*. NATO ASI, Geilo, Springer, 2006.

[30] G. G. Hammes. *Principles of Chemical Kinetics*. Academic Press, 1978.

[31] L. B. Freund. Crack propagation in an elastic solid subjected to general loading. *Journal of the Mechanics and Physics of Solids*, 20(3):129 – 152, 1972. ISSN 0022-5096. doi:10.1016/0022-5096(72)90006-3.

[32] M.L. Hattali, J. Barés, L. Ponson, and D. Bonamy. Low velocity surface fracture patterns in brittle material: A newly evidenced mechanical instability. In *THERMEC 2011*, volume 706 of *Materials Science Forum*, pages 920–924. Trans Tech Publications Ltd, 1 2012. doi:10.4028/www.scientific.net/MSF.706-709.920.

[33] G. Perrin, J. R. Rice, and G. Zheng. Self-healing slip pulse on a frictional surface. *Journal of the Mechanics and Physics of Solids*, 43(9):1461 – 1495, 1995. ISSN 0022-5096. doi:10.1016/0022-5096(95)00036-I.

[34] J. R. Dormand and P. J. Prince. A family of embedded Runge-Kutta formulae. *Journal of Computational and Applied Mathematics*, 6(1):19 – 26, 1980. ISSN 0377-0427. doi:10.1016/0771-050X(80)90013-3.

[35] E. Hairer, S. P. Nørsett, and G. Wanner. *Solving Ordinary Differential Equations I, nonstiff problems*. Springer-Verlag Berlin Heidelberg, 1993. doi:10.1007/978-3-540-78862-1.

[36] A. Zerwer, M. A. Polak, and J. C. Santamarina. Wave propagation in thin plexiglas plates: implications for Rayleigh waves. *NDT and E International*, 33(1): 33 – 41, 2000. ISSN 0963-8695. doi:10.1016/S0963-8695(99)00010-9.

[37] A.-L. Barabási and H. E. Stanley. *Fractal Concepts in Surface Growth*. Cambridge University Press, 1995. doi:10.1017/CBO9780511599798.

[38] Technical information, Altuglas sheets. Technical report, Arkema, 2017. URL https://www.altuglas.com/export/sites/altuglas/.content/medias/downloads/literature/UK-brochure-technique-BD.pdf.

[39] A. Stormo, O. Lengliné, J. Schmittbuhl, and A. Hansen. Soft-clamp fiber bundle model and interfacial crack propagation: Comparison using a non-linear imposed displacement. *Frontiers in Physics*, 4:18, 2016. ISSN 2296-424X. doi:10.3389/fphy.2016.00018.

[40] E. Bouchaud, J.P. Bouchaud, D.S. Fisher, S. Ramanathan, and J.R. Rice. Can crack front waves explain the roughness of cracks? *Journal of the Mechanics and Physics of Solids*, 50(8):1703 – 1725, 2002. ISSN 0022-5096. doi:https://doi.org/10.1016/S0022-5096(01)00137-5.

[41] R. Scorretti, S. Ciliberto, and A. Guarino. Disorder enhances the effects of thermal noise in the fiber bundle model. *Europhysics Letters (EPL)*, 55(5):626–632, sep 2001. doi:10.1209/epl/i2001-00462-x.

[42] S. Roux. Thermally activated breakdown in the fiber-bundle model. *Phys. Rev. E*, 62:6164–6169, Nov 2000. doi:10.1103/PhysRevE.62.6164.

ON DISORDERED INTERFACES AND THERMAL WEAKENING

ABSTRACT

In the previous article, we have looked into the behaviour of fronts in disordered 2D interfaces, while neglecting any thermal effect on the crack dynamics. Here, I reintroduce the Joule heating at the front, and show that thermal avalanches can be triggered if loading the crack with enough intensity. I show however that the adiabatic approximation, considered in the previous pages, likely holds, as thermal exchanges should be of negligible effect with the parameters that we have considered there.
Additionally, by varying one of the dynamics parameter (l, the heat production zone size) to obtain some simulations near the critical point of our model, I give some insight on how 2D avalanches behave in this critical vicinity.
Finally, I discuss experimental tries I made to trigger some hot avalanches using the PMMA interfacial crack set up, that we have previously introduced.

I. ON THE ADIABATIC HYPOTHESIS OF THE PRECEDING ARTICLE

We here consider the same overall parameters as those inverted to reproduce the experiments from Tallakstad et al. [2]. A front propagates, with the same Arrhenius-based model including a stress redistribution, through the same disordered interface. The mean fracture energy of this interface is thus $\overline{G_c} = 250\,\mathrm{J\,m^{-2}}$, its standard deviation $\delta G_c = 35\,\mathrm{J\,m^{-2}}$ and its correlation length $l_c = 50\,\mu\mathrm{m}$. Additionally, some thermal dissipation around the crack front is now considered, and the temperature at the front is described with the same, quasi-static, model that we have now introduced several times (e,g, [1, 3, 4]). The parameters for this thermal model are considered the same as those inverted for bulk PMMA in Ref. [1], that are: a heat conductivity and capacity $\lambda = 0.18\,\mathrm{J\,s^{-1}\,m^{-1}\,K^{-1}}$ and $C = 1.5\,\mathrm{MJ\,m^{-3}}$, a heat conversion efficiency $\phi = 20\%$, and a heat production zone around the front of radius $l = 10\,\mathrm{nm}$.
Of course, applying this bulk PMMA thermal parameters (in particular l and ϕ) to the rupture dynamics of sintered interfacial PMMA is already an assumption, as these are, in practice, two different (although similar) materials. However, in the absence of a better characterisation of these parameters, it is a likely reasonable starting point.
We can now rerun the numerical simulation that reproduced at best the experimental observations from Tallakstad et al. [2], with the added thermal effect. When compared to the simulations already presented (without heat dissipation), no significant difference was observed (see Fig. 1a), as any temperature elevation ΔT was there negligible.

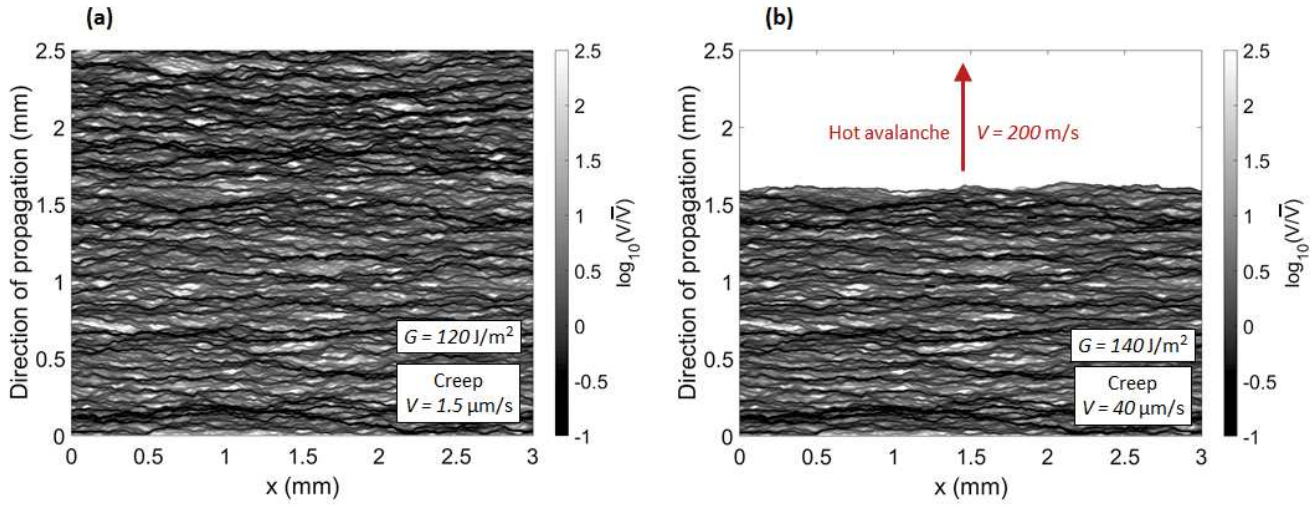

FIG. 1. Spatial crack velocity map for a mean energy release rate of $120\,\mathrm{J\,m^{-2}}$ (top) and $14\,\mathrm{J\,m^{-2}}$ (bottom), with the same parameters as in the preceding article and thermal parameters from Vincent-Dospital et al. [1]. In the latter case, a thermal avalanche is triggered (Large white area, with an average velocity of $200\,\mathrm{m\,s^{-1}}$). The mean velocity defining the colour scale is that of the creep (slow) phase, without an avalanche.

As briefly discussed in the previous article, such similitude does not come as a surprise, as the maximal temperature elevation reached in the creeping (low velocity) regime, approximated by

$$\Delta T_{\max} \sim \frac{\phi\,\overline{G} \times \max(V)}{\lambda}, \tag{1}$$

is about 0.2 K and thus not significant compared to the room temperature $T_0 = 298\,\mathrm{K}$. As a reminder, $\overline{G}$ was $120\,\mathrm{J\,m^{-2}}$ and the maximal simulated velocity was about $1\,\mathrm{mm\,s^{-1}}$. The adiabatic hypothesis of the previous article is thus verified.
Pushing this numerical work slightly further, we can actually infer that the experimental fronts were, likely, even colder than what we have here considered. Indeed, running a simulation at a higher driving load ($\overline{G} = 140\,\mathrm{J\,m^{-2}}$) leads to an average front velocity of about $40\,\mu\mathrm{m\,s^{-1}}$. There, a dramatic thermal avalanches is modelled (see Fig. 1b), whereas Tallakstad et al. [2] could run fracturing experiments at higher average creep velocities (up to $140\,\mu\mathrm{m\,s^{-1}}$) without observing such a dramatic event.

II. 2D THERMAL AVALANCHES CLOSER TO THE CRITICAL POINT

From this section onward, we will work with a slightly less disordered fracture energy defined as follows: $\overline{G_c} = 250\,\mathrm{J\,m^{-2}}$, $\delta G_c = 20\,\mathrm{J\,m^{-2}}$ and $l_c = 25\,\mu\mathrm{m}$. We keep the same thermal parameters: $\lambda = 0.18\,\mathrm{J\,s^{-1}\,m^{-1}\,K^{-1}}$ and $C = 1.5\,\mathrm{MJ\,m^{-3}}$, $\phi = 20\%$, and $l = 10\,\mathrm{nm}$.
To obtain some non negligible temperature elevations, with Eq. (1), and hence some thermal weakening, we loaded a numerical crack in this interface with $\overline{G} = 171\,\mathrm{J\,m^{-2}}$. Figure 2 shows the simulated velocity maps for $\overline{G} = 170$ and $171\,\mathrm{J\,m^{-2}}$, with only the latter triggering a thermal avalanche. The corresponding average creep velocity, thus allowing thermal weakening to initiate, is $6\,\mathrm{mm\,s^{-1}}$, with velocity bursts due to the rough fracture energy landscape of about

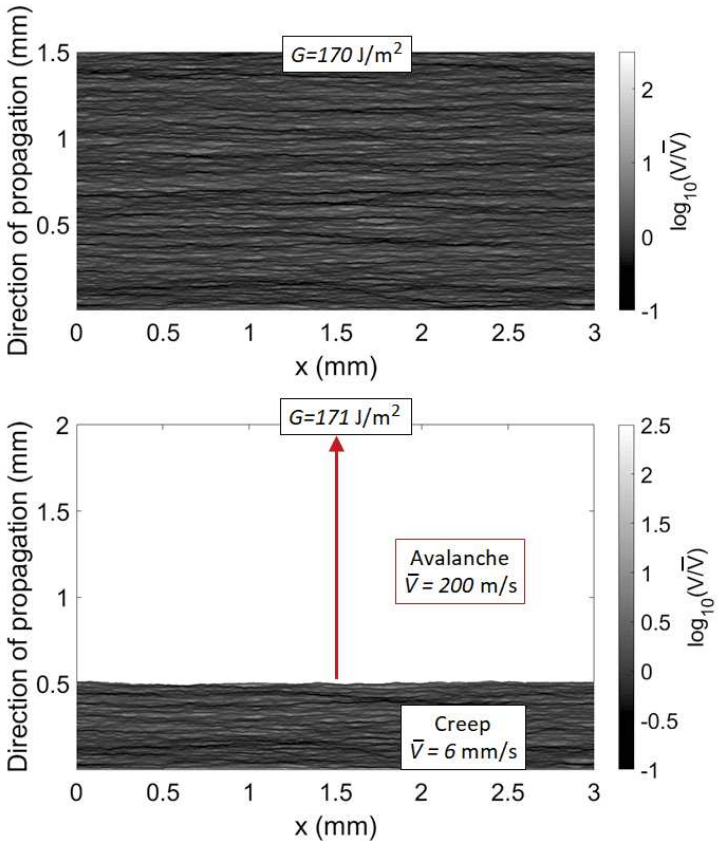

FIG. 2. Spatial crack velocity map for a mean energy release rate of $170\,\mathrm{J\,m^{-2}}$ (top) and $171\,\mathrm{J\,m^{-2}}$ (bottom), with the parameters described in section II. In the latter case, a thermal avalanche is triggered (white area, with an average velocity of $200\,\mathrm{m\,s^{-1}}$). The mean velocity defining the colour scale is that of the creep (slow) phase, without an avalanche: $\overline{V} = 6\,\mathrm{mm\,s^{-1}}$.

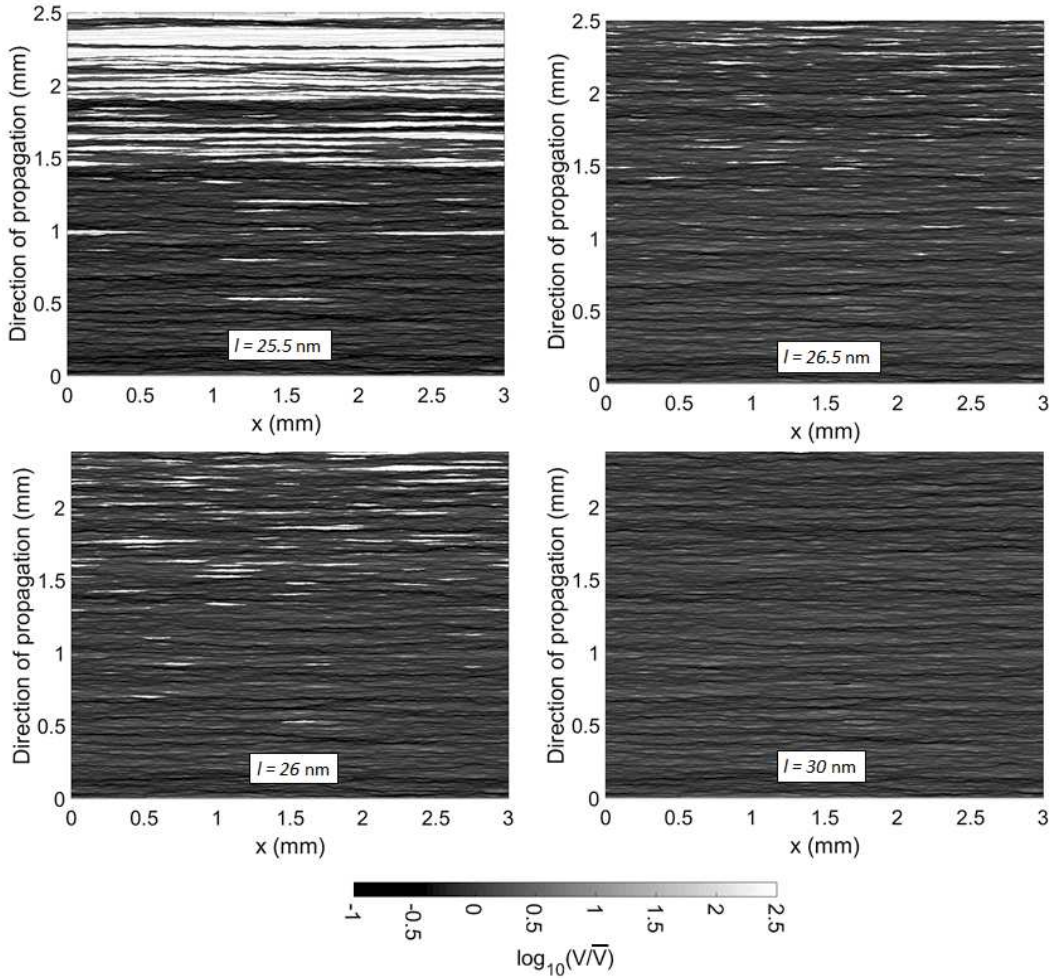

FIG. 3. Spatial crack velocity map for three different sizes l of the thermal production zone. The average velocity for the creeping zones is $\overline{V} = 6\,\mathrm{mm\,s^{-1}}$. The white areas are thermal avalanches which velocity can reach up to $200\,\mathrm{m\,s^{-1}}$.

$60\,\mathrm{cm\,s^{-1}}$. As per Eq. 1, the front temperature in the creep regime now reaches 110 K and is thus significant.
The thermal avalanche shown in Fig. 2 reaches the full system size (which is here $L = 3\,\mathrm{mm}$). It is somewhat expected as, as we are likely not particularly close to the critical point of the modelled dynamics [4]. Indeed, in the considered disordered landscape, the variations of the driving field G induced by the front roughness likely makes the slow and fast phases metastable, making a change in phase prone to propagate quickly to the whole system [5].
We next look for sets of parameters that place the simulations in situations which are close to the critical vicinity. Thus we should observe avalanches of all sizes, and not limited to L. I have here decided to vary the size l of the heat emission zone. Indeed, while not affecting much the triggering of avalanches (mainly controlled by Eq. (1)), a larger l implies a cooler fast propagation phase, so that thermal runaways will be more easily stopped. In fine, a very large l brings the crack to a cold case again (brings it beyond the critical vicinity), as the limiting temperature ΔT_{lim} that a front can reach is limited by l:

$$\Delta T_{\mathrm{lim}} \sim \frac{\phi \overline{G}}{\pi C l}. \tag{2}$$

In Fig. 3, the spatial velocity maps are shown for various values of l. One can see how the avalanches end up disappearing with larger l, while having transited from the rupture of full crack length to only patches of fast propagation. Note that the size to mainly look at in this figure is the horizontal extent of the avalanches as, although these maps are 2D, the studied system is only a line-crack along the x direction. In theory [4], for a simulation that would exactly stand on the critical point, one would expect fast phase clusters of all sizes without a clear correlation length and displaying a fractal arrangement.

Note that the evolution shown in Fig. 3 could be observed by varying other parameters than l in the right range, such as the ambient temperature T_0 (the thermal parameter describing the phase behaviour in our phase description), the amount of energy ϕ going into heat or the amplitude δG_c of the surrounding quenched disorder.
Note also that, in the same figure, the distribution of avalanches is somewhat top heavy. This may arise from a cumulative effect, as a first avalanche highly deforms the front, hence favouring stress concentrating, and then facilitating further avalanches.

III. LIMITATIONS

As a perspective and continuation work to this thesis, one could thus study further this interfacial dynamics around the critical point, notably to derive additional critical exponents to those proposed in Ref. [4]. I have only here presented a few related potential points of interest.
Doing so, one should however keep in mind the numerous limitations that the model has. In particular, the temperature model we have used here was initially derived [3] for a straight front propagating at a unique velocity. Applying this model that only depends on the local crack velocity and load to a rugous front with a inhomogeneous velocity distribution could be rather inaccurate.
Furthermore, the model is still a quasi-static one, and supposes that changes in front temperature are instantaneous when the velocity varies. We discussed in Ref. [4] how this approximation is likely reasonable in the case of long enough avalanches, when the typical transient times in the system dynamics, to warm or cool a crack fronts, are small compared to the duration of the avalanches. Investigating the critical point (i.e., potentially looking at small and short avalanches, as shown in Fig. 3) might place us in situations where this criterion is not met.
This latter point might be more important for the modelling of interfacial (line) cracks than for that of point fronts. Indeed, in the former case, the lateral progression of fast avalanches is likely dependent on the thermal transient times. In a static and elastic only description, when an avalanche nucleates at a given front position, the neighbouring points that should instantaneously be under a high stress due to the high velocity gradient along the front. There are indeed several orders of magnitudes between the speed of a creeping crack section and that of a thermally weakened one, which is to cause a significant front deformation, as schematically illustrated in Fig. 4. Thus, the transition between a fast and a slow portion of the front shall depend on the thermal transient time, or another time dependent phenomena, such as a viscoplastic behaviour of the matrix or as the inertia of the two PMMA plates.Without modelling such time dependent dynamics, as we indeed did not do to obtain Fig. 3, one would likely obtain a lateral avalanche dynamics which is depending on the numerical solver time step in a non physical way.
Truly, it is in theory possible to solve the whole thermal dynamics, including the rugosity of the fronts and the transient time, as analytically described by a Fourier equation (i.e., [4]). In this case, however, I have for now failed to write a solver whose run time is manageable enough to output any exploitable result. Indeed, integrating the moving heat sources over space (over the front shape) and over time (over the thermal history) to compute an accurate temperature everywhere along the crack is a rather demanding computation.
Finally, let me point out that the fast lateral growth of avalanches in the rupture of cohesive interfaces can be measured experimentally and characterised, as recently shown by De Zotti et al. [6] in the peeling of tape. Thus, reference experiments to be reproduced by models are available. In the case of tape peeling, the instabilities nucleate at the border of the peeled adhesive band, so that significant edge effects are probably at play.

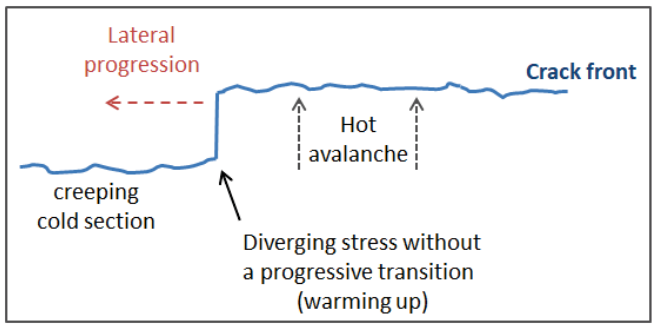

FIG. 4. Schematic of the transition between a creeping crack section and an avalanching one. The thermal transient time are likely of importance for the transition from one to the other, and thus the lateral progression of an avalanche. Alternatively the transition could be governed by some viscoplastic component of the material reology.

IV. AVALANCHE ARREST

Moving back away from the critical points, when avalanches become big compared to the system size, note that the constant average load $\overline{G}(t) = \overline{G}$ hypothesis used in reproducing the interfacial experiments [2], and here in Figs 1, 2 and 3, is likely incorrect. In a realistic set-up, a crack front is to very quickly unload when running away from the load application point at velocities close to that of the mechanical waves. As $\overline{G}$ then decreases, the avalanche would naturally stop when a portion of the front reaches the arrest threshold G_s, as explained in ref. [4]. How $\overline{G}$ decreases with the advance of the crack is of course highly dependent on the loading configuration and system geometry.

V. EXPERIMENTAL TRIES

I had the opportunity to experiment myself with the interfacial rupture in PMMA set-up, from the preparation of the sand blasted and sintered samples to the rupture tests. It was the same set-up, located in Porelab at the university of Oslo, as the one used by Tallakstad et al. [2]. Besides gaining some knowledge on an experiment whose results I have, in the preceding article, tried to numerically reproduce, my main goal was to look for the nucleation of microscopic defaults ahead of the main crack fronts. The observation of such a nucleation had been believed to be observed during earlier exploration works on the set-up. However, testing numerous PMMA samples, I was unable to repeat this observation and could not spot any damage nucleation in front of the interfacial cracks. As of today, it remains unclear whether their previous observation was the consequences of very particular experimental parameters, luckily met but now unknown, or only artefacts in the imaging of the progressing fronts.
Additionally to this unsuccessful search, I have also tried the experimental set-up to trigger and, hopefully, characterise some fast avalanches. Indeed, while those have been well studied in bulk PMMA (e.g., [1]), the interfacial set-up could allow to study the nucleation and lateral progression of the avalanches, that we have discussed above. This set-up was, however, designed to study creep. Some brutal sample rupture was then, in historical test runs, considered as a failed experiment rather than data to be analysed.
To try forcing an avalanche, I first introduced a default in the PMMA plates before sintering them: a cutter cut perpendicular to the direction of crack propagation. The idea was to create a weak (low fracture energy) zone during the sintering, so that a rupture front would there accelerate up to the thermal weakening threshold. A picture of the corresponding set-up is shown in Fig. 5. In this configuration, what seemed to be an avalanche could indeed be observed: an abrupt crack propagation after a slower creep, accompanied with a distinct cracking noise. However, this avalanche actually triggered before the crack met the default. It was then questioned whether the avalanche was at all related to the cut, especially as it was noticed that the loading lever, driving the rupture (see Fig. 5), was subject to a strong deformation during the fracturing test, which was maximal at the onset of the avalanche. Such

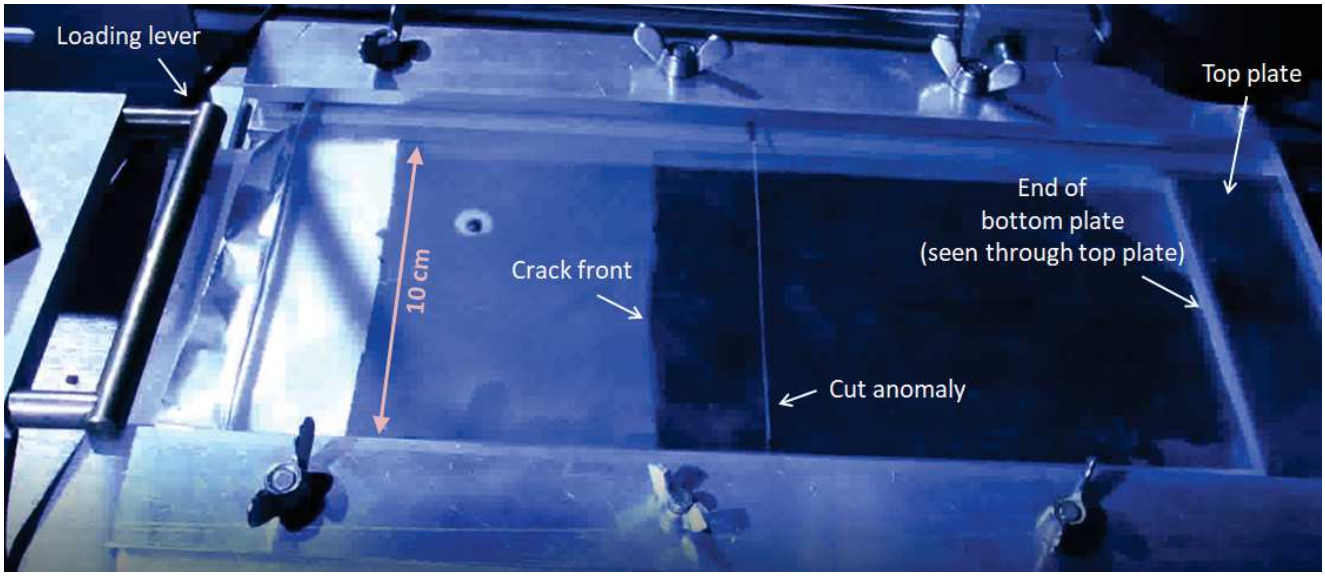

FIG. 5. Top view of the experimental setp-up for the interfacial rupture of PMMA.

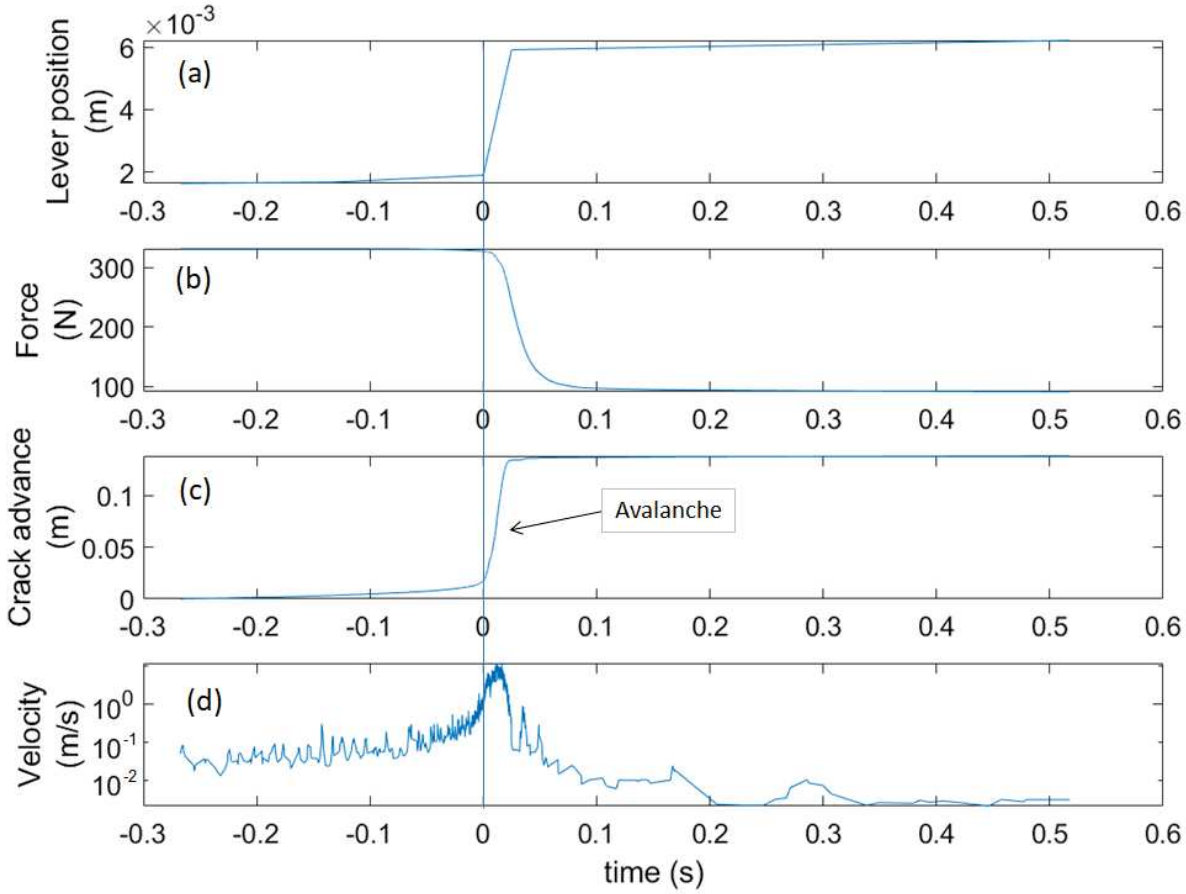

FIG. 6. (a): Lever altitude during the rupture test. The lever is driven with a constant voltage (targeting a constant velocity). Yet, an uncontrolled avalanche occurs in its course from the loading system lack of stiffness. (b): Force measurement during the rupture test. A brutal decrease of the force coincide with the sudden release of the lever potential energy. (c): Simultaneously the crack avalanches. It is unclear if a transition of phase occurs (i.e., if a hot avalanche it at stake), or if the acceleration is only due to the release of the lever. (d): Crack velocity, which is the time derivative of the previous measurement.

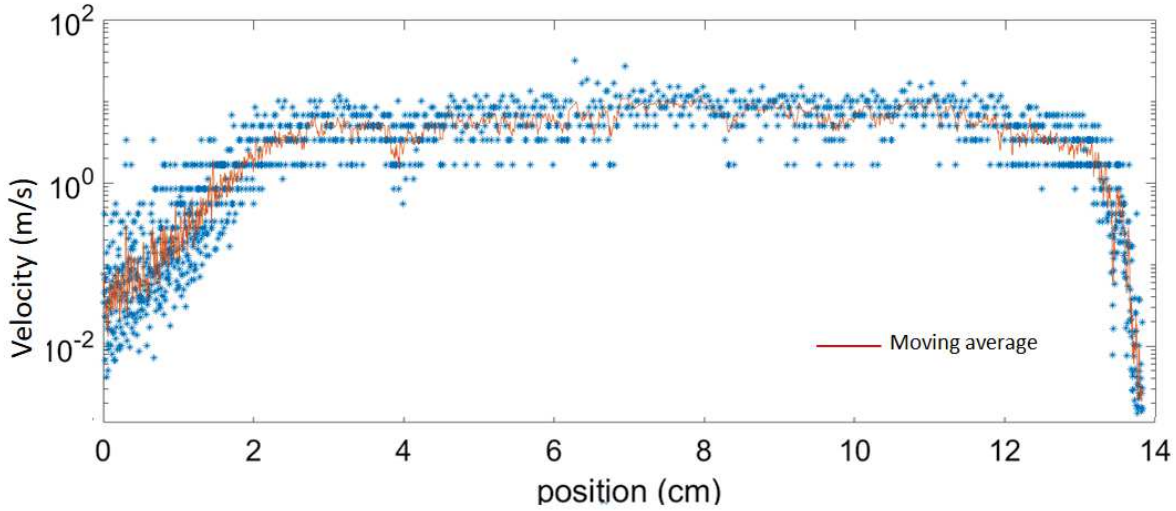

FIG. 7. Crack velocity as a function of the front position (dots). It is a crossplot of Figs. 4c and 4d. The plain line is a moving average.

a deformation was a consequence for the set-up not being designed for fast propagation tests and thus lacking the necessary stiffness. The observed avalanche was then likely caused by the restitution of potential energy from the unstiff loading system. Of course, it does not mean that no phase shift in the crack dynamics was at stake, but one could not state it for certain. I then performed an experiment without a cutting anomaly and monitoring the lever with a standard 30 fps camera, to properly monitor its deformation and the deflection of the lower plate during the rupture experiment. The images are then analysed by manually picking the lever position frame by frame.
The result I present here are from this experiment. The crack progression is monitored under a strong lighting by a Photron fast camera with a frame rate of $50,000$ fps. The front is then automatically picked, frame by frame, by detecting the colour change due to the passage of the crack (which can be seen in Fig. 5). Due to the memory limitation of the camera, only a crack width of 8 pixels $= 2$ mm was monitored (for a total crack length of 10 cm). The total front propagation spanned over 14 cm. The force applied by the lever was additionally measured at the same $50,000$ fps rate by a piezoelectric captor plugged to a data acquisition card. Figure 6 summarises all measurements as time series, and Fig. 7 shows the crack velocity as a function of the crack position. One can notice the uncontrolled avalanche occurring in the lever course, due to the loading system lack of stiffness. Unfortunately the 30 fps monitoring of the lever position does not allow to resolve this burst, as it fully happens in between two frames. This makes analysing the crack avalanche rather difficult, as it is unclear whether it is only due to the restitution of some potential energy by the lever or if some (hot) phase shift is also at stake.
A way to answer this question would be to accurately measure the V versus G relation, because an hysteresis in this relation would likely indicate a complex phase transition dynamics. Yet, the poor resolution of the lever position and the unknown crack morphology (as only a small portion of the front was recorded with the high speed camera) makes it hazardous to asses G. What is certain is that the recorded crack acceleration was rather smooth (see Fig. 7), and does not seem to hold an abrupt phase transition as forecasted by our model. Additionally, one can notice that some creep (that is, some slow propagation without any avalanche) with a velocity as high as centimetres per second could be measured and that the avalanche velocity barely reached $10\,\mathrm{m\,s^{-1}}$. The simulations presented in Fig.1 or 2 are hence not a good representation of this experiment, as they predict that creep ends around $\overline{V} = 6\,\mathrm{mm\,s^{-1}}$ and that the velocity of avalanches reach a few hundred of meters per seconds. Of course the thermal parameters that we have considered (i.e., ϕ and l), as well as the considered interface disorder, might be inappropriate to the description of this particular sintered, interfacial, PMMA. Possibly, the experiment was performed in an all ductile material (in a condition past the critical point) so that any propagation velocity can be regarded as creep and no discontinuity exists in the crack dynamics. The best way to further study issue would be to ensure having a loading system that is far stiffer than the PMMA sintered plates.

[1] T. Vincent-Dospital, R. Toussaint, S. Santucci, L. Vanel, D. Bonamy, L. Hattali, A. Cochard, K. J. Måløy, and E. G. Flekkøy. How heat controls fracture: the thermodynamics of creeping and avalanching cracks. *Soft Matter*, 2020. doi: 10.1039/d0sm010. accepted.
[2] K. T. Tallakstad, R. Toussaint, S. Santucci, J. Schmittbuhl, and K. J. Måløy. Local dynamics of a randomly pinned crack front during creep and forced propagation: An experimental study. *Phys. Rev. E*, 83:046108, 04 2011. doi: 10.1103/PhysRevE.83.046108.
[3] R. Toussaint, O. Lengliné, S. Santucci, T. Vincent-Dospital, M. Naert-Guillot, and K. J. Måløy. How cracks are hot and cool: a burning issue for paper. *Soft Matter*, 12:5563–5571, 2016. doi:10.1039/C6SM00615A.
[4] T. Vincent-Dospital, R. Toussaint, A. Cochard, K. J. Måløy, and E. G. Flekkøy. Thermal weakening of cracks and brittle-ductile transition of matter: A phase model. *Physical Review Materials*, 02 2020. doi:10.1103/PhysRevMaterials.4.023604.
[5] H. B. Callen. *Thermodynamics and an introduction to thermostatistics; 2nd ed.* Wiley, 1985.
[6] V. De Zotti, K. Rapina, P.-P. Cortet, L. Vanel, and S. Santucci. Bending to kinetic energy transfer in adhesive peel front microinstability. *Phys. Rev. Lett.*, 122:068005, Feb 2019. doi:10.1103/PhysRevLett.122.068005.

Chapter V
Frictional anisotropy of 3D-printed fault surfaces

Where friction also depends on material disorder, and in particular in its anisotropy, and where you can 3D-print seismic faults

---

Pending submission to Frontiers in Earth Science
The experimental work has now been performed, see arXiv: 2011.05012

Résumé (*French abstract*):

Anisotropie de friction de surfaces de failles imprimées en 3D

La morphologie des failles sismiques contrôle l'anisotropie spatiale de leurs propriétés de friction, et donc, celle de leur stabilité. Une telle anisotropie est rarement étudiée dans les modèles sismologiques de glissement de faille, bien qu'elle puisse être importante pour la rupture sismique de zones particulières, notamment en cas de glissement oblique. Afin de quantifier le rôle de l'anisotropie de surfaces des failles sur la directionalité de leur coefficient de friction, nous testons ici des failles synthétiques en plâtre de Paris. Ces plans de glissement striés ont été produits en imprimant en 3D des surfaces réelles dont la rugosité fut scannée sur le terrain, à des échelles spatiales allant du millimètre au mètre.

Cet article est encore dans un état préliminaire, car l'obtention des données expérimentales nécessaires a été retardée par la situation sanitaire du premier semestre 2020. Nous présentons, cela-dit, des résultats exploratoires montrant, à l'aide du dispositif expérimental proposé, une anisotropie de friction de faille significative.

Frictional anisotropy of 3D-printed fault surfaces

Tom Vincent-Dospital,[1,*] Alain Steyer,[1] Aldo Mellado Aguilar,[1] François Renard,[2,3] and Renaud Toussaint[1,†]

[1] *Université de Strasbourg, CNRS, IPGS UMR 7516, F-67000 Strasbourg, France*
[2] *University of Oslo, The Njord Centre, Department of Geosciences, N-0316 Oslo, Norway*
[3] *Université Grenoble Alpes, Université Savoie Mont Blanc, CNRS, IRD, IFSTTAR, ISTerre, Grenoble, France*

The surface morphology of faults controls the spatial anisotropy of their frictional properties, and hence in their stability. Such anisotropy is only rarely studied in seismology models of fault slip, although it might be paramount to understand the seismic rupture in particular areas, notably where some oblique slip occurs. To quantify how the anisotropy of fault surfaces affects their static coefficient of friction during sliding, we sheared synthetic fault planes made of plaster of Paris. These fault planes were produced by 3D-printing actual striated fault surfaces whose 3D roughness was measured in the field at spatial scales from millimeters to meters.
This article is still a draft, as the collection of the necessary supporting data sets was unfortunately postponed due to the spring 2020 sanitary situation. We however present exploratory results showing a significant fault frictional anisotropy with the proposed experimental set-up.

I. INTRODUCTION

Seismic faults in the Earth's crust are complex objects along which earthquakes nucleate and propagate [1]. They hold structures and heterogeneities at all scales [2–4]. While faults are often simplified to their simplest two-dimensional description (i.e., the fault plane), increasing complexity is now added to faults models [5]. It is indeed believed that, to fully understand the seismicity of various areas [6–9], it is paramount to account for some disorder in the faults frictional properties such as secondary faulting, off-fault damage or roughness of the fault plane. Yet, another degree of complexity is rarely considered when modelling geological contacts: the possible anisotropy in their frictional properties. Morphological anisotropy is a known feature of faults, notably impacting the seismic waves velocity in their vicinity [10–12] or the mobility of natural and injected fluids [13] in the subsurface. Frictional anisotropy, interestingly, is also regularly studied in other fields than seismology, for instance the tribology of rubber tires [14, 15], the strength of advanced adhesives [16], or the mitigation of water condensation [17]. It is also believed to play a major role in nature [18], for instance in the motion of numerous animals [16, 19, 20] and in the hydration of some plants [21, 22]. In most cases, these frictional anisotropies derive from the existence of preferential topographic orientations on, at least, one of the contact surfaces [23]. The various scales for such structural directivity can be as small as micrometer [24] to nanometer [25, 26]. In seismic faults, such preferential directions in their topography are observed at all scales [2–4] and originate from several processes. At the molecular level, rock forming crystals may display some frictional anisotropy. It is notably the case for antigorite [27], a mineral abundant in the Earth's upper mantle. Fault zones are, besides, initiated by early fractures that often propagate in highly layered sediments. It can result [28] in an anisotropic ramp-flat morphology of these fracture surfaces. For more mature faults having accumulated enough displacement, and above a given length scale [29], the topography of the fault planes is also marked by slip induced wear, with striations and grooves of various wavelengths and amplitudes [30, 31] oriented in the main direction of slip. If such morphological anisotropy of fault surfaces is well-known, its effect on the anisotropy of the frictional properties remains to be characterised.
Here, we study how fault morphology controls the static coefficient of friction and the anisotropy of friction with regards to the main stress direction during slip. To reach this goal, we produce 3D-prints of actual faults surfaces whose topography was measured in the field [32]. We perform friction experiments with plaster of Paris casts of these printed faults. Results show that the friction coefficient along faults is highly anisotropic, a property that should henceforward be considered in numerical models of slip on seismic faults.

II. 3D PRINTING AND PLASTER CASTING OF FAULT PLANES

The actual morphology of natural faults can be difficult to assess, even if their long wavelength structures can be inferred by surface or subsurface imaging techniques [31, 33, 34]. Yet, some fault planes are accessible to direct, high resolution, measurements, notably as they were exhumed by erosion and tectonic processes. For this study, we have used a series of digital fault surfaces. These fault roughness data were acquired with Light Detection and Ranging (LIDAR) or white light interferometry. These data are available on an online public database [32]. Note that, should the reader hold some similar data, these authors welcome additions to this database. We have specifically selected fault roughness measurements

* vincentdospitalt@unistra.fr
† renaud.toussaint@unistra.fr

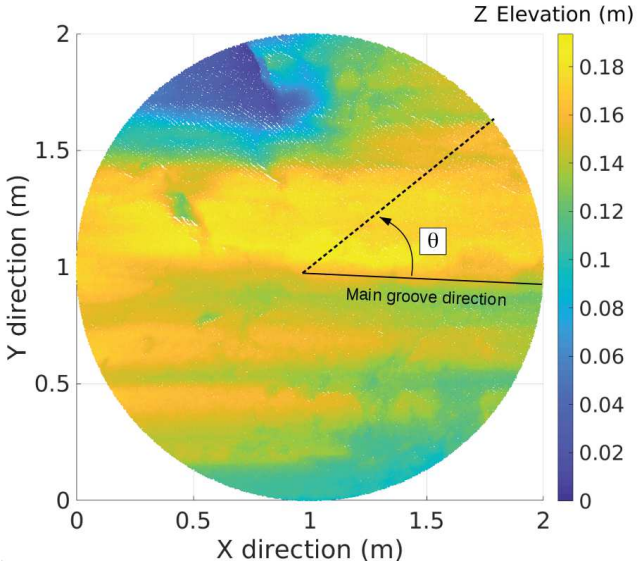

FIG. 1. Topography (i.e. roughness) of the Corona Heights fault at the meter scale [32]. This surface is called S_m, has a radius of 1 m and is defined on a 5 mm grid with a 1.25 mm elevation resolution. A parametric angle θ is defined from the main groove direction.

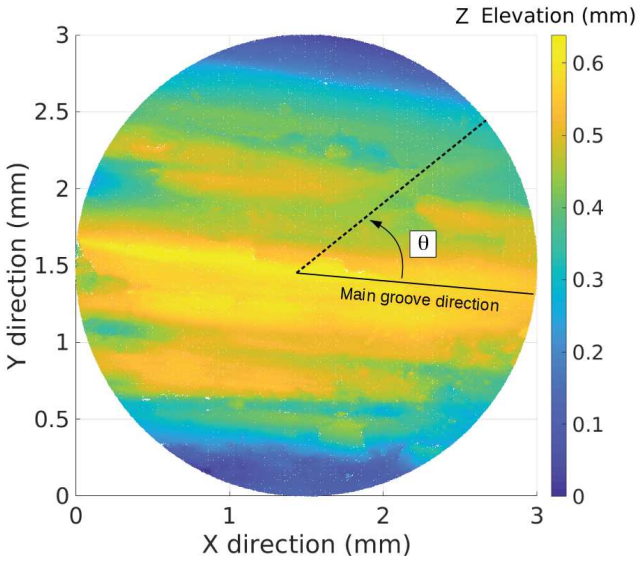

FIG. 2. White light interferometry topography of the Corona Heights fault plane at the millimeter scale. This surface is called S_{mm}, has a radius of 1.5 mm and is defined on a 2 µm grid with a 0.025 µm elevation resolution. A parametric angle θ is defined from the main groove direction.

performed on the Corona Heights fault [35] that outcrops near the Peixotto playground in San Francisco, California. These data cover surface areas with spatial scales in the range of millimeters to meters. Figures 1 and 2 show the fault surface at two spatial scales, one surface at the meter scale and one surface at the millimeter scale. We will further on refer to these two surfaces as respectively S_m and S_{mm}. Already, one can notice some preferential directions in these topographies, and that the fault roughness is somewhat higher at smaller scales (S_{mm}) than at larger ones (S_m) [36].

For our tests, we chose to limit these surfaces to a circular (i.e., isotropic) geometry, and applied a mild median filter to smooth out spikes in the measured surfaces. To run the friction experiments, we also needed to generate some opposing surfaces to the one presented in Figs. 1 and 2. These opposing surfaces could not be measured, as the actual fault walls that were facing S_m and S_{mm} are now eroded. To reconstruct them, we have applied the following transformation to the 3D coordinates (X, Y, Z) of S_m and S_{mm}:

$$\begin{aligned} X' &\sim X \\ Y' &\sim -Y \\ Z' &\sim -Z, \end{aligned} \tag{1}$$

where X', Y' and Z' are the coordinates of the generated opposing surfaces and (X, Y) give the map location of a given surface point of elevation Z, as represented in Fig. 1. We have thus assumed that the missing fault walls are only complementary to the measured ones, so that, when pressed together before the friction tests, they form

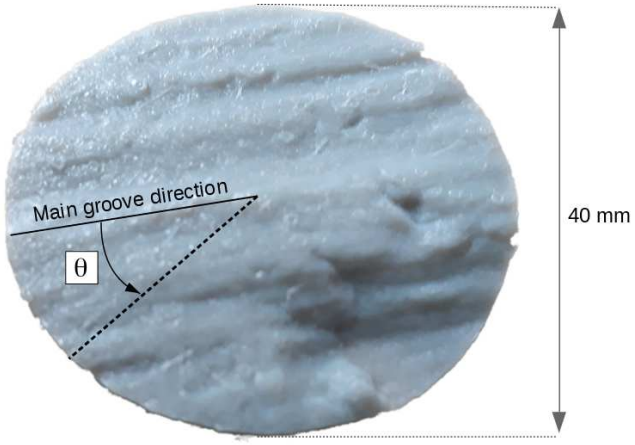

FIG. 3. Polylactic Acid 3D-print of S_m.

a bulk with no empty interstice. Such assumption for in situ faults would only be partly verified, as, when having accumulated some slip the two opposing sliding surfaces do not perfectly match in fault. However, this assumption may be relevant for the youngest faults with only a small amount of slip. We have also assumed that erosion did not significantly alter the fault plane, such that the measured topography is representative of the one of an actual buried fault. For the Corona Heights fault, this assumption is valid because the fault offsets silica-rich chert rocks with a high resistance to weathering.

Once having thus obtained the surfaces, we isotropically down- or up-scaled S_m and S_{mm} to fit a standard 4 cm diameter disk that matches the clamp size of our

FIG. 4. Plaster faults as moulded from the 3D-printed moulds (i.e., an example of which is shown in Fig. 4). Left: S_m (top) and its complementary surface (bottom). Right: (top) and its complementary surface (bottom). The samples have a 40 mm diameter.

shear deformation apparatus. We also re-gridded the surfaces to match the lateral resolution of our 3D-printer ('Ultimaker^2 Extended+' [37]) that has a nozzle size of 250 µm. The four surfaces (two fault surfaces and two opposing surfaces) were then 3D-printed into Polylactic Acid (PLA) material, as shown for instance in Fig. 3. It should be noted that, even when designed to be flat, printed objects can present a natural roughness [38], at a scale however smaller than the grooves observed on the printed faults. These intrinsic imperfections shall be comparable to 60 µm, the elementary thickness of the PLA layers deposited by our printer. In comparison, the standard deviation and maximal elevation in our printed objects topography are respectively 0.66 mm and 3.7 mm for S_m and respectively 1.7 mm and 8.3 mm for S_{mm}. We thus assume that the small scale roughness from the printer's limit in resolution has a second order effect on the frictional properties of the surfaces.

Although we could have performed the friction experiments with the plastic pieces out of the printer, we have rather casted them into plaster of Paris (gypsum) blocks. The goal of such casts was to work with a rock-like material, notably because Paris plaster may wear and deform differently than plastic under shear. The casts were generated with the following protocol: four volumes of water for one volume of powder of plaster of Paris brand were mixed and poured over the plastic moulds. A plaster setting time of one hour was then used, and the samples were then let to dry during at least twelve hours. The moulds, an example of which is shown in Fig. 3, were coated before each cast with some silicon grease to avoid some of the fine plaster details to stick to the PLA during the mould release. Finally, we have produced fault planes in plaster of Paris, as shown in Fig. 4.

III. EXPERIMENTAL SET-UP

The shear apparatus used to perform the friction tests is represented in Fig. 5. The two complementary surfaces are pressed together and mounted one on top of the other between the clamps of the shear apparatus. A normal force F_N is applied on the top surface by using adjustable weights. In addition, a spring system of stiffness 625 N m^{-1} allows, if desired, to compensate for the machine empty weight of 13.6 N (i.e., the normal weight transmitted to the friction surfaces by the machine top clamp and structure when no extra mass is used). A tangential driving shear force F_T is then applied to the top fault wall in a given direction of the (X, Y) plane. The amplitude of the force is measured by a Sauter® [39] force gouge. The shear direction direction is defined by the angle $\theta \in [0, 2\pi]$ from the direction of main grooves on the fault surface, as defined in Figs. 1 and 2. An horizontal mechanical slider makes sure that the friction is evaluated in the direction of interest only, and a vertical slider allows upward or downward displacement of the top surface. While these sliders would ideally be perfectly lubricated, we have estimated their intrinsic coefficient of static friction $\mu_c = 0.35 \pm 0.1$ by performing a friction test with no fault installed in the machine (that is, with only air between the two clamps represented in Fig. 5). Doing series of tests in various directions, the

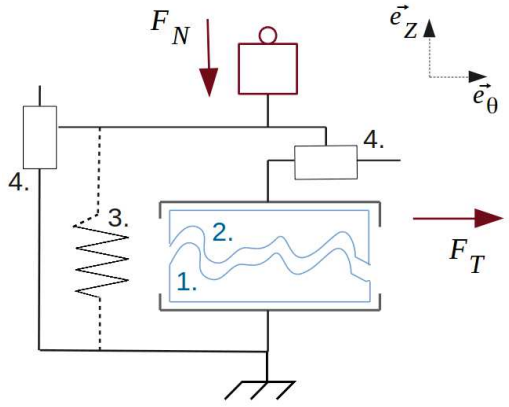

FIG. 5. The shear apparatus contains: the complementary plaster-casted fault surfaces (1 and 2) installed between two clamps; the compression spring (3) necessary to obtain a null normal loading when required; and two horizontal and vertical sliders (4) used to force the motion in the direction of interest while allowing for vertical displacement. The shear force F_T is applied on the top fault wall in the $\boldsymbol{e_\theta}$ direction, while the bottom surface is kept fixed. It is measured by a Sauter® FH500N force gauge [39]. The normal force F_N is applied by a dead weight that acts oppositely to the $\boldsymbol{e_Z}$ direction) on the top surface.

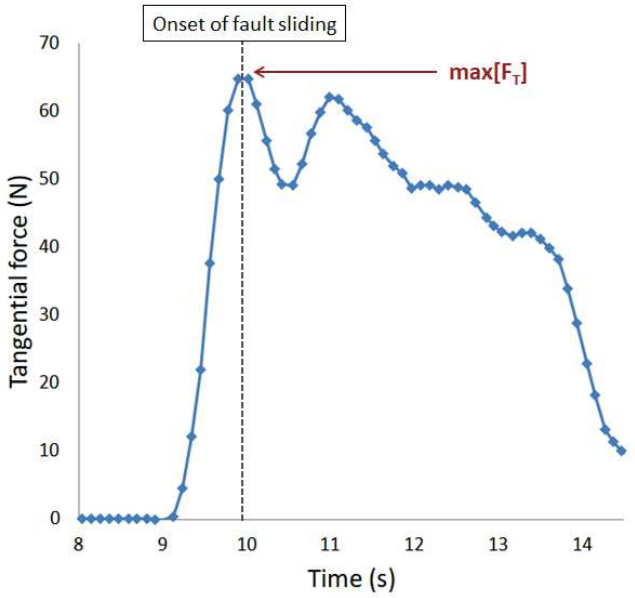

FIG. 6. Typical tangential force versus time for a given slide angle ($\theta = 90^{\circ}$) and a given normal force ($F_N = 4.9\,\mathrm{N}$) applied to the S_m fault. From the maximal value of the tangential force, a friction coefficient $\mu_s(4.9\,\mathrm{N}, 90^{\circ}) = 12.9$ can here be determined, as per Eq. (2).

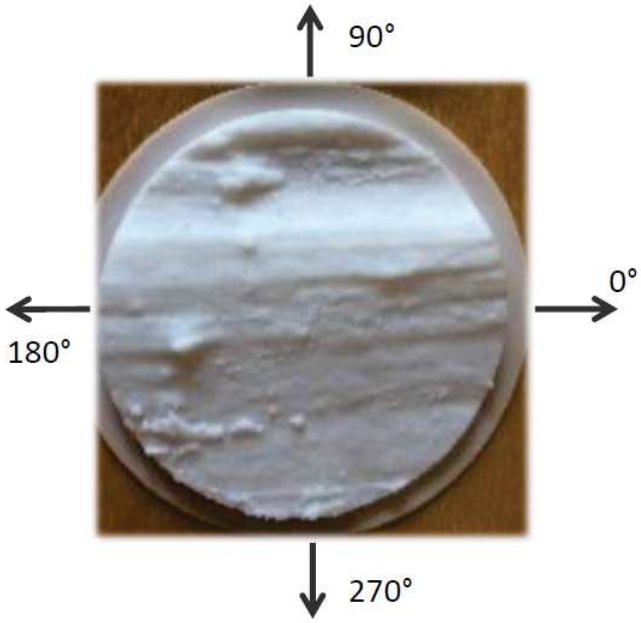

FIG. 7. 3D-print of a Dixie valley fault. The arrows correspond to given sliding directions during the friction tests, for which the coefficient of friction is summarised in Fig. 8. This plastic sample has a diameter of 5.5 cm, which is a magnification accounting for a real - field measured - diameter of 1 mm.

anisotropy of static friction for both the S_m and S_{mm} surfaces was measured. A new cast was used for each test so the potential wear of the surfaces does not impact the next measurements. At the onset of slip, the static friction coefficient is defined using a standard Coulomb's law [40]:

$$\mu_s(F_N, \theta) = \frac{\max\left[F_T(F_N, \theta)\right]}{F_N} - \mu_c, \qquad (2)$$

where μ_s is the coefficient of static friction and $\max\left[F_T\right]$ is the maximum tangential force applied at the onset of slip. Figure 6 shows a typical measurement from a single friction test, from which $\max\left[F_T\right]$, and hence μ_s, are calculated. For the record, the target speed of the test bench speed (that is, the demanded slip velocity) was fixed to a constant $3.077\,\mathrm{mm\,s^{-1}}$

IV. RESULTS

By performing frictional tests along various directions θ, we can now characterise the anisotropy of friction of our fault planes. Unfortunately the tests on S_m and S_{mm} have been postponed due to the infamous Covid-19 situation and limited access to the lab. The present article will be updated with these tests once performed. In the mean time, I here present the results obtained on an early exploratory set of tests, done by Aldo Mellado Aguilar under my supervision and that of Renaud Toussaint, with casts of another seismic fault from the Dixie valley (Nevada). The experimental protocol and set-up were similar (although slightly less advanced) than the ones presented above. The 3D-printed mould is shown in Fig. 7 and the angular dependent coefficient of static friction are shown in Fig. 8. One can notice the strong anisotropy, with μ_s that varies by more than a factor 2 depending on the glide direction. Naturally, the friction is less along the direction of grooves ($\theta = 0^{\circ}$ and $\theta = 180^{\circ}$) than perpendicularly to it.

V. DISCUSSION AND CONCLUSION

In this work, we have shown how the anisotropy, at various scales, in fault plane topography leads to some anisotropy in their friction properties. It notably confirms that seismic faults are prone to slide along some preferential directions, the most likely one being the historical one they have previously slid along, and which has shaped some guiding grooves in their morphology. Yet, displacements following other orientations are possible. Predicting the rupture direction of the next earthquake on a fault is thus not only depending on assessing that of the main regional stress. The question should rather be along which orientation a rupture criterion [40] will first be exceeded. Such a subtlety might be of little importance for mature faults for which the stress principle directions have not changed with time, as, in this case, the main stress is likely to act along

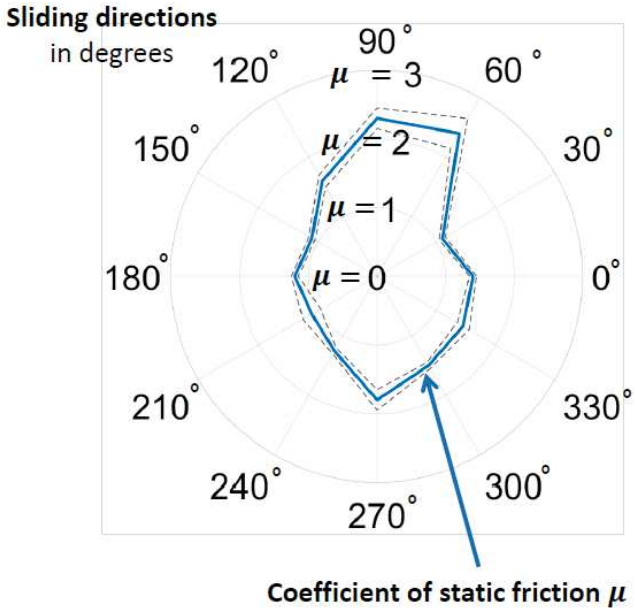

FIG. 8. Anisotropy of the static coefficient of friction for the surface presented in Fig. 7. The plain line is an average of three different tests and the width between the dotted line is the standard deviation. A clear anisotropy, exceeding the noise level, is shown.

the lowest coefficient of friction anyway. Yet, it could be paramount for faults under a changing geological load, where this alignment is not verified, or for the most recent faults, where the slip could be mainly governed by the early surfaces anisotropy. Earthquakes occurring along abnormal directions (i.e., not inline with what is expected from the local stress state) do happen [41–43], and their understanding might be eased by accounting for the possible frictional anisotropy of their surfaces [44]. While we have here only looked at the static coefficient of friction, note that the same considerations are to apply to the dynamical one. Hence, not only the initial slip direction of an earthquake could be impacted by frictional anisotropy, but its complete trajectory [45]. We have also illustrated how the 3D-printing technology can help with new experimental designs for the study of Earth sciences, and it indeed seems to get a growing attention from the community [46–49]. A direct continuation of the present work, for instance, could be to 3D-print and to test some faults surfaces beforehand filtered with various band-pass filters, in order to understand how the various scales of the topography contribute to its global frictional coefficient. Additionally, to better characterise the effect of wear on the friction coefficient, one could quantify the amount of damage caused to the plaster by the frictional slide, by imaging the surfaces before and after each tests.

ACKNOWLEDGEMENT

Author contributions: RT proposed the guidelines of this work, AS built the test machine and performed the friction experiments, AMA performed the friction experiments for the early results with the Dixie valley fault, TVD wrote the first version of this manuscript and FR and RT contributed to the writing of the final version of the manuscript. We are grateful for the early experimental explorations performed by Marine-Sophie Jacob, Céline Fliedner, Gaëtan Leca and Laifa Rahmi, all students from the EOST/IPGS faculty at the University of Strasbourg. We thank the Strasbourg AV.Lab association for the use of their 3D printer.
Author declarations: The authors declare no competing interest. A funding support from the University of Strasbourg is acknowledged. Readers are welcome to comment and correspondence should be addressed to vincentdospitalt@unistra.fr or renaud.toussaint@unistra.fr.

[1] Christopher A. J. Wibberley, Graham Yielding, and Giulio Di Toro. Recent advances in the understanding of fault zone internal structure: a review. *Geological Society, London, Special Publications*, 299(1):5–33, 2008. ISSN 0305-8719. doi:10.1144/SP299.2.

[2] François Renard, Christophe Voisin, David Marsan, and Jean Schmittbuhl. High resolution 3d laser scanner measurements of a strike-slip fault quantify its morphological anisotropy at all scales. *Geophysical Research Letters*, 33 (4), 2006. doi:10.1029/2005GL025038.

[3] Thibault Candela, François Renard, Yann Klinger, Karen Mair, Jean Schmittbuhl, and Emily E. Brodsky. Roughness of fault surfaces over nine decades of length scales. *Journal of Geophysical Research: Solid Earth*, 117 (B8), 2012. doi:10.1029/2011JB009041.

[4] Stephen R. Brown and Christopher H. Scholz. Broad bandwidth study of the topography of natural rock surfaces. *Journal of Geophysical Research: Solid Earth*, 90(B14):12575–12582, 1985. doi:10.1029/JB090iB14p12575.

[5] J. R. Rice and Y. Ben-Zion. Slip complexity in earthquake fault models. *Proceedings of the National Academy of Sciences*, 93(9):3811–3818, 1996. ISSN 0027-8424. doi: 10.1073/pnas.93.9.3811.

[6] James C. Pechmann and Hiroo Kanamori. Waveforms and spectra of preshocks and aftershocks of the 1979 imperial valley, california, earthquake: Evidence for fault heterogeneity? *Journal of Geophysical Research: Solid Earth*, 87(B13):10579–10597, 1982. doi: 10.1029/JB087iB13p10579.

[7] Telemaco Tesei, Cristiano Collettini, Massimiliano R. Barchi, Brett M. Carpenter, and Giuseppe Di Stefano. Heterogeneous strength and fault zone complexity of carbonate-bearing thrusts with possible implications for seismicity. *Earth and Planetary Science Letters*, 408:307 – 318, 2014. ISSN 0012-821X. doi:

https://doi.org/10.1016/j.epsl.2014.10.021.

[8] Ryosuke Ando, Naoto Takeda, and Teruo Yamashita. Propagation dynamics of seismic and aseismic slip governed by fault heterogeneity and newtonian rheology. *Journal of Geophysical Research: Solid Earth*, 117(B11), 2012. doi:10.1029/2012JB009532.

[9] Hideo Aochi and Satoshi Ide. Complexity in earthquake sequences controlled by multiscale heterogeneity in fault fracture energy. *Journal of Geophysical Research: Solid Earth*, 114(B3), 2009. doi:10.1029/2008JB006034.

[10] Russ Evans. Anisotropy: a pervasive feature of fault zones? *Geophysical Journal International*, 76(1):157–163, 01 1984. ISSN 0956-540X. doi:10.1111/j.1365-246X.1984.tb05031.x.

[11] Elizabeth S. Cochran, John E. Vidale, and Yong-Gang Li. Near-fault anisotropy following the Hector Mine earthquake. *Journal of Geophysical Research: Solid Earth*, 108(B9), 2003. doi:10.1029/2002JB002352.

[12] Zefeng Li, Zhigang Peng, Yehuda Ben-Zion, and Frank L. Vernon. Spatial variations of shear wave anisotropy near the San Jacinto fault zone in southern California. *Journal of Geophysical Research: Solid Earth*, 120(12):8334–8347, 2015. doi:10.1002/2015JB012483.

[13] Luigi Vadacca, Claudia Maria Colciago, Stefano Micheletti, and Anna Scotti. Effects of the anisotropy of the fault zone permeability on the timing of triggered earthquakes: Insights from 3d-coupled fluid flow and geomechanical deformation modeling. *Pure and Applied Geophysics*, 175(12):4131–4144, Dec 2018. ISSN 1420-9136. doi:10.1007/s00024-018-1936-4.

[14] G. Carbone, B. Lorenz, B. N. J. Persson, and A. Wohlers. Contact mechanics and rubber friction for randomly rough surfaces with anisotropic statistical properties. *The European Physical Journal E*, 29(3):275–284, Jul 2009. ISSN 1292-895X. doi:10.1140/epje/i2009-10484-8.

[15] A. Tiwari, L. Dorogin, B. Steenwyk, A. Warhadpande, M. Motamedi, Fortunat G., Ciaravola V., and B. N. J. Persson. Rubber friction directional asymmetry. *Europhysics Letters*, 116(6):66002, dec 2016. doi:10.1209/0295-5075/116/66002.

[16] Kejia Jin, Yu Tian, Jeffrey S. Erickson, Jonathan Puthoff, Kellar Autumn, and Noshir S. Pesika. Design and fabrication of gecko-inspired adhesives. *Langmuir*, 28:5737–5742, 2012. ISSN 0743-7463. doi:10.1021/la204040p.

[17] Nicolas Pionnier, Julie Vera, Elise Contraires, Stéphane Benayoun, Rémi Berger, and Stéphane Valette. The effect of the orientation and the height of periodic sub-micrometric texturing on dropwise condensation. *Journal of Colloid and Interface Science*, 526:184 – 193, 2018. ISSN 0021-9797. doi:https://doi.org/10.1016/j.jcis.2018.04.043.

[18] Alexander Filippov and Stanislav N. Gorb. Frictional-anisotropy-based systems in biology: structural diversity and numerical model. *Scientific Reports*, 3:1240, 2013. ISSN 2045-2322. doi:10.1038/srep01240.

[19] A. E. Filippov, G. Westhoff, A. Kovalev, and S. N. Gorb. Numerical model of the slithering snake locomotion based on the friction anisotropy of the ventral skin. *Tribology Letters*, 2018. ISSN 1023-8883. doi:0.1007/s11249-018-1072-4.

[20] Yongmei Zheng, Xuefeng Gao, and Lei Jiang. Directional adhesion of superhydrophobic butterfly wings. *Soft Matter*, 3:178–182, 2007. doi:10.1039/B612667G.

[21] A. Roth-Nebelsick, M. Ebner, T. Miranda, V. Gottschalk, D. Voigt, S. Gorb, T. Stegmaier, J. Sarsour, M. Linke, and W. Konrad. Leaf surface structures enable the endemic namib desert grass Stipagrostis Sabulicola to irrigate itself with fog water. *Journal of The Royal Society Interface*, 9(73):1965–1974, 2012. doi:10.1098/rsif.2011.0847.

[22] Fapeng Wang, Li Wang, Huaping Wu, Jiuyin Pang, Di Gu, and Song Li. A lotus-leaf-like sio2 superhydrophobic bamboo surface based on soft lithography. *Colloids and Surfaces A: Physicochemical and Engineering Aspects*, 520:834 – 840, 2017. ISSN 0927-7757. doi:https://doi.org/10.1016/j.colsurfa.2017.02.043.

[23] Chengjiao Yu and Q. Jane Wang. Friction anisotropy with respect to topographic orientation. *Scientific Reports*, 2:988, 2012. ISSN 2045-2322. doi:10.1038/srep00988.

[24] Stanisław Stupkiewicz, Maciej J. Lewandowski, and Jakub Lengiewicz. Micromechanical analysis of friction anisotropy in rough elastic contacts. *International Journal of Solids and Structures*, 51(23):3931 – 3943, 2014. ISSN 0020-7683. doi:https://doi.org/10.1016/j.ijsolstr.2014.07.013.

[25] Gregor Fessler, Ali Sadeghi, Thilo Glatzel, Stefan Goedecker, and Ernst Meyer. Atomic friction: Anisotropy and asymmetry effects. *Tribology Letters*, 67(2):59, Apr 2019. ISSN 1573-2711. doi:10.1007/s11249-019-1172-9.

[26] Hanjun Gong, Pengzhe Zhu, Lina Si, Xiaoqing Zhang, and Guoxin Xie. "M-shape" nanoscale friction anisotropy of phosphorene. *Computational Materials Science*, 150:364 – 368, 2018. ISSN 0927-0256. doi:https://doi.org/10.1016/j.commatsci.2018.04.013.

[27] Marcello Campione and Gian Carlo Capitani. Subduction-zone earthquake complexity related to frictional anisotropy in antigorite. *Nature Geoscience*, 6:847, 2013. ISSN 1752-0908. doi:10.1038/ngeo1905.

[28] D. C.P. Peacock and D. J. Sanderson. Effects of layering and anisotropy on fault geometry. *Journal of the Geological Society*, 149(5):793–802, 10 1992. ISSN 0016-7649. doi:10.1144/gsjgs.149.5.0793.

[29] Thibault Candela and Emily E. Brodsky. The minimum scale of grooving on faults. *Geology*, 44(8):603–606, 08 2016. ISSN 0091-7613. doi:10.1130/G37934.1.

[30] James T. Engelder. Microscopic wear grooves on slickensides: Indicators of paleoseismicity. *Journal of Geophysical Research*, 79(29):4387–4392, 1974. doi:10.1029/JB079i029p04387.

[31] Joel H. Edwards, Jared W. Kluesner, Eli A. Silver, Emily E. Brodsky, Daniel S. Brothers, Nathan L. Bangs, James D. Kirkpatrick, Ruby Wood, and Kristina Okamoto. Corrugated megathrust revealed offshore from costa rica. *Nature Geoscience*, 11:197–202, 2018. ISSN 1752-0908. doi:10.1038/s41561-018-0061-4.

[32] Thibault Candela and François Renard. Fault morphology database, 2012. URL https://www.isterre.fr/french/recherche-observation/equipes/mecanique-des-failles/moyens-et-outils/article/donnees.html.

[33] Didier Massonnet, Marc Rossi, César Carmona, Frédéric Adragna, Gilles Peltzer, Kurt Feigl, and Thierry Rabaute. The displacement field of the Landers earthquake mapped by radar interferometry. *Nature*, 364:138–142, 1993. ISSN 1476-4687. doi:10.1038/364138a0.

[34] Richard J. Blakely, Ray E. Wells, Craig S. Weaver, and Samuel Y. Johnson. Location, structure, and seismicity of the Seattle fault zone, Washington: Evidence from aeromagnetic anomalies, geologic mapping, and seismic-reflection data. *GSA Bulletin*, 114(2):169–177, 02 2002. ISSN 0016-7606. doi:10.1130/0016-7606(2002)114¡0169:LSASOT¿2.0.CO;2.

[35] Thibault Candela, François Renard, Jean Schmittbuhl, Michel Bouchon, and Emily E. Brodsky. Fault slip distribution and fault roughness. *Geophysical Journal International*, 187(2):959–968, 11 2011. ISSN 0956-540X. doi:10.1111/j.1365-246X.2011.05189.x.

[36] Emily E. Brodsky, James D. Kirkpatrick, and Thibault Candela. Constraints from fault roughness on the scale-dependent strength of rocks. *Geology*, 44(1):19–22, 01 2016. ISSN 0091-7613. doi:10.1130/G37206.1.

[37] Technical information, Ultimaker2 Extended+. Technical report, Ultimaker. URL https://ultimaker.com/download/7386/UserManual-UM2Extended-v2.1.pdf.

[38] Yann Quinsat, Claire Lartigue, Christopher A. Brown, and Lamine Hattali. Characterization of surface topography of 3d printed parts by multi-scale analysis. *International Journal on Interactive Design and Manufacturing*, 12(3):1007–1014, Aug 2018. ISSN 1955-2505. doi:10.1007/s12008-017-0433-9.

[39] Technical information, Sauter FH-S. Technical report, Sauter. URL https://dok.kern-sohn.com/manuals/files/English/FH-S-BA-e-1819.pdf.

[40] F. P. Bowden and D. Tabor. The friction and lubrication of solids. *American Journal of Physics*, 19(7):428–429, 1951. doi:10.1119/1.1933017.

[41] Jean-Philippe Avouac, Francois Ayoub, Shengji Wei, Jean-Paul Ampuero, Lingsen Meng, Sebastien Leprince, Romain Jolivet, Zacharie Duputel, and Don Helmberger. The 2013, Mw 7.7 Balochistan earthquake, energetic strike-slip reactivation of a thrust fault. *Earth and Planetary Science Letters*, 391:128 – 134, 2014. ISSN 0012-821X. doi:10.1016/j.epsl.2014.01.036.

[42] Kenji Satake and Hiroo Kanamori. Abnormal tsunamis caused by the june 13, 1984, torishima, japan, earthquake. *Journal of Geophysical Research: Solid Earth*, 96 (B12):19933–19939, 1991. doi:10.1029/91JB01903.

[43] Bernard Célérier. Seeking anderson's faulting in seismicity: A centennial celebration. *Reviews of Geophysics*, 46 (4), 2008. doi:10.1029/2007RG000240.

[44] M. H. P. Bott. The mechanics of oblique slip faulting. *Geological Magazine*, 96(2):109–117, 1959. doi:10.1017/S0016756800059987.

[45] F. Tapia, D. Le Tourneau, and J.-C. Géminard. Anisotropic friction: assessment of force components and resulting trajectories. *EPJ Techniques and Instrumentation*, 3:1, 2016. ISSN 2195-7045. doi:10.1140/epjti/s40485-016-0029-y.

[46] Li Wang, Yang Ju, Heping Xie, Guowei Ma, Lingtao Mao, and Kexin He. The mechanical and photoelastic properties of 3D printable stress-visualized materials. *Scientific Reports*, 2017. ISSN 2045-2322. doi:10.1038/s41598-017-11433-4.

[47] Xia-Ting Feng, Yan-Hua Gong, Yang-Yi Zhou, Zheng-Wei Li, and Xu-Feng Liu. The 3D-printing technology of geological models using rock-like materials. *Rock Mechanics and Rock Engineering*, 52:2261–2277, 2019. ISSN 1434-453X. doi:10.1007/s00603-018-1703-y.

[48] Andrew Squelch. 3D printing rocks for geo-educational, technical, and hobbyist pursuits. *Geosphere*, 14(1):360–366, 11 2017. ISSN 1553-040X. doi:10.1130/GES01364.1.

[49] Jiannan Wang, Robert R. Stewart, and Nikolay I. Dyaur. *Seismic response analysis of a 3D-printed dual-porosity physical model: Marine case*, pages 301–305. Society of Exploration Geophysicist, 2018. doi:10.1190/segam2018-2997200.1.

Chapter VI
Thermo-mechanical pain:
the signaling role of heat dissipation in biological tissues

Where hot cracks might be painful

Next submission to PRE
arXiv: 2005.04991

Résumé (*French abstract*):

La douleur thermo-mécanique :
le rôle d'avertissement de la dissipation thermique dans les tissus biologiques.

L'algésie mécanique est un processus important dans la préservation des organismes vivants, permettant des réflexes et des décisions potentiellement vitales lorsque des parties du corps sont sollicitées. Pourtant, ses divers mécanismes sous-jacents doivent encore être dénoués. Nous discutons ici quantitativement de comment la détection de stimuli mécaniques douloureux par le système nerveux peut se baser, en partie, sur des mesures thermiques. En effet, la plupart des fractures dans un corps, y compris celles microscopiques, dégagent de la chaleur, qui se diffuse ensuite dans les tissus avoisinant. A travers ce processus, les protéines thermosensibles TRP, qui traduisent des températures anormales en potentiels d'action, peuvent réagir à des dommages mécaniques. L'implication de ces récepteurs polymodaux dans l'algésie mécanique a longtemps été rapportée, et nous proposons ici une explication physique pour le couplage entre la douleur thermique et la douleur mécanique. En particulier, dans le cas de la peau humaine, nous montrons que les neurites voisines d'une fibre de collagène rompue peuvent connaitre une brusque élévation de température, de la fraction de degré à plusieurs dizaines de degrés. Cette anomalie thermique théorique étant compatible avec la sensibilité des canaux cationiques TRPV3 et TRPV1, connus pour déclencher des potentiels d'action dans le système neuronal, un degré de douleur mécanique peut ainsi être généré.

Thermo-mechanical pain: the signaling role of heat dissipation in biological tissues

Tom Vincent-Dospital[1, *] and Renaud Toussaint[1, †]

[1] *Université de Strasbourg, CNRS, Institut de Physique du Globe de Strasbourg, UMR 7516, F-67000 Strasbourg, France*

Abstract: Mechanical algesia is an important process for the preservation of living organisms, allowing potentially life-saving reflexes or decisions when given body parts are stressed. Yet, its various underlying mechanisms remain to be fully unravelled. Here, we quantitatively discuss how the detection of painful mechanical stimuli by the human central nervous system may, partly, rely on thermal measurements. Indeed, most fractures in a body, including microscopic ones, release some heat, which diffuses in the surrounding tissues. Through this physical process, the thermo-sensitive TRP proteins, that translate abnormal temperatures into action potentials, shall be sensitive to damaging mechanical inputs. The implication of these polymodal receptors in mechanical algesia has been regularly reported, and we here provide a physical explanation for the coupling between thermal and mechanical pain. In particular, in the human skin, we show how the neighbouring neurites of a broken collagen fiber can undergo a sudden thermal elevation that ranges from a fraction to tens of degrees. As this theoretical temperature anomaly lies in the sensibility range of the TRPV3 and TRPV1 cation channels, known to trigger action potentials in the neural system, a degree of mechanical pain can hence be generated.

Introduction: on rupture and energy dissipation

The growth of mechanical damages through a body is an irreversible thermodynamic process [1]. Indeed, when a fracture progresses by a given surface unit, it dissipates a specific amount of energy, that is referred to, by rupture physicists, as the energy release rate, expressed in $\mathrm{J\,m^{-2}}$. In most engineering materials (e.g., [2]), this quantity, denoted G, is well studied, since it characterizes the loading necessary for a crack to propagate [3]. For instance, it is in the order of $10\,\mathrm{J\,m^{-2}}$ in weak glasses [4] and can reach $100\,\mathrm{kJ\,m^{-2}}$ in the strongest media, as titanium [5] or steel [6].

When it comes to biological tissues, this energy release rate can also be estimated, and was notably measured to be about $G \sim 2000\,\mathrm{J\,m^{-2}}$ in the human hand skin [7]. An important question, then, is how is this dissipated mechanical energy received and felt by the human body? Most generally, there are many possible ways for it to be transformed, ranging from its storage as surface potential energy on the walls of the new fractures [8] to its emission to the far field as mechanical [9] or electromagnetic [10] waves, that is, sound and luminescence. It was, in particular, shown that a significant part of the mechanical input is converted into heat close to the damage [11–14], as the rupture of stretched atomic and molecular bonds is prone to generate a local and incoherent -thermal- atomic motion.

The related elevations in temperature have been measured in various synthetic solids (e.g., [12, 13, 15]), and are believed to be more than only a side effect of the fracturing process. Indeed, from its positive feedback on the dynamics of rupture, it was pointed out as a likely cause for the brittleness of matter [16, 17] and for the instability of some seismic faults [18–20].

We here propose that, in the human body, this damage-induced heat is to be sensed by the neuronal network, and may hence explain a degree of coupling between the thermal and mechanical pain, which has been regularly suspected (e.g., [21–23]).

THERMO-MECHANICAL NOCICEPTION

The perception of pain (i.e., nociception or algesia) arises from the bio-electrical signals (referred to as action potentials) that sensory neurons send from the aggressed body part to the nervous system (e.g, [26]). To initiate such messages, the dolorous inputs, being mechanical, thermal or chemical, need to be converted accordingly, at the surface of neurites (i.e., the extensions of neurons cell bodies).

We will here focus, as an example, on nociception in the human skin. As for other body parts, the TRPs proteins (Transient Receptor Potential cation channels) are notably believed to be responsible for the reporting of its temperature to the brain [21, 27]. For instance, TRPV3 send action potentials between 30 and 40°C, with an activation intensity that is gradual with temperature [28, 29], leading to a harmless perception of warmth. The feel of a more intense, potentially more noxious, heat occurs when TRPV1 is activated, at higher skin temperatures above 43°C. The physico-chemical mechanism to translate heat into current is, in all cases, believed to be a temperature dependant shifts in the TRPs voltage-dependent activation curves [30], that is, in their ability to pass ions

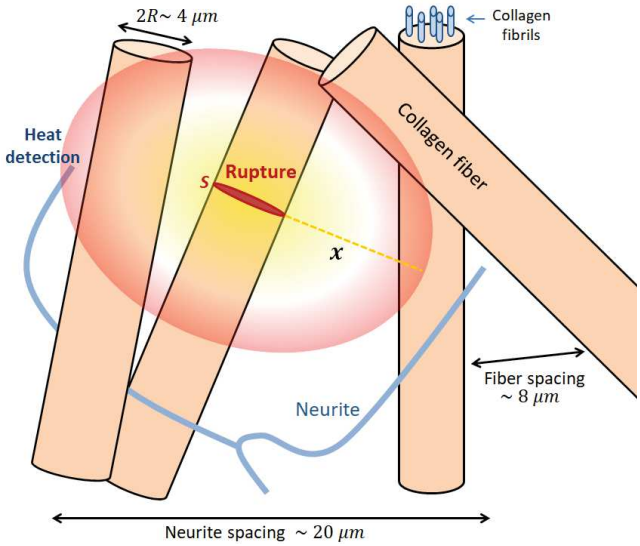

FIG. 1. Damage induced heat dissipation in the human skin. A collagen fiber is supposed to brutally snap, after which heat progressively diffuses to the surrounding molecules, as per Eq (1). If significant enough, this heat migh be detected by the TRPs proteins of the surrounding cells and neurites. In this figure, the schematic collagen and neurites geometries are inspired from [24] and [25].

through a neuron membrane depending on the balance of charge on each side of this membrane.

The role of the TRP proteins is, however, not limited to thermal sensing, and some TRPs are known to be sensitive to chemical aggression, responding for instance to abnormal pH, to capsaïcine (i.e., the component of chilli pepper that is felt as hot), to menthol (that is felt as cold), or to arachnid acids [21, 22]. They are hence often referred to as polymodal nociceptors. Similarly, a growing suspicion seems to have risen that they could also be involved in the feeling of mechanical pain [21–23]. While the latter is complex, and shall rely on many types of nociceptors other than the TRPs [31], the detection of thermal and mechanical inputs has indeed been shown to be somewhat coupled. In particular, the pain threshold of human subjects was reported to be a decreasing function of the ambient temperature [32], and the drug-induced inhibition of TRPV1 and TRPV3 has proven to reduce mechanical hyperalgesia [33–35] (i.e., the increased sensibility to mechanical pain after a first stimulus). We suggest that this apparent coupling may be explained by the actual (physical) coupling between mechanical damage and heat dissipation. It is for instance well known that burns can be induced by friction on the skin (e.g., [36]), due to the heat that is there generated. Similarly, a micro-crack of the epidermis, that is caused by some mechanical input, is to release some heat in the surrounding tissues, and this heat may well be detected by the skin thermal nociceptors, as illustrated in Fig. 1.

TEMPERATURE ELEVATION AROUND A BROKEN COLLAGEN FIBER

As the major structural cutaneous constituent, let us consider a collagen fiber, which has a typical radius [24] $R \sim 2\,\mu\text{m}$. While it is itself composed of many fibrils and proteins [37], the failure of this unit is likely a characteristic step [38] in any wider damage of the surrounding matter, as it is the case for engineered fibrous materials (e.g., [13]). As per the energy release rate G of skin [7], the rupture of this fiber shall dissipate an energy $\pi R^2 G \sim 25\,\text{nJ}$, that is here assumed to be mainly converted into heat on the atomic scale, which then diffuses [39] to the surrounding skin molecules. For simplicity, we suppose that the collagen fiber break is brutal, that is, with a rupture velocity comparable to that of sound in skin [40, 41], $V_0 \sim 1500\,\text{m}\,\text{s}^{-1}$. We can then, for various times τ after the fracture that are superior enough to $2R/V_0 = 2.5\,\text{ns}$, compute the temperature rise ΔT around the damage, by integrating the heat diffusion kernel [39] over the broken surface S:

$$\Delta T = \iint_S \mathrm{d}s\, \frac{G\sqrt{C}}{(4\pi\lambda\tau)^{3/2}} \exp\left(\frac{-Cr^2}{4\lambda\tau}\right). \qquad (1)$$

In this equation, r is the integration distance between a given point where the temperature is computed, and the various infinitesimal heat sources of S, that have an elementary surface $\mathrm{d}s$. In addition, the heat conductivity and volumetric heat capacity of skin are respectively denoted λ and C, whose values are about $\lambda \sim 0.4\,\text{J}\,\text{m}^{-1}\,\text{s}^{-1}\,\text{K}^{-1}$ and $C \sim 4\,\text{MJ}\,\text{K}^{-1}\,\text{m}^{-3}$ [42].

If the rise in temperature described by Eq. (1) can be captured by the human neuronal system, it could then be treated as mechanical pain. In a healthy skin, the density of neurites was estimated [25] to be about $\rho_n \sim 2000\,\text{mm}^{-2}$, a quantity from which we derive an order of magnitude for the maximum distance between the surface of a broken collagen bundle and that of a neuronal receptor: $1/(2\sqrt{\rho_n}) - R \sim 9\,\mu\text{m}$. We have here assumed very thin, evenly distributed, neurites, that are all thermo-sensitive. This might of course be rather simplified, considering the various types of cutaneous neurons (e.g., [31]) and their respective densities in different body parts [26]. In addition, the expression of the TRPs in the skin (and their role in thermo-sensing) is not limited to its sensory neurons, as they also appear, notably, in keratinocyte cells [21, 43]. Interestingly, however, such an approximate maximum distance (9 μm) is similar to the typical gap between the surfaces of two collagen fibers, which was measured [24] in average to be about 8 μm. Thus, if only two contiguous fibers were to break in response to a mechanical stimuli, one of it would, probably, be rather close (that is, in the micrometer range) to a neurite. We therefore show, in Fig. 2, the evolution of the temperature $T_0 + \Delta T$ predicted by Eq. (1), at various distances x up to 9 μm perpendicularly to the broken

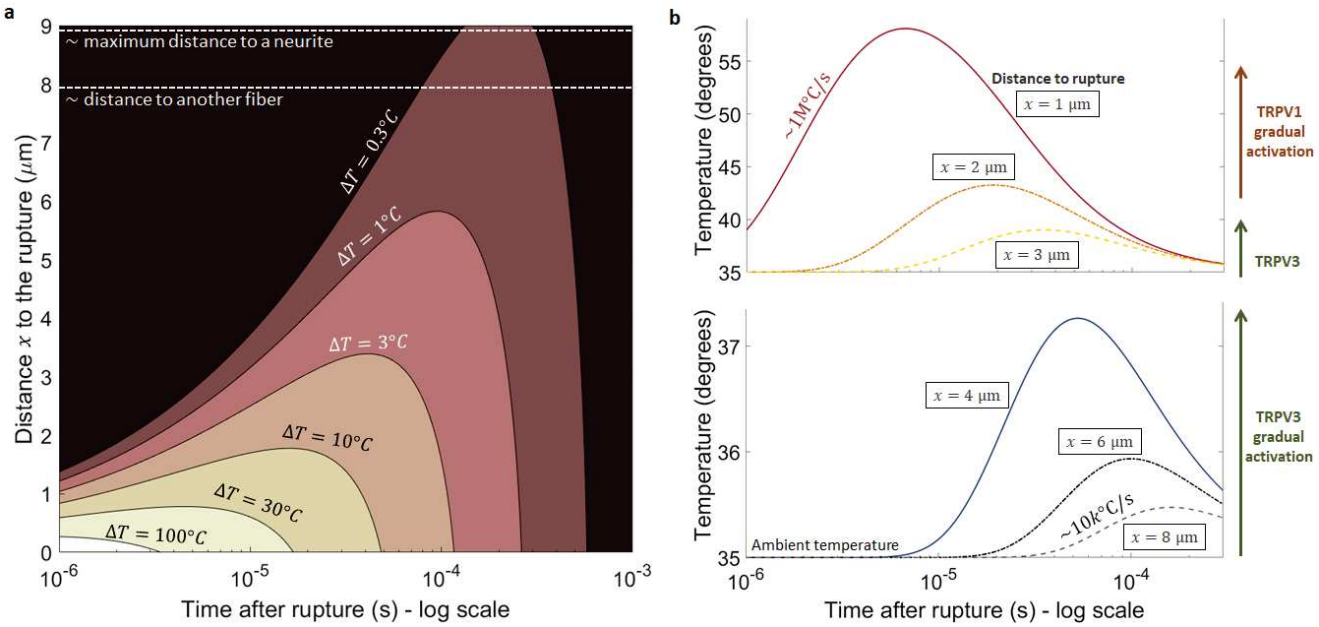

FIG. 2. (a): Temperature elevation ΔT close to a fractured collagen fiber, as a function of the distances in space and time to the rupture event, as predicted by Eq. (1). (b): Local skin temperature felt at various distances and times from the fractured fiber. Each plots corresponds to a horizontal section of inset (a), to which an ambient skin temperature $T_0 = 35°\mathrm{C}$ was added. For readability, two graphs with different temperature scales are shown. (Top): temperature at a distance $x = 1$, 2 and 3 µm from the fracture. (Bottom): temperature at $x = 4$, 6 and 8 µm. An approximate maximal distance between a neurite and the surface of a collagen fiber is about 9 µm, as we developed in the core text. The vertical arrows show the domains of increasing activation of the TRPV1 [22] (strong heat) and TRPV3 [28] (warm feeling) protein channels at the surface of neurites.

fiber surface, T_0 being the normal internal skin temperature. We have here used $T_0 \sim 35°\mathrm{C}$. Typical surface skin temperatures can indeed be measured (e.g., [44]) to lie between 30°C and 34°C, with an internal one that should be slightly higher, transiting to about 37°C (e.g., [45]). Of course, a lower skin temperature (for instance at extremities) means that a stronger thermal anomaly would be needed for the TRPs threshold to be reached . Additionally to Fig. 2, we show, in Fig. 3, the related spatial temperature maps at three given times τ after the fracture.

Close to the rupture plane, that is, for $x < 2$ µm, modelled temperatures superior to that of the activation of TRPV1 ($\sim 43°\mathrm{C}$) are quickly reached, in about 10 µs. A painful message can thus be triggered. More conservatively, if the thermal transducers are further away from the rupture point ($x = 2$ to 9 µm), they undergo a temperature elevation of half a degree to a few degrees, about 0.1 ms after the damage. While this quantity is not enough to trigger TRPV1, and not vastly outside the range of the normal temperature oscillations of the human skin [46], it could still be perceived as some abnormally sudden and localised heat by the brain. TRPV3 was indeed shown to be rather sensitive to small temperature changes around the normal body temperature [28, 29], and with a more intense response the faster these changes are [29]. Here, as shown in Fig. 2, we expect very high heating rates ranging from $10\,\mathrm{k°C\,s^{-1}}$ to $1\,\mathrm{M°C\,s^{-1}}$.

The temperature bursts reaching the neurons in less than a millisecond, they could in theory trigger pain reflexes, whose characteristic delays are an order of magnitude bigger, and mainly arise from the two-way travel time of the bio-electrical signals from the neurites to the central nervous system (e.g, [26]).

DISCUSSION

On the thermal model simplicity

The thermal model we have considered is also rather simple, supposing in particular the thermal properties of skin to be homogeneous. As an example, the TRP proteins reside within the cell membranes, and the heat capacity and conductivity of these lipid bilayers [47] are to slightly differ from the surrounding, aqueous, environment. The extra heat could also be preferably conducted inside the collagen network rather than outside of it. Overall, however, the various components of skin shall have comparable thermal properties, so that a homogeneous approach likely leads to a reasonable estimation.

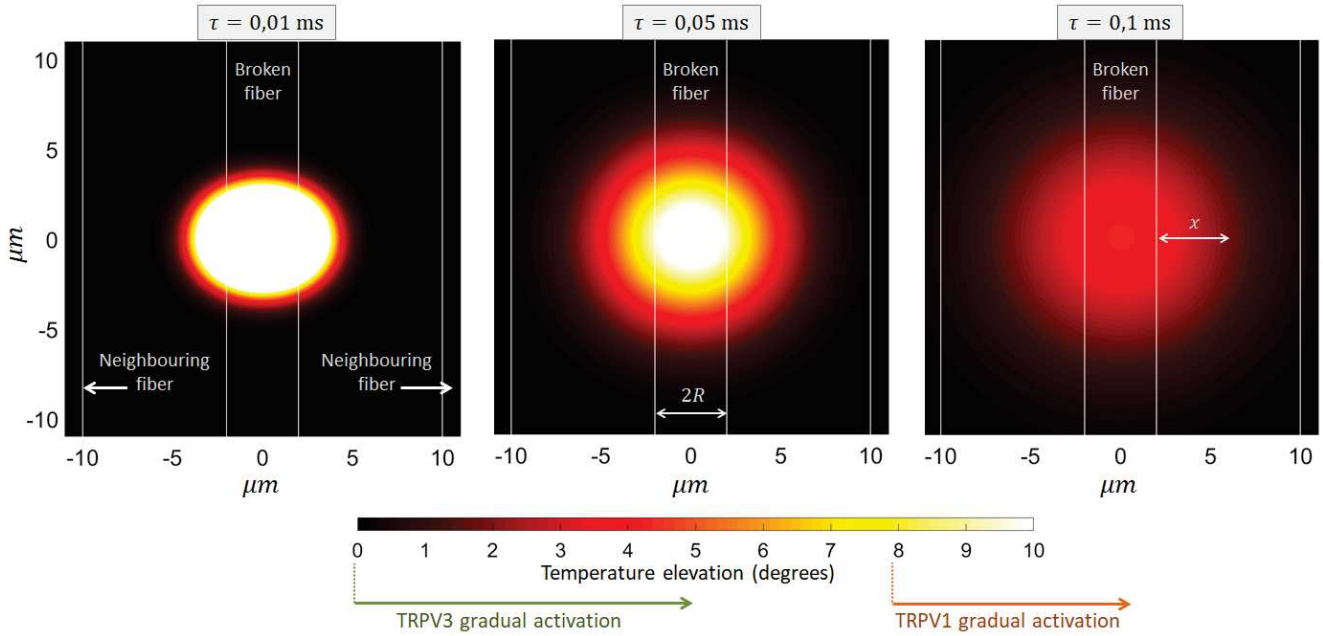

FIG. 3. Modelled temperature anomaly (ΔT) around a brutally broken collagen fiber, as per Eq. (1). Three times τ after the rupture are shown in chronological order. The color scale is saturated at 10°C for readability. In each frame, the volume integral $\iiint C\Delta T \mathrm{d}v = \pi R^2 G$ is conserved. The white vertical lines mark the border of the broken fiber and of its closest neighbours [24]. Each map is a cross-section cutting though the central fiber center and has an area of about $1/\rho_n$, where ρ_n is the typical neurite density in the human skin [25]. Thus, at least one neurite is likely to be present on the displayed surface. The two arrows below the color bar represents the domains of activation of the TRPV3 and TRPV1 channels, when assuming a background temperature of 35°C.

On the thermal anomaly duration and strength

The time interval during which the temperature elevation holds at a given location is of importance. In our case, it is of the order of 0.1 ms and less (see Fig. 2), and a question stands on the response time of in situ TRPs proteins. Recent laboratory studies [48, 49], applying fast temperature rise to patch clamp samples, indeed suggest that the TRPs reach a steady current emission in times as large as a few milliseconds. It may imply that the temperature signal we have here described should, in practice, be low-pass filtered. While it could stand as a predicament of the present theory, a early (transient) response from the proteins channels may be enough information to be interpreted as pain by the central nervous system. Furthermore, the response of nociceptors is to be multifactor, depending for instance in ions concentration and voltage, and the behavior of TRP proteins are known to hold a complex hysteresis. They have notably shown [50] an improved response time to temperature jumps after a first excitation. Overall, and while an activation time longer than the millisecond is likely in regard to the current state in the art, the actual responsiveness of in situ channels has not been measured.

When it comes to the strength of the temperature anomaly, only part, rather than the whole, of the released energy G could be transformed into heat, leading to an equivalent reduction in our computed temperatures. And, if collagen fibers were to slowly creep rather than brutally snap, more time would be given to the thermal diffusion to evacuate the thus progressively generated heat, so that ΔT would also be significantly smaller [17]. As an example, if only 50% of G was to be dissipated into heat, the local temperature elevation would be twice less than what is shown in Figs. 2 and 3, and the threshold for TRPV1 activation would barely be reached, even close to the damage. In practice, this conversion efficiency in organic tissues is not known, and would benefit from some experimental characterisation. However, in a soft polymer (which skin partly is), Vincent-Dospital et al. [14] have shown it to be close to 100%, so that this value, although not conservative, is not unsound.

The preceding points suggest that the time and amplitude spans of our modelled anomaly are truly at the limit of the acknowledge sensitivity of TRPs. However, note that we have here only considered a microscopic lesion. While the rupture of a single fiber is likely representative of the orders of magnitude at stake in this very local phenomenon, larger traumas, in particular if not limited to collagen bundles, could be accompanied

with stronger and longer thermal anomalies. There, the spatial extent of the warmed-up neurites may also play some role in the nociception (e.g., [26]).

On hyperalgesia rather than algesia

Interestingly, the suspected involvement of TRPs [33–35] in mechanical sensibility was reported for hyperalgesia rather than for algesia itself, and we propose that it could be explained by our computed temperatures. Indeed, as we suspect that the energy that is converted into heat lies at the limit of the thermal nociceptors sensibility, the damaged tissues might need to already be inflamed (that is, warmer) for a noxious signal to be generated. Alternatively, the limitation of the TRPs action to hyperalgesia could arise from the hysteresis in these channels response. It has for instance been shown [49, 51] that TRVP3 needs a first activation at a noxious heat level before responding to temperature changes in a more normal range, that our model does cover.

On membrane stretching and other mechano-nociceptors

We should here restate that the thermo-mechanical pain process that we have described shall certainly not exhaustively account for any sense of mechanical pain. It is rather an explanation to its coupling with the ambiant temperature [32] and the involvement of TRP proteins. Other mechano-nociceptors are however likely at play (e.g., [31]): for instance, the well named Piezo channels, which opening is believed to be directly related to the cell membranes strain, and which could contribute to noxious mechanical sensing [52].
Interestingly, as another explanation to the mechanical sensitivity of TRPs, it was proposed [53] that the stretching of cell membranes could similarly force the opening of these proteins. This view and that we have developed are not exclusive, as the activation of a channel may, in practice, be polymodal, that is, the thermal responsiveness of a nociceptor could be enhanced by its abnormal strain.

Concluding remarks

Note finally that other and similar phenomena than those we have discussed could also be at play in thermo-mechanical sensing. For instance, it was shown (e.g., [54]) that the important toughness of skin is explained by the reorientation and the sliding of collagen fibrils in a stretched skin. The related friction between these collagen units, which occurs before their actual rupture, is also to generate some heat bursts. By contrast, the vasoconstriction in a compressed body would be prone to induce a local cooling [55], which could also be sensed. While we have focused on the example of skin, the main concepts we have here discussed are also general enough to stand for both somatic (that is, related to the skin, tissues and muscles) and visceral (i.e., related to internal organs) pain, in which the TRPs are likely involved [56]. Let us conclude by amusingly pointing out that temperature monitoring has regularly been used by material scientists, including the authors of the present manuscript, to monitor the ongoing damage of engineered solids (e.g., [10, 13, 15]). In these experiments, we might have unknowingly mimicked our own biology.

Acknowledgements and conflicts of interest

The authors acknowledge the support of the IRP France-Norway D-FFRACT, and of the University of Strasbourg. They declare no competing financial interests in the publishing of this work. We also thank Charlotte Kruckow for her insightful suggestions.

* vincentdospitalt@unistra.fr
† renaud.toussaint@unistra.fr

[1] J. R. Rice. Thermodynamics of the quasi-static growth of Griffith cracks. *Journal of the Mechanics and Physics of Solids*, 26(2):61 – 78, 1978. doi:10.1016/0022-5096(78)90014-5.
[2] G. T. Hahn, M. F. Kanninen, and A. R. Rosenfield. Fracture toughness of materials. *Annual Review of Materials Science*, 2(1):381–404, 1972. doi: 10.1146/annurev.ms.02.080172.002121.
[3] A. Griffith. The Phenomena of Rupture and Flow in Solids. *Philosophical Transactions of the Royal Society of London A: Mathematical, Physical and Engineering Sciences*, 221(582-593):163–198, January 1921. ISSN 1471-2962. doi:10.1098/rsta.1921.0006.
[4] S. M. Wiederhorn. Influence of water vapor on crack propagation in soda-lime glass. *Journal of the American Ceramic Society*, 50(8):407–414, 1967. doi: 10.1111/j.1151-2916.1967.tb15145.x.
[5] S. M. L. Sastry, R. J. Lederich, and B. B. Rath. Subcritical crack-growth under sustained load in Ti-6AI-6V-2Sn. *Metallurgical Transactions A*, 12(1):83–94, Jan 1981. ISSN 1543-1940. doi:10.1007/BF02648512.
[6] J. H. Huang and C. J. Altstetter. Internal hydrogen-induced subcritical crack growth in austenitic stainless steels. *Metallurgical Transactions A*, 22(11):2605–2618, Nov 1991. ISSN 1543-1940. doi:10.1007/BF02851354.

[7] B. P. Pereira, P. W. Lucas, and T. Swee-Hin. Ranking the fracture toughness of thin mammalian soft tissues using the scissors cutting test. *Journal of Biomechanics*, 30(1):91 – 94, 1997. ISSN 0021-9290. doi:10.1016/S0021-9290(96)00101-7.

[8] J. R. Rice and D. C. Drucker. Energy changes in stressed bodies due to void and crack growth. *International Journal of Fracture Mechanics*, 3:19–27, 1967. ISSN 1573-2673. doi:10.1007/BF00188642.

[9] J. W. Morrissey and J. R. Rice. Crack front waves. *Journal of the Mechanics and Physics of Solids*, 46(3): 467 – 487, 1998. ISSN 0022-5096. doi:10.1016/S0022-5096(97)00072-0.

[10] G. Pallares, C. L. Rountree, L. Douillard, F. Charra, and E. Bouchaud. Fractoluminescence characterization of the energy dissipated during fast fracture of glass. *Europhysics Letters*, 99(2):28003, 2012.

[11] J. R. Rice and N. Levy. Local heating by plastic deformation at a crack tip. *Physics of Strength and Plasticity*, pages 277–293, 1969.

[12] K. N. G. Fuller, P. G. Fox, and J. E. Field. The temperature rise at the tip of fast-moving cracks in glassy polymers. *Proceedings of the Royal Society of London A: Mathematical, Physical and Engineering Sciences*, 341(1627):537–557, 1975. ISSN 0080-4630. doi: 10.1098/rspa.1975.0007.

[13] R. Toussaint, O. Lengliné, S. Santucci, T. Vincent-Dospital, M. Naert-Guillot, and K. J. Måløy. How cracks are hot and cool: a burning issue for paper. *Soft Matter*, 12:5563–5571, 2016. doi:10.1039/C6SM00615A.

[14] T. Vincent-Dospital, R. Toussaint, S. Santucci, L. Vanel, D. Bonamy, L. Hattali, A. Cochard, K. J. Måløy, and E. G. Flekkøy. How heat controls fracture: the thermodynamics of creeping and avalanching cracks. *Soft Matter*, 2020. doi:10.1039/d0sm010. accepted.

[15] D. Palumbo, R. De Finis, F. Ancona, and U. Galietti. Damage monitoring in fracture mechanics by evaluation of the heat dissipated in the cyclic plastic zone ahead of the crack tip with thermal measurements. *Engineering Fracture Mechanics*, 181:65 – 76, 2017. ISSN 0013-7944. doi:10.1016/j.engfracmech.2017.06.017.

[16] G. Carbone and B. N. J. Persson. Hot cracks in rubber: Origin of the giant toughness of rubberlike materials. *Phys. Rev. Lett.*, 95:114301, Sep 2005. doi: 10.1103/PhysRevLett.95.114301.

[17] T. Vincent-Dospital, R. Toussaint, A. Cochard, K. J. Måløy, and E. G. Flekkøy. Thermal weakening of cracks and brittle-ductile transition of matter: A phase model. *Physical Review Materials*, 02 2020. doi: 10.1103/PhysRevMaterials.4.023604.

[18] J. R. Rice. Heating and weakening of faults during earthquake slip. *Journal of Geophysical Research: Solid Earth*, 111(B5), 2006. doi:10.1029/2005JB004006.

[19] C. Wibberley and T. Shimamoto. Earthquake slip weakening and asperities explained by fluid pressurization. *Nature*, 436:689–92, 09 2005.

[20] J. Sulem and V. Famin. Thermal decomposition of carbonates in fault zones: Slip-weakening and temperature-limiting effects. *Journal of Geophysical Research: Solid Earth*, 114(B3), 2009. doi:10.1029/2008JB006004.

[21] H. Wang and C. J. Woolf. Pain TRPs. *Neuron*, 46(1):9 – 12, 2005. ISSN 0896-6273. doi: 10.1016/j.neuron.2005.03.011.

[22] M. J. Caterina and U. Park. Chapter 4 TRPV1: A polymodal sensor in the nociceptor terminal. In *The Nociceptive Membrane*, volume 57 of *Current Topics in Membranes*, pages 113 – 150. Academic Press, 2006. doi: 10.1016/S1063-5823(06)57003-6.

[23] M. B. Goodman. Sensation is painless. *Trends in Neurosciences*, 26(12):643 – 645, 2003. ISSN 0166-2236. doi: 10.1016/j.tins.2003.09.013.

[24] P. D.H.M. Verhaegen, J. Van Marle, A. Kuehne, H. J. Schouten, E. A. Gaffney, P. K. Maini, E. Middelkoop, and P. P.M. Van Zuijlen. Collagen bundle morphometry in skin and scar tissue: a novel distance mapping method provides superior measurements compared to fourier analysis. *Journal of Microscopy*, 245(1):82–89, 2012. doi:10.1111/j.1365-2818.2011.03547.x.

[25] A.-L. Oaklander. The density of remaining nerve endings in human skin with and without postherpetic neuralgia after shingles. *Pain*, 92, 2001. ISSN 0304-3959.

[26] A.-L. Oaklander and S. M. Siegel. Cutaneous innervation: Form and function. *Journal of the American Academy of Dermatology*, 53:1027–1037, 2005. doi: 10.1016/j.jaad.2005.08.049.

[27] B. I. Tóth, A. Oláh, A. Gábor Szöllősi, and T. Bíró. TRP channels in the skin. *British journal of pharmacology*, 171:2568 – 2581, 2014. doi:10.1113/jphysiol.2005.088377.

[28] A. K. Singh, L. L. McGoldrick, L. Demirkhanyan, M. Leslie, E. Zakharian, and A. I. Sobolevsky. Structural basis of temperature sensation by the TRP channel TRPV3. *Nature Structural and Molecular Biology*, 26: 994–998, 2019. doi:10.1038/s41594-019-0318-7.

[29] H. Xu, I. S. Ramsey, S. A. Kotecha, M. M. Moran, J. A. Chong, D. Lawson, P. Ge, J. Lilly, I. Silos-Santiago, Y. Xie, P. S. DiStefano, R. Curtis, and D. E. Clapham. TRPV3 is a calcium-permeable temperature-sensitive cation channel. *Nature*, 418:181–186, 2002. doi: 10.1038/nature00882.

[30] B. Nilius, K. Talavera, G. Owsianik, J. Prenen, G. Droogmans, and T. Voets. Gating of TRP channels: a voltage connection. *The Journal of physiology*, 567:35 – 44, 2005. doi:10.1113/jphysiol.2005.088377.

[31] R. Z. Hill and D. M. Bautista. Getting in touch with mechanical pain mechanisms. *Trends in Neurosciences*, 43:311 – 325, 2020. ISSN 0166-2236. doi: 10.1016/j.tins.2020.03.004.

[32] W. J. Culp, J. Ochoa, M. Cline, and R. Dotson. Heat and mechanical hyperalgesia induced by capsaisin: cross modality threshold modulation in human C nociceptors. *Brain*, 112(5):1317–1331, 10 1989. ISSN 0006-8950. doi: 10.1093/brain/112.5.1317.

[33] K. M. Walker, L. Urban, S. J. Medhurst, S. Patel, M. Panesar, A. J. Fox, and P. McIntyre. The vr1 antagonist capsazepine reverses mechanical hyperalgesia in models of inflammatory and neuropathic pain. *Journal of Pharmacology and Experimental Therapeutics*, 304(1):56–62, 2003. ISSN 0022-3565. doi: 10.1124/jpet.102.042010.

[34] J. D. Pomonis, J. E. Harrison, L. Mark, D. R. Bristol, K. J. Valenzano, and K. Walker. A novel, orally effective vanilloid receptor 1 antagonist with analgesic properties. in vivo characterization in rat models of inflammatory and neuropathic pain. *Journal of Pharmacology and Experimental Therapeutics*, 306(1):387–393, 2003. ISSN 0022-3565. doi:10.1124/jpet.102.046268.

[35] S. McGaraughty, K. L Chu, J. Xu, L. Leys, R. J. Radek, M. J. Dart, A. Gomtsyan, R. G. Schmidt, P. R. Kym, and J.-D. Brederson. TRPV3 modulates nociceptive signaling through peripheral and supraspinal sites in rats. *Journal of neurophysiology*, 118:904–916, 2017. ISSN 1522-1598. doi:10.1152/jn.00104.2017.

[36] M. M. Al-Qattan, K. Al-Zahrani, B. Al-Shanawani, and N. Al-Arfaj. Friction Burn Injuries to the Dorsum of the Hand After Car and Industrial Accidents: Classification, Management, and Functional Recovery. *Journal of Burn Care and Research*, 31(4):610–615, 07 2010. ISSN 1559-047X. doi:10.1097/BCR.0b013e3181e4d6b9.

[37] M. J. Buehler. Nature designs tough collagen: Explaining the nanostructure of collagen fibrils. *Proceedings of the National Academy of Sciences*, 103(33):12285–12290, 2006. ISSN 0027-8424. doi:10.1073/pnas.0603216103.

[38] T.I. Zohdi. A computational framework for network modeling of fibrous biological tissue deformation and rupture. *Computer Methods in Applied Mechanics and Engineering*, 196(31):2972 – 2980, 2007. ISSN 0045-7825. doi: 10.1016/j.cma.2006.06.015. Computational Bioengineering.

[39] H. S. Carslaw and J. C. Jaeger. *Conduction of Heat in Solids*. Oxford: Clarendon Press, 1959.

[40] L. B. Freund. Crack propagation in an elastic solid subjected to general loading. *Journal of the Mechanics and Physics of Solids*, 20(3):129 – 152, 1972. ISSN 0022-5096. doi:10.1016/0022-5096(72)90006-3.

[41] S. A. Goss and F. Dunn. Ultrasonic propagation properties of collagen. *Physics in Medicine and Biology*, 25(5): 827–837, sep 1980. doi:10.1088/0031-9155/25/5/001.

[42] M. L. Cohen. Measurement of the thermal properties of human skin. a review. *Journal of Investigative Dermatology*, 69(3):333 – 338, 1977. ISSN 0022-202X. doi: 10.1111/1523-1747.ep12507965.

[43] A. Moqrich, S. W. Hwang, T. J. Earley, M. J. Petrus, A. N. Murray, K. S. R. Spencer, M. Andahazy, G. M. Story, and A. Patapoutian. Impaired thermosensation in mice lacking TRPV3, a heat and camphor sensor in the skin. *Science*, 307(5714):1468–1472, 2005. ISSN 0036-8075. doi:10.1126/science.1108609.

[44] K. Otsuka, S. Okada, M. Hassan, and T. Togawa. Imaging of skin thermal properties with estimation of ambient radiation temperature. *IEEE Engineering in Medicine and Biology Magazine*, 21(6):49–55, 2002. doi: 10.1109/MEMB.2002.1175138.

[45] V.P. Saxena and D. Arya. Steady-state heat distribution in epidermis, dermis and subdermal tissues. *Journal of Theoretical Biology*, 89(3):423 – 432, 1981. ISSN 0022-5193.

[46] V. Shusterman, K. P. Anderson, and O. Barnea. Spontaneous skin temperature oscillations in normal human subjects. *American Journal of Physiology-Regulatory, Integrative and Comparative Physiology*, 273(3):R1173–R1181, 1997. doi:10.1152/ajpregu.1997.273.3.R1173.

[47] A. R. N. Bastos, C. D. S. Brites, P. A. Rojas-Gutierrez, C. DeWolf, R. A. S. Ferreira, J. A. Capobianco, and L. D. Carlos. Thermal properties of lipid bilayers determined using upconversion nanothermometry. *Advanced Functional Materials*, 29(48):1905474, 2019. doi: 10.1002/adfm.201905474.

[48] J. Yao, B. Liu, and F. Qin. Kinetic and energetic analysis of thermally activated TRPV1 channels. *Biophysical journal*, 99:1743–1753, 2010. ISSN 1542-0086. doi: 10.1016/j.bpj.2010.07.022.

[49] B. Liu and F. Qin. Patch-clamp combined with fast temperature jumps to study thermal TRP channels. In *TRP Channels*, volume 1987 of *Methods in Molecular Biology*. Humana, New York, NY, 2019. doi:10.1007/978-1-4939-9446-5˙9.

[50] B. Liu and F. Qin. Use dependence of heat sensitivity of vanilloid receptor TRPV2. *Biophysical journal*, 110:1523–1537, 2016. ISSN 1542-0086. doi: 10.1016/j.bpj.2016.03.005.

[51] Beiying Liu, Jing Yao, Michael X. Zhu, and Feng Qin. Hysteresis of gating underlines sensitization of TRPV3 channels. *Journal of General Physiology*, 138(5):509–520, 10 2011. ISSN 0022-1295. doi:10.1085/jgp.201110689.

[52] S. E. Murthy, M. C. Loud, I. Daou, K. L. Marshall, F. Schwaller, J. Kühnemund, A. G. Francisco, W. T. Keenan, A. E. Dubin, G. R. Lewin, and A. Patapoutian. The mechanosensitive ion channel Piezo2 mediates sensitivity to mechanical pain in mice. *Science Translational Medicine*, 10(462), 2018. ISSN 1946-6234. doi: 10.1126/scitranslmed.aat9897.

[53] C. Liu and C. Montell. Forcing open TRP channels: Mechanical gating as a unifying activation mechanism. *Biochemical and Biophysical Research Communications*, 460(1):22 – 25, 2015. ISSN 0006-291X. doi: 10.1016/j.bbrc.2015.02.067.

[54] W. Yang, V. R. Sherman, B. Gludovatz, E. Schaible, P. Stewart, R. O. Ritchie, and M. A. Meyers. On the tear resistance of skin. *Nature Communications*, 6:6649, 2015. ISSN 2041-1723. doi:10.1038/ncomms7649.

[55] E.-H. Rubinstein and Daniel I. Sessler. Skin-surface Temperature Gradients Correlate with Fingertip Blood Flow in Humans. *Anesthesiology: The Journal of the American Society of Anesthesiologists*, 73(3):541–545, 09 1990. ISSN 0003-3022.

[56] S. Sikandar and A. H. Dickenson. Visceral pain: the ins and outs, the ups and downs. *Current opinion in supportive and palliative care*, 6:17–26, 2012. doi: 10.1097/SPC.0b013e32834f6ec9.

.

THESIS SUMMARY AND PERSPECTIVE

Dear reader, you have now reached the end of this document and I hope that you found it pleasant to go through. In the next lines, I will summarise what I think should be the main take away points and perspectives of this work.

Summary of the main thesis conclusions

We have mainly defended the idea that the propagation of a crack in a brittle solid matrix is a subcritical, thermally activated, phenomenon, at both slow and fast propagation velocity. Truly, a subcritical description was already common for slow creeping fractures, but it had not been extended to the description of fast, dynamical, ruptures. We have here merged these two regimes, which are often observed in the rupture of numerous materials, in a single thermodynamics framework, and, this way, we proposed an explanation to a long lasting question of rupture physics. To explain the transition between slow and fast cracks, we have in particular stated that the well known thermal dissipation at their tips can be strong and concentrated enough to lead to very high temperatures, which are, in return, prone to deeply impact the fracturing growth rate. We have indeed shown evidences that a significant portion of the fracture energy release rate G is released into heat, over only a few atomic lengths, leading to thousands of degrees hot crack tips. We have then discussed how such hot temperatures are compatible with many observables, reported over decades of scientific literature, and how they can strongly accelerate a subcritical crack propagation.

In this statistical physics framework, we have still acknowledged that an overcritical crack propagation can occur, but only after the fracture growth rate has already reached the fastest propagation branch, rather than at the onset of this fast regime. This overcritical propagation likely coincides with new energy dissipation processes, such as the complexification of cracks, possibly nucleating around temperature related phase changes around the main front.

Because we proposed that the slow to fast transition happens when the tip temperature becomes significant compared to the intensity of the background thermal bath, we have also predicted that fast rupture avalanches should be inhibited at high environmental temperatures. Thus, we have proposed a new explanation to the brittle-ductile transition of matter, for which we have characterised the critical behaviour in the theory we have developed.

The most quantitative result of this thesis is, no doubt, the demonstration that our proposed theory is compatible with the dynamics of rupture in two materials that have, over the last century of experiments, become quite canonical in fracture tests, that is, PMMA and adhesive glues. We have indeed shown that one can quantitatively reproduce the crack velocity to mechanical load curves in these materials, over many orders of magnitude of front growth rate, and with model parameters values seemingly in reasonable ranges. We have also demonstrated, although truly to a lesser extent, that our model could be applicable to the rupture of a very vast range of other materials.

Interestingly, rather than developing completely new physical concepts, the framework we have proposed for the physics of rupture is, on the contrary, a concatenation of many ideas that have been considered since the seminal work of Griffith, a hundred years ago, from the use of thermodynamics to the possibility of hot cracks. I suspect that this simple model may also be compatible with many other past and present works in fracture physics, not directly considered in this thesis, because it only encompasses a simple statistical physics description, which may be extensively complexified to account for various phenomena.
I find it actually quite beautiful and surprising that classical physics and thermodynamics, which are now taught everyday to most students in science, can still help to unravel very down to earth problems, such as the propagation of cracks.

Although they have long been known and described, thermal effects in rupture still likely have many secrets to be revealed. Besides arguing on their important role in the dynamics of fracture, I have tried to illustrate this idea with the last chapter of this thesis, in which I have defended that they could be partly responsible for the pain we may feel.
I can only hope that more warm secrets will be revealed or confirmed in the future, and that an increased interest by the community will be brought to rupture-induced thermal effects during the years to come.

Perspectives

As mentioned several times in this manuscript, transposing the proposed framework into a frictional, mode II, rupture problem may be a beneficial future step. It could lead to a new understanding of slip weakening mechanisms, with, as discussed, notable applications in geophysics to the stability of faults [1] but also to other domains.
For instance, one could better understand the cutting of materials, when it is obtained by solid-solid friction, in which a stick-slip phenomena can be observed and traced back to thermo-mechanics [2]. Solid friction is a very common process of everyday life. After all, we are partly solids ourselves. Thermal weakening could thus intervene in activities as different as ice skating [3] or music playing [4], where it is believed that the melting of the contact water, in the former case, and of the coating of the violin bow, in the latter one, can lead to significantly altered friction properties. Such melting is there maybe not necessarily called for to explain some thermal weakening in friction, as an improved subcritical slide due to the friction induced heat, in the spirit of what we have here proposed for mode I rupture, could there solely or partly be at stake.
Thermal weakening in friction might also not be limited to solid contacts. In particular, it was reported [5] that slip, and also stick-slip, can occur in the flow of surfactant solutions through nanopores (and also in larger tubes, although in a more negligible manner). In this case, a rearrangement of the surfactant molecules at high driving pressure was proposed to explain stick-slip, and we note that such rearrangement could be accompanied with thermal exchanges.
In summary, friction has always been known as a heat dissipation mechanism and the retroactive effect of this heat could, in part, be due to simple thermal activation.

Coming back to and ending with mode I rupture, it is to be said that there are many concepts which we have introduced in this thesis that would call for further exploration. In particular, an accurate characterisation of the hysteretical rupture of many materials and its comparison to our model would be beneficial to further discuss the validity of this model. Indeed, while our third chapter dealt with the study of many different solids, the full (three branches) velocity to load relation of these solids was mostly unknown, so that an accurate model matching, as done in chapter II for two polymers, was not actually done.
It could also be interesting to understand the lateral dynamics of thermal avalanches of non-punctual fracture fronts. We have here often simplified crack fronts to their simplest 0D description, when such a lateral propagation of avalanches has been shown to be significant for the rapid crack dynamics in some materials [6]. On a related topic, and, more generally, the question of how material disorder helps to trigger fast ruptures in a three dimensional solid remains of particular interest for real engineering applications. As discussed in chapter IV, one of the challenge here is the experimental characterisation of disorder, so that fracture models can be applied to known materials rather than supposed ones. Of course, a perfect characterisation of disorder would make the word disorder rather inappropriate.

Finally, I can only admit that an absolute validation or dismissal of our model, that has truly been welcome with quite some scepticism by peers, will not come before an actual and accurate measurement of temperature or atomic motion at the nanoscale around fast running crack tips. Such scepticism, and the conversations that resulted from it, has undoubtedly helped to improve some of the articles that you have read, at the unfortunate price of making the publication of these articles a rather frustrating process.
What remains certain is that some thermal measurements already suggest, and have actually long suggested, that a strong thermal dissipation is at play in the propagation of fast running cracks (e.g., [7]), and we have here shown that one should not overlook their potential effect on the dynamics of rupture.

---

[1] H. Noda, E. M. Dunham, and J. R. Rice. Earthquake ruptures with thermal weakening and the operation of major faults at low overall stress levels. *Journal of Geophysical Research: Solid Earth*, 114(B7), 2009. doi:10.1029/2008JB006143.
[2] Q. Wang, G. G. Ye, L. H. Dai, and C. Lu. Modelling the tuned criticality in stick-slip friction during metal cutting. *Modelling and Simulation in Materials Science and Engineering*, 23:17, 2015. ISSN 0965-0393. doi:10.1088/0965-0393/23/5/055013.
[3] A.-M. Kietzig, S. G. Hatzikiriakos, and P. Englezos. Physics of ice friction. *Journal of Applied Physics*, 107(8):081101, 2010. doi:10.1063/1.3340792.
[4] J.H. Smith and J. Woodhouse. The tribology of rosin. *Journal of the Mechanics and Physics of Solids*, 48(8):1633 – 1681, 2000. ISSN 0022-5096. doi:10.1016/S0022-5096(99)00067-8.
[5] Christophe Cheikh and Ger Koper. Stick-slip transition at the nanometer scale. *Phys. Rev. Lett.*, 91:156102, Oct 2003. doi:10.1103/PhysRevLett.91.156102.
[6] V. De Zotti, K. Rapina, P.-P. Cortet, L. Vanel, and S. Santucci. Bending to kinetic energy transfer in adhesive peel front microinstability. *Phys. Rev. Lett.*, 122:068005, Feb 2019. doi:10.1103/PhysRevLett.122.068005.

[7] G. Pallares, C. L. Rountree, L. Douillard, F. Charra, and E. Bouchaud. Fractoluminescence characterization of the energy dissipated during fast fracture of glass. *Europhysics Letters*, 99(2):28003, 2012.

Acknowledgement

I would like to close this document by thanking the many people that have made, remotely or directly, its writing possible. I hope I am here as exhaustive as possible.

- On a very personal level, I would like to thank Mathilde for having borne sharing my life through this work, including during the less happy moments, when I might have been moody about it.

- I thank Renaud Toussaint and the ED413 school, for having trusted me with this thesis, which was both a great opportunity and a source of many learnings for me. To Renaud Toussaint and Alain Cochard, I am grateful for the directions, pieces of advice and, more generally, to the great supervision they have provided me during the past three years.

- I thank Knut Jorgen Måløy and Eirik Flekkøy for having made possible the cotutelle with the University of Oslo, and for their great advice. I am also grateful for having been able to spend a few months among their team and their lab.

- On this laboratory note, I would like to thank Marcel Moura and Alain Steyer, for their guidance in using the labs in, respectively, Oslo and Strasbourg.

- I thank my co-authors without whom the articles and drafts in this thesis would not be half as complete. Namely: Renaud Toussaint, Alain Cochard, Knut Jorgen Måløy, Eirik Flekkøy, Stéphane Santucci, Loïc Vanel, Daniel Bonamy and François Renard.

- By advance, I thank the examiners of this thesis for having read this far, and for the time they will spend on assessing my work.

- I acknowledge and am grateful for the structural and financial support of the Universities of Strasbourg and Oslo, of the IRP France-Norway D-FFRACT and of CNRS INSU ALEAS.

- I am grateful to my co-workers and fellow PhD students in Strasbourg, Shahar Ben Zeev and Laciel Alonso, for having shared my office and my everyday thoughts, being about fracture physics or not.

- I have also a thought for the many physics teachers I have encountered during my education. Many of their teaching were first-hand useful in this research.

- Of course, I want to thank my wonderful parents, Anne and Michel, without whom I would never have followed this education in the first place.

Université de Strasbourg

Tom VINCENT-DOSPITAL

Fracturation interfaciale : effets thermiques et désordre matériel

École doctorale Sciences de la terre et de l'environnement | ED 413

Résumé

La dynamique de propagation des fissures est importante en science des matériaux et en ingénierie, pour la compréhension de la résistance des solides et des structures qui nous entourent. Ce sujet est aussi central en sciences de la Terre, notamment pour la compréhension de l'instabilité des failles sismiques.

Lors de la rupture d'un milieu élastique fragile, une partie du chargement extérieur fourni à la matrice est dissipée dans une zone plastique en tête de fissure. Cette dissipation irréversible, qui peut-être caractérisée par un taux de libération d'énergie macroscopiquement mesurable, s'appuie sur divers mécanismes physiques. En particulier, l'élévation de la température induite par friction intermoléculaire, directement au sein de la zone plastique.

Plus qu'un simple marqueur de l'endommagement, cette dissipation thermique pourrait, en retour, avoir un impact significatif sur la dynamique de la rupture. Dans cette thèse, nous étudions cette possibilité et proposons une loi d'activation dans laquelle l'élévation thermique en tête de rupture est réintroduite. Nous montrons que ce modèle permet de reproduire la rupture de différents matériaux et fournit une explication à la transition fragile-ductile de la matière.

Mots-clés : dynamique de rupture, dissipation thermique, fissures, fractoluminescence

Résumé en anglais

The dynamics of cracks is of paramount importance in material sciences and in everyday engineering, to correctly grasp the toughness of matter and of structures. It is also rather central in geosciences, for instance in the instability of seismic faults.

During the rupture of a brittle elastic medium, a portion of the external mechanical load, provided to the matrix, is dissipated in a plastic zone at the fracture tip. This irreversible dissipation, which can be characterized by a macroscopically measurable energy release rate, derives from various physical processes. In particular, a rise in temperature from the intermolecular friction, directly inside the plastic zone.

More than a marker for the damage, such a thermal dissipation at the tip can lead to an increase in the fracture velocity, as understood by statistical physics. In the present thesis, we study this possibility and propose an activation law in which the fracture induced heat is reintroduced. We show that it allows a good reproduction of the actual rupture of several materials and can explain the brittle-ductile transition of matter.

Keywords: rupture dynamics, thermal dissipation, cracks, fractoluminescence